

Javier Ballestín Fuertes

Mejora de sistemas de electrónica  
de potencia para el despliegue  
masivo de recursos energéticos  
distribuidos y vehículo eléctrico en  
redes de distribución de baja  
tensión

Director/es

Sanz Osorio, José Francisco  
Muñoz-Cruzado Alba, Jesús

<http://zaguan.unizar.es/collection/Tesis>

© Universidad de Zaragoza  
Servicio de Publicaciones

ISSN 2254-7606

Tesis Doctoral

MEJORA DE SISTEMAS DE ELECTRÓNICA DE  
POTENCIA PARA EL DESPLIEGUE MASIVO DE  
RECURSOS ENERGÉTICOS DISTRIBUIDOS Y  
VEHÍCULO ELÉCTRICO EN REDES DE  
DISTRIBUCIÓN DE BAJA TENSIÓN

Autor

Javier Ballestín Fuertes

Director/es

Sanz Osorio, José Francisco  
Muñoz-Cruzado Alba, Jesús

**UNIVERSIDAD DE ZARAGOZA**  
**Escuela de Doctorado**

Programa de Doctorado en Energías Renovables y Eficiencia Energética

2022





UNIVERSIDAD DE ZARAGOZA

MEJORA DE SISTEMAS DE  
ELECTRÓNICA DE POTENCIA PARA EL  
DESPLIEGUE MASIVO DE RECURSOS  
ENERGÉTICOS DISTRIBUIDOS Y  
VEHÍCULO ELÉCTRICO EN REDES DE  
DISTRIBUCIÓN DE BAJA TENSIÓN

Tesis doctoral presentada por Javier Ballestín Fuertes  
dentro del Programa de Doctorado en Energías Renovables y Eficiencia Energética

Dirigida por Dr. José Francisco Sanz Osorio  
y Dr. Jesús Muñoz-Cruzado Alba





UNIVERSIDAD DE ZARAGOZA

MEJORA DE SISTEMAS DE ELECTRÓNICA DE  
POTENCIA PARA EL DESPLIEGUE MASIVO DE  
RECURSOS ENERGÉTICOS DISTRIBUIDOS Y  
VEHÍCULO ELÉCTRICO EN REDES DE  
DISTRIBUCIÓN DE BAJA TENSIÓN

Tesis doctoral presentada por Javier Ballestín Fuertes  
dentro del Programa de Doctorado en Energías Renovables y Eficiencia Energética

Dirigida por Dr. José Francisco Sanz Osorio  
y Dr. Jesús Muñoz-Cruzado Alba

El doctorando

El director

El director

Zaragoza, Agosto de 2022



*Mejora de sistemas de electrónica de potencia para el despliegue masivo de recursos energéticos distribuidos y vehículo eléctrico en redes de distribución de baja tensión*

Autor: Javier Ballestín Fuertes

Director: Dr. José Francisco Sanz Osorio

Director: Dr. Jesús Muñoz-Cruzado Alba

Agosto de 2022

---







## Publicaciones

La presente tesis doctoral recoge los resultados de trabajos de investigación que han sido previamente publicados en revistas científicas indexadas y congresos internacionales. A continuación, se listan las seis referencias bibliográficas seleccionadas para poder defender la tesis doctoral en la modalidad de compendio de publicaciones.

1. Ballestín-Fuertes, J.; Muñoz-Cruzado-Alba, J.; Sanz-Osorio, J.F.; Hernández-Callejo, L.; Alonso-Gómez, V.; Morales-Aragones, J.I.; Gallardo-Saavedra, S.; Martínez-Sacristan, O.; Moretón-Fernández, Á. “Novel Utility-Scale Photovoltaic Plant Electroluminescence Maintenance Technique by Means of Bidirectional Power Inverter Controller”. *Appl. Sci.* 2020, 10, 3084. doi: 10.3390/app10093084.  
*Q2 en Engineering, Multidisciplinary. Factor de impacto 2,736 (2020).*
2. Ballestín-Fuertes, J.; Muñoz-Cruzado-Alba, J.; Sanz-Osorio, J.F.; Laporta-Puyal, E. ”Role of Wide Bandgap Materials in Power Electronics for Smart Grids Applications”. *Electronics* 2021, 10, 677. doi: 10.3390/electronics10060677.  
*Q2 en Engineering, Electrical & Electronic. Factor de impacto 2,397 (2020).*
3. Javier Ballestín Fuertes, Jesús Muñoz-Cruzado Alba y José Francisco Sanz Osorio. “4L D-STATCOM para redes débiles desbalanceadas de baja tensión”. VII Congreso Smart Grids, Madrid (España), 16 de Diciembre de 2020.
4. J. Ballestín-Fuertes, J. F. Sanz-Osorio, J. Muñoz-Cruzado-Alba, E. L. Puyal, J. Leiva and J. R. Rivero, “Four-Legs D-STATCOM for Current Balancing in Low-Voltage Distribution Grids”. *IEEE Access*, vol. 10, pp. 779-788, 2022, doi: 10.1109/ACCESS.2021.3138827.

*Q2 en Engineering, Electrical & Electronic. Factor de impacto 3,367 (2020).*

5. Muñoz-Cruzado-Alba, J.; Musca, R.; Ballestín-Fuertes, J.; Sanz-Osorio, J.F.; Rivas-Ascaso, D.M.; Jones, M.P.; Catania, A.; Goosen, E. "Power Grid Integration and Use-Case Study of Acid-Base Flow Battery Technology". *Sustainability* 2021, 13, 6089. doi: 10.3390/su13116089.

*Q2 en Environmental Sciences. Factor de impacto 3,251 (2020).*

6. A. M. Munoz, J. Ballestin-Fuertes, G. Fernandez, D. Marquina and R. Igea, "Four-leg EV Chargers for Grid Supporting," PCIM Europe 2022; International Exhibition and Conference for Power Electronics, Intelligent Motion, Renewable Energy and Energy Management, 2022, pp. 1-7, doi: 10.30420/565822235.

## Resumen

Con el objetivo de reducir los gases contaminantes un 55 % para el año 2030, la Comisión Europea ha establecido como objetivos prioritarios un aumento de la generación renovable hasta el 32 % de la generación energética total y un incremento de la eficiencia energética del 32,5 %. El cumplimiento de estos objetivos acarrea una serie de desafíos para el sistema eléctrico que deben ser considerados durante este proceso de transformación. El cierre de los grandes generadores síncronos, fuente de estabilidad para la red, y su reemplazo por fuentes renovables, de gran variabilidad y escasa o nula aportación inercial, están centrando gran parte del esfuerzo de la comunidad investigadora en el sector.

En este contexto, los convertidores de electrónica de potencia están despertando un gran interés debido a dos factores determinantes. En primer lugar, el gran número de convertidores que se espera sean instalados en los próximos años. Desde los grandes inversores fotovoltaicos a dispositivos más pequeños, pero mucho más numerosos, como equipos de climatización o cargadores de vehículo eléctrico. Por otro lado, la gran controlabilidad de estos sistemas incrementa la posibilidad de implementar técnicas que contribuyan a asegurar la estabilidad de la red eléctrica durante el proceso de cierre de las centrales térmicas.

La presente tesis doctoral contribuye al estado del arte del sector por medio de las aportaciones en el estudio de los convertidores de electrónica de potencia, los nuevos materiales que prometen ampliar las capacidades de estos dispositivos y la implementación de técnicas para la prestación de servicios auxiliares a la red. Debido al creciente protagonismo de la red distribución, así como el interés despertado por la creación de comunidades energéticas y las redes inteligentes, más conocidas como *Smart Grids*, este trabajo se centra en la aplicación de servicios orientados a la casuística de las redes de distribución en baja tensión.

En este documento se presta especial atención al problema de los desequilibrios, un problema frecuente en las redes de distribución. Este evento tiene lugar cuando la tensión o la corriente diverge entre las tres fases, ocasionando perjuicios en los usuarios de la red, así como posibles daños en distintos elementos del sistema, como los conductores y transformadores.

A continuación, se realiza el diseño y fabricación de un convertidor D-STATCOM de 30 kVA para la atenuación de desequilibrios en la red de baja tensión. El prototipo ha sido validado en un entorno real perteneciente a una línea de la red de distribución. De los resultados obtenidos durante el periodo de evaluación se han cuantificado los beneficios de la mitigación de desequilibrios, tales como la mejora de la calidad de red y la reducción de las pérdidas técnicas en la línea.

Posteriormente, se propone la aplicación de esta solución a diferentes convertidores comerciales tales como cargadores de vehículo eléctrico, inversores fotovoltaicos y sistemas de baterías. El trabajo concluye con el desarrollo de un cargador de vehículo eléctrico de 50 kW con la capacidad de proveer los servicios auxiliares propuestos en el estudio.

## Agradecimientos

Son muchas las personas sin las cuales hoy no estaría escribiendo estas palabras. Ante el miedo de que esta sección se alargue demasiado, o lo que sería peor, que me deje a alguien sin nombrar, he decidido no citar ninguno de sus nombres. Así, todas estas personas encontrarán un huequecito en estos párrafos.

En primer lugar, quiero agradecerles a mis directores su confianza y apoyo de principio a fin. Gracias a ellos comencé mi carrera profesional, empecé la tesis y he podido terminarla.

A mis compañeros de sistemas electrónicos. A los que me acogisteis desde mi llegada y, aunque con algunos no siga compartiendo el día a día, me habéis enseñado todo lo que sé. Por esas tardes de escapada tan necesarias para desconectar. Todos vosotros hacéis que sea muy fácil levantarse por las mañanas.

Alguien me dijo que los amigos de la carrera son para toda la vida, no le faltaba razón. Gracias por tantos momentos inolvidables.

A mi peña del pueblo, sé que no he podido compartir tanto tiempo con vosotros como nos hubiese gustado, gracias por estar ahí siempre.

Y lo más importante, a mi familia. Gracias por animarme siempre a perseguir lo que he querido. A mis padres, por apoyarme en todo momento, desde pequeñito, pero sobre todo por corregirme cuando no he hecho las cosas bien. A mis abuelos, por preguntarme incansablemente “¿pero eso cuándo termina?”, lo podéis ver, he terminado. Y, finalmente, haré una excepción. Aarón, sin la presión de verte por el retrovisor no habría llegado hasta aquí, ahora te toca a ti escribir tu propio camino.

*Gracias,*

Javier

Agosto de 2022



# Índice general

<b>1. Introducción</b>	<b>1</b>
1.1. Contexto y antecedentes . . . . .	2
1.1.1. Electrificación del sector energético . . . . .	2
1.1.2. Importancia de la red de distribución . . . . .	5
1.1.3. Antecedentes . . . . .	7
1.2. Motivación y objetivos . . . . .	9
1.3. Presentación de los estudios publicados . . . . .	11
1.4. Justificación de la unidad temática de los estudios . . . . .	14
<b>2. Estudio de las topologías de convertidores de electrónica de potencia más empleadas</b>	<b>17</b>
<b>3. Aplicación de materiales con gran ancho de banda para la mejora de sistemas de electrónica de potencia en Smart Grids</b>	<b>41</b>
<b>4. Diseño de sistemas trifásicos de electrónica de potencia de cuatro hilos para el equilibrado de corriente en líneas de baja tensión</b>	<b>69</b>
<b>5. Análisis de los efectos de la instalación de un sistema D-STATCOM de cuatro ramas para el equilibrado de corriente en una red urbana de baja tensión</b>	<b>77</b>
<b>6. Sistemas de almacenamiento en baterías de flujo y sus interfaces de potencia para la prestación de servicios auxiliares a la red</b>	<b>89</b>

## ÍNDICE GENERAL

---

<b>7. Implementación de servicios auxiliares en cargadores públicos para vehículo eléctrico y evaluación de su efecto en la red</b>	<b>117</b>
<b>8. Discusión</b>	<b>125</b>
8.1. Estudio 1 . . . . .	126
8.2. Estudio 2 . . . . .	132
8.3. Estudios 3 y 4 . . . . .	142
8.4. Estudio 5 . . . . .	154
8.5. Estudio 6 . . . . .	157
<b>9. Conclusiones</b>	<b>161</b>
9.1. Conclusiones del estudio . . . . .	162
9.2. Líneas de trabajo futuro . . . . .	165
<b>Bibliografía</b>	<b>167</b>
<b>A. Lista de publicaciones</b>	<b>173</b>
A.1. Publicaciones en revistas científicas . . . . .	175
A.2. Publicaciones en congresos . . . . .	176

# Acrónimos

- B2B** Back-to-Back. 6
- BESS** Battery Energy Storage Systems. 12, 13, 128
- BT** Baja Tensión. 131, 133–135, 139
- CE** Comisión Europea. 2, 4
- CUF** Current Umbalance Factor. 131
- D-STATCOM** Distribution static synchronous compensator. 10, 75, 130, 131, 135, 138
- DERs** Distributed Energy Resources. 4, 128, 134, 135, 139, 140
- EL** Electro-Luminiscencia. 9, 15
- EMC** Compatibilidad Electro-Magnética. 128
- EMI** Interferencia Electro-Magnética. 128
- FACTS** Flexible Alternating Current Transmission Systems. 128
- FV** Fotovoltaica. 4, 6, 126–128, 134
- NECPs** National Energy and Climate Plans. 4
- NPC** Neutral Point Clamped. 126, 127, 130
- SGAM** Smart-Grid Architecture Model. 133
- THD** Total Harmonic Distortion. 130
- TIC** Tecnologías de la Información y la Comunicación. 5
- TRL** Technology Readiness Level. 7
- UE** Unión Europea. 2, 5, 135
- VE** Vehículo Eléctrico. 4, 6, 11, 12, 127, 128, 134, 135, 139
- VUF** Voltage Umbalance Factor. 131, 139
- WBG** Wide-Band-Gap. 10, 39, 128, 129, 135, 138, 140



# Capítulo 1

## Introducción

**RESUMEN:** La amenaza del cambio climático ha empujado a gobiernos de todo el mundo a intensificar sus inversiones en energías renovables, con el objetivo de conseguir una reducción de los gases de efecto invernadero a nivel global. Sin embargo, las altas tasas de generación renovable planificadas no serán posibles si no se avanza en paralelo hacia una red más interconectada, flexible e inteligente. Con estos precedentes, se espera una explosión tanto en la cantidad como en la variedad de dispositivos de electrónica de potencia conectados a la red eléctrica. Generación fotovoltaica, climatización eléctrica, sistemas de almacenamiento, vehículos eléctricos... son sistemas cada vez más comunes en nuestro día a día que favorecen la electrificación del sector energético pero que, a su vez, complican la predictibilidad y operación de la red eléctrica. En este contexto, y alineados con el desafío de conseguir unos convertidores de electrónica de potencia que permitan una mayor penetración de energías renovables en la red, en esta sección se fijan los principales objetivos de la presente tesis doctoral, que serán desarrollados a lo largo de los siguientes capítulos.

## 1. INTRODUCCIÓN

---

### 1.1 Contexto y antecedentes

#### 1.1.1 Electrificación del sector energético

En la actualidad, el cambio climático representa una amenaza no solo para regiones específicas alrededor del mundo, sino para el ecosistema completo de la tierra. El calentamiento de la atmósfera no se detiene, y el clima de la tierra cambia año tras año [1]. Se estima que un millón de especies animales, de los más de 8 millones que habitan el planeta, se encuentran en peligro de extinción, mientras continúa la progresiva contaminación del aire y los océanos [2].

Es en este contexto en el que los gobiernos de todo el mundo han manifestado su compromiso de cambiar esta tendencia. El pasado mes de mayo se cumplieron treinta años de la suscripción de la Comisión Marco de las Naciones Unidas sobre el Cambio Climático (CMNUCC), dentro de lo que se conoció como la Cumbre de la Tierra de Río de Janeiro, celebrada en Nueva York y ratificada por 197 países [3]. Este acuerdo fue actualizado en los años posteriores con la adición al tratado en 1997 del Protocolo de Kioto, que cuenta con nuevas medidas energéticas y jurídicamente vinculantes [4]. Con la entrada del nuevo milenio, en 2006 el Protocolo fue enmendado en Nairobi y actualizado en México en 2010 con la adopción de un nuevo protocolo. Finalmente, en el año 2015 se estableció el Acuerdo de París, con el objetivo de limitar el calentamiento global por debajo de los 2 °C [5].

La energías renovables tienen un rol crucial en ayudar a la humanidad a cumplir con sus necesidades energéticas futuras. Hoy en día, más del 30 % de la generación eléctrica de la Unión Europea (UE) proviene de fuentes de energía renovable, frente al 12 % conseguido en el año 2000 [6]. En 2017, la UE fijó el objetivo de reducir durante la siguiente década sus emisiones de efecto invernadero al menos un 40 % por debajo de los niveles de 1990 [6, 7]. Sin embargo, este objetivo fue recientemente revisado y, como parte del *European Green Deal*, la Comisión Europea (CE) propuso en septiembre de 2020 un objetivo más ambicioso, reducir las emisiones para el año 2030 un 55 %, considerando emisiones y absorción, por debajo de las registradas en 1990. Además, este plan fija que este objetivo debe cumplirse mediante la consecución de una serie de objetivos: la reducción de las emisiones en un 40 % (por debajo de los límites de 1990), una penetración de generación eléctrica

renovable de, al menos, el 32 % y una mejora de la eficiencia energética del 32,5 % [8].

En el año 2022, debido a la gran incertidumbre energética, generada por la inestabilidad de suministro de gas ruso, la UE se ha visto obligada a fijarse unos objetivos todavía más ambiciosos. De este modo, en mayo de 2022, la CE publicaba el plan *REPowerEU* [9], que fija una serie de objetivos para reducir la dependencia de los combustibles rusos acelerando la ya iniciada transición hacia energías sostenibles. Para esto, el plan *REPowerEU* se basa en tres pilares: ahorro energético, generación renovable y diversificación de proveedores. Como muestra en la Figura 1.1, las nuevas medidas introducidas actualizan el objetivo de generación renovable fijado en el *European Green Deal* del 32 % al 45 % para el año 2030. Además, este plan especifica que los países miembros deben realizar un fuerte esfuerzo para conseguir un aumento del ahorro energético del 1,5 % anual desde el año 2024 hasta el 2030, aumentando el límite anterior fijado en el 0,8 % [10].

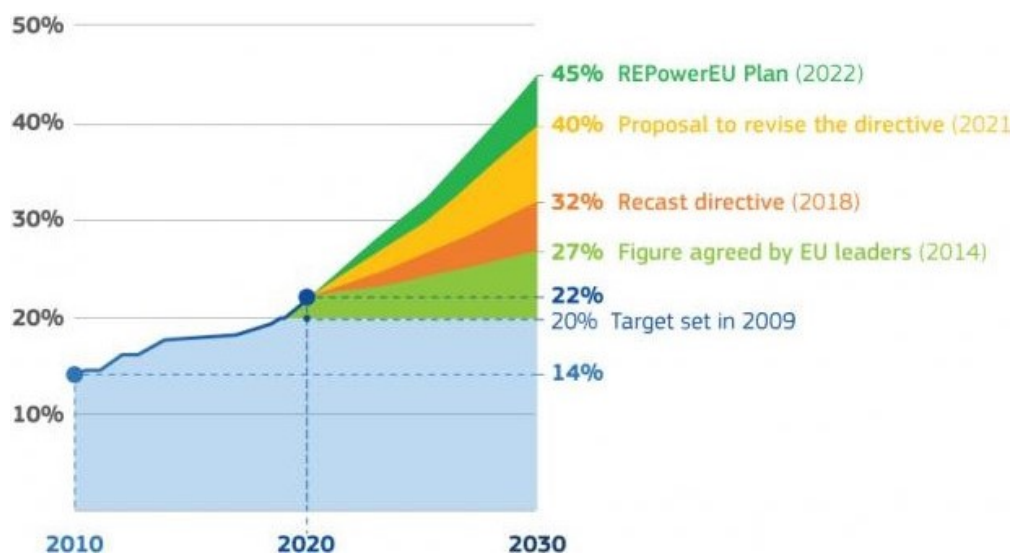


**Figura 1.1:** Evolución de los objetivos de generación renovable de la UE desde 2009 hasta 2022 [11].

De acuerdo con lo anterior, en el año 2030, la generación eléctrica renovable en España supondrá el 74 % del total, continuando esta trayectoria hacia un sector 100 % renovable en 2050 [12]. Como muestra la Figura 1.2, para alcanzar este

## 1. INTRODUCCIÓN

objetivo, en España se deberá incrementar la tasa actual de instalación de energías renovables si se desea alcanzar la meta fijada.

Porcentaje de energías renovables en generación eléctrica					
Método cálculo	Escenario	2015*	2020	2025	2030
Directiva 2018/2001	Escenario Tendencial	37%	41%	48%	53%
	Escenario Objetivo		42%	64%	86%
Porcentaje directo	Escenario Tendencial	38%	41%	47%	52%
	Escenario Objetivo		42%	60%	74%

\* Los datos del año 2015 son reales, el resto son proyecciones realizadas por el MITECO

**Figura 1.2:** Previsión del ratio de energías renovables en el sector de la generación de energía eléctrica en España [12].

Por otra parte, la eficiencia energética presenta una correlación inversa con las necesidades de energías renovables para alcanzar los objetivos fijados. Se estima que, para un incremento del 5 % en la eficiencia energética, las necesidades de instalación de energías renovables decrecerán aproximadamente un 7,5 % para conseguir el mismo objetivo de reducciones de gases de efecto invernadero [6]. De este modo, los esfuerzos para reducir las emisiones de efecto invernadero hechos de ambas formas, despliegue de renovables y mejora de la eficiencia energética, son igualmente efectivos. En consecuencia, la Figura 1.3 muestra que para el año 2030, en España, se ha fijado el objetivo de reducir el consumo energético un 19 % respecto a los niveles de 2020.

Consumo final de energía incluyendo usos no energéticos en el Escenario Objetivo (ktep)				
Años	2015	2020	2025	2030
Carbón	1.503	1.440	1.438	1.408
Productos petrolíferos	40.674	41.930	37.153	29.275
Gas natural	13.139	15.119	14.711	13.774
Electricidad	19.952	20.534	20.813	21.294
Energías renovables	5.292	6.943	7.195	7.426
Otros no renovables	2	309	309	385
No energéticos	4.350	5.105	5.400	5.639
Total	84.912	91.382	87.019	79.199

**Figura 1.3:** Objetivo de reducción del consumo energético en España para el año 2030 [12].

Además, la reducción de emisiones de efecto invernadero pueden conseguirse mediante la sustitución de las centrales térmicas que emplean combustibles fósiles

por energías renovables, o utilizando estas nuevas fuentes de energía para otras aplicaciones como la climatización y el transporte, conduciendo ambas formas a un crecimiento de la electrificación del sector energético. En las próximas décadas, se espera que el consumo eléctrico global crezca ligeramente más rápido que lo que muestran las tendencias actuales. Sin embargo, esta transformación será mucho más rápida en algunos países y regiones específicas. Esto incluye áreas con una rápida expansión de la energía solar residencial y Vehículo Eléctrico (VE), y en países que favorezcan el cierre de sus centrales térmicas [6].

La bajada de precios de algunas tecnologías al alcance de los consumidores, como la climatización eléctrica, la Fotovoltaica (FV) y el VE, hace que estas comiencen a ser competitivas sin la necesidad de ser subvencionadas. Esto ocasiona que los gobiernos pierdan la capacidad de controlar las tasas de despliegue de estas tecnologías.

### 1.1.2 Importancia de la red de distribución

La inminente electrificación a nivel global hace que el rol de las redes inteligentes, más conocidas como Smart Grids, tome una especial importancia. La siguiente generación de Smart Grids debe resolver un escenario con un gran número de dispositivos conectados, y con una mayor capacidad de coordinación entre los mismos. De hecho, esta tendencia ya ha comenzado.

En este contexto, las grandes plantas de generación basadas en fuentes de energía no renovables serán progresivamente sustituidas por grandes plantas renovables. Por otro lado, se prevé que el autoconsumo, la gestión de la demanda y el fomento de las comunidades energéticas locales contribuirán a promover un papel más proactivo de la ciudadanía en la descarbonización, incrementando la diversidad de actores participantes tanto en la generación de energía renovable como en el conjunto del sistema eléctrico. En consecuencia, se espera que emerjan las ciudades inteligentes con una gran penetración de recursos energéticos distribuidos, comúnmente conocidos como DERs por sus siglas en inglés, donde se incluirán pequeñas plantas FV, cargadores de VE, sistemas de almacenamiento, bombas de calor, etc.

## 1. INTRODUCCIÓN

---

Tal es el crecimiento de DERs instalados en las redes de distribución que, los principales planes estratégicos tanto a nivel nacional como internacional trazan objetivos específicos destinados a la mejora de estas redes que garanticen la seguridad de suministro eléctrico [13]. Como consecuencia del *European Green Deal*, el gobierno de cada uno de los países de la CE definió su Plan Nacional de la Energía y el Clima, denominados NECPs por sus siglas en inglés. Dentro de los objetivos establecidos por cada uno de estos países de acuerdo a sus condiciones particulares, los cinco miembros más importantes de la UE (Alemania, Francia, Italia, España y Países Bajos) [14], coinciden en la importancia de garantizar un suministro eléctrico seguro durante este proceso de transición, que supondrá el apagado de las grandes centrales nucleares, de gas y carbón, encargadas tradicionalmente de proveer estabilidad a la red.

Para ello, estos planes fijan objetivos similares en materia de seguridad eléctrica e interconectividad [12, 15, 16, 17, 18]. La variabilidad de estas fuentes de energía requerirá una mayor flexibilidad tanto a generadores como a consumidores de energía. Este aspecto evidencia la necesidad de convertir el modelo unidireccional usado en la actualidad, en el que la energía fluye largas distancias de una forma ineficiente desde las grandes centrales hacia los puntos de consumo; a un modelo energético integrado, en el que la energía fluye entre usuarios y productores reduciendo el desperdicio de recursos como se muestra en la Figura 1.4. Esta estrategia involucra nuevas tecnologías, procesos y modelos de negocio como las Tecnologías de la Información y la Comunicación (TIC) y la digitalización, las Smart Grids y los mercados de flexibilidad.

Uno de los mejores ejemplos del potencial de un sistema energético integrado es la electrificación del transporte. En la actualidad, sabemos que los vehículos eléctricos conectan el sector del transporte y de la energía. Sin embargo, los puntos de recarga, habitualmente ubicados en las residencias de los usuarios, ofrecen un interfaz muy limitado para el intercambio energético entre ambos sectores.

Por el contrario, los nuevos dispositivos en las Smart Grids deberán cumplir una serie de requisitos antes de ser aceptados por los consumidores y, así, ayudar a su penetración en el mercado: estos deberán ser económicos, conseguir altas eficiencias y ser silenciosos, fiables y compactos. En la actualidad, los convertidores de

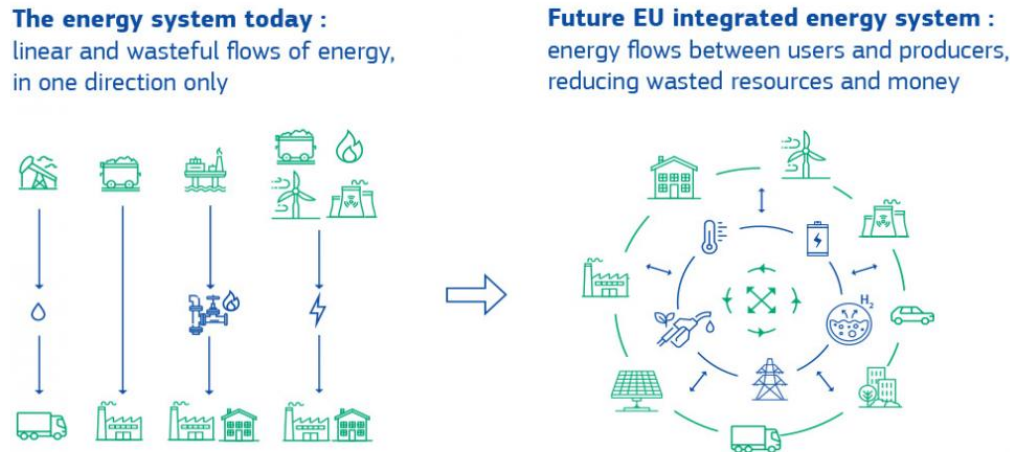


**Figura 1.4:** Evolución del modelo energético actual a un sistema integrado [19].

electrónica de potencia no cumplen con varias de las condiciones citadas anteriormente, por lo que será necesaria una evolución de estos dispositivos que permita un despliegue masivo entre los consumidores.

### 1.1.3 Antecedentes

La presente tesis se enmarca en la línea de las investigaciones llevadas a cabo, en el ámbito del desarrollo de sistemas para el soporte a la red eléctrica, por el grupo de Sistemas Electrónicos de la Fundación CIRCE [20]. En esta línea se han llevado a cabo desarrollos de electrónica de potencia para diferentes aplicaciones (generación eólica y FV, baterías, VE...), con una orientación hacia la creación de Smart Grids que maximice el aprovechamiento de las energías renovables asegurando la estabilidad de la red. A continuación, la Tabla 1.1 muestra algunos de los proyectos que sirvieron de precursores para el desarrollo de esta tesis:

## 1. INTRODUCCIÓN

---

**Tabla 1.1:** Descripción de los proyectos precedentes relacionados con la tesis.

<b>FLEXICIENCY</b>	Este proyecto demostró el despliegue de nuevos servicios de control y flexibilidad en mercados minoristas.	[21, 22]
<b>EV-OPTIMANAGER</b>	El objetivo principal del proyecto consistió en el desarrollo de productos en torno a la carga de vehículo eléctrico que facilitarán la previsión, gestión y acumulación de energía eléctrica.	[23, 24]
<b>REDACTIVA</b>	En este proyecto se desarrolló un convertidor B2B de cuatro ramas con una topología NPC tipo-I para la realización de pruebas anti-isla sobre inversores.	[25, 26]

## 1.2 Motivación y objetivos

El desafío principal de esta tesis nace de la necesidad de continuar con la inclusión de energías renovables en el sistema eléctrico, asegurando la estabilidad del mismo. En concreto, se aborda este reto desde el punto de vista de los convertidores de electrónica de potencia conectados a la red de baja tensión, y cómo estos pueden contribuir a la mejora de la seguridad y la calidad de suministro.

Derivado de los retos generales descritos anteriormente, los objetivos específicos abordados durante la investigación se resumen en la tabla 1.2. En ella, se numera cada uno de los objetivos con el fin de relacionar estos objetivos con los estudios publicados durante la investigación en apartados posteriores.

**Tabla 1.2:** Objetivos específicos de la tesis.

---

<b>Objetivo 1</b>	Estudio de las características actuales de los convertidores de electrónica de potencia, las futuras necesidades que deberán satisfacer en las Smart Grids en función de los diferentes casos de uso.
<b>Objetivo 2</b>	Estudio de los materiales semiconductores, tanto los empleados actualmente y los que se encuentran en fases de desarrollo, para la fabricación de equipos de electrónica de potencia; determinando los más apropiados para aplicaciones conectadas a la red eléctrica.
<b>Objetivo 3</b>	Planteamiento y diseño de mejoras hardware que permitan la adición de nuevos servicios auxiliares de red a los convertidores de electrónica de potencia, así como los algoritmos de control necesarios para llevarlos a cabo.
<b>Objetivo 4</b>	Evaluación del desempeño de un prototipo con las funcionalidades desarrolladas en el objetivo anterior en un entorno de funcionamiento real, equivalente a un nivel de madurez tecnológica o TRL de 7 según [27].
<b>Objetivo 5</b>	Integración de las técnicas de soporte a la red desarrolladas en dispositivos en los cuales esta no es su función principal.

---

Estos objetivos se encuentran alineados con los retos definidos en el *European Green Deal* [8] y la *Estrategia Europea para la Integración del Sistema Energético*

## 1. INTRODUCCIÓN

---

[28] que define el objetivo de perseguir “un sistema «multidireccional», en el que los consumidores desempeñen un papel activo en el suministro de energía”. De forma análoga, el *Plan Nacional Integrado de Energía y Clima 2021-2030 (PNIEC)* [12] destaca los retos tecnológicos que en materia de seguridad energética presentan los cambios en el mix energético y el necesario “aumento de la flexibilidad del sistema energético nacional”.

### 1.3 Presentación de los estudios publicados

La presente tesis doctoral está compuesta por un compendio de seis estudios publicados en revistas y congresos internacionales. Estos estudios se relacionan con los objetivos detallados en el apartado anterior. A continuación se presenta una breve descripción de cada uno de los estudios publicados, destacando la aportación de cada uno de ellos al cumplimiento de los objetivos de la tesis.

- **Estudio 1:** Ballestín-Fuertes, J.; Muñoz-Cruzado-Alba, J.; Sanz-Osorio, J.F.; Hernández-Callejo, L.; Alonso-Gómez, V.; Morales-Aragones, J.I.; Gallardo-Saavedra, S.; Martínez-Sacristan, O.; Moretón-Fernández, Á. “Novel Utility-Scale Photovoltaic Plant Electroluminescence Maintenance Technique by Means of Bidirectional Power Inverter Controller”. *Appl. Sci.* 2020, 10, 3084. doi: 10.3390/app10093084.

La primera parte de este artículo se alinea con el **Objetivo 1**. Ésta se centra en el estudio de las topologías más comunes de inversores de electrónica de potencia, particularizando en aplicaciones fotovoltaicas, así como el análisis de sus técnicas de control. A continuación, este estudio es utilizado para el diseño de un inversor fotovoltaico bidireccional, capaz de tomar energía de la red para inyectarla en los paneles con el objetivo de realizar la inspección mediante la técnica de la Electro-Luminiscencia (EL). De esta forma se permite la aplicación de esta técnica sin la necesidad de desmontar los paneles para evaluarlos en unas instalaciones acondicionadas para ello. Finalmente, presenta los resultados obtenidos en una planta piloto compuesta por 11 paneles fotovoltaicos.

- **Estudio 2:** Ballestín-Fuertes, J.; Muñoz-Cruzado-Alba, J.; Sanz-Osorio, J.F.; Laporta-Puyal, E. “Role of Wide Bandgap Materials in Power Electronics for Smart Grids Applications”. *Electronics* 2021, 10, 677. doi: 10.3390/electronics10060677.

Este estudio completa, en su primera mitad, el **Objetivo 1** mediante el análisis de las funcionalidades exigibles en el futuro por los códigos de red a los convertidores de electrónica de potencia para proveer servicios auxiliares a la red. A continuación, se estudian las características técnicas que deberán

## 1. INTRODUCCIÓN

---

satisfacer estos dispositivos en el futuro para llevar a cabo las funcionalidades analizadas en aplicaciones relacionadas con Smart Grids. Dadas las limitaciones del silicio como material semiconductor para satisfacer estas necesidades, se realiza un estudio de los límites teóricos de los principales materiales semiconductores llamados a reemplazar al silicio, conocidos como materiales de gran ancho de banda o WBG, en aplicaciones de potencia; así como un análisis del estado de madurez de estos materiales y su proximidad a un mercado a gran escala. Finalmente, se completa el **Objetivo 2** mediante la comparación de los materiales analizados, concluyendo los más apropiados para este tipo de aplicaciones de potencia.

- **Estudio 3:** Ballestín Fuertes, Jesús Muñoz-Cruzado Alba y José Francisco Sanz Osorio. “4L D-STATCOM para redes débiles desbalanceadas de baja tensión”. VII Congreso Smart Grids, Madrid (España), 16 de Diciembre de 2020.

Este estudio satisface el **Objetivo 3**, para lo que se abordan las posibilidades que ofrece la modificación de los ampliamente utilizados convertidores trifásicos de tres hilos por sistemas equivalentes de cuatro hilos. Esta nueva configuración posibilita que cada una de las fases trabaje de forma independiente a las demás, debido a la presencia de un conductor conectado al neutro de la red que permite el retorno de la corriente desequilibrada. Esta característica permite realizar el filtrado de las corrientes desequilibradas de la red, mediante la eliminación de la corriente de secuencia inversa y homopolar, con las consiguientes mejoras obtenidas en la eficiencia y la calidad de suministro de la red.

- **Estudio 4:** J. Ballestín-Fuertes, J. F. Sanz-Osorio, J. Muñoz-Cruzado-Alba, E. L. Puyal, J. Leiva and J. R. Rivero, “Four-Legs D-STATCOM for Current Balancing in Low-Voltage Distribution Grids”. IEEE Access, vol. 10, pp. 779-788, 2022, doi: 10.1109/ACCESS.2021.3138827.

Este artículo parte de los análisis realizados en el **Estudio 4** para desarrollar un compensador estático de distribución, más conocido como D-STATCOM por sus siglas en inglés. En este artículo se detalla el diseño del hardware y de la estrategia de control de un prototipo de 30 kW. Finalmente, se analizan los resultados de su operación en una red de distribución en la ciudad de

### 1.3 Presentación de los estudios publicados

---

Málaga durante un periodo de un mes para completar los retos propuestos en el **Objetivo 4**.

- **Estudio 5:** Muñoz-Cruzado-Alba, J.; Musca, R.; Ballestín-Fuertes, J.; Sanz-Osorio, J.F.; Rivas-Ascaso, D.M.; Jones, M.P.; Catania, A.; Goosen, E. “Power Grid Integration and Use-Case Study of Acid-Base Flow Battery Technology”. *Sustainability* 2021, 13, 6089. doi: 10.3390/su13116089.

En este estudio se aborda el **Objetivo 5** mediante el análisis de los casos de uso de los sistemas de baterías en diferentes tipos de redes y a diferentes escalas. Posteriormente, se analiza la integración de un sistema de baterías de flujo para el soporte de una pequeña red aislada en la isla de Pantelleria.

- **Estudio 6:** A. M. Munoz, J. Ballestin-Fuertes, G. Fernandez, D. Marquina and R. Igea, ”Four-leg EV Chargers for Grid Supporting,”PCIM Europe 2022; International Exhibition and Conference for Power Electronics, Intelligent Motion, Renewable Energy and Energy Management, 2022, pp. 1-7, doi: 10.30420/565822235.

En este artículo, alineado con el **Objetivo 5**, se expone el desarrollo de un cargador para VE de 50 kW desarrollado con tecnología de semiconductores de carburo de silicio. Este equipo es capaz de proporcionar servicios auxiliares a la red gracias a su topología trifásica con cuatro ramas. Para concluir, este estudio analiza a través de simulación los beneficios obtenidos de los servicios auxiliares prestados por el cargador en varias redes: la red de baja tensión de IEEE para redes europeas de baja tensión [29] y en cuatro redes reales pertenecientes al sur, centro y norte de Europa.

### 1.4 Justificación de la unidad temática de los estudios

La Figura 1.5 recoge la relación entre los estudios que conforman el compendio de esta tesis. En primer lugar, los **Estudios 1 y 2** completan el estado de la técnica. En el **Estudio 1** se analizan las topologías trifásicas más importantes de inversores fotovoltaicos que son representativas a su vez de los interfaces de potencia empleados en todo tipo de aplicaciones. Por su parte, el **Estudio 2** analiza las potenciales necesidades exigibles por los códigos de red a los equipos conectados a la red de distribución. De estas necesidades se extraen las características técnicas que deberán tener los semiconductores que componen estos equipos, tales como una mayor frecuencia de conmutación o unas menores pérdidas. Posteriormente se realiza un estado del arte de las principales tecnologías llamadas a reemplazar al silicio como material semiconductor, tanto en el corto como en el medio plazo. Finalmente, se realiza una comparativa entre todos estos materiales para concluir cual de ellos será el más apropiado para este tipo de aplicaciones.

El **Estudio 3** parte de las conclusiones obtenidas en el **Estudio 2**, se seleccionan una serie de funcionalidades que pueden introducirse en distintos tipos de recursos energéticos distribuidos y propone unas modificaciones sobre las topologías y estrategias de control analizadas en el **Estudio 1** que permiten su cumplimiento.

Posteriormente, el **Estudio 4** parte de la propuesta de diseño llevada a cabo en el **Estudio 3** para desarrollar el prototipo de un convertidor de 30 kW que cumpla con las funcionalidades seleccionadas. Este prototipo ha sido instalado en un entorno real y se ha validado su funcionamiento durante un periodo de tiempo relevante para demostrar su influencia sobre la red de distribución.

En paralelo, el **Estudio 5** analiza los principales casos de uso de los interfaces de sistemas de almacenamiento energético en baterías (BESS) y las funcionalidades que estos pueden proporcionar a la red.

Finalmente, el **Estudio 6** propone la implementación de servicios auxiliares adicionales en todo tipo de convertidores electrónicos conectados a la red, en particular en cargadores de VE. La tendencia actual en este mercado es que los VE permitan una carga bidireccional, es decir, que estos no solo carguen sus baterías utilizando la energía de la red sino que, en momentos puntuales en los que se requiera, estos puedan suministrar energía a la red para favorecer su estabilidad. Este

#### **1.4 Justificación de la unidad temática de los estudios**

---

comportamiento permite tratar a los puntos de recarga como BESS extrapolando las conclusiones del **Estudio 5**. Por su parte, se ha empleado una topología análoga a la validada en el **Estudio 4**, que permita replicar sus resultados sin la necesidad de instalar equipos especialmente diseñados para este cometido. En último lugar, tomando las conclusiones del **Estudio 2**, el cargador desarrollado se ha diseñado empleando dispositivos semiconductores basados en carburo de silicio.

# 1. INTRODUCCIÓN

---

**01**

**Estado de la técnica**

Novel Utility-Scale Photovoltaic Plant Electroluminescence Maintenance Technique by Means of Bidirectional Power Inverter Controller. 2020. Appl. Sci.

**02**

**Estado de la técnica**

Role of Wide Bandgap Materials in Power Electronics for Smart Grids Applications. 2021. Electronics.

**03**

**Conceptualización y diseño**

4L D-STATCOM para redes débiles desbalanceadas de baja tensión. 2020. VII Congreso Smart Grids.

**04**

**Validación en campo**

Four-Legs D-STATCOM for Current Balancing in Low-Voltage Distribution Grids. 2021. IEEE Access

**05**

**Estudio de los casos de uso**

Power Grid Integration and Use-Case Study of Acid-Base Flow Battery Technology. 2021. Sustainability.

**06**

**Despliegue en dispositivos comerciales**

Four-leg EV Charger for Grid Supporting. 2022. PCIM Europe 2022

**Figura 1.5:** Relación entre los estudios que componen la tesis.

# Capítulo 2

## **Estudio de las topologías de convertidores de electrónica de potencia más empleadas**

### **RESUMEN:**

La inspección de los paneles fotovoltaicos mediante la técnica de EL es una de las más precisas en la detección de fallos en las células de las que se dispone hoy en día. En la actualidad, para su realización es necesaria la desconexión y transporte de los paneles para su análisis en instalaciones aptas para esta finalidad. En este artículo se propone la realización de estos ensayos in-situ mediante la inversión del flujo de corriente en el convertidor de la planta fotovoltaica. Para ello, en este estudio se analizan las principales topologías de convertidores trifásicos y las variaciones de estas más empleadas en la industria, destacando las principales ventajas e inconvenientes de cada una de ellas.

Article

# Novel Utility-Scale Photovoltaic Plant Electroluminescence Maintenance Technique by Means of Bidirectional Power Inverter Controller

Javier Ballestín-Fuertes <sup>1</sup>, Jesús Muñoz-Cruzado-Alba <sup>1</sup>, José F. Sanz-Osorio <sup>2</sup>,  
Luis Hernández-Callejo <sup>3,\*</sup>, Victor Alonso-Gómez <sup>3</sup>, José Ignacio Morales-Aragones <sup>3</sup>,  
Sara Gallardo-Saavedra <sup>3</sup>, Oscar Martínez-Sacristan <sup>4</sup> and Ángel Moretón-Fernández <sup>4</sup>

<sup>1</sup> Fundación CIRCE, Parque Empresarial Dinamiza, Avenida Ranillas Edificio 3D, 1ª Planta, 50018 Zaragoza, Spain; jballesin@fcirce.es (J.B.-F.); jmunoz@fcirce.es (J.M.-C.-A.)

<sup>2</sup> Instituto Universitario de Investigación CIRCE (Universidad de Zaragoza—Fundación CIRCE), Edificio CIRCE, Campus Río Ebro, C / Mariano Esquillor Gómez, 15, 50018 Zaragoza, Spain; jfsanz@unizar.es

<sup>3</sup> Campus Universitario Duques de Soria, Universidad de Valladolid, 42004 Soria, Spain; victor.alonso.gomez@uva.es (V.A.-G.); ziguratt@coit.es (J.I.M.-A.); s.gallardosaavedra@gmail.com (S.G.-S.)

<sup>4</sup> Campus Miguel Delibes, Universidad de Valladolid, 47011 Valladolid, Spain; oscar@fmc.uva.es (O.M.-S.); angel.moreton@outlook.es (Á.M.-F.)

\* Correspondence: luis.hernandez.callejo@uva.es; Tel.: +34-975129418

Received: 20 March 2020; Accepted: 24 April 2020; Published: 28 April 2020



**Featured Application:** The paper proposes a new utility-scale photovoltaic plant maintenance method to evaluate the degradation of photovoltaic panels. The method takes advantage of the installed power inverters and combiner boxes of the solar photovoltaic plant to use them as a way of energising the panels as light emitters, in order to look for defects in them without the need of an expensive uninstalling and reinstalling process.

**Abstract:** Nowadays, photovoltaic (PV) silicon plants dominate the growth in renewable energies generation. Utility-scale photovoltaic plants (USPVPs) have increased exponentially in size and power in the last decade and, therefore, it is crucial to develop optimum maintenance techniques. One of the most promising maintenance techniques is the study of electroluminescence (EL) images as a complement of infrared thermography (IRT) analysis. However, its high cost has prevented its use regularly up to date. This paper proposes a maintenance methodology to perform on-site EL inspections as efficiently as possible. First, current USPVP characteristics and the requirements to apply EL on them are studied. Next, an increase over the automation level by means of adding automatic elements in the current PV plant design is studied. The new elements and their configuration are explained, and a control strategy for applying this technique on large photovoltaic plants is developed. With the aim of getting on-site EL images on a real plant, a PV inverter has been developed to validate the proposed methodology on a small-scale solar plant. Both the electrical parameters measured during the tests and the images taken have been analysed. Finally, the implementation cost of the solution has been calculated and optimised. The results conclude the technical viability to perform on-site EL inspections on PV plants without the need to measure and analyse the panel defects out of the PV installation.

**Keywords:** electroluminescence; photovoltaic panels; power inverters; utility-scale photovoltaic plants; solar plants maintenance; photovoltaic panels degradation

## 1. Introduction

Energy use worldwide is changing quickly due to the need to mitigate climate change. Renewable energies (RE) have a crucial role in helping the world to meet its energy needs, with the possibility to supply four-fifths of the world's electricity by 2050, massively cutting down carbon emissions. Nowadays, new legislation is promoting the installation of RE power plants to increase their penetration level in the power generation system [1,2]. However, photovoltaic (PV) and wind power have to exploit their full potential, decreasing the installation and maintenance costs of power plants.

Currently, the proportion of electricity generation of the European Union (EU) from renewable energy sources has increased from only 12% in 2000 to more than 30% in 2020 [3]. This represents an average growth of 1.7% per year. Moreover, RE power installation worldwide has changed from a 20% of the shared electricity net in 2010, to a value over 30% in 2020, and the forecast is to reach the 50% by year 2050 [4]. In particular, wind and solar plants dominate the growth in renewable energy generation.

Nowadays, the reduction of needed investment cost for new utility-scale photovoltaic plants (USPVPs), up to 6 times in respect to one decade ago [5], has placed the PV technology in a competitive scenario regarding other generation sources, both conventional and renewable. This situation is accelerating the rate of PV power penetration into the international power system, turning solar power generation into an important actor in the transformation of the future electric market [6,7]. In addition, in order to substitute conventional power plants, the size and rated power of USPVPs have increased exponentially in the last decade, recently reaching rated powers up to 2.2 GW [8].

The area needed to place USPVPs grows linearly related to the rated power capacity [9], and therefore it is crucial to develop efficient and optimum maintenance techniques for USPVPs, which can cover huge extensions of terrain in a short time at a competitive cost.

One of the most promising maintenance techniques in the current state-of-the-art is the evaluation method of PV panels damage through the study of images. This method covers up two different technologies: the study of infrared thermography (IRT) images and the study of electroluminescence (EL) images. On the one hand, the study of IRT images analyses hot and cold spots on the PV cells while they are generating power during the daylight [10]. On the other hand, the study of EL images analyses the PV panels while they are in the direct polarisation working zone, detecting the damaged modules from the emitted spectrum in the non-visible zone [11].

The paper focus on the latter category, which will be explained in detail in the following section. The main objective of this paper is to present a new method to reduce the maintenance costs of EL testing, using the hardware provided by the PV solar inverters and a sequencing of the PV strings to polarise them accordingly. The paper analyses hardware and software used in current and future USPVPs, and points out the required changes in order to apply the developed technique conveniently. Finally, the paper provides a discussion about the expected outcomes and costs of the new method.

This paper is organised as follows. First, Section 2 describes the principles of EL technology applied to PV panels and the current maintenance procedure, as well as a comparison with the most commonly used image processing analysis: the IRT technology. After that, Section 3 describes power inverters used currently in USPVPs and how to adapt them to run EL tests. Section 4 introduces the control technique added to the power inverter to induce a direct polarisation of the PV panels, as well as how to synchronise the whole plant in order to perform the EL maintenance action in the proper way. Following this, Sections 5 and 6 show the built prototype, the demo-plant and the results obtained from the experiments. Section 7 introduces a cost analysis of the solution in order to evaluate its feasibility. Finally, Section 8 summaries the most important conclusions of the research.

## 2. Electroluminescence Technique

### 2.1. EL Principles Applied to PV Panels

The working principle of a PV solar cell is based on a photoreceiver diode which captures the photons doing a photoelectric conversion. According to this fact, the classic electric model of a PV panel is shown in Figure 1a [12,13].

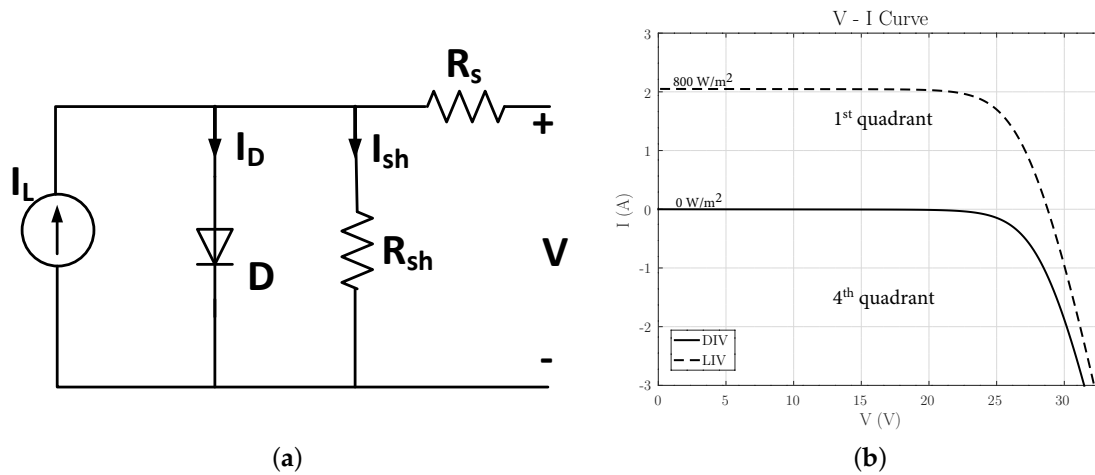


**Figure 1.** Classic electric model of photovoltaic (PV) panel (a) and light I–V (LIV) and dark I–V (DIV) curves of a standard 36 PV cell module according to the work in [14] (b).

Therefore, the current provided by the PV cell is defined by expression (1),

$$I = I_L - I_D - I_{sh} \tag{1}$$

where  $I_L$  is the current generated by the captured light,  $I_{sh}$  is the dissipated current by the shunt PV panel resistor and  $I_D$  is the lost current due to the recombination. In particular,  $I_D$  is defined by the following expression,

$$I_D = I_0 \left( e^{\frac{V+IR_s}{nV_T}} - 1 \right) \tag{2}$$

where  $I_0$  is the inverse saturation current of the diode,  $V_T$  is the thermal voltage,  $n$  is the diode ideality factor and  $R_s$  is the series resistance.

Consequently, the characteristic I–V curve of a PV panel is described by the dashed curve in Figure 1b [14], known as the LIV curve. It has a behaviour determined by the electric characteristics of the diode, and the vertical position is determined by the irradiation value. Besides, the dashed curve at Figure 1b has been calculated for an irradiance value of  $800 \text{ W/m}^2$ . On the other hand, when the irradiation is equal to zero it reaches the solid curve, known as the DIV curve. Due to the physical characteristics of PV cells, they start to work as photo-emitters (4th quadrant), instead of phosphorescent (1st quadrant), when a current is supplied to them, in the same way as the light-emitting diode (LED) technology [14].

However, the light emitted in the 4th quadrant is relatively low, due to the fact that in the PV silicon panels this process is done through the carriers recombination in a forbidden indirect band of the semiconductor, by means of the recombination by defects or Auger [15]. Nevertheless, there is a small radiative recombination, which is enough to be detected by an external sensor. This phenomenon means that the EL technique could be useful as a non-destructive and fast evaluation method to get the health state of PV cells.

## 2.2. EL Analysis Procedure

The health state of a PV silicon panel could be determined using the EL technique by means of supplying current to the panel. Typically, the hardware needed to perform tests such as is a power supply able to provide the short-circuit current of the panel under test,  $I_{sc}$ , and at a voltage level higher than the panel open circuit value at the rated irradiance,  $V_{oc}$ .

Consequently, current injection produces near-infrared (IR) light emission in the solar panel. In an industrial solar plant scenario, this operation is performed by qualified technical staff, taking the PV panel photograph in the plant-site, and conducting the post-image process and analysis of results afterwards. The image is taken with an appropriate digital camera, and focused in the wavelength of interest, paying special attention to avoid parasitic light and camera vibrations [16].

The technical specification International Electrotechnical Commission (IEC) 60904 defines methods to capture images of PV panels by means of EL technique. It also defines postprocessing procedures to get quantitative descriptors and provide a guideline to understand the results. The standard is oriented to the measurement in a controlled scenario, forcing the current flow thanks to a voltage power supply in the panel under test terminals. In addition, captures with low signal-to-noise ratio (SNR) are provided by thermoelectric cooling of charge-coupled device (CCD) or complementary metal-oxide-semiconductor (CMOS) cameras. Relevant parameters such as the number of pixels, noise, wide length, and dynamic range are taken into account in the selection of the right detectors. Moreover, the images should have enough quality, and therefore they should be obtained in dark scenarios, by means of walls, curtains or otherwise, in order to avoid the parasitic light [16].

The EL technique is very useful in the manufacturing step of PV panels, where the controlled described test could be run easily. However, applying EL evaluation over existing USPVPs implies one of these alternatives: (i) to dismount, test and remount every single panel individually; (ii) to perform the EL images on the PV panels without dismounting them by means of an external power supply. In the first case, cell breaking due to transport is a very common issue. In the second case, it is necessary to carry an external power source to the plant site. Additionally, in both cases, the processes are invasive, so there is a potential danger of damaging facilities and workers.

If the PV solar inverter was adapted conveniently to work in a bidirectional way, it would be possible to force the panels to work in the 4th quadrant and apply EL recognition during low irradiation time slots (at night, sunrise and sunset) directly on the installed panels.

## 2.3. IRT Versus EL Inspections

IRT is the most extended technique in PV image processing to detect failures in panels. It is a non-destructive measurement technique, which provides fast, real-time and two-dimensional distributions of characteristic features from PV modules [17–19]. In addition, IRT can be performed in illuminated or dark conditions [16,20–22].

In the former instance, the illuminated IRT or IRT under common operating conditions of the PV system are similar to luminescence, where the current flowing through cells increases PV module temperature. In this case, it is used as a contactless method for diagnosing of common thermal and electrical defects in PV modules [23–25]. Typical anomalies detected by illuminated IRT arise whenever one component becomes warmer than the surrounding ones or the expected rated values, for instance: modules; bypass diodes; single cells without following any pattern, in the lower parts or closer to the frame; a part of a cell respect to the rest; or pointed heating or a bypass diode string part respect to the others when they are equally shaded [26].

However, results reveal that IRT could not detect all possible failures in PV modules. Recently research about EL shows that it can give complementary information to IRT techniques, adding value to individual findings [27,28]. Performed IRT measurements proved that not all identified defects lead to an increase in temperature [28]. It has been experimentally observed how using EL is especially interesting to detect cell cracks in PV modules, appearing as dark lines on the solar cell in the EL image, as well as interrupted contacts, or a number of process failures (e.g., shunts or defects in

the anti-reflection layer) [28]. Irregular areas indicate the presence of cracks in the silicon wafers while regular rectangular dark areas can be due to broken front grid fingers. In this case, EL locating can complement outdoor IRT technique by detecting defects that does not produce a temperature increment [29].

In the latter instance, IRT in dark conditions shares some similarities with EL technique, being the module subjected to a forward voltage. In the EL test, modules operate under forwarding bias like a LED, and therefore have to be power supplied. The excitation current can be less than or equal to  $I_{sc}$  [21]. It has been observed from visual inspection of EL and IR images in the fourth quadrant that most of the defects detected in the dark IRT images under the forwarding bias condition can also be identified in the EL images, whereas not all the defects detected in the EL images can be detected with dark-IRT, as some broken cells or soldering defects over one or more buses [29]. Therefore, the high resolution of the EL images enables resolving most defects more precisely than the dark IRT images.

### 3. USPVPs Power Inverters

#### 3.1. USPVPs Retrofit Requirements to Apply EL on-Site

Several automatic tools must be introduced in a USPVP in order to perform the EL image processing technique diagnosis successfully, leading the PV panels to the 4th quadrant working area sequentially, and in the right order.

Firstly, it is mandatory to have a way of getting the EL images with the required requisites, being the optical device installed in a drone, vehicle, tripod, etc. Afterwards, the images taken by the camera will be sent to a central controller site, where they will be saved, post-processed, and a final diagnosis will be obtained.

On the other hand, the power electronics inverter will have to fulfil a list of requirements to allow the direct polarisation of the PV panel strings and lead them to the 4th quadrant for the EL evaluation. Following, the characteristics that must fulfil the power converters are pointed out.

- **Working-mode as a current source:** the inverter must be able to work as a power supply with the capability of producing the PV panel string  $I_{sc}$  at a voltage near the PV panel open-circuit value,  $V_{oc}$ . Therefore, the inverter must have a completely bidirectional feature.
- **Starting-up without irradiation:** in order to avoid parasitic light irradiance and PV plant power losses, all tests must be carried out during sunrise, sunset or at night. Therefore, the DC-Link precharge of the inverter must be done from the alternating current (AC) grid side, instead of doing it in the usual way, from the PV panels. Consequently, the PV inverter must include a precharge mechanism from its grid side.
- **PV string sequencing:** especially in the cases of large solar inverters, the number of PV string arrays in parallel can be considerable, covering a large ground area. Thus, it is desirable to apply direct polarisation to a single fraction of all panels connected to the inverter, limiting the action area, and therefore minimising the power needed to carry out the EL inspection. Therefore, it is recommended to replace isolators with several lower power automatic switches connected to one or a few strings.

#### 3.2. USPVPs Power Inverters Topologies

Nowadays, there is a wide variety of power electronics converter topologies oriented to solar plant applications. The state-of-the-art is extensive and there is not an homogeneous answer about which is the best solution [30–37], providing very different solutions according to the needs of each specific application.

There are many possible classifications of solar inverters according to different factors: galvanic isolation or not; single-stage or multi-stage; central, multi-string, string or module inverter; bi-level or multi-level converter; voltage source inverter (VSI), current source inverter (CSI) or impedance source; grid-connected or isolated; hard or soft switching, etc. [33].

In particular, this study focuses on the application of automated EL technique to large PV plants. Therefore, we will consider grid-connected high-power inverters. In these applications, VSI non-isolated inverters are commonly used. Besides, hard-switching is usually chosen because there are no space or weight limitations in the case of solar micro-inverters for domestic applications.

According to the conversion stages inside the PV inverter, single-stage and multi-stage topologies can be found. Multi-stage topologies are suitable for direct current (DC) voltage adjustment, providing galvanic isolation through high-frequency (HF) intermediate stages if needed. However, specially in high-power plants, single-stage inverters are widely used due to the fact that strings are grouped reaching the highest possible voltage, up to 1500 V, and achieving a maximum power between 1 MW and 3.5 MW [38–43]. The objective is to reduce the DC current at the rated power and, consequently, reduce the power losses in the DC installation.

Finally, as the case of study are large PV installations, only three-phase topologies will be considered. Four-leg configurations or several single-phase devices in parallel are also possible, but they are not usually used in industrial environment, and thus they will not be studied in this paper. Within this context, the most representative topologies are described below (although the state-of-the-art is not limited to these topologies).

Firstly, nowadays the bi-level three-phase inverter is the simplest and most used topology in the market. This topology, shown in Figure 2a, consists of only six full-controlled semiconductor devices (usually metal-oxide-semiconductor field-effect transistor (MOSFETs) or (insulate gate bipolar transistors (IGBTs))).

In the following, several multilevel topologies for PV inverters are presented [44,45]. These topologies can be extended in the case of 3, 5 or N levels, but, for the sake of simplicity, only the three-level cases are presented. The objective of increasing the number of levels is to add step levels in the voltage waveform, reducing the low-pass filter size and, therefore, improving the inverter response, as well as reducing its cost and size.

One of the most used multilevel topology is the neutral point clamped (NPC) topology type I. Figure 2b shows an example of 3-level NPC topology; this configuration has a floating medium point in the DC-link that allows it to modulate 0 V in addition to  $+V_{DC}$  and  $-V_{DC}$ . There are some variants on this configuration; Figure 2e shows one representative modification [46]. This configuration has some advantages over the previous one as lower harmonics introduction, smaller passive components, higher efficiency, and solves the leakage current problem inherent in PV panels. Besides, the new capacitor in parallel to the medium-point diodes facilitates the semi-buses balancing: the main problem in standard NPC topology.

NPC topology type T is another of the most used topologies in PV applications. Figure 2c shows the T-type topology in a three-level example. This configuration reduces the number of semiconductor elements removing the antiparallel diodes required by the I-type topology. Besides, T-type inverters have a slightly higher efficiency due to the fact that, in active mode, only one switch is conducting [47].

Another common multilevel configuration is the flying-capacitor topology, for example, Figure 2d shows a three-level flying-capacitor inverter. This topology allows low harmonics injection, and a better power control and capacitor balancing than the NPC topology. On the contrary, the DC-link bus capacity becomes larger and, for a higher number of levels, this solution becomes more complex and bulky. Moreover, this topology achieves a lower efficiency and a worse use of the effective switching frequency than others alternatives. In addition, like in the case of NPC topology, there are some variations on this configuration that provides certain advantages [44].

In conclusion, all the discussed topologies in this section allow bidirectional current flow and, therefore, they can be used for EL inspections. Consequently, the hardware available in current large PV plants can be modified in most cases to allow EL maintenance at low or zero cost.

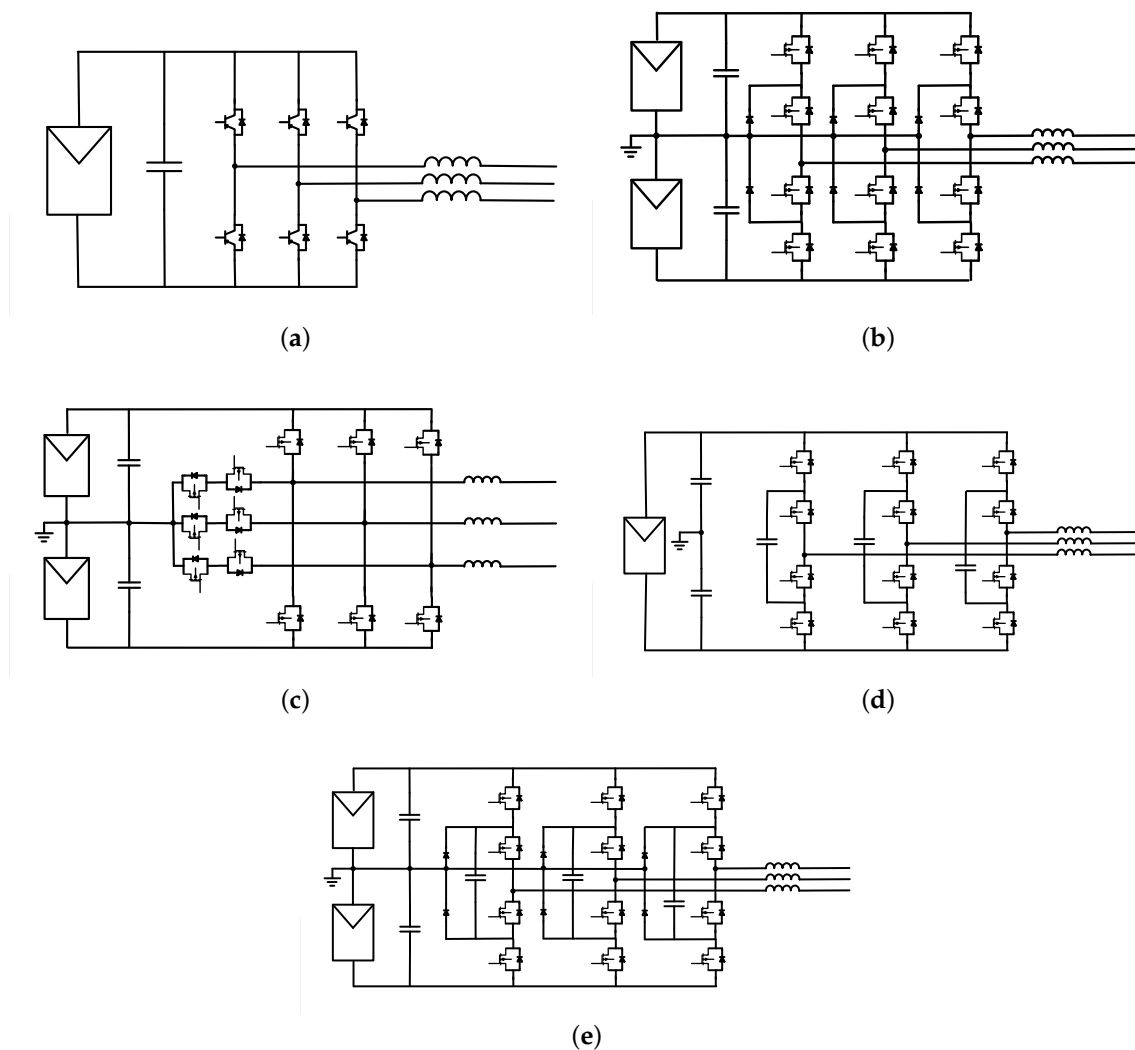


**Figure 2.** Representative power inverter topologies for utility-scale photovoltaic plants (USPVPs) applications: (a) two-level three-phase inverter, (b) three-level three-phase NPC I-type inverter, (c) three-level three-phase neutral point clamped (NPC) T-type inverter, (d) three-level three-phase flying capacitor inverter and (e) three-level three-phase NPC I-type modified inverter.

#### 4. USPVPs Control for Applying EL Technique

##### 4.1. Power Inverter Controller Structure

As discussed in the previous section, industrial high-power grid-tie converters usually use a single-stage inverter topology in PV applications [48,49]. A three-level NPC type-I three-phase topology has been selected for the purposes of this study; however, nevertheless, the same techniques could be applied in the same way to other topologies.

Figure 3 shows a classical DG converter control block scheme. The controller is divided into four layers [50,51]:

- **High level controller:** The highest level control is responsible for providing the right active and reactive power set-points to the lower level controllers. Its objective is to maximise the active power generation and to help the utility grid with the reactive power injection.

- **Middle level controller:** The middle level controller is tasked to follow the higher level control references. Besides, it is in charge of checking the power inverter limitations due to restrictions (such as temperature and over voltages), and setting up priorities whenever necessary.
- **Low level controller:** The low level controller includes both the instantaneous current controller based on a proportional-integrative-derivative (PID) controller, a direct-quadrature-zero (DQ0) transformation and the modulation control technique, which provides the switching pulse width modulation (PWM) signal to the power converter semiconductors.
- **Hardware level:** Finally, the hardware level is in charge of translating the control signals to the physical pulses of the converter in order to produce the expected voltage signal behaviour by the power converter.

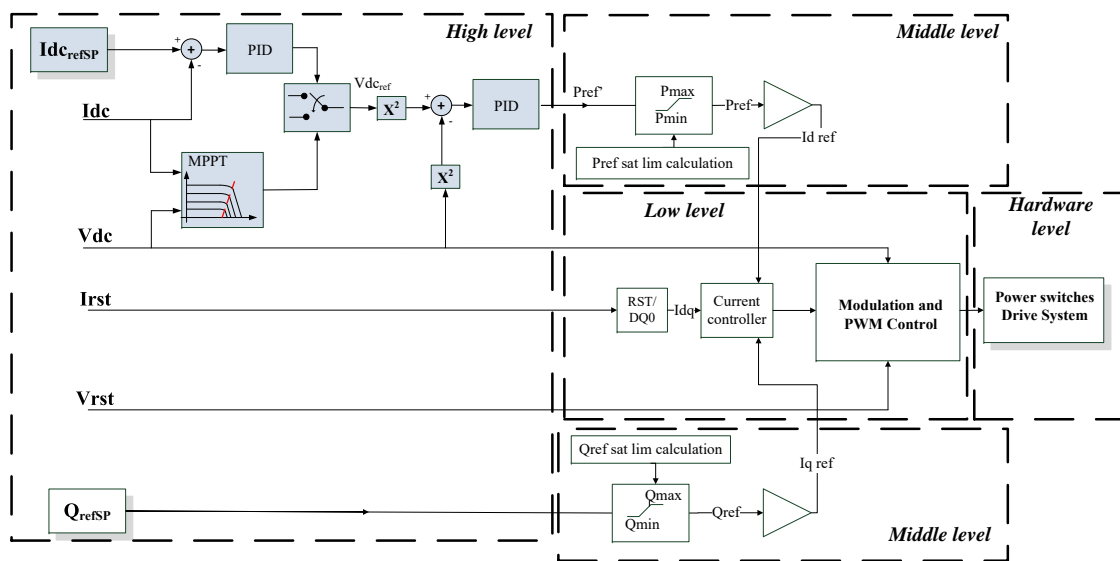


**Figure 3.** Main control diagram of a photovoltaic (PV) inverter controller: in blue are marked the high-level control blocks related to the maximum power point tracking (MPPT) and electroluminescence (EL) evaluation working modes.

In particular, the EL control action is performed inside the high level controller layer. Figure 3 highlights in blue the blocks concerning EL functionality. The PV power inverter has a maximum power point tracking (MPPT) algorithm that looks for the optimum working point of the inverter in order to get the maximum output power from the PV panels [52–55].

The proposed algorithm introduces a switch that allows to change between the MPPT controller and a specific DC current controller for the EL operation. Therefore, the high-level goal, instead of being the maximum output power generation, is to establish a predefined negative DC current reference, in order to force the PV panels to work as light emitters. Consequently, the controller finds the right DC voltage reference in which the current set-point is acquired by means of, for example, a PID controller. Theoretically, the transition between the EL and the MPPT working modes could be done on the fly; however, it is necessary to stop the device in order to change the combiner box breakers state conveniently [56,57].

#### 4.2. Complete System Control Architecture

In order to perform the EL inspection in USPVPs, a higher automation control level should be achieved. On the one hand, it is mandatory to have a system that is capable of taking the images automatically. Nowadays, due to its autonomy and profitability, unmanned aerial vehicles are the most studied inspection system [58,59], and several studies are focused on the applications of drones to the autonomous monitoring of large-scale PV plants [60]. On the other hand, the direct polarisation



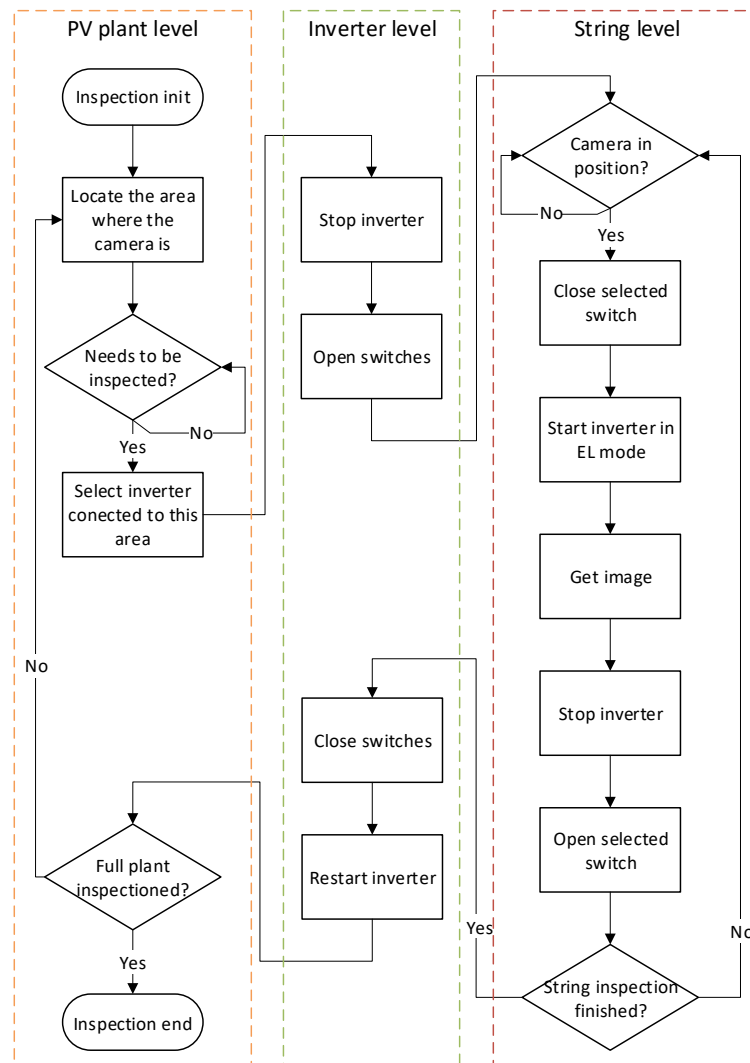
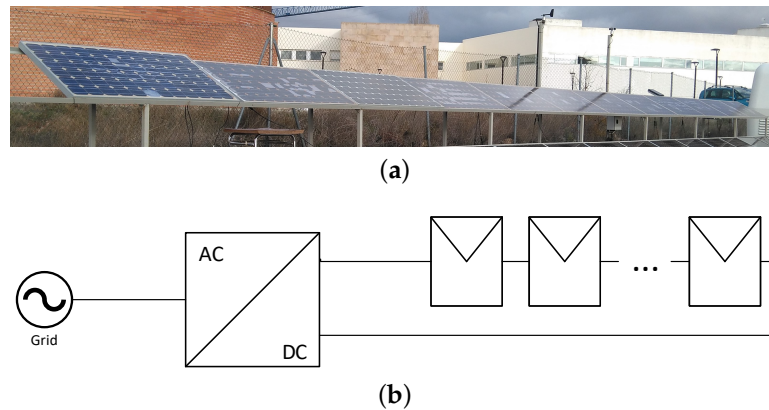


Figure 5. Complete system flow diagram for the maintenance of USPVPs.

### 5. Prototype Design and Installation on the Demo Site

In order to test the proposed inspection procedure, a small pilot plant is available. The pilot, shown in Figure 6a, consists of 11 PV panels with several damaged cells. The datasheet contains the main specifications of the panels: every panel has a maximum peak power of 175 W, a  $V_{oc}$  of 44.35 V and a  $I_{sc}$  of 5.45 A. Summarising, the full plant achieves a maximum power point (MPP) of 2.1 kW, with 488 V  $V_{oc}$  and 5.45 A  $I_{sc}$ . It is important to emphasise that these characteristics are provided by the manufacturer for the newly manufactured panels, but the pilot plant have several defects, and therefore the showed values may vary significantly.

A three-level NPC I-type converter, which is prepared to allow the bidirectional current flow, has been developed for the purpose of performing an EL inspection on the pilot plant. The inverter, shown in Figure 7, achieves a maximum power of 3 kW. As Figure 6b shows, the inverter AC side has been connected to the 400 V three-phase grid, whereas the PV side can set its voltage between 330 and 550 Vdc. During the EL test execution, this voltage range is enough to allow the current control between 10%  $I_{sc}$  and 100%  $I_{sc}$ . Besides, the DC-link pre-charge allows the panels direct polarisation in night time conditions.



**Figure 6.** Panels with several defects used in the pilot plant (a), and connection diagram between panels and the inverter (b).

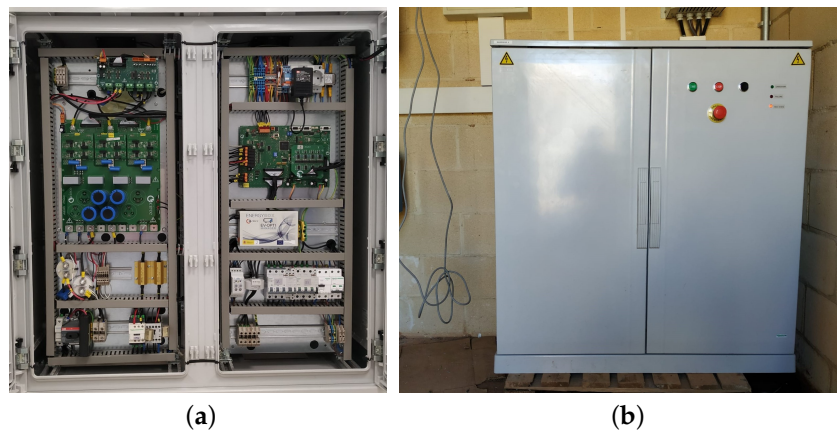


**Figure 7.** Bidirectional inverter developed for the direct polarization of the panels (a), and inverter installed in the demo site facilities (b).

## 6. Simulation and Experimental Results

### 6.1. Simulation

Previously to the inverter assembly, the full system behaviour has been analysed in the PSCAD simulation environment. A model of the bidirectional converter and its controller has been simulated connected to a PV array. In this way, the PV array has been modelled according to the pilot plant characteristics, so that the obtained results can be extrapolated to the experimental set-up.

Current EL legislation [64] establishes that two tests must be completed in order to detect defects of different nature. A current equal to 10% and 100% of  $I_{sc}$  must be injected during the first and second test, respectively. Starting from a scenario where the PV panels are connected to the inverter without current flowing between them, the current controller has been tested under different irradiance levels and current set-points, always within the limits set in legislation.

Figure 8 shows the PID controller response to a reference in the form of 200 ms pulse. Thus, voltage, current and power results are summarised in Table 1 for the analysed cases, allowing the calculation of power consumption required during the inspection.

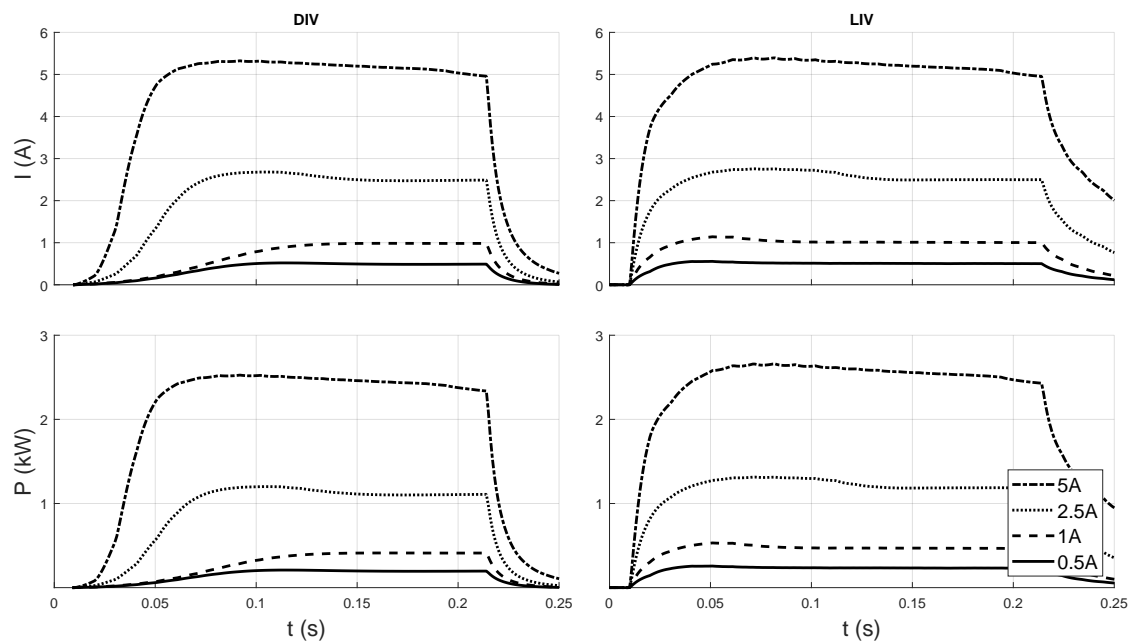


**Figure 8.** Controller response to a pulse of 200 ms under different irradiance conditions—DIV ( $1 \text{ W/m}^2$ ) and LIV ( $800 \text{ W/m}^2$ )—and for several current references scenarios.

**Table 1.** Behaviour of PV panels under different conditions during direct polarisation: Daytime ( $800 \text{ W/m}^2$ ) and Night-time ( $1 \text{ W/m}^2$ ).

Irradiance	Daytime				Nighttime			
	0.5	1	2.5	5	0.5	1	2.5	5
Current (A)	0.5	1	2.5	5	0.5	1	2.5	5
Voltage (V)	461	464	475	490	401	418	446	472
Avg. power (W)	231	465	1186	2445	200	419	1114	2359

On the one hand, the simulations conclude that irradiance is not strongly related with voltage and power levels required to achieve the current reference. On the other hand, a slight increase in voltage produces an important current variation. Consequently, if current set-point is increased, the voltage increases slightly also, and therefore the needed power variations are approximately linear with current. In conclusion, power consumption and, consequently, inspection cost, depends strongly on the current level necessary to achieve the light emission required to the defect detection.

### 6.2. Field Test

The developed inverter installed in the pilot plant has been tested in current source working mode in order to compare the simulation results with the experimental ones. The current controller allows different set-points levels according to the requirements of the inspection. Tests has been performed at four current levels: 10%, 25%, 50% and 100% of  $I_{sc}$ . Table 2 shows the voltage and power measurements obtained from the pilot tests. These results confirm the simulation conclusions: power mainly depends on current and is practically independent of irradiance. On the other hand, small variations in voltage produce substantial changes in current. This conclusion ensures that the necessary voltage to carry out the inspection is around the  $V_{oc}$  in the inverter, values within the inverter working range.

**Table 2.** Behaviour of PV panels under different conditions during direct polarisation: Daytime (800 W/m<sup>2</sup>), Night-time (1 W/m<sup>2</sup>).

Irradiance	Daytime				Nighttime			
Current (A)	0.5	1	2.5	5	0.5	1	2.5	5
Voltage (V)	462	468	486	512	439	460	498	528
Power (W)	231	468	1215	2560	220	460	1245	2640

The controller implemented in the inverter allows to follow a current reference externally set. Figure 9 shows a transitory measurement when the current set-point, injected to the panels, change from 5 A to 0.5 A. The response time and over oscillation strongly depends on the implemented controller, in this case a PID controller.

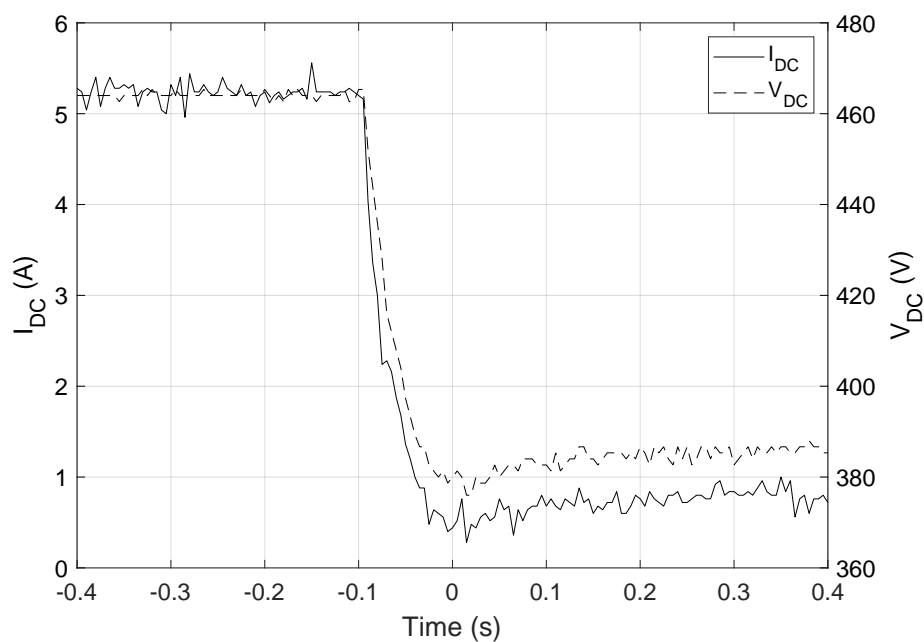


**Figure 9.** Experimental results: current set-point changed from 5A to 0.5A.

In order to corroborate the validity of the techniques used in the pilot plant, both in the inverter, and in the capture of images with the use of unmanned vehicles, EL measurements were made in the pilot plant. Figure 10 shows the EL image of a PV panel, obtained in the experimental plant with an injected current of 10% of  $I_{sc}$  (approximately 0.5 A). Figure 11 shows the image obtained from the same PV panel in the plant with the injection of the  $I_{sc}$  (approximately 5 A). The EL image of the same PV panel, but obtained previously to be mounted in the plant, in darkness (inside the laboratory), using a power supply, at  $I_{sc}$ , is shown in Figure 12.

Some assessments can be made from the previous figures. It could be observed the existence of fractures in many of the cells of Figures 10 and 11 that are not seen in Figure 12. Such fractures are the result of blows during transport or in the installation of the PV panels. For example, highlighted in red, the three figures show a pair of adjacent cells that present a diagonal fracture in the pilot plant, but that did not appear in the PV panel previous to its installation. The same type of fractures can be detected in other cells throughout the PV panel, especially at the edges and less sharply in the centre. These fractures were not carried out consciously, nor was the PV panel hit during its transfer or installation. However, this fact reinforces the need to carry out on-site inspections, without having to disassemble the PV panels and take them to a dark chamber to perform EL.

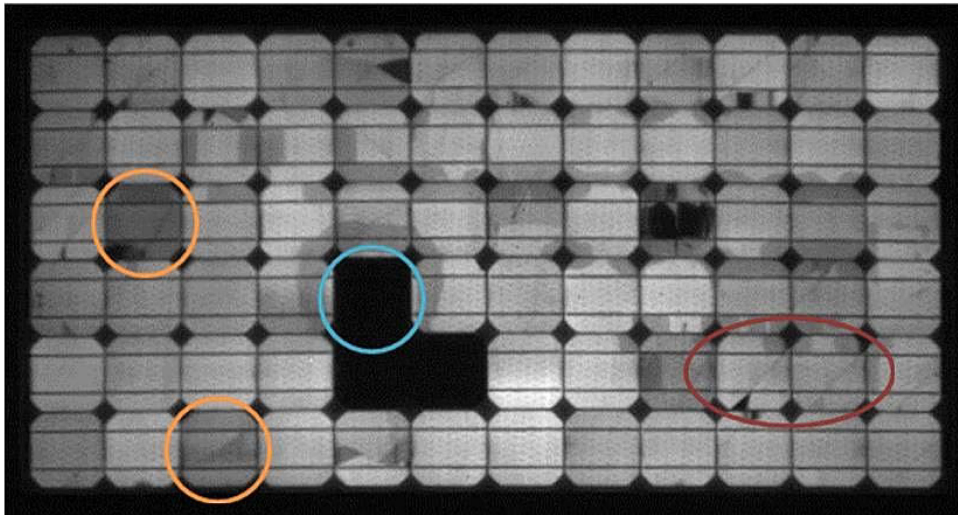


**Figure 10.** EL image of the 0.5A PV panel ( $10\% I_{sc}$ ) in the pilot plant. Capture made with the camera fixed on a tripod.

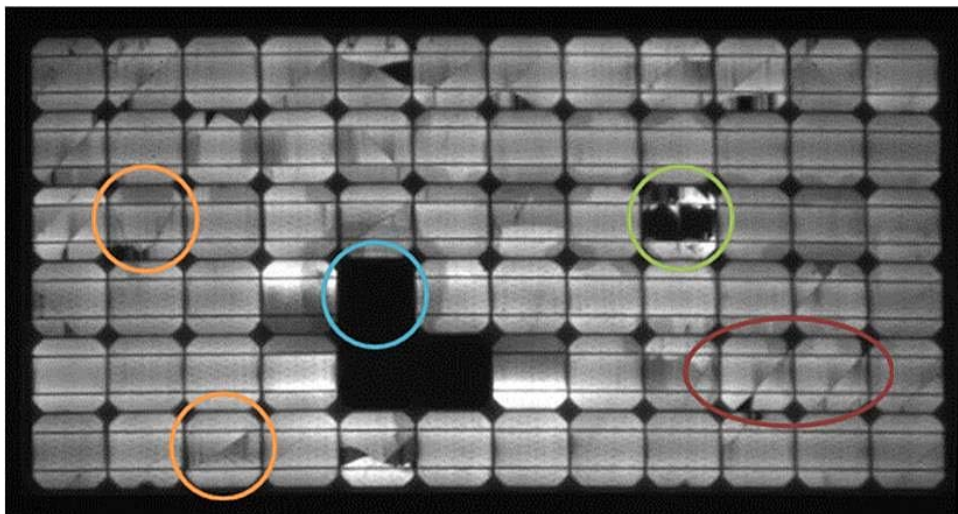


**Figure 11.** EL image of the 5A PV panel ( $100\% I_{sc}$ ) in the pilot plant. Capture made with the camera fixed on a tripod.

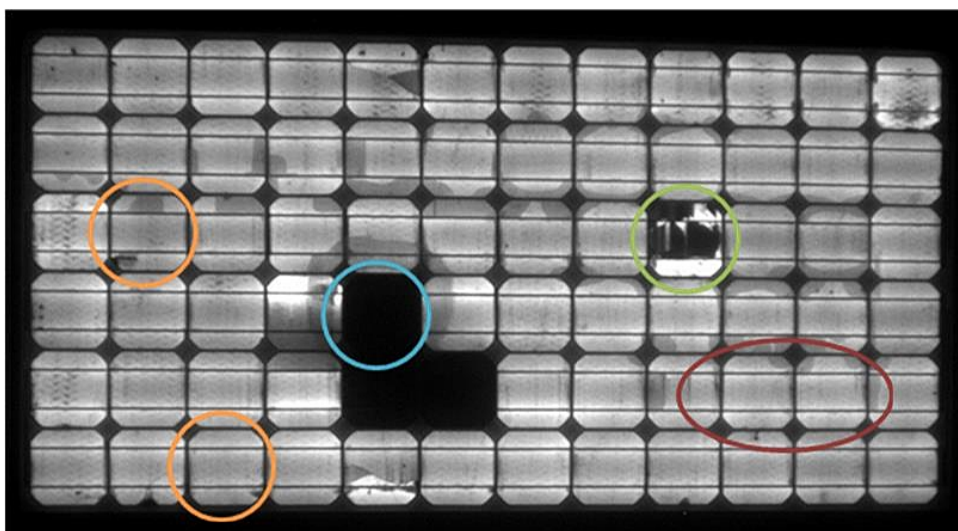


**Figure 12.** EL image of a the same PV panel, to at  $I_{sc}$ , previous to be installed in the plant (indoors and with the use of a power supply). Capture made with the camera fixed on a tripod.

Regardless of possible damage done in transport and installation, it is confirmed that the device designed for the injection of current into the PV panels is capable of working properly to obtain EL images, both at very low currents (10% of  $I_{sc}$ ) and at the working currents of the PV panels ( $I_{sc}$ ). The images obtained indicate that photographs can be obtained with the appropriate quality, and that they obtained photographs highlight the behaviour of the cells. This step is indispensable for the viability of the subsequent capture of EL images with the use of a mobile camera.

Moreover, the proposed procedure using bidirectional inverter allows us to easily perform EL image capture at different currents. A localisable defect with low current intensity is that of potential-induced degradation. This type of panel failure is evidenced by the presence of cells that have a markedly lower brightness than other existing cells. However, at high currents, they have a brightness similar to the rest, so it is not possible to distinguish them. Several examples of this phenomenon can be seen in Figure 10, which are not seen in Figure 11 or Figure 12. Two of these cells have been highlighted in orange in the three previous images.

## 7. Economic Analysis of Solution Cost

### 7.1. Solution Cost

This section analyses the extra installation cost of upgrading a new USPVP to allow for the proposed EL maintenance technique. In addition, installation costs will be compared to current plant costs in order to evaluate the additional needed investment. As Section 3 shows, power inverters allow bidirectional power flow; therefore, only some minor additional features have to be added.

Firstly, an inspection control is required in order to perform the new features. Due to the low computational requirements of the needed software, hardware upgrades are not required by the control system. Besides, software development costs will be amortised for all manufactured inverters worldwide, so its impact on the final price will be negligible.

Secondly, the AC pre-charge system is required to apply EL inspections. The device is implemented in the inverter and allows to raise the DC-link voltage from the grid side. Pre-charge is carried out by means of the following components; an auxiliary power transformer to level-up the input voltage, a breaker to activate the pre-charge process, a resistor to limit the peak current and a diode-based bridge to rectify the AC voltage. These components must be chosen for each case, but their cost will not differ significantly. For instance, a grid-tied inverter with an output grid voltage of 400 V, pre-charge system cost would be zero if the PV plant had a functionality that requires it, for example, reactive power injection at night feature; otherwise, it would be approximately 135 € according to up to date market values [65–67].

Finally, string sequencing requires several breakers in order to energise a small panel area and to minimise the energy consumption. Thus, the number of breakers is not predefined, and its estimation is carried out in the following section.

On the other hand, plant power generation will not be affected as the best accuracy for the EL technique is obtained at night, sunrise or sunset. Thus, the inspection will be carried out during non-productive hours, and therefore there will not be any power production losses and the operational costs of the solution will not increase.

### 7.2. Economic Optimisation of the Solution

Obviously, choosing the optimal number and size of breakers is an important task, but it is not an easy one. On the one hand, if too many breakers are installed, the initial investment cost will raise significantly. On the other hand, a high number of breakers divide the full plant in smaller areas with a lower energy consumption per test. Moreover, although a higher number of breakers would be required, dividing the plant into smaller sectors will lead to breakers with less power cutting capability

and, therefore, cheaper ones. Expression (3) gives a relationship between power and price of the required breakers:

$$C_{Brkr} = \alpha P_N + \beta \quad (3)$$

where  $C_{Brkr}$  is the unitary cost in €,  $P_N$  the rated power in kW and  $\alpha$  and  $\beta$  are two parameters to establish a linear regression about the cost of breakers in the working range of the selected scenario.

In order to calculate the optimal amount of breakers, an optimisation analysis is going to be carry out in a selected application. For a typical USPVP application using power solar inverters of 1 MW,  $\alpha$  and  $\beta$  have been estimated according to current market prices [68–74] as 1.475 and 325, respectively. Additionally, several costs could be taken into account, but only the exposed above are relevant to this study. These costs are represented by the initial investment and the energy consumption during the inspection process. The investment in breakers ( $C_0$ ) can be formulated as

$$C_0 = C_{Brkr} N_{Brkr} \quad (4)$$

where  $N_{Brkr}$  is the amount of breakers, the variable to optimise.

Regarding electricity power consumption, current legislation specifies that two inspections must be performed at 10% and 100% of  $I_{sc}$ . This cost can be calculated by means of expression (5),

$$C_{Insp} = \frac{C_{Energy}(P_{10\%I_{sc}} + P_{100\%I_{sc}})t}{N_{Brkr}} \quad (5)$$

where the inspection energy cost per MWp of PV panels installed ( $C_{Insp}$ ) depends on the energy price ( $C_{Energy}$ ), the power consumed during both tests ( $P_{10\%I_{sc}}$  and  $P_{100\%I_{sc}}$ ) and the time required to inspect 1 MWp-equivalent-area; moreover, it is inversely proportional to the number of breakers used. Electricity cost is ~10 cent €/kWh [75,76], the energy consumption has been taken from Table 2, and the inspection time using unmanned vehicle techniques is estimated to be ~13 min/MWp.

These costs have been calculated for a one-year period, assuming a plant expected life of 25 years. Furthermore, increasing plant automatism would improve the capacity to carry out the maintenance tasks, being able to perform inspections more frequently. In this case, it is assumed that an inspection is completed monthly. In order to show the costs on an annual basis, the initial investment ( $C_0$ ) has been divided for the 25 years of expected plant life; inspection energy cost ( $C_{Insp}$ ) has been multiplied by 12 annual inspections; and finally, total costs are the sum of both of them. Selected costs are represented in Figure 13, where the minimum cost is found installing 4 or 5 breakers per PV-panel-MWp, which, according to expressions (3) and (4), it represents an investment of 2775 €.

Accordingly to these estimations, the price to adapt a new USPVP to EL inspection can be calculated as the addition of pre-charge cost (135 €) and breaker cost (2775 €), which gives a result of 2910 €. On the other hand, it should be noted that inverters already have a switch to disconnect the panels; so the extra cost will be 2910 € minus the cost of 1-MW-breaker (1800 €), which is an extra cost of 1110 € per MWp. Major studies assert that the average installation cost of a large PV plant is 1112 €/kW [5]. Based on this information, it can be concluded that an increase of 0.10% on the initial investment would allow the on-site EL maintenance of the PV plant.

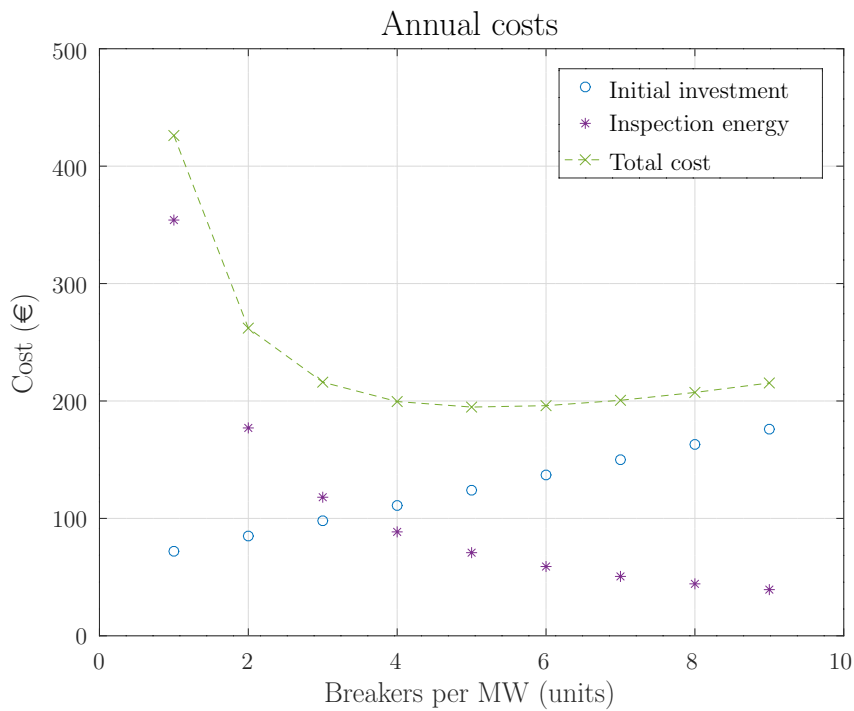


**Figure 13.** Annual prorated costs resulting from the EL maintenance application for installed MWp for the selected use case.

### 8. Discussion

Section 2 compares EL and IRT technology from the point of view of both technique performances. Later, a solution to apply on-site EL maintenance is developed. The technical feasibility of the proposed method is analysed in Section 6. Moreover, Section 7 concludes that the extra cost required to include the direct polarisation feature in a USPVP is no relevant to the cost of these plants. An analysis showing economic viability and the increment over productivity produced by early detection of damaged panels can be carried out in detail, but it is not relevant to reach the main objectives of the study and, therefore, it is out of the paper’s scope.

Finally, Table 3 summarise the comparison between the most important image processing USPVP maintenance methods. As can be seen, IRT and EL could be both used at a low cost, and without incurring in power plant production losses. EL tests require more time to perform the test because it needs a higher image resolution than IRT but, on the other hand, it gives also more information than IRT techniques.

**Table 3.** Features and costs comparison between state of the art and proposed USPVP image processing methods.

Technology	Illuminated IRT	Dark IRT	Off-site EL	On-site EL
<b>Implementation test cost</b>	+	+	++++	+
<b>Plant production losses</b>	-	-	+++	-
<b>Results accuracy</b>	++	+	+++	+++
<b>Time per test</b>	+	+	+++	++

-: null, +: low, ++: moderate, +++: high, ++++: very high.

### 9. Conclusions

The size and rated power of USPVPs have been increasing exponentially in the last decade, increasing the need for optimisation and automation of maintenance processes. Currently, one of the

most extended practices in the maintenance of PV panels is the analysis of IRT images. However, as has been explained through the text, IRT technique has some limitations in the detection of defects in PV panels.

One of the most promising techniques to complement the results of IRT tests is the study of EL images. Unfortunately, EL procedures involves dismantling the modules or to use external power supplies and, therefore, they have a high cost and require qualified staff and special equipment.

In this context, the paper has presented a novel USPVP maintenance technique based on on-site EL image acquisition by means of the bidirectional inverters usually installed in USPVPs. The proposed procedure retains the high capability to characterise defects inherent in EL technique, achieving a high automatism level and, as a consequence, a time and cost reduction.

The behaviour of the system has been calculated by simulation, and has been validated with experimental results in a small-scale PV plant successfully, afterwards. The results confirm the technical feasibility of performing this technique on a USPVP, without the need to uninstall and reinstall the panels for their evaluation. Consequently, on the one hand, the presented technique allows a full evaluation of the plant at a low operational cost, due to the low energy consumption performing the test. Moreover, on the other hand, the technique could be applied to both new and existing plants at a low installation cost, due to the fact that only minor hardware and software changes are needed. In particular, hardware costs of the installation for a real scenario have been calculated, representing a neglecting increment in the plant installation cost per megawatt, and the cost of software modifications is almost zero too, because it is very simple, with low computational requirements, and easy to implement algorithm in any commercial inverter control unit.

In conclusion, the paper has provided a new cheap and valuable solution to improve the maintenance of USPVPs; a method that could be used as an alternative or complementary with IRT technique. Indeed, some resources such as the unmanned vehicle could be shared between the two methods, reducing the overall installation cost for both of them.

Following the evaluation in the pilot-site with successful results, future work will test the solution in a real USPVP, in order to evaluate the solution in an industrial environment.

**Author Contributions:** Conceptualization, J.B.-F., J.M.-C.-A. and L.H.-C.; methodology, J.M.-C.-A., J.F.S.-O. and L.H.-C.; software, J.B.-F., J.M.-C.-A.; validation, J.B.-F., J.M.-C.-A., L.H.-C. and V.A.-G.; formal analysis, J.B.-F., J.M.-C.-A., L.H.-C. and J.F.S.-O.; investigation, J.B.-F., J.M.-C.-A., L.H.-C. and O.M.-S.; resources, J.B.-F., J.M.-C.-A., V.A.-G., Á.M.-F., J.I.M.-A. and S.G.-S.; data curation, J.B.-F., J.M.-C.-A., V.A.-G., J.I.M.-A., S.G.-S. and Á.M.-F.; writing—original draft preparation, J.B.-F., J.M.-C.-A., L.H.-C. and V.A.-G.; writing—review and editing, J.B.-F., J.M.-C.-A., L.H.-C. and V.A.-G.; visualization, J.B.-F., J.M.-C.-A., J.F.S.-O., L.H.-C. and V.A.-G.; supervision, J.F.S.-O., L.H.-C., O.M.-S. and V.A.-G.; project administration, J.M.-C.-A., J.F.S.-O. and L.H.-C.; funding acquisition, J.M.-C.-A., J.F.S.-O., L.H.-C., V.A.-G. and O.M.-S.; All authors have read and agreed to the published version of the manuscript.

**Funding:** This research was funded by the “Ministerio de Industria, Economía y Competitividad” grant number “RTC-2017-6712-3” with name “Desarrollo de herramientas Optimizadas de operación y mantenimiento Predictivo de Plantas fotovoltaicas—DOCTOR-PV”. The authors want to thank the support and collaboration of the Centro para el Desarrollo Tecnológico Industrial, E.P.E. (CDTI) funds through the RED CERVERA CER-20191002 “ENERISLA: SISTEMAS ENERGÉTICOS AISLADOS 100% RENOVABLES”. This work has been partially financed by the Junta de Castilla y León under project VA283P18.

**Conflicts of Interest:** The authors declare no conflicts of interest.

## References

1. European Commission. Europe leads the global clean energy transition: commission welcomes ambitious agreement on further renewable energy development in the EU. *Int. Energy Agency* **2018**, *1*, 718. doi:10.1016/0960-1481(94)90358-1. [CrossRef]
2. European Parliament. U targets: More Renewables, Better Energy Efficiency (Video). 2018. Available online: <https://www.europarl.europa.eu/news/en/headlines/economy/20181031STO18175/eu-targets-more-renewables-better-energy-efficiency-video> (accessed on 19 February 2020).

3. Agora Energiewende and Sandbag. *The European Power Sector in 2017. State of Affairs and Review of Current Developments*; 128/02-A-2018/EN; Agora Energiewende and Sandbag: Berlin, Germany, 2018.
4. U.S. Energy Information Administration. Energy Information Administration. *Choice Rev. Online* **2007**, *44*, 44–3624–44–3624. doi:10.5860/choice.44-3624. [CrossRef]
5. IRENA. *Renewable Power Generation Costs in 2018*; International Renewable Energy Agency: Abu Dhabi, UAE, 2019; ISBN 978-92-9260-126-3
6. InterSolarEurope. *Global Market Outlook for Solar Power 2018-2022*; InterSolarEurope: Brussels, Belgium, 2018; ISBN 978-908-271-431-9.
7. Rakhshani, E.; Rouzbehi, K.; Adolfo, J.S.; Tobar, A.C. Integration of Large Scale PV-Based Generation into Power Systems: A Survey. *Energies* **2019**, *12*, 1425. [CrossRef]
8. SolarInsure. *Larges Solar Power Plants of the World*; SolarInsure: Costa Mesa, CA, USA, 2019.
9. Wikipedia. Direct and Indirect Band Gaps. Available online: [https://en.wikipedia.org/wiki/Direct\\_and\\_indirect\\_band\\_gaps](https://en.wikipedia.org/wiki/Direct_and_indirect_band_gaps) (accessed on 5 July 2019).
10. Glavaš, H.; Vukobratović, M.; Primorac, M.; Muštran, D. Infrared thermography in inspection of photovoltaic panels. In Proceedings of the International Conference on Smart Systems and Technologies 2017, Osijek, Croatia, 19 October 2017; pp. 63–68. doi:10.1109/SST.2017.8188671. [CrossRef]
11. Frazão, M.; Silva, J.A.; Lobato, K.; Serra, J.M. Electroluminescence of silicon solar cells using a consumer grade digital camera. *Meas. J. Int. Meas. Confed.* **2017**, *99*, 7–12. doi:10.1016/j.measurement.2016.12.017. [CrossRef]
12. Rodriguez, P.; Sera, D.; Teodorescu, R.; Rodriguez, P. PV Panel Model Based on Datasheet Values PV. In Proceedings of the 2007 IEEE International Symposium on Industrial Electronics, Vigo, Spain, 4–7 June 2007. pp. 2392–2396. doi:10.1109/ISIE.2007.4374981. [CrossRef]
13. PV Performance Modeling Collaborative. Single Diode Equivalent Circuit Models. Available online: <https://pvpmmc.sandia.gov/modeling-steps/2-dc-module-iv/diode-equivalent-circuit-models/> (accessed on 20 February 2020).
14. Liu, S.; Dugal, R.A. Dynamic Multi-Physics Model for Solar Array. *IEEE Power Eng. Rev.* **2002**, *22*, 66. doi:10.1109/MPER.2002.4312200. [CrossRef]
15. Wu, F.; Lin, H.; Yang, Z.; Liao, M.; Wang, Z.; Li, Z.; Gao, P.; Ye, J.; Shen, W. Suppression of surface and auger recombination by formation and control of radial junction in silicon microwire solar cells. *Nano Energy* **2019**, *58*, 817–824. doi:10.1016/j.nanoen.2019.02.021. [CrossRef]
16. IEA International Energy Agency. *Review on Infrared and Electroluminescence Imaging for PV Field Applications*; Technical Report IEA-PVPS T13-10:2018, IEA-PVPS Task 13; IEA International Energy Agency: Paris, France, 2018.
17. Waqar Akram, M.; Li, G.; Jin, Y.; Chen, X.; Zhu, C.; Zhao, X.; Aleem, M.; Ahmad, A. Improved outdoor thermography and processing of infrared images for defect detection in PV modules. *Solar Energy* **2019**, *190*, 549–560. doi:10.1016/j.solener.2019.08.061. [CrossRef]
18. Meola, C.; Boccardi, S.; maria Carlomagno, G. Nondestructive Testing With Infrared Thermography. In *Infrared Thermography in the Evaluation of Aerospace Composite Materials*; Elsevier: Cambridge, MA, USA, 2017; pp. 85–125. doi:10.1016/b978-1-78242-171-9.00004-8. [CrossRef]
19. Botsaris, P.N.; Tsanakas, J.A. Infrared Thermography as an Estimator Technique of a Photovoltaic Module Performance Via Operating Temperature Measurements. In Proceedings of the 10th ECNDT, Moscow, Russia, 7–11 June 2010; pp. 199–202.
20. Ebner, R.; Kubicek, B.; Ujvari, G.; Novalin, S.; Rennhofer, M.; Halwachs, M. Optical characterization of different thin film module technologies. *Int. J. Photoenergy* **2015**, *2015*. doi:10.1155/2015/159458. [CrossRef]
21. Berardone, I.; Lopez Garcia, J.; Paggi, M. Quantitative analysis of electroluminescence and infrared thermal images for aged monocrystalline silicon photovoltaic modules. In Proceedings of the 2017 IEEE 44th Photovoltaic Specialist Conference (PVSC), Washington, DC, USA, 25–30 June 2017; pp. 402–407. doi:10.1109/pvsc.2017.8366338. [CrossRef]
22. Gallardo-Saavedra, S.; Hernández-Callejo, L.; Alonso-García, M.d.C.; Santos, J.; Morales-Aragonés, J.I.; Alonso-Gómez, V. Failure diagnosis on photovoltaic modules using thermography, electroluminescence, RGB and I-V techniques. In Proceedings of the 36th European Photovoltaic Solar Energy Conference and Exhibition, Marseille, France, 9 September 2019; pp. 1171–1175.

23. Tsanakas, J.A.; Ha, L.; Buerhop, C. Faults and infrared thermographic diagnosis in operating c-Si photovoltaic modules: A review of research and future challenges. *Renew. Sustain. Energy Rev.* **2016**, *62*, 695–709, doi:10.1016/j.rser.2016.04.079. [[CrossRef](#)]
24. Salazar, A.M.; Macabebe, E.Q.B. Hotspots Detection in Photovoltaic Modules Using Infrared Thermography. *MATEC Web Conf.* **2016**, *70*, 10015. doi:10.1051/MATECCONF/20167010015. [[CrossRef](#)]
25. Jaffery, Z.A.; Dubey, A.K.; Irshad.; Haque, A. Scheme for predictive fault diagnosis in photo-voltaic modules using thermal imaging. *Infrared Phys. Technol.* **2017**, *83*, 182–187. doi:10.1016/j.infrared.2017.04.015. [[CrossRef](#)]
26. Köntges M.; Kurtz S.; Packard C.; Jahn U.; Berger K.A.; Kato, K.; Friesen T.; Liu H.; Van Iseghem M. *IEA-PVPS T13-01 2014 Review of Failures of Photovoltaic Modules Final*; Technical Report IEA-PVPS T13-01:2014, IEA-PVPS Task 13; IEA International Energy Agency: Paris, France, 2014.
27. Deitsch, S.; Christlein, V.; Berger, S.; Buerhop-Lutz, C.; Maier, A.; Gallwitz, F.; Riess, C. Automatic classification of defective photovoltaic module cells in electroluminescence images. *Sol. Energy* **2019**, *185*, 455–468, doi:10.1016/j.solener.2019.02.067. [[CrossRef](#)]
28. Ebner, R.; Zamini, S.; Újvári, G. Defect analysis in different photovoltaic modules using electroluminescence (EL) and infrared (IR)-thermography. In Proceedings of the 25th European Photovoltaic Solar Energy Conference and Exhibition/5th World Conference on Photovoltaic Energy Conversion, Valencia, Spain, 6–10 September 2010. doi:10.4229/25thEUPVSEC2010-1DV.2.8. [[CrossRef](#)]
29. Gallardo-Saavedra, S.; Hernández-Callejo, L.; Alonso-García, M.d.C.; Santos, J.; Morales-Aragón, J.I.; Alonso-Gómez, V. Nondestructive characterization of solar PV cells defects by means of electroluminescence, infrared thermography, I-V curves and visual tests: experimental study and comparison. *Energies* **2020**, pending publication.
30. Seth, N.; Goel, V.; Kulkarni, R.D. Three phase innovative multilevel inverter topologies for research and industrial applications: A review. In Proceedings of the 2017 International Conference on Nascent Technologies in Engineering, Navi Mumbai, India, 27 January 2017. doi:10.1109/ICNTE.2017.7947934. [[CrossRef](#)]
31. Cabrera-Tobar, A.; Bullich-Massagué, E.; Aragüés-Peñalba, M.; Gomis-Bellmunt, O. Topologies for large scale photovoltaic power plants. *Renew. Sustain. Energy Rev.* **2016**, *59*, 309–319. doi:10.1016/j.rser.2015.12.362. [[CrossRef](#)]
32. Kjaer, S.; Pedersen, J.; Blaabjerg, F. Power inverter topologies for photovoltaic modules—a review. In Proceedings of the Conference Record of the 2002 IEEE Industry Applications Conference. 37th IAS Annual Meeting (Cat. No.02CH37344), Pittsburgh, PA, USA, 13–18 October 2002; Volume 3, pp. 782–788. doi:10.1109/ias.2002.1042648. [[CrossRef](#)]
33. Dogga, R.; Pathak, M.K. Recent trends in solar PV inverter topologies. *Sol. Energy* **2019**, *183*, 57–73. doi:10.1016/j.solener.2019.02.065. [[CrossRef](#)]
34. Deshpande, S.; Bhasme, N.R. A review of topologies of inverter for grid connected PV systems. *Innov. Power Adv. Comput. Technol.* **2018**, *2017*, 1–6. doi:10.1109/IPACT.2017.8245191. [[CrossRef](#)]
35. Smyth, D. *What Is the Best Grid Connected PV Inverter Topology and Why?*; Technical Report; AC Solar Warehouse. 2016. Available online: [www.acsolarwarehouse.com](http://www.acsolarwarehouse.com) (accessed on 15 February 2020).
36. Zhao, T.; Bhavaraju, V.; Nirantare, P.; Xu, J. Evaluation of commercial scale transformerless solar inverter technology. In Proceedings of the 2015 IEEE Energy Conversion Congress and Exposition, ECCE 2015, Montreal, QC, Canada, 20–24 September 2015; pp. 5342–5348. doi:10.1109/ECCE.2015.7310411. [[CrossRef](#)]
37. Shehadeh, S.H.; Aly, H.H.; El-Hawary, M.E. An overview of topologies for photovoltaic electrical energy. In Proceedings of the IEEE Electrical Power and Energy Conference, Halifax, NS, Canada, 21–23 August 2013; pp. 1–8.
38. SMA Solar Technology AG. Sunny Central 1000CP Xt. Technical report. Available online: [www.SMA.de](http://www.SMA.de) (accessed on 20 February 2020).
39. Schneider Electric Solar. 1500V Context SmartGen. Available online: <https://solar.schneider-electric.com/product/conext-smartgen/> (accessed on 20 February 2020).
40. Ingeteam. INGECON SUN Power (1000V/1500V). Available online: [https://www.ingetteam.com/us/en-us/sectors/photovoltaic-energy/p15\\_24\\_36/ingecon-sun-power-1000v-1500v.aspx](https://www.ingetteam.com/us/en-us/sectors/photovoltaic-energy/p15_24_36/ingecon-sun-power-1000v-1500v.aspx) (accessed on 20 February 2020).

41. ABB Central Inverters, PVS980, 1818 to 2091 kVA—Data Sheet. Available online: <http://search.abb.com/library/Download.aspx?DocumentID=3AXD50000027473&LanguageCode=en&DocumentPartId=&Action=Launch> (accessed on 20 February 2020).
42. GPTech. SmartPV. Available online: <http://www.greenpower.es/en/gptech-solutions/products/smartpv/#!tab1> (accessed on 20 February 2020).
43. FreesunHEM | Power Electronics. Available online: <https://power-electronics.com/productos/solar-products/freesun-hem/> (accessed on 27 February 2020).
44. Tayab, U.B.; Bashir, M.A. Multilevel inverter topologies for photovoltaic power system: A review. *ARPN J. Eng. Appl. Sci.* **2017**, *12*, 3537–3549.
45. Prabakaran, N.; Palanisamy, K. A comprehensive review on reduced switch multilevel inverter topologies, modulation techniques and applications. *Renew. Sustain. Energy Rev.* **2017**, *76*, 1248–1282. doi:10.1016/j.rser.2017.03.121. [[CrossRef](#)]
46. Busquets-Monge, S.; Rocabert, J.; Rodriguez, P.; Alepuz, S.; Bordonau, J. Multilevel Diode-Clamped Converter for Photovoltaic Generators with Independent Voltage Control of Each Solar Array. *IEEE Trans. Ind. Electron.* **2008**, *55*, 2713–2723. doi:10.1109/TIE.2008.924011. [[CrossRef](#)]
47. Ma, L.; Kerekes, T.; Teodorescu, R.; Jin, X.; Floricau, D.; Liserre, M. The high efficiency transformer-less PV inverter topologies derived from NPC topology. In Proceedings of the 2009 13th European Conference on Power Electronics and Applications, Barcelona, Spain, 8–10 September 2009; pp. 1–10.
48. Burkart, R.; Kolar, J.W.; Griepentrog, G. Comprehensive comparative evaluation of single- and multi-stage three-phase power converters for photovoltaic applications. In Proceedings of the IEEE 34th International Telecommunications Energy Conference (INTELEC), Scottsdale, AZ, USA, 30 September–4 October 2012; pp. 1–8.
49. Tahir, S.; Wang, J.; Baloch, M.H.; Kaloi, G.S. Digital control techniques based on voltage source inverters in renewable energy applications: A review. *Electronics (Switzerland)* **2018**, *7*. doi:10.3390/electronics7020018. [[CrossRef](#)]
50. Muñoz-Cruzado-Alba, J.; Villegas-Núñez, J.; Vite-Frías, J.A.; Carrasco-Solís, J.M.; Galván-Díez, E. New Low-Distortion Q-f Droop Plus Correlation Anti-Islanding Detection Method for Power Converters in Distributed Generation Systems. *IEEE Trans. Ind. Electron.* **2015**, *62*, 5072–5081. doi:10.1109/TIE.2015.2405894. [[CrossRef](#)]
51. Muñoz-Cruzado-Alba, J.; Villegas-Núñez, J.; Vite-Frías, J.A.; Solís, J.M.C. A new fast peak current controller for transient voltage faults for power converters. *Energies* **2016**, *9*, 1–18. doi:10.3390/en9010001. [[CrossRef](#)]
52. Kalogerakis, C.; Koutroulis, E.; Lagoudakis, M.G. Global MPPT Based on Machine-Learning for PV Arrays Operating under Partial Shading Conditions. *Appl. Sci.* **2020**, *10*, 700. doi:10.3390/app10020700. [[CrossRef](#)]
53. Basha, C.H.; Rani, C. Different conventional and soft computing MPPT techniques for solar PV systems with high step-up boost converters: A comprehensive analysis. *Energies* **2020**, *13*, 371. doi:10.3390/en13020371. [[CrossRef](#)]
54. Costanzo, L.; Vitelli, M. A Novel MPPT technique for single stage grid-connected PV systems: T4S. *Energies* **2019**, *12*, 4501. doi:10.3390/en12234501. [[CrossRef](#)]
55. Tobón, A.; Peláez-restrepo, J.; Montano, J.; Durango, M. MPPT of a Photovoltaic Panels Array with Partial Shading Using the IPSPM with Implementation Both in Simulation as in Hardware. *Energies* **2020**, *13*, 815. doi:10.3390/en13040815. [[CrossRef](#)]
56. What is a Combiner Box? Available online: <https://power-electronics.com/productos/solar-products/freesun-hem/> (accessed on 27 February 2020).
57. Solar String Combiner Boxes—ABB Enclosures. Available online: <https://new.abb.com/low-voltage/products/enclosures/solar-combiners> (accessed on 29 February 2020).
58. Niccolai, A.; Gandelli, A.; Grimaccia, F.; Zich, R.; Leva, S. Overview on photovoltaic inspections procedure by means of unmanned aerial vehicles. In Proceedings of the 2019 IEEE Milan PowerTech, PowerTech 2019, Milan, Italy, 23–27 June 2019; pp. 1–6. doi:10.1109/PTC.2019.8810987. [[CrossRef](#)]
59. Luo, X.; Li, X.; Yang, Q.; Wu, F.; Zhang, D.; Yan, W.; Xi, Z. Optimal path planning for UAV based inspection system of large-scale photovoltaic farm. In Proceedings of the 2017 Chinese Automation Congress, CAC 2017, Jinan, China, 20–22 October 2017; pp. 4495–4500. doi:10.1109/CAC.2017.8243572. [[CrossRef](#)]

60. Sizkouhi, A.M.M.; Esmailifar, S.M.; Aghaei, M.; Vidal de Oliveira, A.K.; Rütther, R. Autonomous Path Planning by Unmanned Aerial Vehicle (UAV) for Precise Monitoring of Large-Scale PV plants. In Proceedings of the 2019 IEEE 46th Photovoltaic Specialists Conference (PVSC), Chicago, IL, USA, 16–21 June 2019; Volume 2, 1398–1402.
61. Cabrera-Tobar, A.; Bullich-Massagué, E.; Aragüés-Peñalba, M.; Gomis-Bellmunt, O. Active and reactive power control of a PV generator for grid code compliance. *Energies* **2019**, *12*. doi:10.3390/en12203872. [CrossRef]
62. Marinopoulos, A.; Papandrea, F.; Reza, M.; Norrga, S.; Spertino, F.; Napoli, R. Grid integration aspects of large solar PV installations: LVRT capability and reactive power/voltage support requirements. In Proceedings of the 2011 IEEE PES Trondheim PowerTech: The Power of Technology for a Sustainable Society, POWERTECH 2011, Trondheim, Norway, 19–23 June 2011; pp. 1–8. doi:10.1109/PTC.2011.6019324. [CrossRef]
63. Cagnano, A.; De Tuglie, E.; Dicorato, M.; Forte, G.; Trovato, M. PV plants for voltage regulation in distribution networks. In Proceedings of the Universities Power Engineering Conference, London, UK, 4–7 September 2012; pp. 1–5. doi:10.1109/UPEC.2012.6398422. [CrossRef]
64. IEC International Electrotechnical Commission. *IEC TS 60904-13 Photovoltaic Devices-Part 13: Electroluminescence of Photovoltaic Modules*; IEC International Electrotechnical Commission: Geneva, Switzerland, 2018.
65. ST 500/69/23 | Transformadores para Panel de Control Block, 230V ac, 500VA, 1 salida | RS Components. Available online: <https://es.rs-online.com/web/p/transformadores-de-montaje-en-panel-y-carril-din/7315208/> (accessed on 18 April 2020).
66. LC1D09BL | Contactor 9 A, 3 NA, Bobina 24 V dc, TeSys D | RS Components. Available online: <https://es.rs-online.com/web/p/contactores/4001899/> (accessed on 17 April 2020).
67. HS200 68R J | Arcol | Resistencias Fijas para Montaje en Panel | RS. Available online: <https://es.rs-online.com/web/p/resistencias-fijas-para-montaje-en-panel/6150583/> (accessed on 17 April 2020).
68. Disyuntor 100A NZMB1-A100 | Eaton | NZMB1-A100 | 259079 | Interruptor potencia protección transfo. eibabo.es. Available online: <https://www.eibabo.es/eaton/disyuntor-100a-nzmb1-a100-eb10784156> (accessed on 17 April 2020).
69. Disyuntor 160A XT2N 160 R160 | ABB | XT2N 160 R160 | 1SDA067058R0001 | Interruptor potencia protección transfo. eibabo.es. Available online: <https://www.eibabo.es/abb/disyuntor-160a-xt2n-160-r160-eb17803409> (accessed on 17 April 2020).
70. Disyuntor 250A XT4N 250 EKIP LS/I | ABB | XT4N 250 EKIP LS/I | 1SDA068147R0001 | Interruptor potencia protección transfo. eibabo.es. Available online: <https://www.eibabo.es/abb/disyuntor-250a-xt4n-250-ekip-ls-i-eb12102121?fs=4278333618> (accessed on 17 April 2020).
71. Disyuntor 400A T5N000040E02403 | ABB | T5N000040E02403 | 1SDA054317R0001 | Interruptor potencia protección transfo. eibabo.es. Available online: <https://www.eibabo.es/abb/disyuntor-400a-t5n000040e02403-eb12102118> (accessed on 17 April 2020).
72. Disyuntor 400A NZMN3-AE400 | Eaton | NZMN3-AE400 | 259114 | Interruptor potencia protección transfo. eibabo.es. Available online: <https://www.eibabo.es/eaton/disyuntor-400a-nzmn3-ae400-eb10703722?fs=2659164480> (accessed on 17 April 2020).
73. Disyuntor 1000A 33241 | Schneider Electric | 33241 | Interruptor potencia protección transfo. eibabo.es. Available online: <https://www.eibabo.es/schneider-electric/disyuntor-1000a-33241-eb15803670> (accessed on 17 April 2020).
74. Disyuntor 1000A IZMX16N3-V10F-1 | Eaton | IZMX16N3-V10F-1 | 183333 | Interruptor potencia protección transfo. eibabo.es. Available online: <https://www.eibabo.es/eaton/disyuntor-1000a-izmx16n3-v10f-1-eb17403569> (accessed on 17 April 2020).
75. Fu, R.; Feldman, D.; Margolis, R. *U.S. Solar Photovoltaic System Cost Benchmark: Q1 2018*; NREL: Golden, CO, USA, 2018; pp. 1–47. doi:10.7799/1325002. [CrossRef]
76. EIA. Cost and Performance Characteristics of New Generating Technologies. In *Annual Energy Outlook 2019*; EIA: Washington, DC, USA, 2019; Volume 2019, pp. 1–3.





# Capítulo 3

## **Aplicación de materiales con gran ancho de banda para la mejora de sistemas de electrónica de potencia en Smart Grids**

**RESUMEN:** La transición energética ha conducido a un creciente despliegue de recursos energéticos distribuidos, los cuales, en la mayoría de ocasiones, requieren de convertidores de electrónica de potencia. Un caso particular es el de los convertidores destinados a ambientes urbanos y Smart Grids. Estas aplicaciones requieren de una serie de características que hacen a los materiales WBG particularmente relevantes. En el artículo *Role of Wide Bandgap Materials in Power Electronics for Smart Grids Applications* se analizan las características más destacadas que se esperan de los convertidores de electrónica de potencia de las Smart Grids del futuro. Posteriormente, mediante el análisis de las principales características de los nuevos materiales, se determinan los más apropiados para estas aplicaciones a corto y medio plazo.

## Article

# Role of Wide Bandgap Materials in Power Electronics for Smart Grids Applications

Javier Ballestín-Fuertes <sup>1,\*</sup>, Jesús Muñoz-Cruzado-Alba <sup>1</sup>, José F. Sanz-Osorio <sup>2</sup> and Erika Laporta-Puyal <sup>1</sup>

<sup>1</sup> Fundación CIRCE, Parque Empresarial Dinamiza, Avenida Ranillas Edificio 3D, 1ª Planta, 50018 Zaragoza, Spain; jmunoz@fcirce.es (J.M.-C.-A.); elaporta@fcirce.es (E.L.-P.)

<sup>2</sup> Instituto Universitario de Investigación CIRCE, Universidad de Zaragoza—Fundación CIRCE, Edificio CIRCE, Campus Río Ebro, C/Mariano Esquilor Gómez, 15, 50018 Zaragoza, Spain; jfsanz@unizar.es

\* Correspondence: jballestin@fcirce.es

**Abstract:** At present, the energy transition is leading to the replacement of large thermal power plants by distributed renewable generation and the introduction of different assets. Consequently, a massive deployment of power electronics is expected. A particular case will be the devices destined for urban environments and smart grids. Indeed, such applications have some features that make wide bandgap (WBG) materials particularly relevant. This paper analyzes the most important features expected by future smart applications from which the characteristics that their power semiconductors must perform can be deduced. Following, not only the characteristics and theoretical limits of wide bandgap materials already available on the market (SiC and GaN) have been analyzed, but also those currently being researched as promising future alternatives (Ga<sub>2</sub>O<sub>3</sub>, AlN, etc.). Finally, wide bandgap materials are compared under the needs determined by the smart applications, determining the best suited to them. We conclude that, although SiC and GaN are currently the only WBG materials available on the semiconductor portfolio, they may be displaced by others such as Ga<sub>2</sub>O<sub>3</sub> in the near future.

**Keywords:** wide bandgap materials; power electronics; smart grids; distributed energy resources; technical requirements



**Citation:** Ballestín-Fuertes, J.; Muñoz-Cruzado-Alba, J.; Sanz-Osorio, J.F.; Laporta-Puyal, E. Role of Wide Bandgap Materials in Power Electronics for Smart Grids Applications. *Electronics* **2021**, *10*, 677. <https://doi.org/10.3390/electronics10060677>

Academic Editor: Fortunato Pezzimenti

Received: 11 February 2021  
Accepted: 9 March 2021  
Published: 13 March 2021

**Publisher's Note:** MDPI stays neutral with regard to jurisdictional claims in published maps and institutional affiliations.



**Copyright:** © 2021 by the authors. Licensee MDPI, Basel, Switzerland. This article is an open access article distributed under the terms and conditions of the Creative Commons Attribution (CC BY) license (<https://creativecommons.org/licenses/by/4.0/>).

## 1. Introduction

At present, climate change represents a threat not only to specific regions around the world but to the entire world ecosystem. Therefore, there is an urgent need to deal with this situation and numerous initiatives have been developed to help in the cutting emissions mission [1].

Renewable energies (REs) have a crucial role in helping the world meet its future energy needs. Today, more than 30% of electricity generation in the European Union (EU) comes from renewable sources, whereas in 2000 it was only 12% [2]. In 2017, the EU planned to reduce greenhouse gas emissions during the following decade at least 40% from 1990 levels [3,4]. However this objective has recently been updated and, as part of the European Green Deal, the European Commission proposed in September 2020 to raise the 2030 greenhouse gas emission reduction objective, including emissions and removals, to at least 55% compared to 1990. This objective should be achieved by means of the following key targets: at least 40% cuts in greenhouse gas emissions (from 1990 levels), 32% share for renewable energy and 32.5% improvement in energy efficiency [5].

To achieve the 2030 targets for RE it is necessary to maintain the current growth levels. On the other hand, energy efficiency requires an inverse correlation with the RE need to achieve these targets. If energy efficiency is increased in 5%, the final requirement for the installation of RE will decrease in 7.5% approximately to achieve the same RE goal [3]. Thus, efforts to reduce greenhouse gas emissions made in both ways, RE share and energy efficiency, are equally valuable. Besides, cutting greenhouse emissions could be achieved

by substituting fossil fuel power plants by RE power plants or by means of using RE sources to provide energy to other applications such as heating and transport, leading to a great growth of the energy sector electrification. In the following decades global electricity consumption will increase slightly faster than recent trends but, however, there will be abrupt changes in individual countries and specific locations. These include areas with rapidly expanding residential solar and/or electric vehicles (EVs), and where major thermal generators will be closed [3].

As consumer-scale technologies, such as photovoltaic (PV) and EV, become cost-competitive without subsidies, governments will lose the ability to control rates of deployment. The change can then become rapid, and may also be derived from increased electric heating and better energy management systems (EMSs) for buildings.

Therefore, the incoming electrification of the world makes especially important the role of smart grids. The next generation of smart grids must answer to a scenario with a higher number of devices connected, and with an improved capability of coordination between them. Indeed, this trend has already started. Figure 1 shows a scheme of the future electric grid. On the one hand, utility-scale power plants based on non-renewable sources (red) will be progressively substituted for utility-scale RE plants (green). On the other hand, smart cities will emerge (blue), and a high penetration of distributed energy resources (DERs) is expected, such as micro PV plants, EV, energy storage systems (ESSs), heat pumps, etc.

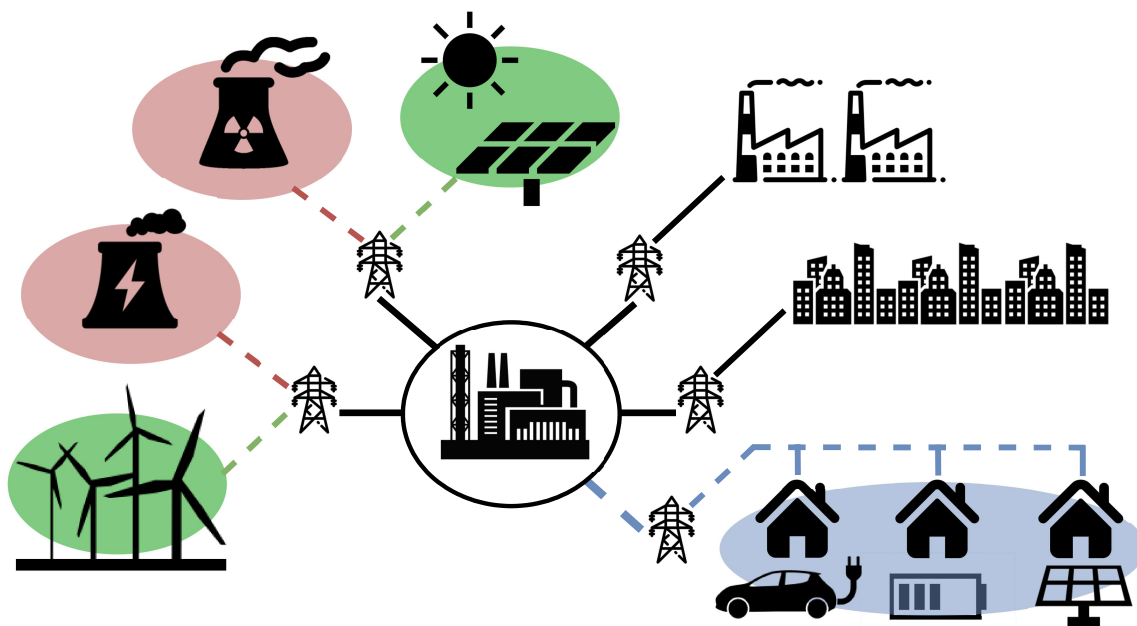


**Figure 1.** Current and future electric grid components: utility-scale non-renewable power plants (red), utility-scale RE plants; large factories and loads (black); future smart grid components such as energy storage systems (ESSs), electric vehicles (EVs), photovoltaic (PV), etc. (blue).

However, the new equipment in smart grids must fulfil several requirements in order to be accepted by consumers and thus help their market penetration: they have to be cost-effective; have a high efficiency (99% or higher); noiseless; reliable; and compact. To achieve these goals, power electronics have to evolve to produce new devices.

Nowadays power electronics products do not comply the requirements exposed above and, therefore, new devices should be developed. wide bandgap (WBG) materials are a series of promising new technologies that try to give an answer to the market needs.

This paper is organized as follows. Section 2 will analyze power electronics applications and requirements in smart grids. For this purpose, the different types of power electronics converters needed by smart grid equipment are studied, the features desired in

this equipment are extracted, and these characteristics are translated into requirements for the semiconductor devices that will make up these power converters. Following, Section 3 will review the current state-of-the-art and future trends of WBG materials in power electronics; focusing on the electrical and physical properties of these semiconductor devices today and developments expected in the coming years, but also paying particular attention to the viability of these products on mass-market applications. Section 4 will introduce the most appropriate figures of merit (FOMs) in order to establish a relationship between the WBG technologies and the most appropriate materials for smart grid applications. Finally, Section 5 will present the most important conclusions of the study.

## 2. Applications and Requirements

Not all power converters are designed for the same type of applications. Besides, other considerations like communications capability or active and reactive power range, leads to particularities making them suitable for different uses. Table 1 establishes a classification of power converters in which only types 2, 3 and 4 are suitable for integrating DER into the smart grid. Following, each type is described briefly:

- Type 1 is usually power converters with a power rating lower than the following types. Moreover they do not have communications with external devices to provide them with the capacity to manage their demand. Thus, type-1 converters are fully controlled by the load or RE. Some of these devices cannot control their reactive power injection while others add a power factor correction (PFC) stage [6,7]. The PFC allows to regulate the reactive power output and cancel it. Some examples are mode-2 EV chargers and micro PV and wind generation.
- Type 2 is similar to type 1 but they also include a communication link that allows an external element to limit the power consumed or generated in order to allow demand management tasks. A typical example of this devices are large EV charging facilities with demand-side management systems.
- Type 3 adds some features to provide grid support tools; giving the possibility to regulate the active and reactive power, among others, in order to provide ancillary services to the grid [8,9]. This group include vehicle to grid (V2G) EV chargers and large wind and PV plants.
- Type 4 introduces, compared to type 3, the possibility of an independent control of the power references for each phase, giving the capability of providing additional grid support against unbalanced scenarios [10].

Table 1. Power converter classification.

Type	Grid-Conditioned Communications	Active Power Control	Reactive Power Control	Topology	Examples
1	No	No	No	single-phase three-phase	Mode-2 EV charger; PV/wind generation
2	Yes	Yes	No	single-phase three-phase	Mode-3/4 EV charger; PV/wind generation
3	Yes	Yes	Yes	single-phase three-phase	V2G EV charger; PV/wind; BESS
4	Yes	Single-phase control	Single-phase control	four-wire	Unbalanced-load grid support

As described previously, type 2, but especially 3 and 4, allow the implementation of advanced functionalities in order to provide new services for a better management and regulation of the power grid. Consequently, they are important features to speed up the penetration of DER in urban environments. Following, some of the most interesting functionalities developed recently for power converters are explained. However, new behaviours could be implemented if future grid codes require them.

- Voltage and frequency disturbances clearance: nowadays, grid codes establish some voltage and frequency curves in which voltage and frequency disturbances are related to a specific clearing time [11]. Grid codes ask for a safety disconnection if the disturbance lasts longer than the specified time; the objective is to guarantee the service and prevent a system blackout. On the other hand, the contrary is asked in some cases too; a disconnection previous to the maximum clearing time, in order to restore the stability of the system before its disconnection.
- Active power curtailment and slew rate: these two features help to mitigate grid instabilities due to load imbalances [12,13]. On one hand, a remote control signal to the DER imposing a maximum power reference will prevent the system of over production. On the other hand, a predefined active power slew rate guarantees a smooth starting, giving the whole system enough time to react consequently. This is especially useful after the clearing of faulty conditions, when a whole section of the system could start simultaneously to maximum power. Moreover, thanks to the advancement in communications on power converters, coordination techniques for a distributed starting could be implemented.
- Synchronism emulation curves: due to inertia, frequency disturbances produce a response in the active power output of the synchronous generators that mitigate this effect. However, power converters used for DER do not have such behaviour. They can regulate its output independently of frequency. Therefore, recent Minimum Technical Requirements (MTRs) are establishing a new concept called as synthetic inertia. The power plant is configured with an active power curve in function of frequency measurement [9,14]. In addition, some active power reserves could be asked to in order to increment the production over the nominal value in case of sub-frequency disturbances [12].
- Voltage regulation: grid codes usually include V-Q curves in order to define a criterion for DER. In the past, MTRs used to define the reactive power injection needed for a determined voltage deviation. However, nowadays recent grid codes define it as an increment because the utility grid usually sends also a reactive power reference to the converter [11]. Furthermore, power converters could be connected to the grid even there are not the needed conditions for power generation. In such cases, the power converter could be used as a static synchronous compensator (STATCOM), in order to inject reactive power and help the utility grid in its task.
- Anti-islanding techniques: the islanding phenomenon has been discussed widely in the literature, and there is a wide range of anti-islanding techniques to be implemented in power converters. The objective is to introduce a control algorithm that determines whenever the inverter is working in an undesired island condition that could produce hazards and damage in equipments, and proceed with a safety disconnection procedure [8,15–17].
- Low voltage ride through: some of the most common requirements present in grid codes for DER are the low voltage ride through requirements. Grid codes require of power converters to remain connected if the fault is not long enough and to help the system regulating the active and reactive current output of the converter conveniently [18].
- Black-start: black-start capability consists in the availability of power converters to restore by themselves the electric grid power supply without the need of the intervention of any central synchronous generator [19,20]. This feature is possible thanks to the development of grid-forming control strategies, in which the power converter works as a voltage source instead of a current source by different techniques: droop-based control, virtual synchronous machine, or power synchronization [21]. They are not asked in any grid code up to date, but actually, it has been discussed widely inside working groups to include it in the future.
- Controlled island operation: the opposite of anti-islanding techniques, controlled island operation tries to hold a micro-grid energized after an opening of the point

of common coupling. This has to be perfectly known by the utility grid in order to avoid hazards and its purpose is to prevent an unjustified cut of the power supply of the micro-grid. As well as with black-start feature, grid-forming control strategies are the way to achieve this goal [20].

The new range of functionalities that could be implemented by the new generation of power converters are specially useful for power electronics applications in urban environments. Following, some of the most promising applications are described briefly in order to determine in which aspects and requirements the efforts of the power converters design must be focused on:

- **Micro-PV:** Regarding urban use-cases there are three technologies of inverters with different features and cost: string inverters, microinverters, and optimizers. Within the systems designed for applications in urban areas we can differentiate two categories, commercial and residential. Commercial applications are characterized by offering a range of power that in most manufacturers covers from 10 to 100 kW. On the other hand, residential systems for connecting to the grid are from 1 to 10 kW. Within the residential inverters we find characteristics such as multi maximum power point tracking (MPPT) input, storage ready, EV charger integrated, built-in Revenue Grade Meter, additional power supply input, or network connectivity [22,23]. Commercial grid-tied inverters include features as seamless switchover, prioritize self-consumption of renewable sources or stored battery, support large loads to avoid grid peak usage, efficient fast charge, scalable battery reserve, embedded controls for sell surplus generation or curtail the production, integrated reactive power regulation functions, multiple MPP trackers, WLAN or Wi-Fi access for system monitoring and control functions [22,23].
- **EV charging systems:** Nowadays there are four modes of EV charging systems defined by the IEC [24,25]. Mode 1 and 2 correspond to slow charging modes, making a direct connection between grid and vehicle via household socket-outlets. On the other hand, modes 3 and 4 correspond to smart charging modes, providing a communication link to control the active power charging reference. Currently, EV is a technology with an extremely high growing rate, and their penetration rate into the distribution grid will be high in a near future [26].  
Nowadays, mode 4 fast chargers in publicly available outlets are replacing slow chargers, due to the necessity of short charging times in stops during journeys: up to 50 kW and/or with vehicle to grid (V2G) functionality [27–29]. Moreover, recent efforts to bring into the market commercial ultra-fast chargers up to 350 kW, and 500 kW are being made [30–32].  
In addition, current research projects [33] lead the integration to a new stage, providing load-balancing techniques over charging points and, therefore, contributing to grid stability [34]. Finally, other research activities look for a final integration of load balancing over buildings, leads to an optimization of the available distributed resources and needs (demand, generation, and energy storage), as well as contributing to the grid stability [35].
- **Battery energy storage systems (BESSs):** BESSs are a key service in the new concept of electric power grid and to provide flexibility in a wide range of scenarios. The evolution of the technology associated to batteries has led to the development of a new generation of very competitive batteries, reducing both cost and volume. Therefore, BESS are growing at tremendous rates nowadays, by the hand of the EV market [26]. Growth in privately owned non-utility energy storage is driven by two primary factors. The first is regulatory initiatives that incentivize non-utility ownership of storage. The second is self-interest, i.e., profit from the use of BESS [36]. A new brand of products have appeared in the market just since a few years back related to domestic BESS [37,38]. The current state-of-the-art has allowed affordable, robust and compact designs able to be installed in most buildings and houses, developing a cutting-edge technology ready for a widespread across the entire electric power grid. Besides,

thanks to the technology improvements and cost reduction of the massive irruption of the EV market [26], nowadays its use as ESS is affordable. In addition, second-life applications could be an interesting low-cost alternative to facilitate the penetration of DER in the near future [39].

Urban BESSs offer a variety of services (peak shaving, load shifting, emergency back-up and demand response) related to flexibility needs in smart grids [40]. This is due they are usually associated with PV generation with a link through alternating current (AC), where both AC outputs are connected to the same house, or direct current (DC), in which case they share a common DC bus. Consequently, BESS can regulate the total power generation/consumption of the building, with available commercial models from up to 15 kW. However, manufacturers usually offer modular solutions in order to scale the product up to the needs of clients [38].

Finally, BESS are being studied under another perspective too. Recently, there are some efforts to develop distributed BESS into the low voltage distribution grid. The objective is not only to provide a device able to adjust the load curve of the grid, but also to deliver ancillary services typical of flexible alternating current transmission systems (FACTS) and to correct active power unbalances between phases to avoid overloads and overheating [41], becoming an interesting tool for distributed system operators (DSOs).

- Energy routers and Distribution (D-)FACTS: The introduction of BESS and small prosumers in the electric grid have changed the unidirectional power flow of a typical power grid. Currently, scenarios with a high penetration of BESS, EV and DER must consider the possibility of bidirectional power flows in the low voltage distribution grid. Consequently, new devices have appeared to optimize the response in such circumstances, substituting current conventional transformers located in the final part of the grid. The main objective is to regenerate the signal and to hold the voltage at its nominal value, in order to avoid disturbances in the consumers, as well as providing other functionalities such as power flow control, total harmonic distortion (THD) reduction, and voltage and frequency regulation and communications [42–44]. Besides, other initiatives [45] are developing special designed D-FACTS for a high share of renewable energies scenarios. Such devices are able to inject reactive power to help in the voltage regulation issue and, at the same time, help the system with low voltage ride through issues, mitigate low order harmonics, and they are able to redistribute active power between the power-line phases in order to avoid overloads.

Summarizing, some conclusions about the power converters requirements could be extracted from the applications and features exposed above:

- Breakdown voltage values of 1200 V will be enough for most low voltage urban applications. Therefore, achieving higher voltages in bidirectional devices is not a priority for this specific use-case.
- The size of power semiconductors will not be relevant either. Their size is small regarding the complete size of the converter, where the heatsink and the passive filters are the most bulky parts.
- The size of the passive components will have a strong importance, and high switching frequencies will be required to reduce them.
- To get compact designs, is mandatory to reduce or remove completely the cooling systems. Consequently, a key design parameter will be to get devices able to hold high working temperatures and with good behaviour respect to thermal conductivity.
- Reducing conduction and switching power losses will improve the efficiency and help to reduce the necessities of the cooling system.
- Power electronics devices must be inaudible in order to avoid discomfort in the final users.
- Devices should fulfil requirements respect to electromagnetic compatibility (EMC) and electromagnetic interference (EMI). Power semiconductors are devices with fast

and abrupt transients and, therefore, are typically a source of problems regarding this issue if they have not been carefully designed [46].

- Finally, as it happens with any domestic product, the manufacturing of huge volumes require both: the use of available and affordable raw materials; and the use of cheap and reliable manufacturing process.

### 3. WBG Materials

Power electronics equipment is manufactured from semiconductor substrates, being silicon (Si) the most commonly used today. Si is a mature technology that has been present for power control applications since 1950s. However, the performance of Si-based power switching devices is reaching its theoretical limits [47]. The main limitations of Si-based devices are high power losses, low switching frequency and poor high-temperature performance. However, a new group of advanced materials known as WBG promises to satisfy DER integration needs, as well as to meet new requirements of urban areas to support the incoming electrification of society. Among others, silicon carbide (SiC), gallium nitride (GaN), diamond, gallium oxide (Ga<sub>2</sub>O<sub>3</sub>), aluminium nitride (AlN), boron nitride (BN) and zinc oxide (ZnO) exhibit better characteristics as semiconductors than Si, and they become in a promising choice for next generation of power conversion systems.

While high switching frequencies could be reached by unipolar devices like metal-oxide-semiconductor field-effect transistors (MOSFETs), they can only provide low rated voltage and current capabilities. However, bipolar Si semiconductors enable high power conversion devices but operating at a relative low frequency. Therefore, larger passive components are required, incrementing the size and weight of power converters. Besides, several applications with high constrains about weight and volume such as automotive, motor drives, aerospace, and power supplies have requirements outside the limits of Si, asking for new solutions to be developed.

WBG materials have demonstrated to be an attractive solution to Si limitations providing powerful characteristics as shown in Figure 2. For instance, they offer a higher electric breakdown field that enable greater voltage blocking capability, thinner layers, and allows deeper doping concentration. Therefore, it results in lower conduction losses and a low drift resistance. Thus, an on-resistance reduction in comparison with Si-based devices. In accordance, same on-resistance WBG can have smaller area implying less capacitance. Likewise, less capacitance and a high saturation drift velocity allow higher switching speeds and lower losses per switching cycle [48]. Additionally, the low intrinsic carrier concentration of WBG materials enables reduced leakage currents and robust high-temperature performance [49].

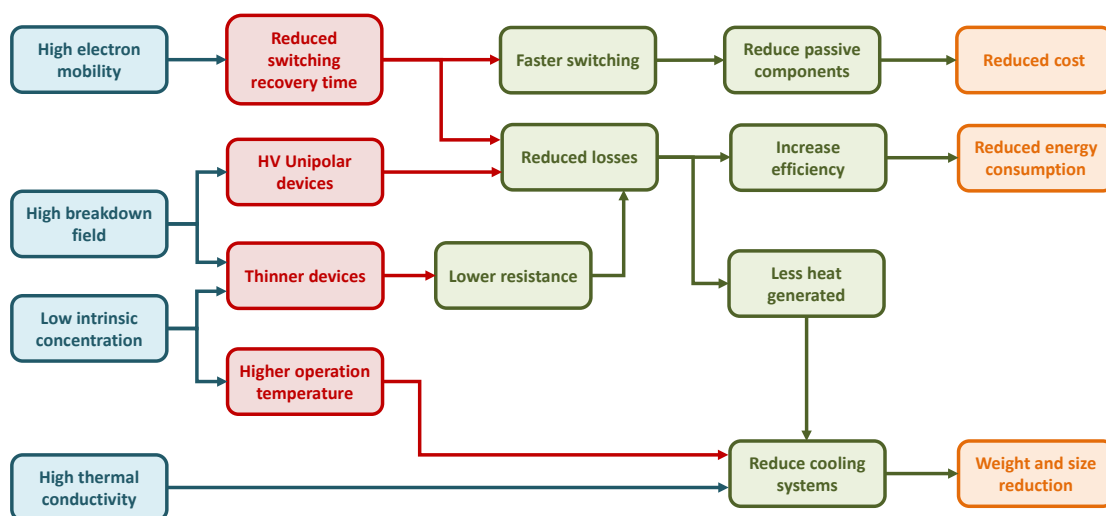


**Figure 2.** WBG semiconductor parameter capabilities (blue); physical properties affected by WBG advantages (red); power electronics characteristics (green); and product benefits (yellow).

As Figure 2 shows, all these features of WBG materials translate to high level output power equipment an improved efficiency, reduced system size, weight, and cost [50]. Low switching losses allow WBG semiconductors reaching efficiencies up to 99%. This means up to 75% energy losses reduction compared with Si devices [51]. Moreover, higher switching frequencies can be reached too. Frequencies higher than 20 kHz have not been possible in power levels of more than tens of kilowatts because of Si limitations so far; therefore, WBG materials allow simpler circuit topologies by reducing size and number of passive components (capacitors, inductors) [52] and offer a better output quality.

### 3.1. SiC

#### 3.1.1. SiC Technology Evolution and Future Trends

Since 1987 SiC has experienced a great development, being currently the most mature of all WBG materials [53,54]. SiC is a crystalline compound of equal parts of carbon and Si; providing more than 170 different polytypes, *4H-SiC* is the most interesting regarding power electronics applications due to its high carrier mobility, particularly in c-axis direction, and its low dopant ionization energy [55].

Due to its higher capabilities, it offers an electric-field breakdown voltage ten times higher than Si. In addition, high thermal conductivity and resistance make SiC useful in high power and temperature applications (up to 350 °C) [55]. Besides, Si is the second most abundant element in Earth crust, actually about 27% of the crust is composed of this material [56]. Its availability makes SiC an extremely attractive alternative to Si, as there is no lack of raw materials as it happens with other WBG choices.

Thanks to the development of SiC epitaxial wafers to form homoepitaxial SiC layers on SiC substrates, the SiC manufacturing technology has grown significantly in the last decades [57]. Moreover, the optimization of epitaxial and bulk processes in *4H-SiC* has made possible to decrease the crystallographic (dislocations and stacking faults) and surface defects (at triangles, carrots, comets, pits), up to values of 0.1 cm<sup>-2</sup> in surface defects density (dislocations), as well as zero micropipe defects [58]. Consequently, the advancement of SiC technology has allowed the increment in SiC wafer size along the last two decades. Nowadays, 150 mm wafers are commercially available, while 200 mm wafers were demonstrated in 2015 and currently there are some commercial examples [58].

The first SiC wafer was developed commercially in 1993, and thanks to its high voltage capacity, it has been applied to a wide range of different power devices. For instance, high-voltage trench U-shape MOSFET (U-MOSFET) of 1.4 kV, lateral 2.6 kV implanted depletion-type MOSFET (D-MOSFET) have been demonstrated since 1997 and, on the other hand, 1.8 kV and 4.5 kV vertical junction field-effect transistors (JFETs) (1998–2000). Besides, in 1999 positive-intrinsic-negative (PIN) diodes were developed with a blocking voltage of 8.6 kV (1999), Junction barrier Schottky (JBS) diodes with a blocking voltage of 3.6 kV, and SiC-Schottky Barrier Diodes (SBDs) with a blocking voltage of 4.9 kV [54]. In addition, bipolar devices as 27 kV PIN diodes [59], 2.6–15 kV gate turn-off (GTO) thyristors (1999–2013) [60,61] and SiC insulated-gate bipolar transistor (IGBT) have been experimentally demonstrated. In the same way, SiC modules (SiC MOSFETs with SiC Schottky diodes) prototypes have been presented with a blocking voltage of 6.5 kV/200 A [62] and 15 kV/10 A [63]. Due to the new features of SiC technology, new packaging designs have been implemented for SiC devices to allow: high-temperature operation, weight and size reduction, and the minimization of parasitic capacitances and inductances. Nowadays, on the one hand, available SiC products use packaging techniques that allow operating temperatures up to 210 °C. On the other hand, 1200–1700 V modules produce parasitic inductances lower than 5 nH, even with models up to high rated currents [52].

The SiC power electronics market is small compared with Si these days but, nevertheless, due to the dramatically cost reduction made during the last decade, and the increasing demand and market availability, a substantial growth is forecasted. In the following years, applications such as PFC, power supply, and PV inverters seem to go on adopting SiC

technology progressively. Nowadays, Tesla is using SiC MOSFETs for its main inverters in the Model 3 and other automakers are evaluating the potential benefits of this technology for their futures EV [64]. In this way, the fast development and penetration of the EV market will contribute to a faster rise during the following decade.

In addition, SiC devices have been available in the market since 2001 with the introduction of the first SBD. In the last two decades, a commercial range of available devices have break into the market such as SiC unipolar diodes and SiC MOSFETs, that can reach breakdown voltages up to 1700 and 3300 V, and current handling capabilities up to 750 A, and some manufacturers are working on a next generation of 6500 V devices [62].

The next step in the advancement for cost reduction is the announce of 4H-SiC 200 mm wafer manufacturing [65]. However, most SiC manufacturers are still doing the transition to 150 mm epitaxial wafer. The incoming generation of 200 mm diameter wafers coupled with a decrease in defects density forecasts that the cost of SiC MOSFETs will drop to become competitive with Si devices. However, the transition will be slow, as it happened with the previous transition from 100 mm to 150 mm wafers.

Consequently, market analysts common conclusion is that SiC technology value for power electronics applications will grow from \$250 M to \$1.4 billion in 2022, and it will accelerate raising to more than \$10 billion before 2027 [66].

However, SiC must not only solve the high device cost and lack of maturity but, it has also to face technical challenges at all levels, including issues related to device performance, module integration, packaging, and the need to define qualification standards. One of the most important challenges that several studies are currently looking for a solution to is the carbon cluster formation in the SiC/SiO<sub>2</sub> interface [67]. Some studies have shown that the formation of carbon clusters in SiC-MOSFETs can cause a reduction in field-effect mobility of up to 100 cm<sup>2</sup>V<sup>-1</sup>s<sup>-1</sup> [68].

Summarizing, SiC semiconductor technology has advanced enormously from the last three decades but, however, considerable efforts are still needed to achieve the full potential of this material. SiC has challenges to deal: performance, reliability, cost, manufacturing process, filter and thermal designs, system layouts, etc. Therefore, the market penetration of SiC technology is increasing but it is still limited to specific applications.

### 3.1.2. SiC Advantages and Disadvantages

Following, SiC main advantages are summarized:

- High efficiency: SiC semiconductors have lower switching power losses than Si devices. This feature allows getting efficiencies above 99.5%. This meant up to 75% energy losses reduction [69].
- Higher switching frequency operation: SiC allows to work at higher switching frequencies of operation than Si without increasing significantly power losses. Thus, units based on SiC reduce the size of passive components, decreasing the device size, weight and cost.
- High level of output voltage: due to their higher electric breakdown field, SiC-based devices can reach higher operation voltages.
- Withstanding high temperatures: SiC-based devices can handle up to 600 °C, while Si-based devices can operate at maximum temperatures of 175 °C.
- Higher thermal conductivity: SiC has 4.5 W/cm·K, therefore it has three times more thermal conductivity than Si. Besides, SiC power devices have a lower junction-to-case thermal resistance (0.02 K/W for SiC and 0.06 K/W for Si). It implies lower cooling requirements and, therefore, smaller and cheaper cooling systems.
- Higher reliability: forward and reverse characteristics of SiC power devices do not vary significantly with temperature and time.
- Component reduction: when replacing Si devices or by reducing active and passive components in both size and number [70].
- Short-circuit withstanding: traditional Si devices have short-circuit withstand times greater than 10 μs, SiC MOSFETs have a typical short circuit withstand time on the

order of 1  $\mu\text{s}$ , but recent research reports SiC MOSFETs at levels higher than 3.3 kV having developed enhanced short circuit capability [71]. Thus, it benefits voltage source base high power conversion systems, giving reliability to SiC MOSFETs by demonstrating being capable of sustaining short-circuit currents up to 13  $\mu\text{s}$  [52].

Many of these advantages are not yet mature and require further development; likewise, SiC technology have some challenges, such as those presented below, that need research and development to accelerate SiC adoption.

- High cost: reducing the cost of SiC is a key to accelerate its adoption. Currently SiC MOSFET plus SiC diode is significantly higher than Si IGBT plus Si diode [72].
- Packaging: this is the primary constraint for the performance of SiC. The advantages of SiC are not being realized when devices are embedded in traditional packages designed for switching at lower frequencies; they must be designed with a symmetrical layout to minimize loop inductance and be more thermally efficient. In addition, the carbon cluster issue must be faced.
- Availability: the availability of SiC devices is limited, there exist only a few wafer suppliers. Despite the investments in expanding production capacity, there is a short SiC wafer supply situation.
- Gate drivers: high-performance gate drivers are required to manage the switching speed of a SiC device. Fast fault response time is needed to protect SiC devices against short-circuits.

### 3.2. GaN

#### 3.2.1. GaN Technology Evolution and Future Trends

GaN has been used in light-emitting diodes (LEDs) and radio devices for decades and, since 2000, has become an interesting option in power applications. GaN bandgap is slightly higher than SiC, and both have a similar breakdown voltage, although its most attractive feature is its high electron mobility which allows high switching frequencies. On the contrary, GaN low thermal conductivity, similar as Si, can be a significant problem in high power applications [55]. GaN devices are limited to 650 V, 150 A in the portfolio of most manufacturers [57,58] but, nevertheless, some studies have shown the development of 1200 V devices [73]. Moreover, some studies expect that GaN on Si semiconductors will achieve price parity with Si devices at the same performance shortly [61,62].

All these characteristics make GaN a promising alternative to substitute Si devices for high-frequency applications, for instance in resonant converters [74]. However, manufacturing of practical devices of this material is challenging. Si and SiC devices use vertical structures; vertical structures for GaN could take the most significant advantage of the superior material properties. Nevertheless, there is a limitation for vertical GaN device manufacturing due to the lack of availability of high quality and low-cost GaN wafers. Accordingly, commercial GaN devices are lateral heterojunction field effect transistors, known as High Electron Mobility Transistors (HEMTs).

Manufacturing of GaN wafers is made through epitaxial growth on GaN substrates. However, due to it is an expensive technique, only a small wafer diameter can be reached by this technique. Heteroepitaxial growth of GaN in different material substrates such as Si (GaN on Si), SiC (GaN on SiC) and sapphire have been carried out [75], choosing Si as the most attractive for commercial applications due to the large-size scalability of inexpensive Si substrates.

Following, a more detailed description of the different power devices developed with GaN is shown.

- Mature: GaN technology is mature in optoelectronics and radio frequency applications (low voltage). On the other hand, GaN-based devices for medium to high voltage power conversion applications are expected to grow significantly in the near future. Therefore, they will probably be ready for an upper scale deployment in the next decade.

- Market: with less than five years in the market, lateral enhanced mode GaN and cascade 600–650 V GaN HEMT devices are available from a dozen of suppliers, and the most recent 900 V GaN HEMT devices and 1200 V/180 A GaN modules are available from a couple of suppliers too.
- Prototype: three suppliers have announced prototypes of 1.2 kV GaN HEMT devices and are expected to be commercially shortly.
- Research: research on GaN power devices has grown exponentially since 2010 and numerous vertical devices as 1.2 kV GaN Schottky blocking diode, 3.7 kV GaN pn-diode [76], 1.5 kV JFET diodes, and GaN transistors with breaking voltage up to 2 kV have been demonstrated. Lateral devices as GaN transistors up to 3.5 kV, Polarization Super Junction (PSJ) GaN FET beyond 3 kV, flexible GaN chips [77], and GaN nanowire metal-semiconductor field-effect transistors (MESFETs) have also been reported experimentally.

Due to the particular characteristics of GaN some issues require efforts in R&D to exploit the full potential of this technology. In the case of achieving high switching frequencies, integration is critical. Active devices as transistors, flyback diodes, rectifiers or drivers can be monolithically integrated to reduce parasitic elements, in order to reach high-performance converters with a reduction over the system cost [78]. Other important aspects to take into account are the implications of the higher power density. GaN HFET area-specific on-resistances are two orders of magnitude smaller than Si-based lateral devices [76]. This considerable reduction in size of GaN devices requires to optimize process and packaging to improve thermal dissipation. Moreover, the worse threshold voltage stability of D-mode metal-insulator-semiconductor (MIS) HEMTs and E-mode MIS-FETs is one of the most important challenges [79], being one of the most discussed issues in the literature [80–86].

GaN-based power devices have similar prices than SiC-based devices for the same characteristics [87,88]. A lower price in GaN devices is possible because they can be developed on Si substrates that are readily available and incur fewer cost than SiC development process. Hence, the cost of GaN power devices is no longer a key driver in system cost. Therefore, efforts must be focus on volume production and research to achieve manufacturing maturity and reliability [89]. Meanwhile, analysts forecast a parity in price per ampere for GaN on Si based devices comparing with Si-based devices to be achieved shortly.

Nowadays, GaN on Si technology is the industry standard for wafer diameters up to 150 mm (6"). Low-voltage applications of GaN lateral devices up to 650 V based on 150 mm wafer are in the market since 2014, and recently 900 V GaN devices have been released by TransPhorm-Fujitsu [90]. After enabling 200 mm GaN on Si wafer different suppliers as Exagan, VisIC and Powdec have announced 1200 V lateral GaN devices shortly [91]. Moreover, Imec recently announced the development of high-performance enhancement-mode p-GaN power devices on 200 mm (8") QST<sup>®</sup> substrates. This fact will enable commercial vertical GaN power devices suitable for high voltage and high current applications (1200 V and beyond) [92].

As mentioned above, breakdown strength and electron mobility allow designing smaller devices. Additionally, the high-frequency operation and lower switching losses allow reduction in size and number of magnetic and passive components. Initially, commercially available GaN-based PV inverters (2013) reduced size in 40% respect the Si-based inverters [93]. Furthermore, these inverters did not need a cooling fan and had a considerable reduction in weight too. A few years later, the Little Box Challenge (2016) presented a 2 kW PV inverter with a power density of 8.8 W/l [53], this single phase GaN-based inverter was more than 10 times smaller in comparison with commercial Si inverters. Currently, a lot of research is being carried out in order to develop more power density GaN-based inverters at commercial levels.

Bidirectional converters for high power and EES will be crucial for the future grid and, as well as SiC, the adoption of GaN in power electronics enables the integration of DER into the grid. High frequencies GaN-based grid-tied inverters generate less grid distortion,

allowing applications that require connecting many inverters to the same grid. A prototype of three phases 8 kW inverter have been presented by Siemens and Texas Instruments with efficiencies of 99% [94], and ensuring easy manufacturing, while reducing cost and system size.

GaN and SiC offer a similar price for low-power semiconductor devices. Given its higher electron mobility, GaN have a place in small high-frequency products as on-board EV chargers or micro PV inverters. However, due to its lower power capability and thermal conductivity SiC will be preferable in larger power products [95,96]. Therefore, a rising demand for GaN high-frequency devices is expected. However, lack of availability of GaN material restrains the growth of the GaN power device market. The global market value for GaN power devices was estimated at 16 million in 2016, and different analysts forecast a significant compound annual growth rate around 49.8% and 79% to reach between \$273 and \$460 million by 2022 [97,98]. Power supply application will be the segment with more importance (50% of total market), and automotive and PV will sum 25%. of market share.

### 3.2.2. GaN Advantages and Disadvantages

The basic material properties of GaN offer a number of valuable advantages for power electronics applications, as shown below:

- High dielectric strength: this allows smaller devices for a given breakdown voltage requirement.
- High operating temperature: GaN has a theoretical maximum operating junction temperature above 400 °C.
- High switching frequency: higher electron mobility of GaN allows higher operation frequency than both Si and SiC. Some latest-generation GaN-based devices can operate in the hundreds of MHz, allowing downsize magnetic and passive components.
- High current density: due to higher carrier density and increased electron mobility, higher currents are possible with very low parasitic capacitance.
- Lower on resistance: due to its low on-resistance, lower conduction losses are achieved so that, GaN-based devices have efficiencies up to 99%.

Even though GaN has superior characteristics than Si, this technology is under development and has some challenges that must to be addressed. Below, some of them are detailed:

- Poor thermal conductivity: GaN has poor thermal conductivity compared to SiC and other WBG.
- Parasitic, packaging, controllability: due to tighter gate voltage margins compared to Si and SiC devices, the influence of parasitic inductances can lead to the device destruction and leg short circuits [77].
- Electromagnetic Interference (EMI): due to high switching speed, GaN-based devices enable higher power densities but require additional EMI filters.
- Reliability: long-term reliability qualification standards of these devices have been developed only recently.

## 3.3. Diamond

### 3.3.1. Diamond Technology Evolution and Future Trends

Diamond is well known for being an exceptional material. Actually, it has superior physical properties respect to all WBG materials. Due to its high breakdown field, high thermal conductivity, high electron mobility and low dielectric constant; diamond-based power devices are expected to considerably reduce both switching and conduction losses for high power and high-temperature applications. Initial research about the use of diamond for switching applications began in the 1980s, using natural diamond crystals, but obtaining poor results due to geometrical problems. Synthetized electronic grade single crystals became commercially available after the establishment of epitaxial growth by chemical vapor deposition (CVD) in the 2000s. Since then, there has been an increase in diamond

power-device studies. However, diamond devices are still in the research phase, and they are not commercially available yet.

Historically, the practical application of diamond devices has been constrained by the lack of availability of single crystal wafer with large size, dislocation free, and low resistivity. Contrary to the other WBG materials, no significant advances in diamond wafer size have been seen in three decades. However, different approaches have been developed to enable both larger and relatively low defect density ( $<10^5 \text{ cm}^{-2}$ ) substrates [99]. Firstly, high-growth-rate CVD has made possible to prepare  $15 \text{ mm} \times 15 \text{ mm}$  substrates. Another approach to obtain large area substrates is mosaic wafer fabrication method. By this technique, several plates of approximately  $1 \text{ cm}^2$  single crystal diamond are synthesized by combining the high rate homoepitaxial growth of CVD diamond and subsequent a lift-off process using ion implantation [100,101]. Through this technique plates, up to  $50 \text{ mm}$  have been reached and are commercially available [102,103].

Another significant advance has been efficient doping. Doped diamond layers are generally prepared by gas-phase doping during plasma-enhanced CVD growth on single-crystal diamond substrates. In the past decade, substantial progress has been made in p-type doping with boron, and just in the last few years, n-type doping with phosphorus has been demonstrated at a few laboratories [99].

These two advances, large area substrates and efficient doping, have allowed the development of diamond power devices with better results. For instance, a diamond-based SBD with up to  $10 \text{ kV}$  of breakdown voltage [104], and a bipolar junction transistor (BJT) with a breakdown voltage of  $1 \text{ kV}$  [99] and forward current density greater than  $500 \text{ A/cm}^2$ .

As discussed before, diamond for power conversion technology is in a very early development stage. Therefore, most of the upcoming advances will be to accelerate the development of diamond for power electronics, in order to advance in the Technology Readiness Levels (TRL) scale. Hence, most of the actions will be aimed to overcome several challenges for the practical application of diamond devices.

Despite the improvement achieved in diamond devices performance due to homoepitaxial growth and doping control techniques, the lack of device fabrication techniques still limits a full technology development. Diamond devices need new processing techniques to form edge-termination structures to take advantage of all semiconductor properties; especially selectively doped substrates using ion implantation or selective area growth, together with metal-oxide-semiconductor (MOS) structures. Additionally, a deeper understanding of interface and defect structures are necessary in order to improve both, device fabrication and performance [105]. To operate at high-temperature, high-voltage and high-frequency, packaging technology must advance to allow full diamond potential exploitation. As well as the challenges facing SiC and GaN devices, packaging technology with the suitable material, thermal, and electrical properties must be developed, but with even more stringent requirements for temperature and electrical performance [99].

There is a joint effort of governments and companies to promote the device research at companies and universities. For example, ambitious projects as GreenDiamond has the objective to develop the first high power electronics device ( $6.5 \text{ kV}$ ,  $10 \text{ kV}$  and then  $20 \text{ kV}$  MOSFETs) based on diamond and build up the first power converter using diamond devices [103]. The project has tried to use  $2 \text{ inches}$  diamond plates and packing material to support  $300 \text{ }^\circ\text{C}$  [103]. Other projects with similar objectives are under progress too [106,107].

The main target application for diamond devices is high voltage and high power applications. These applications require vertical device structure and a corresponding diamond wafer to achieve a device over  $100 \text{ A}$ . In order to reach these high voltages and high currents levels, a  $6\text{-inch}$  wafer is a target. However, according to research roadmap for diamond technology, it will not be available until 2030 [108].

In conclusion, the diamond power market is in the emerging stage and the cost of diamond materials is exceptionally high compared with its counterparts. The adoption of diamond for power devices manufacturing has been limited due to the high cost of

diamond wafers. As a result, low demand is expected in the short term and no investment in fabrication facilities is expected. There is a growing challenge regarding high investment cost principally in synthetic diamond production and the process equipment to support its production [109].

### 3.3.2. Diamond Advantages and Disadvantages

Diamond intrinsic properties offer an alternative to current semiconductors with more potential benefits for high power applications. Some of the most important characteristics of diamond as a power semiconductor are presented below.

- High switching frequency: diamond-based devices may have faster switching and lower losses compared with the other technologies as has been partially demonstrated by SBD [110].
- High-temperature operation: diamond has the highest thermal conductivity known for any semiconductor material (five times better than copper, 15 times better than Si) and low thermal expansion. This property allows diamond devices more heat to dissipated, operate at higher junction temperatures than other technologies enabling applications without cooling systems. Thereby, a diamond-based diode has been demonstrated to operate at 1000 °C [111].
- Radiation hardness: thanks to the high atomic displacement energy (42 eV/atom) and low atomic number, diamond can demonstrate a higher stability to radiation than other solid state materials [112].
- High output power: diamond has higher electric breakdown field than both SiC and GaN materials. Therefore, diamond has the ability to isolate massive voltages with a small fraction of the material required compared to current technologies. For example, the amount of diamond needed to isolate 10 kV is 50 times lower than the required for Si [113]. theoretically, a single diamond power device could switch power at voltages approaching 50 kV [114].
- Composition: diamond is a solid form of carbon that can be synthesized by CVD process into a single crystal to be used for electronic devices; hence it is free from natural resources depletion problem.

In spite of all the advantages of using diamond for power electronics, some disadvantages have to be overcome before the technology could achieve a commercial level. Following this, the main important issues are pointed out:

- Maturity: using diamond for power electronics is still in the research and development phase. Further research about the designing and processing stage is needed to obtain diamond's full potential.
- Cost and availability: due to its incipient development, processing problems have not been solved yet. There is not a reliable technique to produce the desirable wafer size and diamond-based devices in mass at affordable commercial costs.

## 3.4. Ga<sub>2</sub>O<sub>3</sub>

### 3.4.1. Ga<sub>2</sub>O<sub>3</sub> Technology Evolution and Future Trends

Gallium (III) oxide, commonly called gallium oxide, has emerged as a new semiconductor material for power electronics devices. Whereas Ga<sub>2</sub>O<sub>3</sub> has been reported since 1952 [115] and was used as an insulator on GaAs wafers during the 1970s [116], it has been only in the last decade when research has been intensified in Ga<sub>2</sub>O<sub>3</sub> as a WBG semiconductor. Ga<sub>2</sub>O<sub>3</sub> has five known polymorphs  $\alpha$ ,  $\beta$ ,  $\gamma$ ,  $\delta$  and  $\epsilon$ . Its most stable beta crystal structure ( $\beta$ -Ga<sub>2</sub>O<sub>3</sub>) is attracting the interest for power electronics devices. It has a larger band gap (4.9 eV) and expected breakdown field (8 MV/cm) than both SiC and GaN. Thanks to its excellent characteristics, Ga<sub>2</sub>O<sub>3</sub> is suitable for high voltage and high power switching applications, and potentially offers better performance than Si, SiC and GaN.

$\beta$ -Ga<sub>2</sub>O<sub>3</sub> has the possibility to produce large native substrate areas by standard melt growth techniques. The melt-growth is a low-energy-consumption, low-cost method of making large substrates. The most common methods of crystal growth for Ga<sub>2</sub>O<sub>3</sub> are

Verneuil Method, Floating Zone (FZ) Method, Flux Method, Czochralski (CZ) Method, Edge-defined Film-fed Growth (EFG) Method and CVD [116]. EFG and CZ are commercial methods, offering large crystal sizes of 2-inch diameter. Additionally, the FZ method may be used commercially for growing large crystals. With the EFG method, Tamura company has demonstrated 4- and 6-inch substrates [117]. Moreover, for  $\beta$ -Ga<sub>2</sub>O<sub>3</sub> thin film growth, many of the techniques developed for SiC and GaN epitaxy can be applied. Some of these techniques are molecular beam epitaxy (MBE), halide vapor phase epitaxy (HVPE), metal-organic chemical vapor deposition (MOCVD), and mist chemical vapor deposition (MIST CVD). An additional growth technique is a hybrid of MOCVD and HVPE (HOVPE). Unfortunately, these technologies do not reach to produce 20  $\mu$  m or greater thick films at a commercially viable rate [118].

Nevertheless, a recent breakthrough was presented in 2018 by FLOSFIA in Japan. FLOSFIA use the corundum structure  $\alpha$ -Ga<sub>2</sub>O<sub>3</sub>, which has superior properties respect to  $\beta$ -Ga<sub>2</sub>O<sub>3</sub>. In addition, FLOSFIA applies the p-type Ir<sub>2</sub>O<sub>3</sub> compatibility with n-type Ga<sub>2</sub>O<sub>3</sub> to demonstrate normally-off MOSFET. The device is made of a novel p-type corundum semiconductor which works as an inversion layer [119].

Besides the high intensity of Ga<sub>2</sub>O<sub>3</sub> research as WBG semiconductor in the last decade, further developments are needed about high-quality bulk crystal growth, epitaxial thin film growth, and device process technologies; as well as a better understanding of Ga<sub>2</sub>O<sub>3</sub> properties: p-type conductivity, dopants and defects such as oxygen vacancies and thin films properties. Nowadays, one of the most challenging points is the absence of p-type dopants, where researchers have demonstrated several effective solutions [120]. In addition, thermal management approaches for power devices will be another challenge to enable the adoption of Ga<sub>2</sub>O<sub>3</sub>. Other areas of research with some importance will be the radiation damage effect on Ga<sub>2</sub>O<sub>3</sub> and related heterostructures as well as process patterning and contacting conditions [121].

According to the exposed above, Ga<sub>2</sub>O<sub>3</sub> can provide superior performance in high voltage applications than other semiconductors in the market. Due to its low cost and the possibility of mass production, Ga<sub>2</sub>O<sub>3</sub> is a firm candidate to substitute both Si, SiC and GaN semiconductors in current and future applications. In spite of that, due to its low grade of maturity, Ga<sub>2</sub>O<sub>3</sub> technology adoption is not expected for several years yet. According to estimations of automotive council UK, it could provide a step change in performance compared to SiC and GaN for the automotive industry in the late 2020s [122].

Given the availability of high quality and large size substrates, the development of electronics devices based on Ga<sub>2</sub>O<sub>3</sub> has been facilitated, and proof of concept of different Ga<sub>2</sub>O<sub>3</sub> power devices have been demonstrated. For instance, a 8.03 kV  $\beta$ -Ga<sub>2</sub>O<sub>3</sub> MOSFET has been recently demonstrated [123]. Furthermore, regardless of the early stage of Ga<sub>2</sub>O<sub>3</sub> development, Denso Corporation announced the adoption of  $\alpha$ -Ga<sub>2</sub>O<sub>3</sub> based semiconductors (provided by FLOSFIA) for its EV power control units targeting commercial production [124], that presumably will take place in the following years.

#### 3.4.2. Ga<sub>2</sub>O<sub>3</sub> Advantages and Disadvantages

Ga<sub>2</sub>O<sub>3</sub> has been a material of eager interest over the last years due to its exceptional potential as a semiconductor. Following, some of the benefits of using Ga<sub>2</sub>O<sub>3</sub> are pointed out:

- Large breakdown electric field: its breakdown field, which exceed the double of GaN and SiC breakdown electric fields, allows us to expect higher breaking voltage than SiC and GaN-based devices while maintaining acceptable low on-resistance. Researchers have demonstrated critical field strength of 3.80 MV/cm from a  $\beta$ -Ga<sub>2</sub>O<sub>3</sub>-based MOSFETs, which is beyond the theoretical limits of SiC and GaN [116].
- Thermal stability: the monoclinic structure of  $\beta$ -Ga<sub>2</sub>O<sub>3</sub> has concentrated almost all research efforts because it is the most stable with a melting point of 1740 °C [125]. Recently, developments have used the semi-stable phase corundum-structured  $\alpha$ -Ga<sub>2</sub>O<sub>3</sub>. Using enhancement thermal stability process on sapphire substrates, the  $\alpha$ -Ga<sub>2</sub>O<sub>3</sub> film can grow at a temperature as high as 800 °C [126].

- Large area single crystal substrates: the good material workability of Ga<sub>2</sub>O<sub>3</sub> and the availability of melt-grown allow the fabrication of a large single crystal.
- Low on-resistance: apart from diamond, Ga<sub>2</sub>O<sub>3</sub> exceed others semiconductors on-resistance characteristics. An SBD has been reported with an outstanding specific on-resistance of 0.1 mΩ cm<sup>2</sup> [127]. This represents 86% less than any SBD SiC-based devices available on the market.
- Cost: single crystal bulk could be grown by using the same melt growth methods than the ones used for sapphire. Consequently, substrates of a large area in a single crystal are available at low cost; this allows the development of high-quality epitaxial layer.

Despite all the properties that made Ga<sub>2</sub>O<sub>3</sub> an excellent semiconductor material, there are three main drawbacks of Ga<sub>2</sub>O<sub>3</sub>.

- Low thermal conductivity: with 0.13–0.21 W/cmK Ga<sub>2</sub>O<sub>3</sub> has the lowest thermal conductivity of the WBG materials. This will be one of the most critical challenges to develop Ga<sub>2</sub>O<sub>3</sub> power devices.
- Lack of a p-type dopant: Ga<sub>2</sub>O<sub>3</sub>-based devices are n-type unipolar, limiting the application of β-Ga<sub>2</sub>O<sub>3</sub> to unipolar Schottky and heterojunction devices. In order to achieve an optimal performance, the device requires controlled n-type and p-type doping of β-Ga<sub>2</sub>O<sub>3</sub> epitaxial layers. Si, Sn, and Ge [118,128] have been demonstrated to be effective n-type dopant materials for Ga<sub>2</sub>O<sub>3</sub>. However, due to the nature of metal-oxides, p-doping is not impossible but challenging. Some works present evidence of p-type conduction [129] and the possibility of doping Ga<sub>2</sub>O<sub>3</sub> by substituting Ga atoms with Zn [130] or by N substituting O [131] atom or both, nevertheless, a considerable research effort is needed before the Ga<sub>2</sub>O<sub>3</sub> potential could be exploited.
- Early-stage development: Ga<sub>2</sub>O<sub>3</sub> technology is a far less mature technology than SiC and GaN, and it is evolving in a small number of laboratories.

### 3.5. Other WBG Materials

While GaN, SiC, Ga<sub>2</sub>O<sub>3</sub>, and diamond have attracted most of the attention in the recent years, other WBG materials such as AlN, BN and ZnO have had relatively less development but, nevertheless, are worthy to be discussed briefly.

#### 3.5.1. AlN

AlN has been used for ceramic packages since the 1960s, but not until the 1980s its potential for electronic applications was realized. AlN stands out with a wider band gap than diamond (6.2 eV). Additionally, its high hardness value, thermal stability at high temperature, high thermal conductivity (340 W/m K) and large critical electric field (12 MV/cm) are attractive for high power electronics applications [132]. However, due to the challenges in material growth, high processing cost and device fabrication, very limited work has been reported on AlN electronics.

Recently, researchers from Arizona State University achieved high-quality AlN epilayers on sapphire substrates allowing to create a 1 kV AlN SBD [133]. This work presents a cost-effective route to AlN-based SBD. Another innovation in the early development of AlN-substrates for power devices is carried out by projects as InRel with the goal to the manufacturing of AlN devices with even higher breakdown voltage (>2.5 kV) and proven reliability [134].

The AlGaN alloy has exceptional properties as semiconductor combining advantages of GaN and AlN, such as high bandgap (3.4 to ~6.0 eV), high breakdown fields (>10 MV/cm for AlN), high electron mobility (up to 1000 cm<sup>2</sup>/(V·s)), high saturation velocities (>107 cm/s), and relative ease at being doped n-type with Si. Besides, having the same crystal structure of InGaN, could take advantage of knowledge and manufacturing infrastructure associated with InGaN LEDs [99].

However, the AlGaN development faces challenges such as the ability to be doped controllably and selectively, the availability of single-crystal substrates with the necessary quality for epitaxial growth and the knowledge to control heteroepitaxial growth [135].

Recent research at Sandia National Laboratories has presented results about devices based in AlGaN alloys. A 30% aluminium mole fraction AlGaN alloy was used over sapphire substrates to develop Quasi-vertical PIN diodes. The highest measured breakdown voltage recorded was 1627 V. These diodes present better performance in comparison with vertical GaN-based diodes. Likewise, an 810 V lateral AlGaN HEMT was demonstrated based in Al-rich epilayers, 85 and 70% of aluminium alloys were used over sapphire substrates [135]. After demonstrating a 2-dimensional electron gas in an  $\text{Al}_{0.85}\text{Ga}_{0.15}\text{N}/\text{Al}_{0.70}\text{Ga}_{0.30}\text{N}$  (barrier/channel) heterostructure, current efforts are focus to achieve a normally-off 5 kV, 5 m  $\Omega \cdot \text{cm}^2$  device [136].

AlGaN, with Al composition in the range of 70–100%, could be a viable material for next-generation of power electronics, in the near future is expected to be used in applications where both extremely high power and a constrained volume are required, and cost may not be a primary constraint.

### 3.5.2. BN

BN is known to be the second hardness material and has low chemical reactivity like the diamond. In its cubic structure (c-BN) BN is isoelectronic with diamond. n-type and p-type doping BN can be manufactured with Si and *Be* respectively. c-BN has advantageous properties such as a bandgap of 6.4 eV, and current research forecasts a breakdown field greater than 15 MV/cm. Finally, it has the second-highest thermal conductivity of all materials (theoretically  $\sim 2145 \text{ W}/(\text{m}\cdot\text{K})$  for isotopically pure material) [99].

c-BN has even better properties than the diamond to be used for high power electronics. However, the development of BN technology faces enormous challenges like growing process of cubic BN, strain, growth temperature, adhesion to the substrate, and crystal quality in the c-BN films. Due to these challenges, progress toward realizing device technologies has been very slow up to date [99].

### 3.5.3. ZnO

The fundamental semiconductor properties of ZnO were extensive study during the late 1950s and the 1960s, including the study of its energy band structure, band gaps, the electrical transport properties of the intrinsic (undoped) material, and others. However, the impossibility of p-type doping and the lack of large, bulk single crystals of ZnO hampered the progress in the development of ZnO-based electronic devices [137].

Nowadays, ZnO is being used as an electronic material in photonics, optoelectronics, varistors, transparent power electronics, surface acoustic wave devices, piezoelectric transducers, ultra-violet (UV) light emitters, sensors, and solar cells [138]. Nevertheless, ZnO properties such as wide band gap (3.3 eV), high melting point (1975 °C), low thermal expansion, and high electron mobility (2000  $\text{cm}^2/(\text{Vs})$ ) [137] give ZnO the advantages of high breakdown voltage, ability to sustain large electrical fields, lower electronics noise, high temperature and high-power operation.

Some recent results on the steady-state and transient electron transport within ZnO suggest that this material, having a higher peak and saturation electron drift velocities than SiC and GaN, may also be considered as an alternative material to SiC and GaN for high-power and high-frequency field effect transistors [139].

## 4. Discussion

In the field of semiconductor materials, a figure of merit is a numerical expression taken as representative of the performance of a given material. As seen above, in power electronics several characteristics, such as breakdown voltage, switching speed or thermal conductivity, can be desired. Consequently, different figures of merit have been used throughout history to evaluate the semiconductor performance of different materials.

Critical breakdown field ( $E_C$ ) increase has been one of the main objectives in the development of WBG materials in order to reduce the number of components needed in applications whose voltages are higher than those supported by Si. However, is expected

that all WBG materials have breakdown voltages higher than typical values in most low voltage applications, in the range of 1200 V to 6500 V [140].

In 1965, Johnson [141] presented a new material figure of merit

$$JFOM = \frac{E_C v_S}{2\pi} \quad (1)$$

which depends on the critical breakdown field ( $E_C$ ) and the carrier saturation drift velocity ( $v_S$ ) of the semiconductor. Johnson's Figure of Merit (JFOM) defines the power-frequency product and it is commonly used to determine the frequency capability for a transistor.

In 1972, Keyes [142] derived a figure of merit

$$KFOM = \lambda \left[ \frac{c \cdot v_S}{4\pi\epsilon} \right]^{1/2} \quad (2)$$

where  $\lambda$  is the thermal conductivity,  $c$  the velocity of light and  $\epsilon$  the dielectric constant. Keyes' Figure of Merit (KFOM) provides a thermal limitation of the transistors used in semiconductor devices. In this way, the lower KFOM, the higher thermal constraint.

In 1983, Baliga [143] derived his first material figure of merit

$$BFOM = \epsilon\mu E_G^3 \quad (3)$$

where  $\mu$  is the carrier mobility and  $E_G$  is the bandgap of the semiconductor. Baliga's Figure of Merit (BFOM) defines the conduction losses in unipolar devices. BFOM is based upon the assumption that the power losses are dominated by the dissipation due to the current flow through the on-resistance of the power device. Thus this figure of merit does not apply to system operating at high frequencies where switching losses are significant.

In this way, in 1989, Baliga [144] proposed his second figure of merit

$$BHFFOM = \mu E_C^2 V_G^{1/2} V_B^{3/2} \quad (4)$$

Here,  $V_G$  and  $V_B$  are the gate drive voltage and the breakdown voltage respectively. These parameters are related to the actual semiconductor device which does not depend on the material itself. In this way, the Baliga's High-Frequency Figure of Merit (BHFFOM) cannot be used to compare different materials but for semiconductor devices.

In 2004 Huang [145] presented three new figures of merit for unidirectional devices

$$HMFOM = E_C \sqrt{\mu} \quad (5)$$

$$HCAFOM = \epsilon \sqrt{\mu} E_C^2 \quad (6)$$

$$HTFOM = \frac{\lambda}{\epsilon E_C} \quad (7)$$

Huang's Material Figure of Merit (HMFOM) determines the best material for high-frequency applications. This figure of merit can be considered as a simplification of the BHFFOM, where the device dependent term has been omitted. Secondly, the larger Huang's Chip Area Figure of Merit (HCAFOM), the smaller size of the device is required. Finally, similar to KFOM, the Huang's Thermal Figure of Merit (HTFOM) defines the maximum working temperature but pays particular attention to the fact that materials with a higher breakdown voltage can be embedded in smaller devices and, therefore, small packages present a lower dissipation area.

Table 2 summarizes the main physical properties of the semiconductors analyzed in Section 3. With this values, the figures of merit detailed above have been calculated and they are shown in Table 3, normalized respect to Si values.

**Table 2.** Main physical properties of different semiconductor materials [54,146,147].

	Si	GaAs	4H-SiC	2H-GaN	$\beta$ -Ga <sub>2</sub> O <sub>3</sub>	2H-AlN	Diamond
$E_g$ (eV)	1.12	1.42	3.26	3.49	4.9	6.2	5.0
$\epsilon_r$	11.7	13.1	9.7	9.0	10.0	8.5	5.7
$\mu_n$ (cm <sup>2</sup> /(V·s))	1480	8400	1000	1200	200	300	2800
$E_C$ (MV/cm)	0.3	0.4	3.18	3.0	8.0	12.0	5.7
$v_{sat}$ (10 <sup>7</sup> cm/s)	2.3	4.4	2.2	1.5	2.0	1.7	2.7
$\lambda$ (W/(cm·K))	1.48	0.52	4.5	1.3	0.27	2.85	20.0
$T_{max}$ (°C)	175	150	600	400	600	250	700

**Table 3.** Comparison of different semiconductor material figures of merit (normalized against Si).

	Si	GaAs	4H-SiC	2H-GaN	$\beta$ -Ga <sub>2</sub> O <sub>3</sub>	2H-AlN	Diamond
JFOM	1	2.6	10.1	6.5	23.2	29.6	22.3
KFOM	1	0.5	3.3	0.8	0.2	1.9	21.0
BFOM	1	13.0	13.8	18.9	9.7	25.0	82.0
HMFOM	1	3.2	8.7	9.0	9.8	18.0	26.1
HCAFOM	1	4.7	76.6	69.3	223.4	523.3	241.9
HTFOM	1	0.24	0.35	0.11	0.01	0.07	1.46
Availability	5	2	4	2	2	2	1
Manufacturing	5	4	4	3	2	1	1

The criteria used to compare the different WBG materials are presented below:

1. Market viability of the semiconductors in the short-medium term.
2. Ability of the material to withstand the typical voltages required by the most common converters in smart grids.
3. Properties that improve the characteristics of the electronics converters, based on three factors:
  - (a) Electrical properties.
  - (b) Thermal properties.
  - (c) Material availability and manufacturing cost.

Between the materials analyzed above, 2H-AlN and diamond are far from reaching a technical and economic viability that would make them accessible for mass-market applications. Besides, all WBG materials reach a sufficiently high breakdown field and a size small enough for the applications analyzed in this work. Therefore, Figure 3 compares the most important properties for urban and smart grid applications: switching frequency in high power applications (JFOM and HMFOM), thermal properties by means of heat dissipation (KFOM) and maximum operation temperature ( $T_{max}$ ), and feasibility of these products on the market, availability of raw material and manufacture of high-quality wafers (Availability) and estimated device-production (doping, packaging, etc.) costs (Manufacturing).

From Table 3 and Figure 3 it can be concluded that, although Ga<sub>2</sub>O<sub>3</sub> presents the best electric properties; as to JFOM and HMFOM point out it will have the highest breakdown field and switching speed. In addition, it presents a great maximum temperature, similar to SiC. However, due to its poor thermal behaviour, it could not be feasible to be used in most of the applications studied. These characteristics will force strong requirements in the cooling systems, increasing the cost and size, and losing the benefits that these materials provide. However, due to soft-switching converters strongly reduce power losses in semiconductors, these applications could take advantage of the high breakdown voltage and high switching frequency provided by Ga<sub>2</sub>O<sub>3</sub> without being penalized by the low thermal conductivity feature of this material.

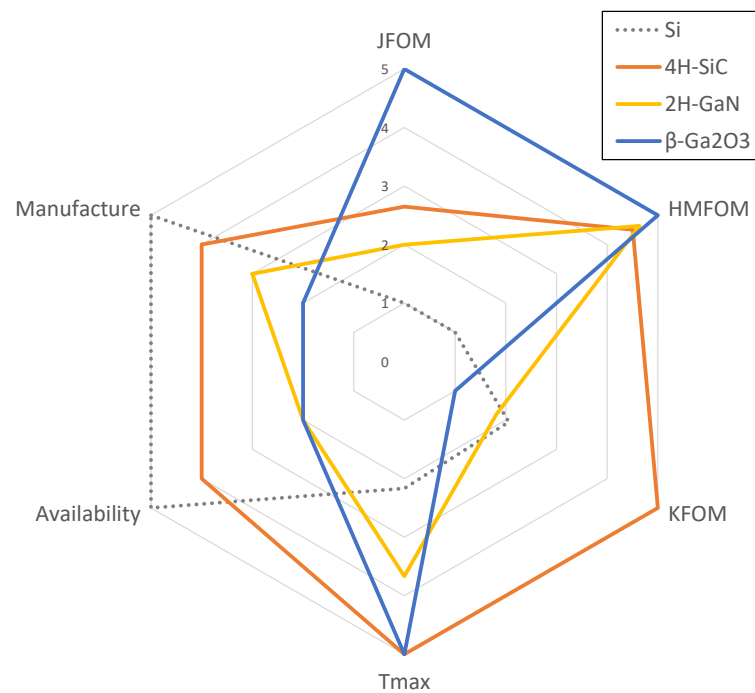


**Figure 3.** Comparison of the most important properties of semiconductors for smart grid applications. (The values have been scaled by assigning 1 to the worst material and 5 to the best)

Power electronics converters for smart grids require high switching frequencies, but also medium-high powers. Although GaN is known for its high switching frequencies, its ability to handle high currents is relatively low. This explains the apparently low value of its figures of merit compared to other materials. On the other hand, SiC presents a thermal conductivity three times higher than Si and GaN, and 16 times higher than Ga<sub>2</sub>O<sub>3</sub>. In addition, SiC has much better electrical properties than Si and similar to GaN. These characteristics, together with the fact that this material is abundant and easily extracted from the Earth crust, will make SiC devices suitable for most consumers equipment.

## 5. Conclusions

The current energy model, based on the combustion of fossil fuels, will inevitably be replaced by a new model where electricity generation is based on clean energies. The policies carried out by governments have led to an increase in the distributed generation of renewable energies in recent years; however, forecasts highlight that this will be even more quick in the coming years due to the maturity reached by these technologies. This will require the massive deployment of power electronics converters. However, the current state of the art of this equipment does not meet some of the desirable requirements in urban environments, thus an improvement in the performance of these devices is required.

Since Si devices are reaching the theoretical limits of this material, a new generation of WBG semiconductor materials have appeared in the last years, surpassing the properties of Si in many applications. Nowadays it is possible to find SiC and GaN devices in the market. Others materials such as Ga<sub>2</sub>O<sub>3</sub> are beginning to show its potential, while others like diamond seem more like a fascinating material to study than a commercially viable alternative.

DER designed for urban and smart grids applications have some requirements that differentiate them from other applications. These devices must be compact, inaudible and economically affordable to be deployed in an urban environment. Consequently, it is mandatory to increase the switching frequency above the limits of Si, holding a competitive cost.

Finally, some figures of merit for the different WBG materials have been analyzed in order to compare the physical properties of these materials and find the most suitable semiconductor for the new generation of DER. SiC, GaN and Ga<sub>2</sub>O<sub>3</sub> are the only materials that seem viable in the medium term and they have shown completely different trends. Since Ga<sub>2</sub>O<sub>3</sub> presents the best electrical properties, its extremely low thermal conductivity makes this material suitable for only a few applications such as soft-switching converters. On the other hand, SiC has more balanced properties. It exceeds the Si electrical properties while having good thermal conductivity, avoiding the need for bulky and expensive heat dissipation systems.

**Author Contributions:** Conceptualization, J.B.-F., J.F.S.-O. and J.M.-C.-A.; methodology, J.B.-F., J.F.S.-O. and J.M.-C.-A.; state-of-the-art analysis, J.B.-F., E.L.-P. and J.M.-C.-A.; writing—original draft preparation, J.B.-F. and J.M.-C.-A.; writing—review and editing, J.M.-C.-A., J.F.S.-O., E.L.-P., J.B.-F.; visualization, J.B.-F.; supervision, J.F.S.-O. and J.M.-C.-A.; project administration, E.L.-P.; funding acquisition, J.M.-C.-A., J.F.S.-O., E.L.-P., J.B.-F. All authors have read and agreed to the published version of the manuscript.

**Funding:** SUDOKET project has been co-funded by the European Union through its ERDF funds within the Territorial Cooperation Programme of the Southwest European Space-SUDOE (SOE2/P1/E0677). The authors want to thank the support and collaboration of the Centro para el Desarrollo Tecnológico Industrial, E.P.E. (CDTI) funds through the RED CERVERA CER-20191002 “ENERISLA: SISTEMAS ENERGÉTICOS AISLADOS 100% RENOVABLES”.

**Conflicts of Interest:** The authors declare no conflict of interest.

## References

1. United Nations. *Moving towards a Climate Neutral UN: The UN System's Footprint and Efforts to Reduce It*; Technical Report; United Nations Environment Programme: Nairobi, Kenya, 2010.
2. Jones, D.; Sakhel, A.; Buck, M.; Graichen, P. *Agora Energiewende and Sandbag (2018): The European Power Sector in 2017. State of Affairs and Review of Current Developments*; Technical Report; Agora Energiewende: Berlin, Germany, 2018.
3. Ecofys Germany GmbH. *National Benchmarks for a More Ambitious EU 2030 Renewables Target*; Technical Report; European Renewable Energy Federation (EREF): Berlin, Germany, 2017.
4. European Commission. *Europe Leads the Global Clean Energy Transition: Commission Welcomes Ambitious Agreement on Further Renewable Energy Development in the EU*; Technical Report; European Commission: Brussels, Belgium, 2018. [[CrossRef](#)]
5. European Commission. *2030 Climate & Energy Framework | Climate Action*; European Commission: Brussels, Belgium, 2020.
6. Kolar, J.W.; Friedli, T. The essence of three-phase PFC rectifier systems Part I. *IEEE Trans. Power Electron.* **2013**, *28*, 176–198. [[CrossRef](#)]
7. Friedli, T.; Hartmann, M.; Kolar, J.W. The essence of three-phase PFC rectifier systems-part II. *IEEE Trans. Power Electron.* **2014**, *29*, 543–560. [[CrossRef](#)]
8. Muñoz-Cruzado-Alba, J.; Villegas-Núñez, J.; Vite-Frías, J.A.; Carrasco-Solís, J.M.; Galván-Díez, E. New Low-Distortion Q-f Droop Plus Correlation Anti-Islanding Detection Method for Power Converters in Distributed Generation Systems. *IEEE Trans. Ind. Electron.* **2015**, *62*, 5072–5081. [[CrossRef](#)]
9. Muñoz-Cruzado-Alba, J.; Rojas, C.; Kouro, S.; Galván Díez, E. Power Production Losses Study by Frequency Regulation in Weak-Grid-Connected Utility-Scale Photovoltaic Plants. *Energies* **2016**, *9*, 317. [[CrossRef](#)]
10. Ballestín, J. *4-Leg D-STATCOM for the Balancing of the Low-Voltage Distribution Grid*; Semana Virtual 2020—CIGRE España; CIGRE España: Alcobendas, Spain, 2020.
11. European Union. *Commission Regulation (Eu) 2016/631*; European Union: Brussels, Belgium, 2016; p. 68.
12. Gevorgian, V.; Booth, S. *Review of PREPA Technical Requirements for Interconnecting Wind and Solar Generation*; Technical Report; National Renewable Energy Laboratory (NREL): Golden, CO, USA, 2013.
13. BDEW Bundesverband der Energie- und Wasserwirtschaft e.V. *Generating Plants Connected to the Medium-Voltage Network*; Technical Guideline; BDEW: Berlin, Germany, 2008; pp. 1–130.
14. National Energy Regulator of South Africa (NERSA). *Grid Connection Code for Renewable Power Plants (RPPs) Connected to the Electricity Transmission System (TS) or Distribution System (DS) in South Africa*; Technical Report; National Energy Regulator of South Africa: Pretoria, South Africa, 2019.
15. Mukarram, M.J.; Murkute, S.V. Sandia Frequency Shift Method for Anti-Islanding Protection of a Gridtied Photovoltaic System. In Proceedings of the 2020 IEEE International Students' Conference on Electrical, Electronics and Computer Science (SCEECS), Bhopal, India, 22–23 February 2020; pp. 1–5. [[CrossRef](#)]
16. Hou, C.C.; Chen, Y.C. Active anti-islanding detection based on pulse current injection for distributed generation systems. *IET Power Electron.* **2013**, *6*, 1658–1667. [[CrossRef](#)]

17. Tao, Y.; Liu, Q.; Deng, Y.; Liu, X.; He, X. Analysis and mitigation of inverter output impedance impacts for distributed energy resource interface. *IEEE Trans. Power Electron.* **2015**, *30*, 3563–3576. [CrossRef]
18. Muñoz-Cruzado-Alba, J.; Villegas-Núñez, J.; Vite-Frías, J.; Carrasco Solís, J. A New Fast Peak Current Controller for Transient Voltage Faults for Power Converters. *Energies* **2015**, *9*, 1. [CrossRef]
19. Noris, L.; Rueda, J.; Rakhshani, E.; Korai, A.W. Power System Black-Start and Restoration with High Share of Power-Electronic Converters. In Proceedings of the 2019 IEEE Power Energy Society General Meeting (PESGM); Institute of Electrical and Electronics Engineers, Atlanta, GA, USA, 4–8 August 2019; pp. 1–5. [CrossRef]
20. Borlase, S. *Smart Grids: Infrastructure, Technology, and Solutions*; CRC Press: Boca Raton, FL, USA, 2013.
21. Tayab, U.B.; Bashir, M.A. Multilevel inverter topologies for photovoltaic power system: A review. *ARPN J. Eng. Appl. Sci.* **2017**, *12*, 3537–3549.
22. Elmakawi, A.M.; Bayindir, K.C. Non-isolated Multi-Port Inverter Topologies for Renewable Energy Applications: A review. In Proceedings of the 2019 IEEE 1st Global Power, Energy and Communication Conference, GPECOM 2019, Nevsehir, Turkey, 12–15 June 2019; pp. 321–330. [CrossRef]
23. Ozkan, Z.; Hava, A.M. A survey and extension of high efficiency grid connected transformerless solar inverters with focus on leakage current characteristics. In Proceedings of the 2012 IEEE Energy Conversion Congress and Exposition ECCE, Raleigh, NC, USA, 15–20 September 2012; pp. 3453–3460. [CrossRef]
24. IEC TC/SC 62196-1, *International Standard: Plugs, Socket-Outlets, Vehicle Couplers and Vehicle Inlets. Conductive Charging of Electric Vehicles*; Technical Report; International Electrotechnical Commission: Geneva, Switzerland, 2003.
25. UNE-EN 61851-23: *Sistema Conductivo de Carga Para Vehículos eléctricos*; Parte 23: Estación de Carga en Corriente Continua para Vehículos Eléctricos' Technical Report; Asociación Española de Normalización y Certificación (AENOR): Madrid, Spain, 2015.
26. International Energy Agency. *Global EV Outlook 2020*; OECD Publishing: Paris, France, 2020; p. 276. [CrossRef]
27. Ingeteam. Electric Mobility. Available online: [https://www.ingeteam.com/us/en-us/sectors/electric-mobility/s15\\_58\\_p/products.aspx](https://www.ingeteam.com/us/en-us/sectors/electric-mobility/s15_58_p/products.aspx) (accessed on 24 September 2020).
28. Webasto. EV Solutions | Electric Vehicle Chargers For Your Business. Available online: <https://www.evsolutions.com/ev-charging-products-for-business> (accessed on 24 September 2020).
29. ABB. EV Charging | Electric Vehicle Chargers | ABB. Available online: <https://new.abb.com/ev-charging> (accessed on 1 September 2020).
30. ABB. High Power Charging | High Power Fast Chargers | ABB. Available online: <https://new.abb.com/ev-charging/products/car-charging/high-power-charging> (accessed on 1 September 2020).
31. PHOENIX CONTACT | High Power Charging—The Technology for Fast Charging Stations. Available online: [https://www.phoenixcontact.com/online/portal/pi?1dmy&uril=wcm:path:/pien/web/main/products/technology\\_pages/subcategory\\_pages/High\\_power\\_charging/b1c8a245-f088-4fad-b144-cea31e7f9a82](https://www.phoenixcontact.com/online/portal/pi?1dmy&uril=wcm:path:/pien/web/main/products/technology_pages/subcategory_pages/High_power_charging/b1c8a245-f088-4fad-b144-cea31e7f9a82) (accessed on 1 September 2020).
32. Fast EV Charging—Infineon Technologies. Available online: <https://www.infineon.com/cms/en/applications/industrial/fast-ev-charging/> (accessed on 1 September 2020).
33. Parker | Parker-Project. Available online: <https://parker-project.com/> (accessed on 1 September 2020).
34. INCIT-EV Project | Electric Charging Solutions for Electric Vehicles; European Union: Brussels, Belgium, 2020. Available online: <https://www.incit-ev.eu/> (accessed on 13 December 2020).
35. FLEXICIENCY | Innovation and Networks Executive Agency; European Union: Brussels, Belgium, 2020. Available online: <https://ec.europa.eu/inea/en/horizon-2020/projects/h2020-energy/grids/flexiciency> (accessed on 1 September 2020).
36. Bird, C.B. *Growth and Legal Implications of Energy Storage Technologies*; Technical Report 1; HeinOnline: Getzville, NY, USA, 2017.
37. National Rural Electric Cooperative Association; National Rural Utilities Cooperative Finance Corporation; CoBank.; NRTC. *Battery Energy Storage Overview*; Technical Report; National Rural Electric Cooperative Association: Arlington, VA, USA, 2019.
38. Hesse, H.; Schimpe, M.; Kucevic, D.; Jossen, A. Lithium-Ion Battery Storage for the Grid—A Review of Stationary Battery Storage System Design Tailored for Applications in Modern Power Grids. *Energies* **2017**, *10*, 2107. [CrossRef]
39. Hossain, E.; Murtaugh, D.; Mody, J.; Faruque, H.M.R.; Sunny, M.S.H.; Mohammad, N. A Comprehensive Review on Second-Life Batteries: Current State, Manufacturing Considerations, Applications, Impacts, Barriers Potential Solutions, Business Strategies, and Policies. *IEEE Access* **2019**, *7*, 73215–73252. [CrossRef]
40. Silva, B.N.; Khan, M.; Han, K. Futuristic Sustainable Energy Management in Smart Environments: A Review of Peak Load Shaving and Demand Response Strategies, Challenges, and Opportunities. *Sustainability* **2020**, *12*, 5561. [CrossRef]
41. Evans, G. *Network Connected Energy Storage New Thames Valley Vision*; Technical Report; New Thames Valley Vision: Chester, UK, 2017.
42. Home | GridBridge. Available online: <http://www.grid-bridge.com/> (accessed on 1 September 2020).
43. ThirdEquation. Available online: <https://www.thirdequation.com/> (accessed on 1 September 2020).
44. Home—Smart Wires Inc. Available online: <https://www.smartwires.com/> (accessed on 1 September 2020).
45. Parity H2020—Parity H2020. Available online: <https://parity-h2020.eu/> (accessed on 1 September 2020).
46. Lin, H.N.; Tseng, W.D.; Wu, C.H.; Yeh, T.H.; Ho, T.H. Root cause analysis and defect ground effect of EMI problem for power electronics. In Proceedings of the 2019 Joint International Symposium on Electromagnetic Compatibility, Sapporo and Asia-Pacific International Symposium on Electromagnetic Compatibility (EMC Sapporo/APEMC), Sapporo, Japan, 3–7 June 2019; pp. 440–443. [CrossRef]

47. Sharma, A.; Lee, S.J.; Jang, Y.J.; Jung, J.P. SiC based Technology for High Power Electronics and Packaging Applications. *J. Microelectron. Packag. Soc.* **2014**, *21*, 71–78. [[CrossRef](#)]
48. Garrido-Diez, D.; Baraia, I. Review of wide bandgap materials and their impact in new power devices. In Proceedings of the 2017 IEEE International Workshop of Electronics, Control, Measurement, Signals and their Application to Mechatronics, ECMSM, Donostia-San Sebastian, Spain, 24–26 May 2017; pp. 1–6. [[CrossRef](#)]
49. Kizilyalli, I.C.; Carlson, E.P.; Cunningham, D.W.; Manser, J.S.; Liu, A.Y. *Wide Band-Gap Semiconductor Based Power Electronics for Energy Efficiency*; Technical Report; USDOE Advanced Research Projects Agency—Energy (ARPA-E): Washington, DC, USA, 2018. [[CrossRef](#)]
50. Das, S.; Marlino, L.D.; Armstrong, K.O. *Wide Bandgap Semiconductor Opportunities in Power Electronics*; Technical Report; Oak Ridge National Laboratory (ORNL): Oak Ridge, TN, USA, 2018; doi:10.2172/1415915. [[CrossRef](#)]
51. Armstrong, K.O.; Das, S.; Cresko, J. Wide bandgap semiconductor opportunities in power electronics. In Proceedings of the 2016 IEEE 4th Workshop on Wide Bandgap Power Devices and Applications (WiPDA), Fayetteville, AR, USA, 7–9 November 2016; pp. 259–264. [[CrossRef](#)]
52. Wang, F.F.; Zhang, Z. Overview of Silicon Carbide Technology: Device, Converter, System, and Application. *CPSS Trans. Power Electron. Appl.* **2016**, *1*, 13–32. [[CrossRef](#)]
53. Kim, K.A.; Liu, Y.C.; Chen, M.C.; Chiu, H.J. Opening the Box: Survey of High Power Density Inverter Techniques From the Little Box Challenge. *CPSS Trans. Power Electron. Appl.* **2017**, *2*, 131–139. [[CrossRef](#)]
54. Chow, T.P.; Omura, I.; Higashiwaki, M.; Kawarada, H.; Pala, V. Smart power devices and ICs using GaAs and wide and extreme bandgap semiconductors. *IEEE Trans. Electron Devices* **2017**, *64*, 856–873. [[CrossRef](#)]
55. Elasser, A.; Chow, T.P. Silicon carbide benefits and advantages for power electronics circuits and systems. *Proc. IEEE* **2002**, *90*, 969–986. [[CrossRef](#)]
56. Skinner, B.J. Earth Resources. *Proc. Natl. Acad. Sci. USA* **1979**, *76*, 4212–4217. [[CrossRef](#)]
57. Kim, M.; Seo, J.H.; Singiseti, U.; Ma, Z. Recent advances in free-standing single crystalline wide band-gap semiconductors and their applications: GaN, SiC, ZnO,  $\beta$ -Ga<sub>2</sub>O<sub>3</sub>, and diamond. *J. Mater. Chem. C* **2017**, *5*, 8338–8354. [[CrossRef](#)]
58. Wolfspeed. *Why Choose Wolfspeed? | Wolfspeed*; Wolfspeed: Durham, NC, USA, 2018.
59. Planson, P.; Brosselard, P.; Isoird, K.; Lazar, M.; Phung, L.V.; Raynaud, C.; Tournier, D. Wide bandgap semiconductors for ultra high voltage devices. Design and characterization aspects. In Proceedings of the 2014 International Semiconductor Conference (CAS), Sinaia, Romania, 13–15 October 2014; pp. 35–40. [[CrossRef](#)]
60. Bakowski, M. Roadmap for SiC Power Devices. *J. Telecommun. Inf. Technol.* **2000**, *3–4*, 19–30.
61. Chenq, L.; Agarwal, A.; Capel, C.; Scozzie, C. 15 kV, Large Area (1 cm<sup>2</sup>), 4H-SiC p-Type Gate Turn-Off Thyristors. *Mater. Sci. Forum* **2013**, *740–742*, 978–981. [[CrossRef](#)]
62. Mitsubishi Electric. *Mitsubishi Electric's New 6.5 kV Full-SiC Power Semiconductor Module Achieves World's Highest Power Density*; Mitsubishi Electric: Tokyo, Japan, 2018.
63. Fraunhofer ISE. *New High-Voltage Silicon Carbide Inverter Enables Stabilization of Medium-Voltage Grids*; Fraunhofer ISE: Freiburg im Breisgau, Germany, 2018.
64. Walz, E. *Auto Supplier Bosch to Manufacture Silicon Carbide Chips That Can Extend the Range of EVs*; FutureCar: Santa Clara, CA, USA, 2019.
65. Kusunoki, K.; Kishida, Y.; Kaido, H.; Kamei, K.; Seki, K.; Moriguchi, K.; Okada, N. *Development of High Quality 4H-SiC Single Crystal Wafers Grown by Solution Growth Technique*; Nippon Steel & Sumimoto Metal Technical Report; J-GLOBAL: Tokyo, Japan, 2017; pp. 50–57.
66. Anderson, K. *SiC and GaN Shine at APEC 2018*; Omdia: London, UK, 2018.
67. Kagoyama, Y.; Okamoto, M.; Yamasaki, T.; Tajima, N.; Nara, J.; Ohno, T.; Yano, H.; Harada, S.; Umeda, T. Anomalous carbon clusters in 4H-SiC/SiO<sub>2</sub> interfaces. *J. Appl. Phys.* **2019**, *125*, 65302. [[CrossRef](#)]
68. Zhang, Z.; Wang, Z.; Guo, Y.; Robertson, J. Carbon cluster formation and mobility degradation in 4H-SiC MOSFETs. *Appl. Phys. Lett.* **2021**, *118*, 031601. [[CrossRef](#)]
69. Hensler, A. Air Cooled SiC Three Level Inverter Reaches Efficiency Levels Above 99 Percent. In Proceedings of the 2017 Power Electronics Europe, Warsaw, Poland, 11–14 September 2017; pp. 3–5.
70. Wang, F.; Zhang, Z.; Ericson, T.; Raju, R.; Burgos, R.; Boroyevich, D. Advances in Power Conversion and Drives for Shipboard Systems. *Proc. IEEE* **2015**, *103*, 2285–2311. [[CrossRef](#)]
71. Knoll, L.; Mihaila, A.; Bauer, F.; Sundaramoorthy, V.; Brianda, E. Robust 3.3 kV Silicon Carbide MOSFETs with Surge and Short Circuit Capability. In Proceedings of the 29th International Symposium on Power Semiconductor Devices & IC, Sapporo, Japan, 28 May–1 June 2017; pp. 243–246. [[CrossRef](#)]
72. RichardsonRFPD. *GaN & SiC Technology Overview Your Source for GaN and SiC Products*; RichardsonRFPD: Geneva, IL, USA, 2018.
73. Zhang, Y.; Sun, M.; Piedra, D.; Hu, J.; Liu, Z.; Lin, Y.; Gao, X.; Shepard, K.; Palacios, T. 1200 V GaN vertical fin power field-effect transistors. In Proceedings of the 2017 IEEE International Electron Devices Meeting (IEDM), San Francisco, CA, USA, 2–6 December 2018; pp. 921–924. [[CrossRef](#)]
74. Chen, K.J.; Haberlen, O.; Lidow, A.; Tsai, C.L.; Ueda, T.; Uemoto, Y.; Wu, Y. GaN-on-Si power technology: Devices and applications. *IEEE Trans. Electron Devices* **2017**, *64*, 779–795. [[CrossRef](#)]

75. Kukushkin, S.A.; Osipov, A.V.; Bessolov, V.N.; Medvedev, B.K.; Nevolin, V.K.; Tcarik, K.A. Substrates for epitaxy of gallium nitride: New materials and techniques. *Rev. Adv. Mater. Sci.* **2008**, *17*, 1–32.
76. Amano, H.; Baines, Y.; Beam, E.; Borga, M.; Bouchet, T.; Chalker, P.R.; Charles, M.; Chen, K.J.; Chowdhury, N.; Chu, R.; et al. The 2018 GaN power electronics roadmap. *J. Phys. Appl. Phys.* **2018**, *51*, 163001. [[CrossRef](#)]
77. Market Research Future. *GaN Semiconductor Devices Market 2018 Emerging Technologies, Industrial Insights, Latest Innovations, Growth Analysis and Global Trends by Forecast 2022—Press Release—Digital Journal*; Market Research Future: Maharashtra, India, 2018.
78. SMA. “The Power Density will Increase Tenfold”, Predicts JUEGEN Reinert from SMA; SMA: Niestetal, Germany, 2017.
79. Ćapajna, M. Current Understanding of Bias-Temperature Instabilities in GaN MIS Transistors for Power Switching Applications. *Crystals* **2020**, *10*, 1153. [[CrossRef](#)]
80. Hua, M.; Yang, S.; Wei, J.; Zheng, Z.; He, J.; Chen, K.J. Hole-Induced Degradation in E-Mode GaN MIS-FETs: Impact of Substrate Terminations. *IEEE Trans. Electron Devices* **2020**, *67*, 217–223. [[CrossRef](#)]
81. Hua, M.; Cai, X.; Yang, S.; Zhang, Z.; Zheng, Z.; Wang, N.; Chen, K.J. Enhanced Gate Reliability in GaN MIS-FETs by Converting the GaN Channel into Crystalline Gallium Oxynitride. *ACS Appl. Electron. Mater.* **2019**, *1*, 642–648. [[CrossRef](#)]
82. He, J.; Hua, M.; Zhang, Z.; Chen, K.J. Performance and VTH Stability in E-Mode GaN Fully Recessed MIS-FETs and Partially Recessed MIS-HEMTs with LPCVD-SiNx/PECVD-SiNx Gate Dielectric Stack. *IEEE Trans. Electron Devices* **2018**, *65*, 3185–3191. [[CrossRef](#)]
83. Hua, M.; Wei, J.; Bao, Q.; Zhang, Z.; Zheng, Z.; Chen, K.J. Dependence of VTH Stability on Gate-Bias under Reverse-Bias Stress in E-mode GaN MIS-FET. *IEEE Electron Device Lett.* **2018**, *39*, 413–416. [[CrossRef](#)]
84. Guo, A.; Del Alamo, J.A. Unified Mechanism for Positive- and Negative-Bias Temperature Instability in GaN MOSFETs. *IEEE Trans. Electron Devices* **2017**, *64*, 2142–2147. [[CrossRef](#)]
85. Hua, M.; Wei, J.; Bao, Q.; He, J.; Zhang, Z.; Zheng, Z.; Lei, J.; Chen, K.J. Reverse-bias stability and reliability of hole-barrier-free E-mode LPCVD-SiNx/GaN MIS-FETs. In Proceedings of the Technical Digest—International Electron Devices Meeting, IEDM, San Francisco, CA, USA, 2–6 December 2018; pp. 33.2.1–33.2.4. [[CrossRef](#)]
86. Lagger, P.; Steinschifter, P.; Reiner, M.; Stadtmüller, M.; Denifl, G.; Naumann, A.; Müller, J.; Wilde, L.; Sundqvist, J.; Pogany, D.; et al. Role of the dielectric for the charging dynamics of the dielectric/barrier interface in AlGaN/GaN based metal-insulator-semiconductor structures under forward gate bias stress. *Appl. Phys. Lett.* **2014**, *105*, 033512. [[CrossRef](#)]
87. IMW65R048M1HXKSA1 by Infineon Technologies AG | MOSFETs | Arrow.com. Available online: <https://www.arrow.com/en/products/imw65r048m1hxksa1/infineon-technologies-ag> (accessed on 1 January 2021).
88. GAN063-650WSAQ by Nexperia | MOSFETs | Arrow.com. Available online: <https://www.arrow.com/en/products/gan063-650wsaq/nexperia> (accessed on 1 January 2021).
89. Moens, P.; Liu, C.; Banerjee, A.; Vanmeerbeek, P.; Coppens, P.; Ziad, H.; Constant, A.; Li, Z.; De Vleeschouwer, H.; Roig-Guitart, J.; et al. An industrial process for 650 V rated GaN-on-Si power devices using in-situ SiN as a gate dielectric. In Proceedings of the International Symposium on Power Semiconductor Devices and ICs, Waikoloa, HI, USA, 15–19 June 2014; pp. 374–377. [[CrossRef](#)]
90. Transphorm. *Transphorm GaN Power FET Portfolio*; Transphorm: Goleta, CA, USA, 2018.
91. Jones, E.A.; Wang, F.F.; Costinett, D. Review of Commercial GaN Power Devices and GaN-Based Converter Design Challenges. *IEEE J. Emerg. Sel. Top. Power Electron.* **2016**, *4*, 707–719. [[CrossRef](#)]
92. IMEC. *Press Release—Imec and Qromis Present High Performance p-GaN HEMTs on 200mm CTE-Matched Substrates*; IMEC: Leuven, Belgium, 2018.
93. Blake, C. *GaN Power Devices Slash Size, Raise Efficiency of 4-kW Solar Inverter*; How2Power: Smithtown, NY, USA, 2013; pp. 2–7.
94. Texas Instruments. *TI & Siemens: Taking GaN on the Grid*; Texas Instruments: Dallas, TX, USA, 2018.
95. Keshmiri, N.; Wang, D.; Agrawal, B.; Hou, R.; Emadi, A. Current Status and Future Trends of GaN HEMTs in Electrified Transportation. *IEEE Access* **2020**, *8*, 70553–70571. [[CrossRef](#)]
96. *GaN vs SiC: Silicon Carbide and Gallium Nitride Compared* | Arrow.com; Arrow Electronics: Centennial, CO, USA, 2020.
97. Sachan, S.; Prajapati, A. *GaN Power Device Market Report*; Technical Report; Allied Market Research: Portland, OR, USA, 2020.
98. Villamor, A.; Zong, Z. *Power GaN 2017: Epitaxy, Devices, Applications, and Technology Trends 2017*; Technical Report; Yole Développement: Lyon, France, 2017.
99. Tsao, J.Y.; Chowdhury, S.; Hollis, M.A.; Jena, D.; Johnson, N.M.; Jones, K.A.; Kaplar, R.J.; Rajan, S.; Van de Walle, C.G.; Bellotti, E.; et al. Ultrawide-Bandgap Semiconductors: Research Opportunities and Challenges. *Adv. Electron. Mater.* **2018**, *4*, 1600501. [[CrossRef](#)]
100. Mokuno, Y.; Chayahara, A.; Yamada, H. Synthesis of large single crystal diamond plates by high rate homoepitaxial growth using microwave plasma CVD and lift-off process. *Diam. Relat. Mater.* **2008**, *17*, 415–418. [[CrossRef](#)]
101. Shikata, S. Single crystal diamond wafers for high power electronics. *Diam. Relat. Mater.* **2016**, *65*, 168–175. doi:10.1016/j.diamond.2016.03.013. [[CrossRef](#)]
102. Applied Diamond Inc. *Diamond Plates: Single Crystal and Polycrystalline* | Applied Diamond, Inc.; Applied Diamond Inc.: Wilmington, DE, USA, 2018.
103. CORDIS. *Periodic Reporting for period 1—GreenDiamond (Green Electronics with Diamond Power Devices)*; Technical Report May 2015; European Commission: Brussels, Belgium, 2016.

104. Pernot, J.; Chicot, G.; Fiori, A.; Traore, A.; Thi, T.N.T.; Volpe, P.N.; Eon, D.; Omnès, F.; Bustarret, E.; Gheeraert, E.; et al. Recent progress of diamond device toward power application. In Proceedings of the EXMATEC 2012: 11th Expert Evaluation and Control of Compound Semicon- Ductor Materials and Technologies conference, Porquerolles Islands, France, 30 May–1 June 2012.
105. Umezawa, H. Recent advances in diamond power semiconductor devices. *Mater. Sci. Semicond. Process.* **2018**, *78*, 147–156. [[CrossRef](#)]
106. ARPA-e. *ARPA-E | SWITCHES*; ARPA-e: Washington, DC, USA, 2018.
107. Agence Nationale de la Recherche. *Project MOVeToDiam (DIAMOND VERTICAL POWER MOSFET) | ANR—Agence Nationale de la Recherche*; Agence Nationale de la Recherche: Paris, France, 2017.
108. Shikata, S.; Umezawa, H. Development of diamond-based power devices. *Synthesiology* **2013**, *6*, 152–161. [[CrossRef](#)]
109. Frost & Sullivan. *Are Diamond Semiconductors the Next-generation Power Devices?* Frost & Sullivan: New York, NY, USA, 2018.
110. Kitabayashi, Y.; Kudo, T.; Tsuboi, H.; Yamada, T.; Xu, D.; Shibata, M.; Matsumura, D.; Hayashi, Y.; Syamsul, M.; Inaba, M.; et al. Normally-Off C-H Diamond MOSFETs with Partial C-O Channel Achieving 2-kV Breakdown Voltage. *IEEE Electron Device Lett.* **2017**, *38*, 363–366. [[CrossRef](#)]
111. Kasu, M. Diamond epitaxy: Basics and applications. *Prog. Cryst. Growth Charact. Mater.* **2016**, *62*, 317–328. [[CrossRef](#)]
112. May, P. *Synthetic diamond: Emerging CVD Science and Technology*; John Wiley & Sons: Hoboken, NJ, USA, 1994; p. 663.
113. eVince Technology. *Why Diamond is Better Than Anything Else*; eVince Technology: County Durham, UK, 2017.
114. Wort, C.J.; Balmer, R.S. Diamond as an electronic material. *Mater. Today* **2008**, *11*, 22–28. [[CrossRef](#)]
115. Pearton, S.J.; Yang, J.; Cary, P.H.; Ren, F.; Kim, J.; Tadjer, M.J.; Mastro, M.A. A review of Ga<sub>2</sub>O<sub>3</sub> materials, processing, and devices. *Appl. Phys. Rev.* **2018**, *5*, 11301–13504. [[CrossRef](#)]
116. Bayraktaroglu, B. *Assessment of Gallium Oxide Technology*; Technical Report; Air Force Research Laboratory, Sensors Directorate WPAFB United States: Wright-Patterson Air Force Base, OH, USA, 2017.
117. Nikolaev, V.I.; Stepanov, S.I.; Romanov, A.E.; Bougrov, V.E. Single Crystals of Electronic Materials: Growth and Properties. In *Single Crystals of Electronic Materials*; Woodhead Publishing: Cambridge, UK, 2019; pp. 487–521. [[CrossRef](#)]
118. Okur, S.; Tompa, G.; Sbrokek, N. *Growth of Ga<sub>2</sub>O<sub>3</sub> for Power Device Production*; Vacuum Technology & Coating: Weston, CT, USA, 2017; pp. 31–39.
119. SemiconductorTODAY. *FLOSFIA Demonstrates First Gallium Oxide Normally-off MOSFET*; SemiconductorTODAY: Cheltenham, UK, 2018.
120. Zhang, H.; Yuan, L.; Tang, X.; Hu, J.; Sun, J.; Zhang, Y.; Zhang, Y.; Jia, R. Progress of Ultra-Wide Bandgap Ga<sub>2</sub>O<sub>3</sub> Semiconductor Materials in Power MOSFETs. *IEEE Trans. Power Electron.* **2020**, *35*, 5157–5179. [[CrossRef](#)]
121. Mastro, M.A.; Kuramata, A.; Calkins, J.; Kim, J.; Ren, F.; Pearton, S.J. Perspective—Opportunities and Future Directions for Ga<sub>2</sub>O<sub>3</sub>. *ECS J. Solid State Sci. Technol.* **2017**, *6*, P356–P359. [[CrossRef](#)]
122. Advanced Propulsion Centre; Automotive Council UK. *Power Electronics Roadmap*; Technical Report; Advanced Propulsion Centre: Coventry, UK, 2017.
123. Sharma, S.; Zeng, K.; Saha, S.; Singiseti, U. Field-Plated Lateral Ga<sub>2</sub>O<sub>3</sub> MOSFETs with Polymer Passivation and 8.03 kV Breakdown Voltage. *IEEE Electron Device Lett.* **2020**, *41*, 836–839. [[CrossRef](#)]
124. Denso Corporation. *DENSO and Kyoto University Startup FLOSFIA will Develop Next-Gen Power Semiconductor Device for Electrified Vehicles*; Denso Corporation: Kariya, Japan, 2018.
125. Li, L.; Wei, W.; Behrens, M. Synthesis and characterization of a-, b-, and g-Ga<sub>2</sub>O<sub>3</sub> prepared from aqueous solutions by controlled precipitation. *Solid State Sci.* **2012**, *14*, 971–981. [[CrossRef](#)]
126. Lee, S.D.; Ito, Y.; Kaneko, K.; Fujita, S. Enhanced thermal stability of alpha gallium oxide films supported by aluminum doping. *Jpn. J. Appl. Phys.* **2015**, *54*, 2–5. [[CrossRef](#)]
127. Flosfia. *Ground Breaking Work on Gallium Oxide Normally-off Transistor*; Flosfia: Kyoto, Japan, 2018.
128. Moser, N.A.; Fitch, R.C.; Walker, D.E.; Green, A.J.; Chabak, K.D.; Heller, E.; McCandless, J.P.; Tetlak, S.E.; Crespo, A.; Leedy, K.D. *Recent Progress of B-Ga<sub>2</sub>O<sub>3</sub> MOSFETs for Power Electronic Applications*; Technical Report; Air Force Research Laboratory Wright Patterson Air Force Base United States: Wright-Patterson Air Force Base, OH, USA, 2017.
129. Chikoidze, E.; Fellous, A.; Perez-Tomas, A.; Sauthier, G.; Tchelidze, T.; Ton-That, C.; Huynh, T.T.; Phillips, M.; Russell, S.; Jennings, M.; et al. P-type β-gallium oxide: A new perspective for power and optoelectronic devices. *Mater. Today Phys.* **2017**, *3*, 118–126. [[CrossRef](#)]
130. Li, C.; Yan, J.L.; Zhang, L.Y.; Zhao, G. Electronic structures and optical properties of Zn-doped β-Ga<sub>2</sub>O<sub>3</sub> with different doping sites. *Chin. Phys. B* **2012**, *21*, 127104. [[CrossRef](#)]
131. Zhang, L.Y.; Yan, J.L.; Zhang, Y.J.; Li, T. Effects of N-doping concentration on the electronic structure and optical properties of N-doped β-Ga<sub>2</sub>O<sub>3</sub>. *Chin. Phys. B* **2012**, *21*, 067102. [[CrossRef](#)]
132. Zhao, Y. Aluminum Nitride (AlN) Power Devices. 2017. Available online: <http://faculty.engineering.asu.edu/zhao/> (accessed on 18 October 2018).
133. Fu, H.; Baranowski, I.; Huang, X.; Chen, H.; Lu, Z.; Montes, J.; Zhang, X.; Zhao, Y. Demonstration of AlN Schottky Barrier Diodes with Blocking Voltage over 1 kV. *IEEE Electron Device Lett.* **2017**, *38*, 1286–1289. [[CrossRef](#)]
134. Rittner, M.; Kessler, U.; Naundorf, J.; Kriegel, K.; Schulz, M.; Meneghesso, G. Innovative Reliable Nitride—Based Power devices and applications. In Proceedings of the CIPS 2018 10th International Conference on Integrated Power Electronics Systems, Stuttgart, Germany, 20–22 March 2018.

135. Kaplar, R.J.; Allerman, A.A.; Armstrong, A.M.; Crawford, M.H.; Dickerson, J.R.; Fischer, A.J.; Baca, A.G.; Douglas, E.A. Review—Ultra-Wide-Bandgap AlGa<sub>N</sub> Power Electronic Devices. *ECS J. Solid State Sci. Technol.* **2017**, *6*, Q3061–Q3066. [[CrossRef](#)]
136. Kaplar, R.J.; Allerman, A.A.; Armstrong, A.M.; Baca, A.G.; Fischer, A.J.; Wierer, J.J.; Neely, J.C. *Ultra Wide Bandgap Semiconductors for Power Electronics*; Technical Report; Sandia National Lab.(SNL-NM): Albuquerque, NM, USA, 2015.
137. Claflin, B.; Look, D.C. Electrical Transport Properties in Zinc Oxide. In *Zinc oxide Materials for Electronic and Optoelectronic Device Applications*, 1st ed.; Litton, C.W., Reynolds, D.C., Collins, T.C., Eds.; John Wiley & Sons, Ltd.: Hoboken, NJ, USA, 2011; pp. 61–86. [[CrossRef](#)]
138. Wu, J.J.; Ku, C.H.; Wu, C.T.; Liao, W.P. 2—Hierarchically Nanostructured One-Dimensional Metal Oxide Arrays for Solar Cells. In *Nanocrystalline Materials*; Tjong, S.C., Ed.; Elsevier: Amsterdam, The Netherlands, 2014; pp. 27–74. [[CrossRef](#)]
139. Siddiqua, P.; Shur, M.; O’Leary, S.K. Zinc Oxide as a Potential Material for Future Electronic Device Applications. In *ECS Meeting Abstracts*; MA2017-01; The Electrochemical Society: Pennington, NJ, USA, 2017; p. 1302. [[CrossRef](#)]
140. Huang, A.Q. Wide bandgap (WBG) power devices and their impacts on power delivery systems. In Proceedings of the International Electron Devices Meeting, IEDM, San Francisco, CA, USA, 3–7 December 2017; pp. 20.1.1–20.1.4. [[CrossRef](#)]
141. Johnson, E. Physical limitations on frequency and power parameters of transistors. In Proceedings of the 1958 IRE International Convention Record, New York, NY, USA, 21–25 March 1965; pp. 27–34. [[CrossRef](#)]
142. Keyes, R.W. Figure of merit for semiconductors for high-speed switches. *Proc. IEEE* **1972**, *60*, 225. [[CrossRef](#)]
143. Baliga, B.J. Semiconductors for high-voltage, vertical channel field-effect transistors. *J. Appl. Phys.* **1982**, *53*, 1759–1764. [[CrossRef](#)]
144. Baliga, B.J. Power Semiconductor Device Figure of Merit for High-Frequency Applications. *IEEE Electron Device Lett.* **1989**, *10*, 455–457. [[CrossRef](#)]
145. Huang, A.Q. New unipolar switching power device figures of merit. *IEEE Electron Device Lett.* **2004**, *25*, 298–301. [[CrossRef](#)]
146. Shenai, K. High-Density Power Conversion and Wide-Bandgap Semiconductor Power Electronics Switching Devices. *Proc. IEEE* **2019**, *107*, 2308–2326. [[CrossRef](#)]
147. Higashiwaki, M.; Fujita, S. Introduction. In *Gallium Oxide: Materials Properties, Crystal Growth, and Devices*, 1st ed.; Springer: Berlin/Heidelberg, Germany, 2020; Volume 293, pp. 1–12. [[CrossRef](#)]



# Capítulo 4

## **Diseño de sistemas trifásicos de electrónica de potencia de cuatro hilos para el equilibrado de corriente en líneas de baja tensión**

**RESUMEN:** El rápido despliegue de fuentes de energía distribuida, unido a la creciente electrificación de servicios como la climatización y la movilidad, está generando un cambio en el paradigma eléctrico mundial, dotando a la red de distribución de un rol cada vez más importante. En esta red conviven cargas monofásicas y trifásicas, que son alimentadas por una red trifásica de cuatro hilos. Esta particularidad genera la aparición de desequilibrios en la red, los cuales perjudican a la eficiencia y estabilidad del sistema. Este capítulo presenta el artículo *4L D-STATCOM para redes débiles desbalanceadas de baja tensión*, en el que se aborda el diseño de un equipo de electrónica de potencia para la compensación de desequilibrios con el objetivo de minimizar su impacto en la red.

## 4L D-STATCOM PARA REDES DÉBILES DESBALANCEADAS DE BAJA TENSIÓN

**Javier Ballestín Fuertes**, Investigador, Fundación CIRCE

**Jesús Muñoz-Cruzado Alba**, Investigador, Fundación CIRCE

**José Francisco Sanz Osorio**, Investigador, Instituto Universitario de Investigación Mixto CIRCE (Universidad de Zaragoza - Fundación CIRCE)

**Resumen:** La generación renovable ha aumentado desde un 12% del total en 2000 hasta un 30% en 2020, y se espera que para el año 2050 esta suponga un 50% del total. La variabilidad de los pequeños sistemas de autoconsumo, típicamente monofásicos, conectados a la red de baja tensión, producen unos consumos desequilibrados que afectan negativamente a la eficiencia y a la estabilidad del sistema. En este artículo se propone el uso de un D-STATCOM cuatro ramas para el equilibrado de redes débiles con consumos desequilibrados. El uso de este equipo reduciría las pérdidas en la línea, y proveería al operador de red de una herramienta adicional para la gestión de sobrecargas en las líneas y de tensiones de suministro desequilibradas. En primer lugar se explica el principio de funcionamiento de este equipo y cómo se realiza su integración en una red desequilibrada. Para la validación de este sistema se ha desarrollado un prototipo de D-STATCOM de 30 kVA, que se ha probado a nivel de laboratorio de forma previa a su instalación en campo. A continuación se presentan y analizan los resultados obtenidos. Finalmente, el trabajo concluye los beneficios de la instalación del D-STATCOM propuesto en redes débiles.

**Palabras clave:** 4-Legs D-STATCOM, Recursos Energéticos Distribuidos, Redes Desequilibradas, Baja Tensión.

### INTRODUCCIÓN

La necesidad de mitigar los efectos del cambio climático está produciendo un cambio del modelo energético a nivel mundial. Para favorecer este cambio, la Unión Europea (UE) ha promovido nuevas directivas con el objetivo de potenciar la instalación de recursos energéticos distribuidos (DER) e incrementar su nivel de penetración en el sistema energético [1]. La generación energética renovable en la UE ha aumentado desde un 12% en el año 2000 hasta más de un 30% en 2020 [2]. Esto representa un crecimiento medio anual del 1,7%. Además, las previsiones apuntan a que este crecimiento se mantendrá durante los próximos años, alcanzando la generación renovable un 50% de la producción energética mundial para el año 2050 [3].

Las líneas de distribución suponen un 95,6% de los más de un millón de kilómetros que componen la red eléctrica española [4]. Entre las redes de distribución, son las redes de baja tensión (BT) las que se ven más afectadas por el incremento en la instalación de DER. Estas redes proveen de suministro principalmente a pequeños consumidores (inferiores a 10 kW) típicamente conectados de manera monofásica. La instalación de pequeños sistemas de autoconsumo se ha incrementado rápidamente en los últimos años como una manera de reducir el coste de la factura eléctrica para usuarios residenciales y comerciales.

Los principales inconvenientes generados por este fenómeno son bien conocidos [5] y se listan a continuación:

- Fluctuaciones de tensión
- Desequilibrios entre fases
- Disminución de la eficiencia
- Flujo inverso de potencia
- Aumento de los armónicos de tensión y corriente
- Aumento de la corriente de cortocircuito

En la actualidad, varios estudios se centran en diferentes técnicas para solucionar estos problemas [6]. Los tres primeros puntos del listado anterior están directamente relacionados con una circulación de corriente no equilibrada por las fases del sistema, lo que motiva la búsqueda de soluciones a este problema. En este artículo se propone un nuevo compensador estático de distribución (D-STATCOM) para corregir el problema de los desequilibrios en redes débiles de BT.

El presente documento se encuentra estructurado en los siguientes apartados: En primer lugar, se realiza una explicación del sistema propuesto, destacando las herramientas que proporciona el equipo al operador de red (DSO). Con el objetivo de probar el funcionamiento de la solución propuesta se ha creado un prototipo del D-STATCOM, el cual se detalla en la siguiente sección. A continuación, se presentan una serie de pruebas que han permitido validar el

funcionamiento del prototipo a nivel de laboratorio, de forma previa a su instalación en una red real. Finalmente se presenta una discusión de los resultados obtenidos y se recogen las conclusiones.

## PROYECTO PARITY

El proyecto PARITY [7] parte de la estructura actual de la red eléctrica para abordar el desarrollo de un mercado eléctrico que mejore la durabilidad y eficiencia de la red de distribución en un escenario en el que la implantación de DER supere el 50% del mix de generación.

En este proyecto se están desarrollando una serie de herramientas que posibiliten una gestión activa de la red. Entre estas herramientas se contempla el desarrollo de un D-STATCOM que permita a los DSO mejorar su capacidad de gestión de la red y aumentar la capacidad de despliegue de DER.

Los STATCOM son equipos, usados habitualmente para la regulación de tensión en la red de transporte, que no disponen de ninguna clase de almacenamiento, generación o carga, por lo que no son capaces de tener un intercambio energético neto con la red. Como se muestra en la Figura 1, los STATCOM actuales se conectan de forma trifásica a la red, pues en la red de transporte no se dispone de cable de neutro. Esto provoca que el equipo solo pueda manejar corrientes equilibradas que, unido a la condición de que la potencia neta debe ser necesariamente cero, imposibilita el intercambio de corriente activa con la red.

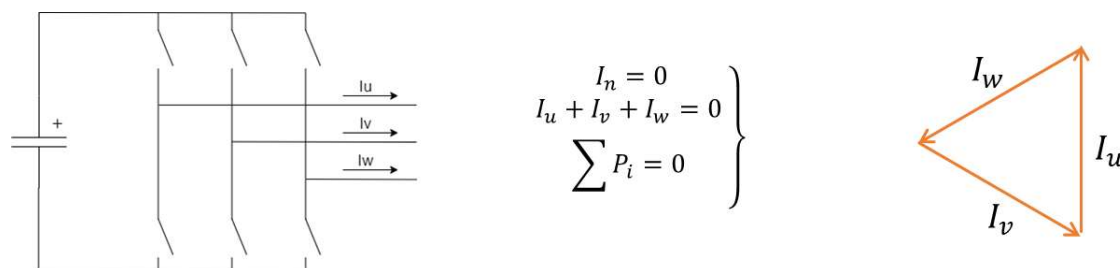


Figura 1. Descripción de un STATCOM 3-ramas.

Por el contrario, en la red de distribución de BT sí se dispone de un neutro físico, lo que permite añadir una cuarta rama (4-Leg) al D-STATCOM conectada a este, que proporciona un camino de retorno para las corrientes desequilibradas, como se muestra en la Figura 2. La capacidad de trabajar con corrientes desequilibradas hace posible el manejo de corriente activa sin incumplir que la potencia activa neta sea nula. Para ello se extrae potencia activa de una o dos fases para inyectarla en la fase o fases restantes, manteniendo el balance de potencia igual a cero y permitiendo una redistribución de la potencia activa circulante en la red.

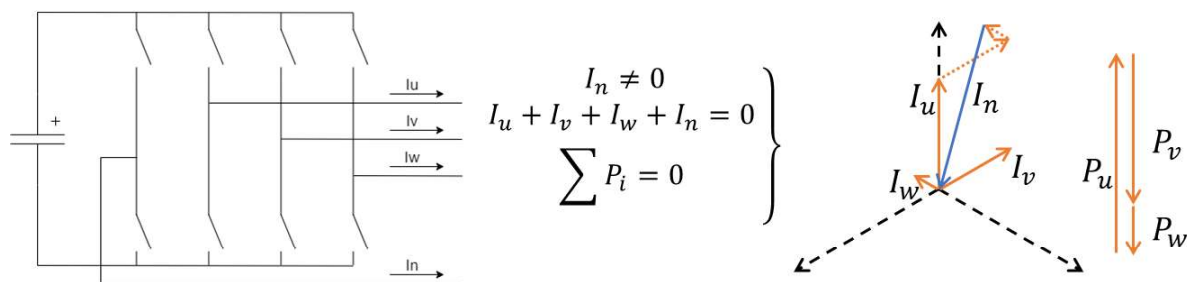


Figura 2. Descripción de un STATCOM 4-ramas.

En este contexto, la introducción de un D-STATCOM con conexión a neutro habilitaría la realización de un control monofásico independiente de cada una de las fases mediante el retorno de la corriente resultante a través del neutro. Esta característica permitiría al D-STATCOM inyectar la corriente calculada en (1) de forma que, como muestra la Figura 3, al sumarse a la corriente que circula hacia las cargas, el desequilibrio se anule y el resultado aguas arriba del equipo fuese la circulación de tres corrientes equilibradas en las fases y una corriente de neutro nula.

$$\begin{pmatrix} I_U^{STAT} \\ I_V^{STAT} \\ I_W^{STAT} \end{pmatrix} = \begin{pmatrix} I_U^{Load} \\ I_V^{Load} \\ I_W^{Load} \end{pmatrix} - \begin{pmatrix} \bar{I}^{Load} \\ \bar{I}^{Load} \\ \bar{I}^{Load} \end{pmatrix} \quad \text{con} \quad \bar{I}^{Load} = \frac{I_U^{Load} + I_V^{Load} + I_W^{Load}}{3} \quad (1)$$

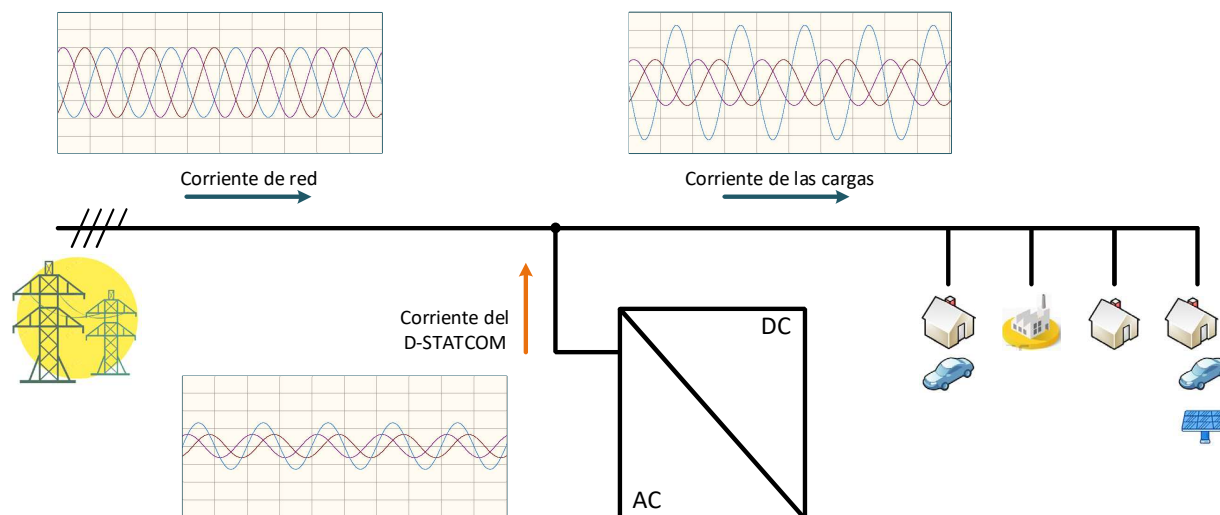


Figura 3. Equilibrado de la corriente en la red por medio de la instalación de un 4L D-STATCOM.

De forma adicional al equilibrado de potencia activa, el D-STATCOM también permitiría la reducción de las pérdidas por medio de la compensación de potencia reactiva, así como la regulación de la tensión de cada una de las fases, mediante la inyección de reactiva de forma independiente.

### 4L-STATCOM

Con el objetivo de probar el funcionamiento del concepto propuesto se ha desarrollado un D-STATCOM 4 ramas con una potencia nominal de 30 kVA a una tensión de red 400 V. Se ha optado por una topología trinivel NPC tipo I basada en silicio, como la mostrada en la Figura 4. Las topologías trinivel consiguen reducir el THD a la salida del convertidor frente a las topologías binivel. En concreto, el empleo de la topología NPC tipo I junto con IGBTs de silicio consigue un compromiso entre prestaciones y costes del equipo.

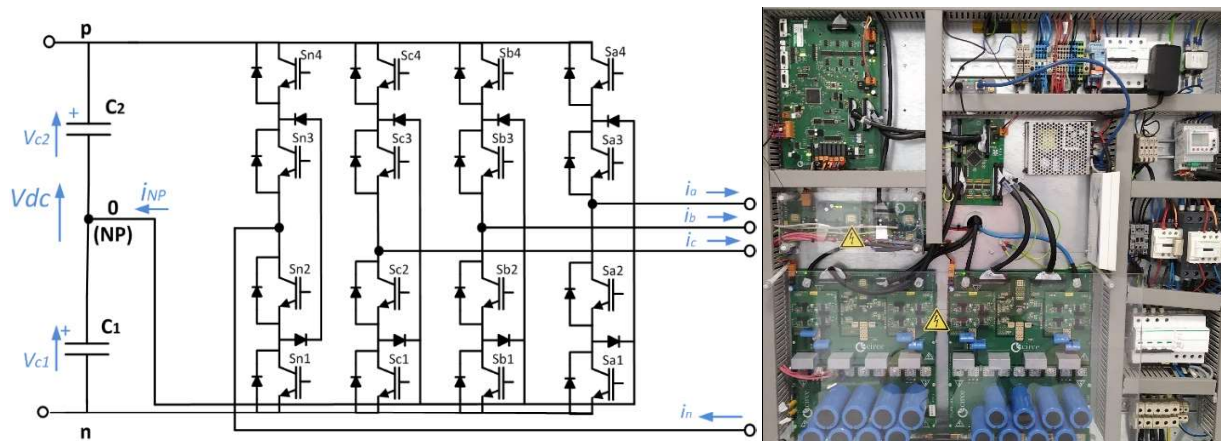


Figura 4. Topología trinivel NPC tipo I empleada en el prototipo del STATCOM.

Las topologías NPC requieren un equilibrado del punto medio del bus de continua (NP), para corregir estas oscilaciones se ha empleado la estrategia de modulación CBPWM con compensación del punto medio propuesta en [8]. Las principales características del D-STATCOM desarrollado se muestran en la Tabla I.

Potencia aparente nominal	30 kVA
Tensión de línea	400 V
Corriente máxima	43 A
Tensión lado de continua	750 V
Capacidad del bus de continua	3.0 mF

Tabla I: Características del D-STATCOM desarrollado.

## RESULTADOS

En esta sección se presentan las pruebas realizadas sobre el D-STATCOM de forma previa a su instalación en una red real. En primer lugar se ha probado el desempeño del equipo en diferentes puntos de funcionamiento. Estos puntos se han escogido de acuerdo a los siguientes casos extremos y a casos intermedios entre los mismos:

- Regulando una corriente nula por cada una de las fases
- Inyectando la corriente reactiva máxima por las tres fases
- Consumiendo la corriente reactiva máxima por las tres fases
- Absorbiendo la potencia activa máxima por una fase e inyectándola por otra
- Absorbiendo la potencia activa máxima por una fase e inyectándola por las otras dos

La Tabla II muestra, en cada uno de los puntos establecidos, la medida del rendimiento y la tasa de distorsión armónica (THD) en la corriente del D-STATCOM. Con estos datos se ha determinado la eficiencia máxima y el THD promedio resultando un 98% y un 1,5% respectivamente. En la Figura 5 se muestran las corrientes en el D-STATCOM para el punto de operación número 6 de la Tabla II.

Punto de operación	Pu (kW)	Pv (kW)	Pw (kW)	Qu (kVAr)	Qv (kVAr)	Qw (kVAr)	Ef	THD
1	2,0	2,0	-4,0	0,0	0,0	0,0	95,99%	1,6%
2	4,0	4,0	-8,0	0,0	0,0	0,0	96,39%	1,6%
3	4,0	0,0	-4,0	0,0	0,0	0,0	95,56%	1,3%
4	7,0	0,0	-7,0	0,0	0,0	0,0	95,83%	1,4%
5	-2,0	-2,0	4,0	0,0	0,0	0,0	96,34%	1,5%
6	-4,0	-4,0	8,0	0,0	0,0	0,0	96,91%	1,5%
7	0,0	0,0	0,0	5,0	5,0	5,0	98,09%	1,5%
8	0,0	0,0	0,0	10,0	10,0	10,0	97,74%	1,4%
9	0,0	0,0	0,0	-5,0	-5,0	-5,0	97,24%	1,8%
10	0,0	0,0	0,0	-10,0	-10,0	-10,0	97,36%	2,2%
11	0,0	0,0	0,0	6,0	4,0	2,0	97,64%	1,7%
12	0,0	0,0	0,0	10,0	8,0	6,0	98,00%	2,1%
13	0,0	0,0	0,0	-6,0	-4,0	-2,0	96,52%	1,7%
14	0,0	0,0	0,0	-10,0	-8,0	-6,0	97,45%	2,8%
15	0,0	0,0	0,0	2,0	0,0	-2,0	95,35%	1,1%
16	2,0	2,0	-4,0	4,0	4,0	4,0	97,35%	1,4%
17	4,0	4,0	-8,0	6,0	6,0	6,0	97,18%	1,6%
18	4,0	0,0	-4,0	4,0	4,0	4,0	97,47%	1,4%
19	7,0	0,0	-7,0	7,0	7,0	7,0	97,07%	1,6%
20	2,0	2,0	-4,0	-4,0	-4,0	-4,0	97,18%	1,8%
21	4,0	4,0	-8,0	-6,0	-6,0	-6,0	96,67%	1,3%

Tabla II: Eficiencia y THD en los diferentes puntos de operación.

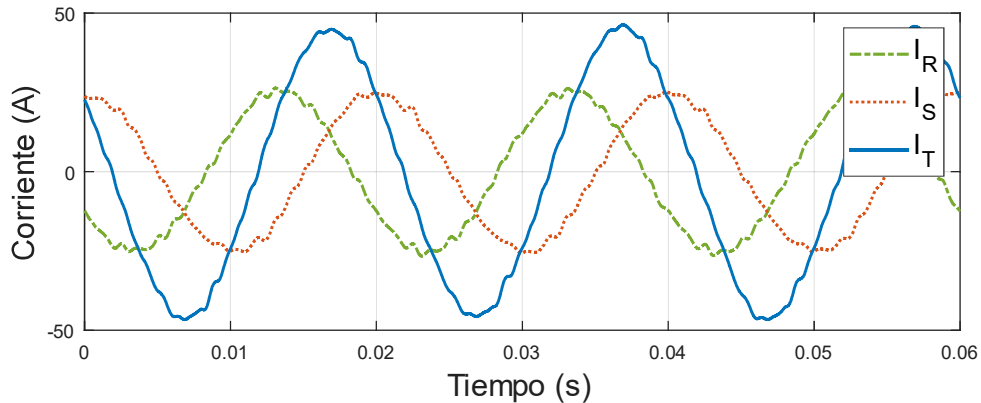


Figura 5. Corrientes del D-STATCOM (Figura 3) equilibrando a una potencia ( $P_r$ ,  $P_s$  y  $P_t$ ) de  $-4$  kW,  $-4$  kW y  $8$  kW.

Durante la realización de estas pruebas se han detectado algunas características que deben ser tenidas en cuenta. En primer lugar, ante un sistema de corrientes desequilibradas típicamente se tendrá una corriente circulando por el neutro no nula. Si se descompone este sistema en sus componentes simétricas, la corriente de neutro está directamente relacionada con la corriente homopolar. La corriente de neutro puede ser en el peor de los casos tres veces superior a la corriente de cualquiera de las fases. En el caso particular de usar el STATCOM para equilibrar potencia activa, esta corriente puede ser hasta 1,7 veces la corriente de fase. Este aspecto puede solucionarse durante el diseño del equipo, dimensionando la cuarta rama para admitir la máxima corriente de neutro, o en el control del mismo, limitando la consigna de corriente para que nunca se exceda la corriente máxima.

Otro aspecto que limita los puntos de operación que se pueden alcanzar son las oscilaciones en la tensión del bus de continua [8]. Estas oscilaciones pueden ser mitigadas aumentando la capacidad del bus, o incluso eliminarse completamente utilizando técnicas de modulación dipolar [9], aunque estas técnicas aumentan el número de conmutaciones en los semiconductores, penalizando la eficiencia.

Por último, como se muestra en la Figura 5, se ha realimentado el D-STATCOM con la medida de un analizador de red ubicado a la entrada del laboratorio con el objetivo de implementar un control en bucle cerrado que permita que el consumo visto desde aguas arriba del mismo sea completamente equilibrado y con un factor de potencia igual a la unidad. Además, también ha podido comprobarse que es posible la regulación de la tensión de las instalaciones del laboratorio por medio de la inyección y consumo de potencia reactiva.

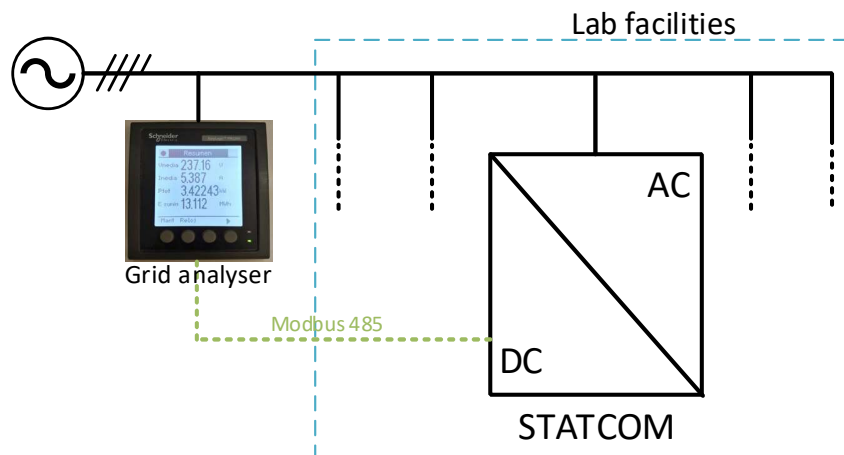


Figura 6. Control en bucle cerrado implementado para equilibrar el consumo del laboratorio.

## CONCLUSIONES

El cambio de modelo energético en el cual se encuentra inmerso el sistema eléctrico actual está haciendo aflorar una serie de problemas los cuales se manifiestan particularmente en la red de baja tensión. El despliegue de DER, en una red compuesta fundamentalmente por cargas monofásicas, produce desbalances que afectan negativamente a la eficiencia y durabilidad de la red.

Este artículo propone utilizar un D-STATCOM de cuatro ramas para realizar el balanceo de la corriente en redes de baja tensión desequilibradas. Esto se traduce en una reducción en el índice de carga de la línea, permitiendo eliminar completamente la corriente de neutro. Por un lado, esto repercute en una disminución de las pérdidas en la línea, evitando a su vez el sobrecalentamiento de los cables. También permite evitar los desequilibrios de tensión, debidos a diferentes caídas de tensión en la línea, producidos a su vez por diferentes flujos de corriente en cada fase.

Además, este equipo permite la inyección y consumo de potencia reactiva de manera independiente por cada una de las fases. Esta característica puede ser usada para cancelar la potencia reactiva que circula por la red, disminuyendo la corriente que circula por la línea. También puede ser utilizada para la regulación de tensión de forma monofásica en redes débiles o incluso para la compensación de huecos de tensión.

A continuación, se ha desarrollado un prototipo de 4L D-STATCOM y se ha realizado su validación en laboratorio previamente a su instalación en una red real. Estas pruebas han permitido caracterizar el equipo en diferentes puntos de funcionamiento y determinar sus aspectos limitantes. Finalmente se ha verificado que el D-STATCOM es capaz de realizar el balanceo de una red y regulación de tensión.

## AGRADECIMIENTOS

Este trabajo se realizó en el marco del proyecto PARITY (Pro-sumer AwaRe, Transactive Markets for Valorization of Distributed flexibility). Este proyecto ha sido financiado por el programa de investigación e innovación Horizonte 2020 de la Unión Europea bajo el acuerdo de concesión N.864319.

## REFERENCIAS

- [1] European Commission, "Europe leads the global clean energy transition: commission welcomes ambitious agreement on further renewable energy development in the EU.," *Int. Energy Agency*, vol. 1, no. February, p. 718, 2018.
- [2] D. Jones, A. Sakhel, M. Buck, and P. Graichen, "Agora Energiewende and Sandbag (2018): The European Power Sector in 2017. State of Affairs and Review of Current Developments," *Agora Energiewende and Sandbag*, p. 49, 2018.
- [3] U.S. Energy Information Administration, "Energy Information Administration," *Choice Rev. Online*, vol. 44, no. 07, pp. 44-3624-44-3624, 2007.
- [4] "Las redes eléctricas en España - FutuRed. Plataforma española de redes eléctricasFutuRed. Plataforma española de redes eléctricas." [Online]. Available: <https://www.futured.es/las-redes-electricas-espana/>. [Accessed: 19-Aug-2020].
- [5] A. Patil, R. Girgaonkar, and S. K. Musunuri, "Impacts of increasing photovoltaic penetration on distribution grid - Voltage rise case study," in *2014 International Conference on Advances in Green Energy, ICAGE 2014*, 2014, pp. 100-105.
- [6] G. Fernández *et al.*, "Photovoltaic Generation Impact Analysis in Low Voltage Distribution Grids," *Energies*, vol. 13, no. 17, p. 4347, Aug. 2020.
- [7] "Parity H2020 – Parity H2020." [Online]. Available: <https://parity-h2020.eu/>. [Accessed: 20-Aug-2020].
- [8] I. López *et al.*, "Generalized PWM-Based Method for Multiphase Neutral-Point-Clamped Converters with Capacitor Voltage Balance Capability," *IEEE Trans. Power Electron.*, vol. 32, no. 6, pp. 4878-4890, 2017.
- [9] I. Lopez *et al.*, "Modulation Strategy for Multiphase Neutral-Point-Clamped Converters," *IEEE Trans. Power Electron.*, vol. 31, no. 2, pp. 928-941, Feb. 2016.



# Capítulo 5

## **Análisis de los efectos de la instalación de un sistema D-STATCOM de cuatro ramas para el equilibrado de corriente en una red urbana de baja tensión**

**RESUMEN:** El artículo *Four-Legs D-STATCOM for Current Balancing in Low-Voltage Distribution Grids* parte del diseño planteado en el capítulo anterior y analiza los efectos de la instalación de un sistema D-STATCOM de cuatro ramas y una potencia nominal de 30 kW en un área residencial de la red de baja tensión. Este capítulo presenta los principales resultados relativos a la mejora en la calidad de suministro, así como la mejora de la eficiencia conseguida durante un periodo de evaluación de un mes.

Received December 3, 2021, accepted December 16, 2021, date of publication December 28, 2021, date of current version January 5, 2022.

Digital Object Identifier 10.1109/ACCESS.2021.3138827

# Four-Legs D-STATCOM for Current Balancing in Low-Voltage Distribution Grids

JAVIER BALLESTÍN-FUERTES<sup>1</sup>, JOSÉ F. SANZ-OSORIO<sup>2</sup>, JESÚS MUÑOZ-CRUZADO-ALBA<sup>1</sup>,  
ERIKA LAPORTA PUYAL<sup>1</sup>, JAVIER LEIVA<sup>3</sup>, AND JACOB RODRIGUEZ RIVERO<sup>4</sup>

<sup>1</sup>CIRCE Foundation, 50018 Zaragoza, Spain

<sup>2</sup>Instituto Universitario de Investigación CIRCE, Universidad de Zaragoza–Fundación CIRCE, 50018 Zaragoza, Spain

<sup>3</sup>Enel Iberia, 29016 Málaga, Spain

<sup>4</sup>E-distribución Redes Digitales, 28042 Madrid, Spain

Corresponding author: Javier Ballestín-Fuertes (jballestin@fcirce.es)

This work was supported in part by the Centro para el Desarrollo Tecnológico Industrial (CDTI), Entidad Pública Empresarial (E.P.E.) Funds through the RED CERVERA “ENERISLA: SISTEMAS ENERGÉTICOS AISLADOS 100% RENOVABLES” under Grant CER-20191002; and in part by the Ministerio de Ciencia, Innovación y Universidades and the European Union Fondo Europeo de Desarrollo Regional (FEDER)-Innterconecta 2018 Program through the Project “Preventive Analysis of Smart Grids with real Time Operation and Renewable Assets Integration” (PASTORA) under Grant ITC-20181102.

**ABSTRACT** The fast deployment of distributed energy resources (DERs) is creating a series of challenges that should be addressed in the coming years. In particular, distribution grids are playing an increasingly important role in the electricity system. Moreover, the three-phase four-wire structure of this network contribute to the appearance of imbalances and a series of problems derived from them. In this context, distribution system operators (DSOs), as the main responsible for the distribution grid, must ensure the quality of supply to consumers. This paper takes advantage of a four-legs D-STATCOM to remove current imbalances in low-voltage power lines. A 35-kVA prototype has been developed and installed in an urban distribution grid. The effect of the D-STATCOM has been analyzed during its first month of operation, studying and measuring the advantages of providing DERs the ability to perform active balancing to the utility grid. The results show a reduction in current imbalances from 21 % to 0 % and neutral current from 10.3 A to 0.4 A. In addition, a 13 % decrease in cable losses has been estimated and a slight improvement in voltage unbalance factor can be noted.

**INDEX TERMS** Distributed energy resources, four-legs D-STATCOM, neutral current, three-phase four-wire network, unbalance compensation.

## I. INTRODUCTION

The gravity of the climate crisis has already initiated a process of electrification of the energy system, increasing the use of electrical energy, maximizing the penetration of renewable energies and the deployment of clean, safe and connected mobility, among others [1], leading to a change in the electric grid as we know it today.

Since 2012, most of the new installed energy capacity has been renewable worldwide, achieving a net addition record of 83 % in 2020 [2]. Moreover, the renewable energies share in Europe reached 23.8 %, surpassing the nuclear energy and making Europe the first region where renewable energies are the dominant power generation source [3].

The associate editor coordinating the review of this manuscript and approving it for publication was Alon Kuperman<sup>1</sup>.

The rapid deployment of renewable energy sources (RES) to replace the traditional large combustion power plants is producing a change, from the current centralized electricity model, to a distributed model where distributed energy resources (DER) are becoming especially relevant, as well as the importance of the distribution network in this process. Furthermore, the growing importance of the distribution network is being increased by changes in the consumption habits of the population, usually connected to the low voltage network. The substitution of gas and oil heating systems by HVAC systems and petrol vehicles by electric vehicles (EV) [4], together with the current profitability of small photovoltaic (PV) installations [5], is evidencing a change in our energy consumption.

In addition, single-phase and three-phase devices coexist in the low-voltage distribution grid, which are supplied by a three-phase four-wire (3P-4W) network, usually connected to

the medium-voltage grid through a delta-wye configured distribution transformer (DT). In this way, single-phase currents return to the DT through the neutral wire, where the three neutral currents are usually canceled.

On the contrary, if the consumption in each of the phases is different the resulting neutral current will increase, and in the worst cases it can be higher than the current in any of the phases. Moreover, the increase in electricity demand, combined with the variability of RES, contributes to the occurrence of unbalanced currents with higher frequency and magnitude. The wide variety of problems caused by imbalances that can compromise the operation of the distribution grid are deeply analyzed in [6], and the most important are listed below:

- Neutral conductor overload: if current is decomposed into its symmetrical components, the neutral current is equal to three times the zero sequence component. If this current is large enough, it can cause heating and degradation of the cable and even failures [7].
- DT overheating: the zero-sequence-current magnetic flux closes via the fuel tank wall of the DT that generates heat, increasing losses and reducing equipment lifetime [8].
- Voltage quality reduction [9], [10].
- Line losses increase: produced by neutral line losses and a non-optimal distribution of phase currents [11].
- Abnormal vibration and malfunction in induction equipment such as rotatory machines [12]–[14].
- Mal-operation of protection relays [14].
- Neutral to ground voltage (NGV) increase [7], [15].

Consequently, the distribution system operator (DSO), as the main responsible for the low voltage grid must guarantee the power supply, and also ensure its power quality. In this way, a wide variety of parameters used to quantify imbalances can be found in the literature [6], [10], [16], [17]. Possibly the most common way to evaluate imbalances is through the unbalance factor (UF), which is defined by decomposing the network into its symmetrical components. Thus, if only positive and negative sequence are considered, the UF is usually expressed as:

$$UF = \frac{|G_{neg}|}{|G_{pos}|} \quad (1)$$

where  $G$  can be current or voltage quantities. However, for 3P-4W networks, the zero sequence should be taken into account in the previous definition, leading to the following expression:

$$UF_0 = \frac{\sqrt{|G_{zero}^2| + |G_{neg}^2|}}{|G_{pos}|} \quad (2)$$

Usually, these parameters are preceded by a  $V$  when they refer to voltages or by a  $C$  when they are calculated from current values. Since most of the problems for consumers are caused by voltage imbalances and not current imbalances, the

most important standards define the voltage unbalance factor (VUF) and their limits. ANSI [18] recommends VUF values lower than 3% since IEC [19] and CIGRE [20] set the limit at 2%, allowing to reach 3% in networks with a high presence of single-phase customers, to ensure the quality of supply. The negative sequence has direct consequences on the malfunctioning of induction machines. However, zero sequence produce neutral currents and heating in electric machines [21], [22], especially in transformers, which reduces the life time of the equipment and can even lead to breakdowns. For this reason, more references to  $VUF_0$  than to VUF are found in academia and research [23]–[25]. Moreover, the current unbalance factors (CUF and  $CUF_0$ ) can be defined in the same way as for voltage. Finally, the neutral current ( $|\bar{I}_n|$ ) is sometimes used as a representative parameter of the line unbalance:

$$|\bar{I}_n| = |\bar{I}_a + \bar{I}_b + \bar{I}_c| \quad (3)$$

To minimize the impact of imbalances, and thus improve the power quality and reliability of supply, several authors propose different methods that can be grouped into two categories [6]. Reconfiguration techniques consist in acting on the switches located in the network to achieve a better distribution of the power flow. In turn, two different methods can be distinguished in this technique: distribution feeder reconfiguration [26], [27] is a method to alter the topological structure of the grid by changing the switch status; whereas phase balancing technique [28], [29] alters the phase connection among phases (known as phase swapping).

The second category mitigates network imbalance by adding special current compensating devices. This category is further classified into three approaches. The first one, reduce the impact of imbalances in the grid by increasing power rating capacity of equipment: oversizing protections, DT and wires or separating the neutral conductor [30]. The next step consists in introducing more resistant to imbalances special transformer configurations e.g. Scott transformer, T-connected transformer and star-hexagon transformer, or by adding active filters to the DT [31]–[34]. Unlike the previous ones, the third technique does not mitigate the consequences of imbalances, but rather combats their origin by installing purpose-built shunt-connected active power filters (APF). The most commonly used APF topologies are three single-phase H-bridge, 3P-4W capacitor midpoint and 3P-4W four legs (4L) topologies [35]–[37].

The aim of this paper is to discuss the effect of removing current imbalances in an urban grid. For this purpose, a D-STATCOM has been designed and installed in a residential area of the Spanish city of Malaga. The remainder of this paper is organized as follows. Section II details the power converter characteristics, including the topology and control algorithms used for current balancing. Section III analyzes the results obtained during one-month field tests. The consequences of the installation of the D-STATCOM are discussed in Section IV. Finally, the conclusions of this paper are drawn in Section V.

## II. PROPOSED SOLUTION

In order to achieve a DER which allows to mitigate the current imbalances in a low-voltage distribution grid, this paper analyses the installation of a D-STATCOM prototype in an urban line where imbalances are frequent. The developed D-STATCOM is a 3P-4W 4L APF. This topology has been chosen due to it reach a greater performance than 3P-4W capacitor midpoint topology and a smaller size and number of components than three single-phase H-bridge converters [38]. In addition, in order to improve the harmonic content and reduce the size and cost of the grid filter, the three-level neutral-point-clamped (NPC) I-type topology [39], shown in Fig. 1a, has been chosen. Moreover, 3P-3W NPC topologies are widely used in vehicle-to-grid (V2G) EV chargers [40], [41], battery energy storage systems and photovoltaic inverters [42], and can be slightly modified to add a fourth leg and improve its performance allowing unbalanced operation. The developed power converter is based on Si IGBTs with a switching frequency of 20 kHz, making its operation completely noiseless. Thus, the prototype shown in 1b has been designed to perform a rated power of 35 kVA with a maximum balancing capacity of 70 A.

In addition, Fig. 2 shows the control scheme implemented in the D-STATCOM to perform the balancing of the line. Firstly, active and reactive power in the grid are measured ( $P_i^{down}$ ,  $Q_i^{down}$ ) and the power references to balance the grid are calculated. The DC-link voltage ( $V_{dc}$ ) is regulated by the D-STATCOM without any external source, therefore a PI controller estimates the power required to maintain a constant voltage in the DC side ( $P_{dc}^{comp}$ ). Then, a SOGI filter [43] is applied to obtain single-phase instantaneous direct and quadrature components from the grid voltages, that are used to determine current references ( $I_i^{ref}$ ) from active and reactive power setpoints. Next, the input error signals for a current controller, obtained from current reference signals and D-STATCOM's output measures, determines the voltage to be applied by the stack to obtain the power setpoints. Moreover, NPC I-type converters suffer from unbalances between the DC-link capacitors ( $V_{c1}$  and  $V_{c2}$ ) that must be compensated. Several modulation techniques with capacitor voltage balance capacity can be found in literature [44], [45]. In this case, the technique presented in [46] has been implemented due to reduce capacitor midpoint oscillation without increase power losses.

According to the Fortescue's theorem [47], any three-phase system can be represented by three symmetrical components. In practice, in a voltage-balanced electrical system, only the direct component of the current is capable of carrying effective power, whereas zero and negative components create pulsed power flows of zero mean value, adversely affecting the efficiency of the grid. Therefore, as Fig. 3 shows, the D-STATCOM is shunt connected to the utility grid to eliminate zero and negative sequence currents, so that upstream of the device the current is completely balanced. In this project, to allow balancing at a different point than the D-STATCOM

installation point, grid values downstream are measured through a commercial grid analyzer, that sends average values of active and reactive power to the control DSP, limiting the line balancing to the fundamental frequency. Thus, given a generic electrical system with unbalanced currents, the power flow of each phase is given by the following expression:

$$\left. \begin{aligned} P_i^{down} &= Re\{\bar{V}_i^{down} \cdot \bar{I}_i^{down*}\} \\ Q_i^{down} &= Im\{\bar{V}_i^{down} \cdot \bar{I}_i^{down*}\} \end{aligned} \right\} \quad (4)$$

where active and reactive power ( $P_i^{down}$  and  $Q_i^{down}$ ) are determined from the complex value of voltage ( $\bar{V}_i^{down}$ ) and current ( $\bar{I}_i^{down}$ ) downstream each phase of the line ( $i = a, b, c$ ).

Of both power components, the active power is the only one that transmits energy, so that the reactive component could be eliminated to minimize the current in the network. In turn, the active power can be redistributed among the three phases as long as power conservation is satisfied ( $\sum P_i^{STAT} = 0$ ). Thus, the desired power flow ( $P_i^{up}$  and  $Q_i^{up}$ ) in each of the phases upstream of the D-STATCOM will be the average power downstream:

$$\left. \begin{aligned} P_i^{up} &= \bar{P} = \frac{\sum P_i^{down}}{3} \\ Q_i^{up} &= 0 \end{aligned} \right\} \quad (5)$$

where  $\bar{P}$  is one third of the total power flowing through the line.

Thus, the power to be injected by the D-STATCOM ( $P_i^{STAT}$  and  $Q_i^{STAT}$ ) can be calculated as the difference between the power downstream and upstream of the device:

$$\left. \begin{aligned} P_i^{STAT} &= P_i^{down} - P_i^{up} = P_i^{down} - \bar{P} \\ Q_i^{STAT} &= Q_i^{down} - Q_i^{up} = Q_i^{down} \end{aligned} \right\} \quad (6)$$

## III. RESULTS

Fig. 4 shows the set up of the D-STATCOM installation in an urban environment. The power electronics cabinet can be seen on the right side of the picture, while the device is connected to the line inside the left enclosure. This enclosure has the protection components (fuses and disconnecter) to allow safe handling of the prototype. In addition, a grid analyzer has been installed to measure the line parameters downstream the connection point which send this information, via Modbus communication, to the unit to perform the balancing algorithm. The D-STATCOM prototype has been installed in an intermediate point of a power line located in a residential area in the city of Malaga (Spain), in the living lab of e-distribución [48]. The prototype is framed in the scope of PASTORA Project (Preventive Analysis of Smart Grids with Real Time Operation and Renewable Assets Integration) [49], that aims at providing AI based solutions for maintenance and flexible operation purposes. Fig. 5 shows the one-line diagram of the network in which the prototype has been installed, where it can be seen that eight different lines depart from the DT, which is equipped with On-Load Tap Changing (OLTC)

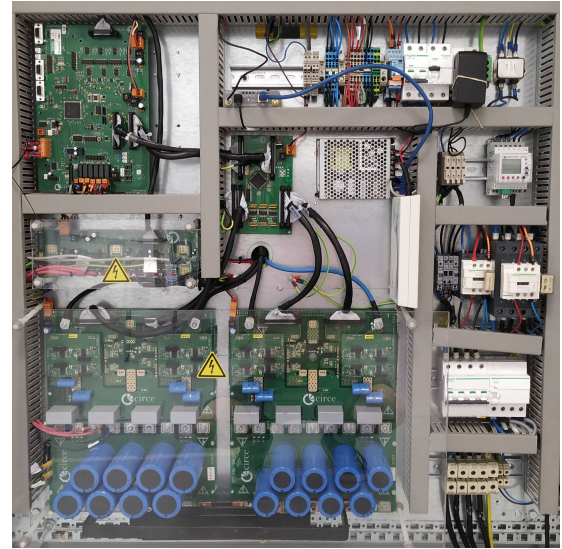
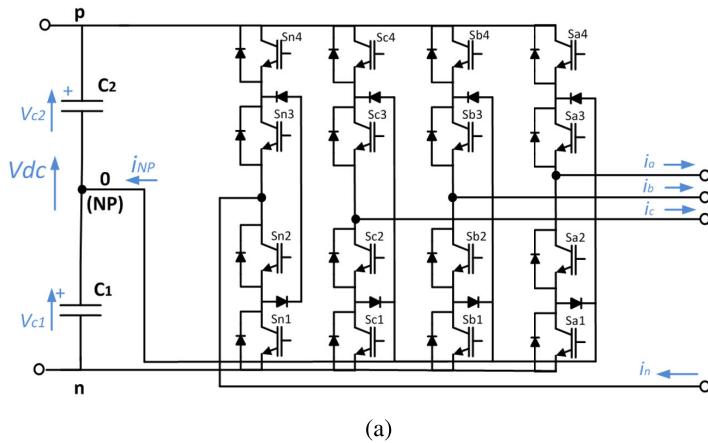


FIGURE 1. NPC I-type topology (a) and power electronics assembled inside the cabinet (b).

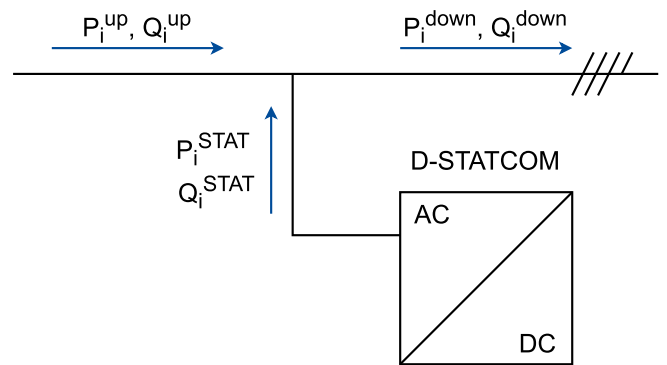
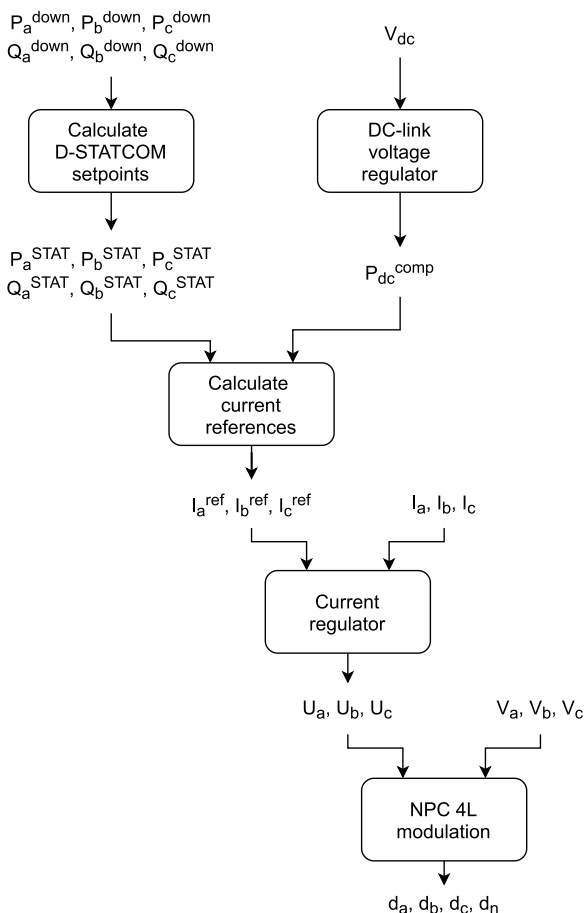


FIGURE 3. The D-STATCOM is shunt connected to the grid, allowing a disconnection without power supply interruptions. The sign convention used for power flows is shown.

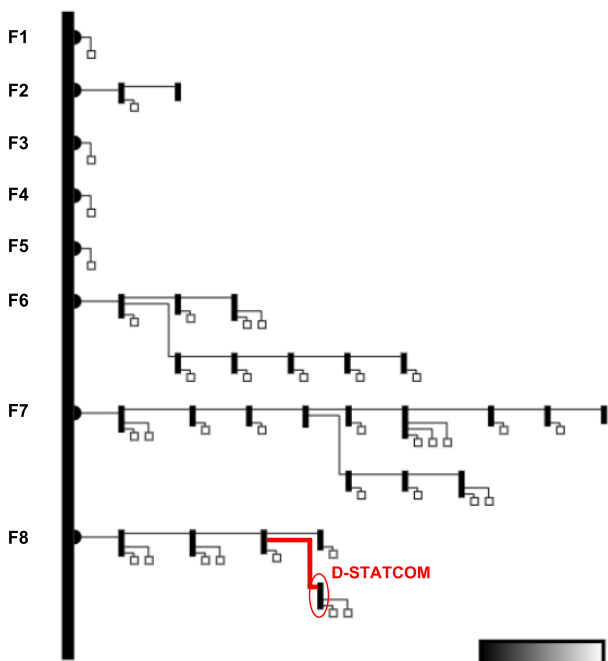
loads connected to the same phase, which causes frequent unbalances on that line. Thus, this location has been chosen for the D-STATCOM deployment to compensate imbalances as close as possible to the point where they are originated. In order to analyze the operation of the D-STATCOM in the grid, the measurements of the currents supplied by the device and downstream the unit have been recorded for one month (February 2021). From both measures the current upstream has been calculated to quantify the impact of the device in the line. With these parameters, the upstream current will be considered as the current corrected by the D-STATCOM and the downstream current as the current flow if the D-STATCOM had never been there, which will be used as a basis for comparison. Fig. 6 shows an oscilloscope snapshot where the prototype is consuming 7 kW from the *c* phase to supply them into the *a* phase whereas *I<sub>b</sub>* current is zero. In addition, DC capacitor voltage oscillations are shown to prove that, although modulation does not completely eliminate the midpoint oscillations, they are reduced and allowing to reach a stable steady state.

FIGURE 2. D-STATCOM control diagram.

capabilities and belongs to a MV/LV Secondary Substation with advanced sensorization in the DT and the low-voltage switchboard. At the end of line F8, section highlighted in red in the image, there is a high concentration of single-phase



**FIGURE 4.** D-STATCOM prototype installed in a residential neighborhood in the city of Malaga. The power converter is installed in the cabinet on the right side, while the enclosure on the left side contains the shunt connection of the prototype to the grid, protection elements and measurements of the line downstream of the device.



**FIGURE 5.** Location where the D-STATCOM prototype has been installed within an urban network in the city of Malaga.

Furthermore, the efficiency of the D-STATCOM has been calculated. Table 1 shows the power losses as a function of the D-STATCOM output power. These measurements have been

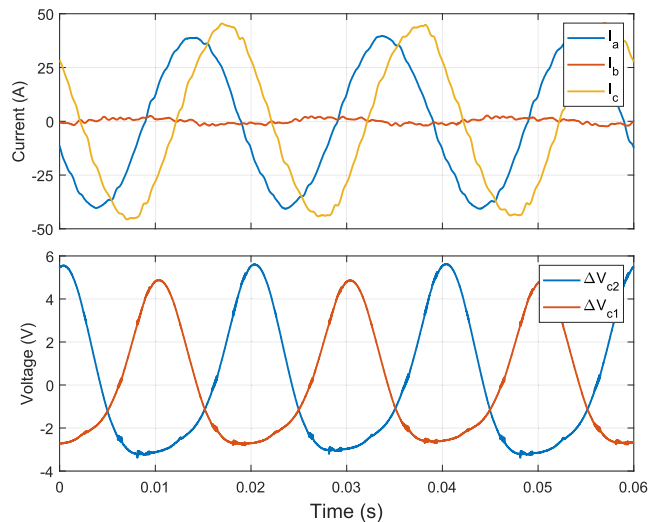


**FIGURE 6.** Three-phase currents (top) and capacitor voltage oscillating component  $\Delta V_{c1}$  and  $\Delta V_{c2}$  (bottom) at  $P_i^{STAT} = \{7, 0, -7\}$  kW and  $Q_i^{STAT} = \{0, 0, 0\}$  kVAR.

taken with the prototype injecting reactive power at balanced setpoints. In addition, according to California Energy Commission (CEC) [50], the prototype achieves a CEC efficiency of 97.7 %.

In order to show the operation of the D-STATCOM in the grid, Fig. 7 represents the current in the three phases and the neutral wire downstream and upstream of the connection

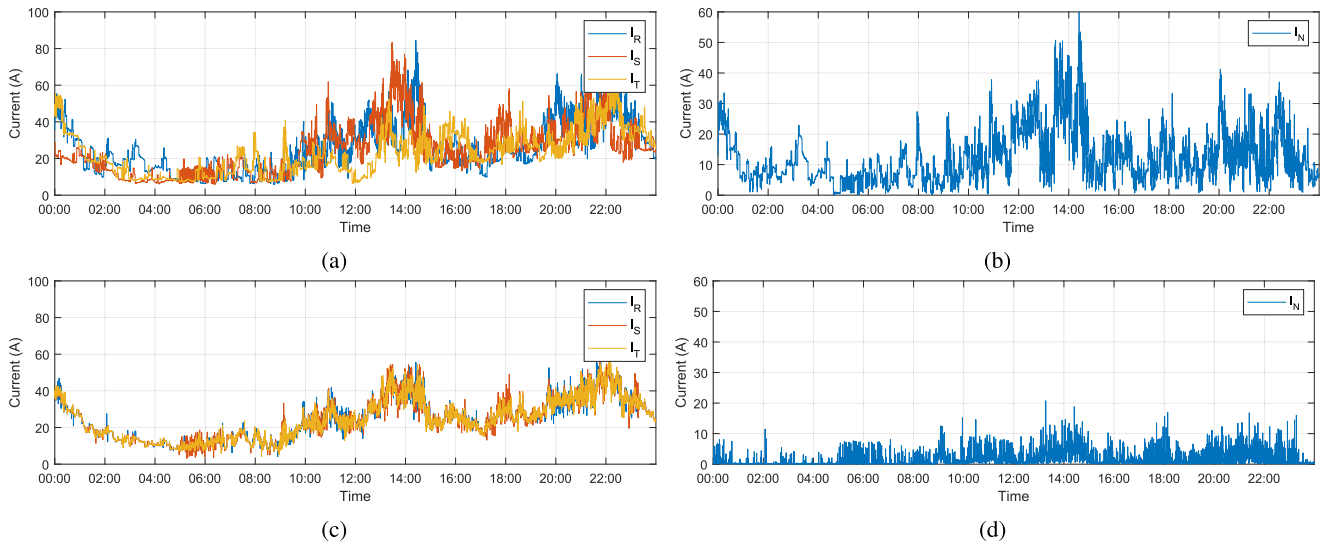


**FIGURE 7.** Comparison of the current through the wires with and without D-STATCOM: phase currents downstream (a), neutral current downstream (b), phase currents upstream (c), and neutral current upstream (d).

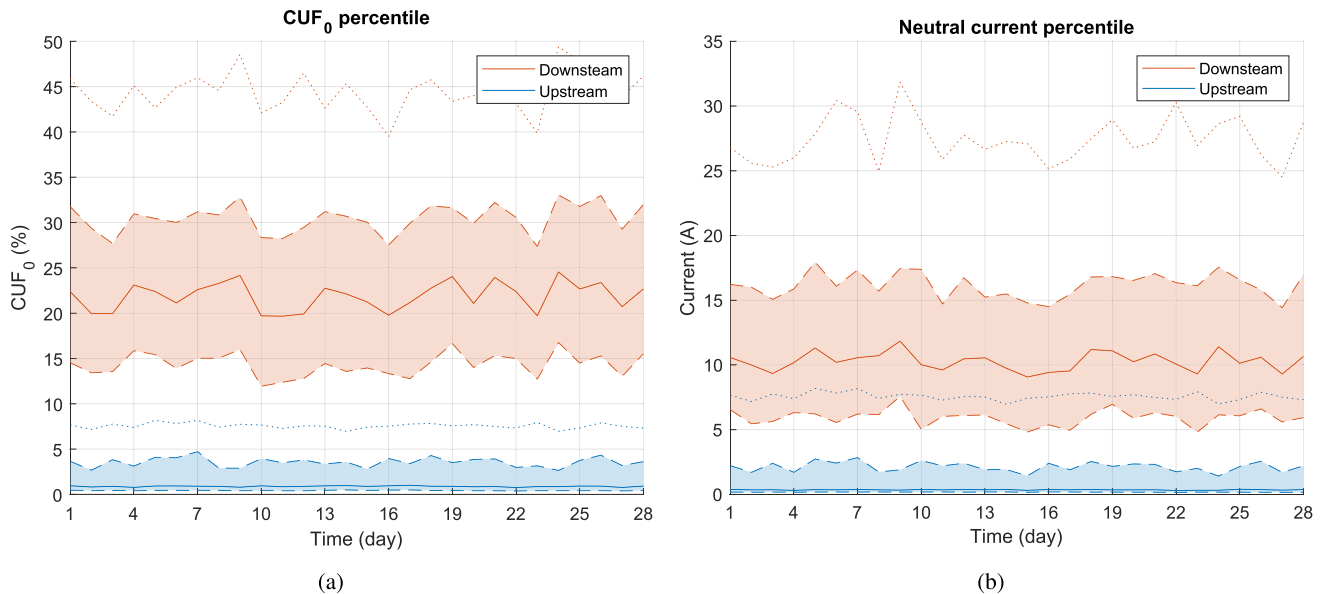


**FIGURE 8.** Effect of the D-STATCOM on the grid comparing 25th, 50th, 75th and 95th percentiles of  $CUF_0$  (a), and neutral current (b) downstream (orange) and upstream (blue) the D-STATCOM.

**TABLE 1.** D-STATCOM power losses and efficiency in function of the three-phase output apparent power.

Load (%)	Output power (kVA)	Power losses (W)	Efficiency (%)
5	174	1.96	91.1
10	170	3.56	95.2
20	187	7.03	97.3
30	250	10.54	97.6
50	370	17.54	97.8
60	450	21.03	97.8
75	580	26.28	97.7
90	730	31.53	97.6
100	810	34.68	97.6

point was first analyzed for 24 hours. On the one hand, it can be noted that the imbalances present downstream, mainly in the period 12:00-15:00 and 20:00-1:00 (Fig. 7a), have been

eliminated upstream where it can be seen that the currents in the three phases are similar (Fig. 7b). As a result, the RMS current in the period between 13:00 and 15:00 present in the most load cable has been reduced from more than 80 A to less than 60 A. On the other hand, the neutral current has been significantly reduced from conducting tens of amperes most of the day (Fig. 7d) to being virtually unloads for the whole day (Fig. 7c). However, total balancing has not been achieved due to three factors: the approximation to the fundamental frequency in the calculation of the references, the delay produced in the communications between the grid analyzer and the D-STATCOM, and the sporadic presence of unbalances higher than the rated power of the prototype.

In order to obtain more significant results, the data analyzed in Fig. 7 has been obtained for a 4-weeks period, from

February 1st to February 28th, 2021. As explained before, the operation of the D-STATCOM proposed in this paper directly acts over current imbalances so that, its results are directly related with CUF. With the information obtained during the 28 days analyzed, the instantaneous values of  $CUF_0$  were calculated and analyzed, obtaining the median of these values and the 25th, 75th and 95th percentiles on a daily basis. The evolution of these results throughout the entire month is shown in Fig. 8a downstream the D-STATCOM in orange, and upstream in blue. The median value is represented by the solid line within the shaded area between 25th and 75th percentiles, whereas the 95th percentile has been represented by the upper dotted lines.

Moreover, as explained above, one of the main consequences and most important benefits of the line balancing is the neutral current reduction. As in the previous case, Fig. 8b shows the 25th, 50th, 75th and 95th percentiles for neutral current upstream and downstream for the 28 days analyzed.

Fig. 8a shows a clear reduction of the  $CUF_0$ , where it can be seen that the shaded area has been reduced from the range 15 % – 30 % downstream to 0 % – 2.5 % upstream. Similarly, the maximum values have been reduced from around 45 % to less than 10 %, and the median value of the whole month has dropped from 21.9 % to 0.9 %.

In the same way, the shaded area of the neutral current has been reduced from the range of 5 A – 15 A to 0 A – 2.5 A (see Fig. 8b). In addition, current peaks through the neutral wire have been minimized from more than 25 A to less than 10 A. Thus, the current in the neutral wire has been practically suppressed, decreasing its average value from 10.3 A to 0.4 A.

The power factor (PF) shows the relationship between active power (P) and apparent power (S) in an electric line. It provides information on how optimal the power transmission is, giving a maximum line utilization when  $P = S$  and  $PF = P/S = 1$ ; hence, the lower PF the lower line efficiency. However, although the calculation of the PF is trivial in balanced three-phase networks, this does not happen in unbalanced grids. [51] shows, how the different ways of calculating S affect PF and proposes the effective apparent power ( $S_e$ ).  $S_e$  assumes a virtual balanced circuit that has exactly the same line power losses as the actual balanced circuit. This equivalence leads to the definition of an effective current  $I_e$

$$3rI_e^2 = r(I_a^2 + I_b^2 + I_c^2 + \rho I_n^2) \quad (7)$$

where  $r$  is the line resistance and  $\rho$  is the ratio of neutral and line wire resistances. In addition, [51] defines the effective voltage ( $V_e$ ) so that  $S_e$  can be calculated in the same way as in a balanced line

$$S_e = 3V_e I_e \quad (8)$$

leading to the definition of the effective power factor

$$PF_e = \frac{P}{S_e} \quad (9)$$

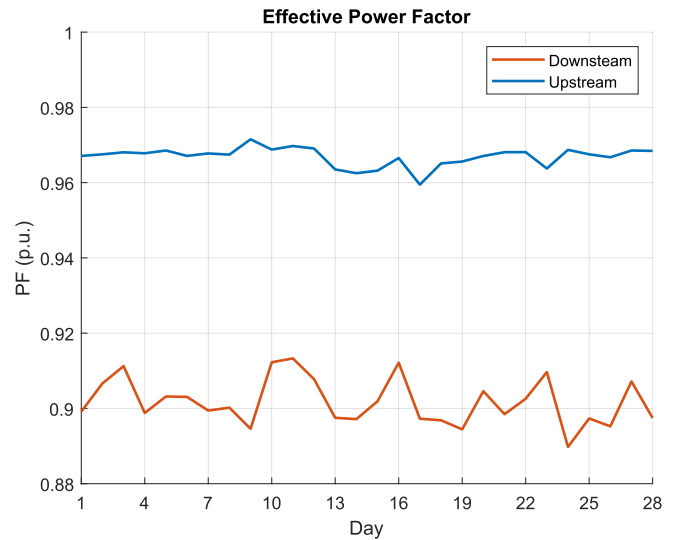


FIGURE 9. Daily average effective power factor downstream (orange) and upstream (blue).

Furthermore, [51] defines  $PF_e$  taking into account harmonics generated by non-linear loads. This approximation has been used to calculate the  $PF_e$  during the operation of the D-STATCOM. Thus, Fig. 9 shows the daily average  $PF_e$  downstream and upstream the power converter, that has been improved from a mean value of 0.901 to 0.967.

As eq. (7) shows, power losses are proportional to the equivalent squared current, so that the reduction in power losses achieved with the D-STATCOM can be calculated as

$$\begin{aligned} \Delta P(\%) &= \frac{3r(I_e^{down})^2 - 3r(I_e^{up})^2}{3r(I_e^{down})^2} \cdot 100 \\ &= \left(1 - \left(\frac{I_e^{up}}{I_e^{down}}\right)^2\right) \cdot 100 \end{aligned} \quad (10)$$

By substituting eq. (8) and (9) in (10), and simplifying  $V_e$  and P that must be equal downstream and upstream, the following relationship between power loss reduction and  $PF_e$  is reached

$$\Delta P(\%) = \left(1 - \left(\frac{PF_e^{down}}{PF_e^{up}}\right)^2\right) \cdot 100 \quad (11)$$

where substituting the  $PF_e$  mean values calculated previously a loss reduction of 13 % is obtained.

As discussed above, the VUF is a key parameter regulated by current legislation. Since, unlike current, the function relating voltage and position on the line is continuous, thus, it is impossible to analyze the VUF in the same way as was done for current indicators. For this reason, the DSO has provided phase voltage measurements from a close-located smart meter and the transformer substation, at the line header. The data analyzed correspond to the months of February 2020 (when the D-STATCOM had not yet been installed) and February 2021.

Thus, the measures from both locations and dates have been analyzed to compare the VUF values without and

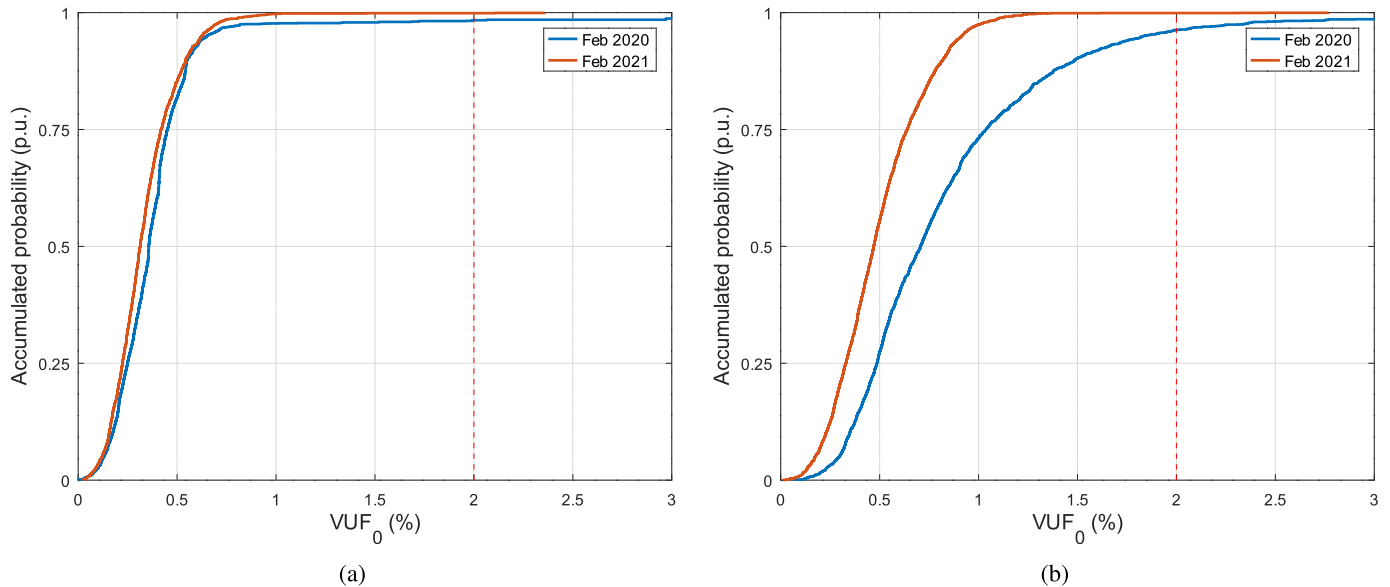


**FIGURE 10.** Comparison of  $VUF_0$  values with D-STATCOM (February 2021) and without D-STATCOM (February 2020), at the transformer substation (a) and at a consumption point close to the location of the prototype (b).

with D-STATCOM, respectively. Fig. 10a shows the  $VUF_0$  cumulative probability diagram at the transformer substation whereas Fig. 10b shows the same results at near to the D-STATCOM. On the one hand, it can be seen that there are no significant differences between the two years analyzed near to the line header. However, in the influence area of the device, a change in trend between the two years can be seen. The results shown a clear decrease in the time that the network is unbalanced, especially noticeable for unbalance values above 0.5 %. Thus, whereas during February 2020, the  $VUF$  value was below 1 % for approximately 75 % of the time, in February 2021, with the D-STATCOM in operation, this value increased to 97 %.

#### IV. DISCUSSION

The legislation establishes the VUF as a normative parameter to ensure the quality of supply to consumers of the electricity grid. However, this parameter do not represent the totality of the problems caused by imbalances in the network. Therefore, other parameters highlighted in the literature have also been analyzed. First, how the D-STATCOM has contributed to the reduction of  $CUF_0$  on the line has been analyzed. The mean value of the current imbalances has dropped from 21.9 % to 0.9 % during the month under analysis. This reduction will mainly impact in a more balanced voltage drop along the line, and therefore in less unbalance in the supply voltage. Another direct consequence of the reduction of current imbalances has been seen in the reduction of neutral current. This conductor must be sized in its design to withstand the maximum current flowing through it. In this case, the maximum current detected during the period analyzed has been reduced by 77 %, from 30 A to 7 A, which would make it possible to use conductors of smaller cross-section and therefore more economical.

Then, an approximation has been established to determine the power losses in the line, since these are proportional to the square of the current flowing through the network. This has resulted in a reduction of 13 % in conduction losses. This reduction only occurs on the line where the prototype has been installed and, since a 13 % reduction in losses in a single line are low compared to those of a complete network, these will not result in significant savings. However, this parameter clearly represents how imbalances affect the efficiency of the grid and how the efficiency could be improved if imbalances are faced.

Finally, the  $VUF_0$  has been calculated in the DT and a smart meter near to the D-STATCOM prototype. Although no improvements were observed at the network header, there was a notable reduction in voltage imbalances at the supply points furthest from the DT. Thus, despite the limited data available for this analysis, there is evidence that the D-STATCOM has also contributed to improving the power quality parameters established by legislation.

#### V. CONCLUSION

The rapid electrification of the power sector is revealing a number of problems that compromise grid stability. This paper has proposed a D-STATCOM for current balancing in low voltage distribution grids. The designed converter has a 4W-4L topology with a switching frequency of 20 kHz, making its operation completely soundless. This prototype achieves a rated power of 35 kVA, which allows a maximum current balancing capacity of 70 A.

The D-STATCOM prototype has been commissioned successfully in a residential area of the city of Malaga (Spain) in order to test its operation in a real environment. The data acquired over a period of one month demonstrates the ability of the unit to decrease neutral current from 30 A to 8 A in

the worst case, reduce technical losses by 13 % and improve power quality in the line. The paper has shown how technical losses have been reduced and quantified them, as well as has pointed out at which level the neutral current has been reduced at the installation site.

Furthermore, the proposed solution can be implemented in a wide range of possible three-phase equipment applications such as EV chargers, PV facilities and energy storage systems, adding an interesting extra-functionality to these devices.

## REFERENCES

- [1] *Going Climate-Neutral by 2050: A Strategic Long-Term Vision for a Prosperous, Modern, Competitive Climate-Neutral EU Economy*. European Union, Maastricht, The Netherlands, 2019.
- [2] *Renewables 2021 Global Status Rep.*, REN21, Paris, France, 2021.
- [3] *Statistical Review of World Energy 2021*, BP, London, U.K., 2021.
- [4] *Global EV Outlook 2021*, IEA, Paris (France), Tech. Rep., 2021.
- [5] *Distributed Energy Resources for Net Zero: An Asset or a Hassle to the Electricity Grid*. Accessed: Sep. 14, 2021. [Online]. Available: <https://www.iea.org/commentaries/distributed-energy-resources-for-net-zero-an-asset-or-a-hassle-to-the-electricity-grid>
- [6] M. R. Islam, H. Lu, M. J. Hossain, and L. Li, "Mitigating unbalance using distributed network reconfiguration techniques in distributed power generation grids with services for electric vehicles: A review," *J. Cleaner Prod.*, vol. 239, Dec. 2019, Art. no. 117932.
- [7] T. M. Gruz, "A survey of neutral currents in three-phase computer power systems," *IEEE Trans. Ind. Appl.*, vol. 26, no. 4, pp. 719–725, Jul./Aug. 1990.
- [8] Q. Song, Z. Yin, J. Xue, and L. Zhou, "Zero-sequence harmonics current minimization using zero-blocking reactor and zig-zag transformer," in *Proc. 3rd Int. Conf. Electr. Utility Deregulation Restructuring Power Technol.*, Apr. 2008, pp. 1758–1764.
- [9] *IEEE Power and Energy Society, IEEE Recommended Practice for Monitoring Electric Power Quality*, Standard 1159-2019, 1995, pp. 1–15.
- [10] C. I. Ciontea and F. Iov, "A study of load imbalance influence on power quality assessment for distribution networks," *Electricity*, vol. 2, no. 1, pp. 77–90, Mar. 2021.
- [11] S. P. Kim, S. G. Song, S. J. Park, and F. S. Kang, "Imbalance compensation of the grid current using effective and reactive power for split DC-link capacitor 3-leg inverter," *IEEE Access*, vol. 9, pp. 81189–81201, 2021.
- [12] S. Deleanu, M. Iordache, M. Stanculescu, and D. Nicolae, "The induction machine operating from a voltage supply, unbalanced and polluted with harmonics: A practical approach," in *Proc. 15th Int. Conf. Eng. Modern Electric Syst. (EMES)*, Jun. 2019, pp. 181–184.
- [13] J. M. Apsley, "Derating of multiphase induction machines due to supply imbalance," *IEEE Trans. Ind. Appl.*, vol. 46, no. 2, pp. 798–805, 2010.
- [14] C.-H. Yang, "Case studies of the impact of voltage imbalance on power distribution systems and equipment," in *Proc. 8th WSEAS Int. Conf. Appl. Comput. Appl. Comput. Sci.*, vol. 1, 2009, pp. 461–465.
- [15] M. J. E. Alam, K. M. Muttaqi, and D. Sutanto, "Alleviation of neutral-to-ground potential rise under unbalanced allocation of rooftop PV using distributed energy storage," *IEEE Trans. Sustain. Energy*, vol. 6, no. 3, pp. 889–898, Jul. 2015.
- [16] Z. Minter, J. Hill, J. C. De Oliveira, K. N. Miu, and S. M. Hughes, "A study of imbalance levels attributed to photovoltaic penetration in distribution systems," in *Proc. IEEE Power Eng. Soc. Transmiss. Distrib. Conf.*, Oct. 2020, pp. 1–4.
- [17] Y. J. Wang, "Analysis of effects of three-phase voltage unbalance on induction motors with emphasis on the angle of the complex voltage unbalance factor," in *Proc. IEEE Power Eng. Soc. Transmiss. Distrib. Conf.*, May 2002, vol. 2, no. 3, p. 1235.
- [18] *Electric Power Systems and Equipment—Voltage Ratings (60 Hertz)*, document ANSI C84.1-2011, 2011.
- [19] *Assessment of Emission Limits for Distorting Loads in MV and HV Power Systems, Technical Report Type 3*, document 61000-3-6:1996, IEC, 2008.
- [20] C. Cigré WG, "CIGRE technical brochure 261, power quality indices and objectives," CIGRE, Paris, France, Tech. Rep. 261, 2004. [Online]. Available: <https://e-cigre.org/publication/261-power-quality-indices-and-objectives>
- [21] M. A. Tsili and S. A. Papathanassiou, "Zero-sequence flux protection of a three-limb core power transformer," in *Proc. 17th Int. Conf. Electr. Mach. (ICEM)*, Sep. 2016, pp. 1–7. [Online]. Available: [http://users.ntua.gr/stpapat/Paper\\_2.65.pdf](http://users.ntua.gr/stpapat/Paper_2.65.pdf)
- [22] X. M. Lopez-Fernandez, C. Alvarez-Mari no, and P. Penabad-Duran, "RNM2D-0 fast stray losses hazard evaluation on transformer tank wall & cover due to zero sequence," in *Proc. 3rd Adv. Res. Workshop Transformers*, Oct. 2010, pp. 338–343.
- [23] F. Shahnia, P. J. Wolfs, and A. Ghosh, "Voltage unbalance reduction in low voltage feeders by dynamic switching of residential customers among three phases," *IEEE Trans. Smart Grid*, vol. 5, no. 3, pp. 1318–1327, May 2014.
- [24] J. Meyer, S. Hähle, P. Schegner, and C. Wald, "Impact of electrical car charging on unbalance in public low voltage grids," in *Proc. Int. Conf. Elect. Power Qual. Utilisation*, 2011, pp. 635–640.
- [25] M. T. Bina and A. Kashefi, "Three-phase unbalance of distribution systems: Complementary analysis and experimental case study," *Int. J. Electr. Power Energy Syst.*, vol. 33, no. 4, pp. 817–826, May 2011, doi: [10.1016/j.ijepes.2010.12.003](https://doi.org/10.1016/j.ijepes.2010.12.003).
- [26] A. Abbasi, "Investigation of simultaneous effect of demand response and load uncertainty on distribution feeder reconfiguration," *IET Gener., Transmiss. Distrib.*, vol. 14, no. 8, pp. 1438–1449, 2020.
- [27] H. Lotfi, R. Ghazi, and M. Naghibi-Sistani, *Multi-Objective Dynamic Distribution Feeder Reconfiguration Along With Capacitor Allocation Using a New Hybrid Evolutionary Algorithm*, vol. 11, no. 3. Berlin, Germany: Springer, 2020, doi: [10.1007/s12667-019-00333-3](https://doi.org/10.1007/s12667-019-00333-3).
- [28] B. Cortés-Cañedo, L. S. Avellaneda-Gómez, O. D. Montoya, L. Alvarado-Barrios, and C. Álvarez-Arroyo, "An improved crow search algorithm applied to the phase swapping problem in asymmetric distribution systems," *Symmetry*, vol. 13, no. 8, pp. 1–20, 2021.
- [29] O. D. Montoya, J. A. Alarcon-Villamil, and J. C. Hernández, "Operating cost reduction in distribution networks based on the optimal phase-swapping including the costs of the working groups and energy losses," *Energies*, vol. 14, no. 15, p. 4535, Jul. 2021.
- [30] A. Hiranandani, "Calculation of cable ampacities including the effects of harmonics," *IEEE Ind. Appl. Mag.*, vol. 4, no. 2, pp. 42–51, Mar. 1998.
- [31] K. Nikum, A. Wagh, R. Saxena, and A. Singh, "Power quality problems in large commercial load and their mitigation: A case study," in *Proc. IEEE 1st Int. Conf. Energy, Syst. Inf. Process. (ICESIP)*, Jul. 2019, pp. 1–5.
- [32] C. Dai and Y. Sun, "Investigation of the imbalance current compensation for transformers used in electric railways," in *Proc. Asia-Pacific Power Energy Eng. Conf.*, 2010, pp. 10–13.
- [33] P. Jayaprakash, B. Singh, and D. P. Kothari, "Three-phase 4-Wire DSTATCOM based on H-bridge VSC with a star/hexagon transformer for power quality improvement," in *Proc. IEEE Region 10 3rd Int. Conf. Ind. Inf. Syst.*, Dec. 2008, pp. 1–6.
- [34] T. H. Chen, "Comparison of Scott and Leblanc transformers for supplying unbalanced electric railway demands," *Electr. Power Syst. Res.*, vol. 28, no. 3, pp. 235–240, Jan. 1994.
- [35] D. Li, T. Wang, W. Pan, X. Ding, and J. Gong, "A comprehensive review of improving power quality using active power filters," *Electr. Power Syst. Res.*, vol. 199, Oct. 2021, Art. no. 107389.
- [36] A. Teke, L. Saribulut, M. E. M. Emin, and M. Tümay, "Active power filter: Review of converter topologies and control strategies," *Gazi Univ. J. Sci.*, vol. 24, no. 2, pp. 283–289, 2011.
- [37] D. Chen and S. Xie, "Review of the control strategies applied to active power filters," in *Proc. IEEE Int. Conf. Electric Utility Deregulation, Restructuring Power Technol.*, Oct. 2004, pp. 666–670.
- [38] A. Hintz, U. R. Prasanna, and K. Rajashekara, "Comparative study of the three-phase grid-connected inverter sharing unbalanced three-phase and/or single-phase systems," *IEEE Trans. Ind. Appl.*, vol. 52, no. 6, pp. 5156–5164, Nov. 2016.
- [39] R. Teichmann and S. Bernet, "A comparison of three-level converters versus two-level converters for low-voltage drives, traction, and utility applications," *IEEE Trans. Ind. Appl.*, vol. 41, no. 3, pp. 855–865, May 2005.
- [40] G. B. Sahinler and G. Poyrazoglu, "V2G applicable electric vehicle chargers, power converters & their controllers: A review," in *Proc. 2nd Global Power, Energy Commun. Conf. (GPECOM)*, Oct. 2020, pp. 59–64.
- [41] M. Yilmaz and P. T. Krein, "Review of battery charger topologies, charging power levels, and infrastructure for plug-in electric and hybrid vehicles," *IEEE Trans. Power Electron.*, vol. 28, no. 5, pp. 2151–2169, May 2013.

- [42] J. Ballestín-Fuertes, J. Muñoz-Cruzado-Alba, J. F. Sanz-Osorio, L. Hernández-Callejo, V. Alonso-Gómez, J. I. Morales-Aragones, S. Gallardo-Saavedra, O. Martínez-Sacristan, and Á. Moretón-Fernández, "Novel utility-scale photovoltaic plant electroluminescence maintenance technique by means of bidirectional power inverter controller," *Appl. Sci.*, vol. 10, no. 9, p. 3084, Apr. 2020.
- [43] J. Xu, H. Qian, Y. Hu, S. Bian, and S. Xie, "Overview of SOGI-based single-phase phase-locked loops for grid synchronization under complex grid conditions," *IEEE Access*, vol. 9, pp. 39275–39291, 2021.
- [44] J. Pou, J. Zaragoza, S. Ceballos, M. Saedifard, and D. Boroyevich, "A carrier-based PWM strategy with zero-sequence voltage injection for a three-level neutral-point-clamped converter," *IEEE Trans. Power Electron.*, vol. 27, no. 2, pp. 642–651, Feb. 2012.
- [45] I. Lopez, S. Ceballos, J. Pou, J. Zaragoza, J. Andreu, I. Kortabarria, and V. G. Agelidis, "Modulation strategy for multiphase neutral-point-clamped converters," *IEEE Trans. Power Electron.*, vol. 31, no. 2, pp. 928–941, Feb. 2016.
- [46] I. López, S. Ceballos, J. Pou, J. Zaragoza, J. Andreu, E. Ibarra, and G. Konstantinou, "Generalized PWM-based method for multiphase neutral-point-clamped converters with capacitor voltage balance capability," *IEEE Trans. Power Electron.*, vol. 32, no. 6, pp. 4878–4890, Jun. 2017.
- [47] C. L. FORTESCUE, "Method of symmetrical co-ordinates applied to the solution of polyphase networks," *Trans. Amer. Inst. Electr. Eng.*, vol. 37, pp. 1027–1140, Oct. 1918.
- [48] *Living Lab de Smartcity Málaga*[Endesa. Accessed: Sep. 14, 2021. [Online]. Available: <https://www.endesa.com/es/proyectos/todos-los-proyectos/transicion-energetica/redes-inteligentes/living-lab-malaga-ciudad-futuro>
- [49] *PASTORA, Inteligencia Artificial Red Distribución*[Endesa. Accessed: Sep. 14, 2021. [Online]. Available: <https://www.endesa.com/es/proyectos/todos-los-proyectos/transicion-energetica/redes-inteligentes/pastora-inteligencia-artificial-red-distribucion>
- [50] J. Newmiller, W. Erdman, J. S. Stein, and S. Gonzalez, "Sandia inverter performance test protocol efficiency weighting alternatives," in *Proc. 40th Photovolt. Spec. Conf.*, 2014, pp. 897–900.
- [51] *IEEE Standard Definitions for the Measurement of Electric Power Quantities Under Sinusoidal, Nonsinusoidal, Balanced, or Unbalanced Conditions*, Standard 1459, 2010.



**JAVIER BALLESTÍN-FUERTE**S received the B.Sc. and M.Sc. degrees in electrical engineering from the University of Zaragoza, Spain, in 2017 and 2019, respectively. He is currently pursuing the Ph.D. degree in power electronics for grid support with the Electronics Systems Group, CIRCE Foundation. Since 2018, he has been working as a Researcher with the Electronics Systems Group, CIRCE Foundation. His main research interests include control of power electronics converters for grid support applications and EV charging.



**JOSÉ F. SANZ-OSORIO** received the Ph.D. degree in industrial engineering from the University of Zaragoza. From 2000 to 2016, he was the Director of the Research group for "Renewable Energy Integration and Power Electronics Configurations," CIRCE Foundation. He is currently a Senior Lecturer with the Electrical Department, University of Zaragoza; the Director of the "Endesa Red" Chair of Aragón; and the Director of the Research Laboratory of Charging Solutions for Electric Vehicles and Impact on the Electricity Grid. His main research interests include renewable energy integration and storage systems, power electronics for grid connection systems, microgrids, smart grids, and development of charging solutions for electric vehicles, both conductive and inductive.



**JESÚS MUÑOZ-CRUZADO-ALBA** was born in Cádiz, Spain, in 1984. He received the B.S. and M.S. degrees in telecommunications and electronics engineering and the Ph.D. degree in power electronics from the University of Seville, Seville, Spain, in 2007, 2011, and 2016, respectively. In 2009, he joined GPTEch, Seville, where he was a part of the Research and Development Department developing power converters for renewable energies applications. Since 2017, he has been a Power Electronics Researcher with Fundación CIRCE, where he is currently a Leader of the Power Electronics Team for Grid Integration Applications.



**ERIKA LAPORTA PUYAL** received the B.Sc. degree in industrial technical engineering (specialized in industrial electronics) and the M.Sc. degree in electronics engineering (power electronics specialization) from the University of Zaragoza, Spain, in 2010 and 2016, respectively. Since March 2009, she has been working as a Project Manager and a Researcher with the Electronic Systems Group, CIRCE Foundation, where she is the responsible of the PCB and hardware design and manufacturing, as well as the management on research and development projects related to: electric vehicle charger (slow, medium, fast, and wireless inductive charge), power storage systems, and power electronics for renewable energies. She has imparted some courses in the renewable energies master of CIRCE and has participated in several Spanish and European research projects.



**JAVIER LEIVA** received the degree (Hons.) in industrial engineering from the University of Malaga, in 2010, the M.Sc. degree in electrical energy systems from the University of Seville, in 2010, and the Ph.D. degree (*cum laude*) from the Inter-University Program in Electrical Power Systems, University of the Basque Country, and the Polytechnic of Catalonia, in 2021. He joined Endesa, in 2010, where he currently works as an Expert in Innovative Business Opportunities within Global Infrastructure and Networks Unit of Enel. He has a strong background in living laboratories and smart cities, in addition to network flexibility, DER integration, and electric mobility. He received the Best Dissertation Award for the M.Sc. degree.



**JACOB RODRIGUEZ RIVERO** is currently a Telecommunication Engineer with the University of Seville and a Executive Master in Business Administration (EMBA) with I. I. San Telmo (IESE). He was with Endesa and Enel for 18 years, he currently works as a Unit Manager with Endesa Ingeniería, an Innovation Project Manager with Endesa Red, and the Head of Subsidized Programs with Edistribución. In addition, he is an Associated Teacher in telecommunication degree at the University of Granada.

•••



# Capítulo 6

## **Sistemas de almacenamiento en baterías de flujo y sus interfaces de potencia para la prestación de servicios auxiliares a la red**

**RESUMEN:** La variabilidad de las fuentes de energía renovable suponen un reto para la consecución de los objetivos de descarbonización del sector eléctrico. La solución a este problema radica en el desarrollo de sistemas de almacenamiento energético. En la literatura se proponen varios sistemas como las centrales hidroeléctricas de bombeo, el hidrógeno verde o sistemas de baterías. Entre estos últimos las baterías de flujo constituyen una alternativa viable en sistemas destinados al ajuste de generación y demanda. El artículo *Power Grid Integration and Use-Case Study of Acid-Base Flow Battery Technology*, propone tres casos de uso para la obtención de servicios de red adicionales, a diferentes escalas, a partir de un tipo específico de baterías de flujo que utilizan la electrolisis de agua como medio de almacenamiento energético.

## Article

# Power Grid Integration and Use-Case Study of Acid-Base Flow Battery Technology

Jesús Muñoz-Cruzado-Alba <sup>1,\*</sup>, Rossano Musca <sup>2</sup>, Javier Ballestín-Fuertes <sup>1</sup>, José F. Sanz-Osorio <sup>3,4</sup>, David Miguel Rivas-Ascaso <sup>1</sup>, Michael P. Jones <sup>1</sup>, Angelo Catania <sup>5</sup> and Emil Goosen <sup>6</sup>

- <sup>1</sup> Fundación CIRCE, Parque Empresarial Dinamiza, Avenida Ranillas Edificio 3D, 1ª Planta, 50018 Zaragoza, Spain; jballestin@fcirce.es (J.B.-F.); dmrivas@fcirce.es (D.M.R.-A.); mpjones@fcirce.es (M.P.J.)
- <sup>2</sup> Engineering Department, University of Palermo, Viale delle Scienze Ed. 9, 90128 Palermo, Italy; rossano.musca@unipa.it
- <sup>3</sup> Instituto Universitario de Investigación CIRCE, Universidad de Zaragoza, Edificio CIRCE, Campus Río Ebro, C/ Mariano Esquillor Gómez, 15, 50018 Zaragoza, Spain; jfsanz@unizar.es
- <sup>4</sup> Instituto Universitario de Investigación CIRCE, Fundación CIRCE, 50018 Zaragoza, Spain
- <sup>5</sup> S.MED.E Pantelleria S.p.a., Viale Strasburgo 189, 90146 Palermo, Italy; angelo.catania@smede.it
- <sup>6</sup> AquaBattery B.V., Lijnbaan 3c, 2352 CK Leiderdorp, The Netherlands; emil.goosen@aquabattery.nl
- \* Correspondence: jmunoz@fcirce.es; Tel.: +34-976-97-68-59

**Abstract:** There are many different types of energy storage systems (ESS) available and the functionality that they can provide is extensive. However, each of these solutions come with their own set of drawbacks. The acid-base flow battery (ABFB) technology aims to provide a route to a cheap, clean and safe ESS by means of providing a new kind of energy storage technology based on reversible dissociation of water via bipolar electro dialysis. First, the main characteristics of the ABFB technology are described briefly to highlight its main advantages and drawbacks and define the most-competitive use-case scenarios in which the technology could be applied, as well as analyze the particular characteristics which must be considered in the process of designing the power converter to be used for the interface with the electrical network. As a result, based on the use-cases defined, the ESS main specifications are going to be identified, pointing out the best power converter configuration alternatives. Finally, an application example is presented, showing an installation in the electrical network of Pantelleria (Italy) where a real pilot-scale prototype has been installed.

**Keywords:** energy storage systems; acid-base flow battery; power converters; power grid integration; distributed energy resources; power flow batteries; acid-base flow battery



**Citation:** Muñoz-Cruzado-Alba, J.; Musca, R.; Ballestín-Fuertes, J.; Sanz-Osorio, J.F.; Rivas-Ascaso, D.M.; Jones, M.P.; Catania, A.; Goosen, E. Power Grid Integration and Use-Case Study of Acid-Base Flow Battery Technology. *Sustainability* **2021**, *13*, 6089. <https://doi.org/10.3390/su13116089>

Academic Editor: Nicu Bizon

Received: 4 May 2021

Accepted: 24 May 2021

Published: 28 May 2021

**Publisher's Note:** MDPI stays neutral with regard to jurisdictional claims in published maps and institutional affiliations.



**Copyright:** © 2021 by the authors. Licensee MDPI, Basel, Switzerland. This article is an open access article distributed under the terms and conditions of the Creative Commons Attribution (CC BY) license (<https://creativecommons.org/licenses/by/4.0/>).

## 1. Introduction

As the gravity of the climate crisis exerts ever increasing pressure on governments and industries alike, the already rapid acceleration of renewable energy procurement will continue to increase at pace. Fueled by the ever-decreasing cost of distributed energy resources (DER) such as photovoltaic (PV) and wind, it currently seems that a successful rollout of renewables will be boosted by providing cheap energy storage technologies.

Historically, a large proportion of power was generated by the burning of fossils fuels. This method of power generation is highly controllable, making it possible to match supply with demand and to respond to any imbalance in the grid. Given the intermittent nature of renewable energy sources (RES), matching supply with demand becomes a much greater task when renewables make up a significant proportion of the energy mix; however, energy storage systems (ESS) can be used to alleviate some of these problems. It is an unfortunate fact that currently, much of the energy generated by renewables must be discarded due to it being generated at a time when demand is low. Some authors reported that in Germany 4% of generated wind energy went to waste in 2015, while China discarded 17% of all its renewable energy generated, due to a lack of sufficient energy storage [1]. Likewise, it is often that the energy generated by renewables is unable to supply the entirety of the

load demand. With adequate energy storage integrated within the grid infrastructure, it becomes possible to store excess of renewable energy when supply is high or demand is low and release it when the opposite is true, adding an element of controllability and thus increasing the total amount of load supplied by renewables. In addition, thus, increasing the sustainability of the power grid generation sources by means of increasing the efficiency of the available resources.

There are many different types of ESS available, and the functionalities that they can provide are extensive. However, each of these solutions come with their own set of drawbacks, primarily their high cost. Operational and environmental safety is another important consideration; there is a growing list of incidents that includes explosions and fires that were caused by unstable ESS such as lithium-ion batteries [2] and important ethical concerns over the mining practices employed for the extraction of key minerals such as cobalt [3]. Therefore, a new type of ESS technology has been proposed recently, the acid-base flow battery (ABFB) [4,5] to help in the integration of RES at an affordable cost and in a more sustainable way, based on the acid/base and salinity concentration of water between several tanks.

It is known that electric power can be produced by exploiting the controlled mixing of salt and fresh water via reverse electro dialysis [6] with a high power energy density. Indeed, the energy released by mixing 1 m<sup>3</sup> of fresh water in seawater is equivalent to the hydropower that could be obtain in a fall of 270 m. This energy is released because of the increase in entropy when mixing solutions with different salinities, and is converted into electric energy by means of ion-exchange membranes in reverse electro dialysis (RED) [4]. Numerous advances have been made in this technology in the last decade [7].

The main principle is based on the selective transport of cations and ions through ion-exchange membranes (IEMs), resulting in a controlled mixing of salt and fresh water while generating an ionic current. On the other hand, the electro dialysis (ED) is the opposite process in which electricity is used to desalinate brackish water to produce fresh and saltwater [8,9]. Thus, using both methods, RED and ED, results in a system that could be used as an ESS (known as “concentration gradient flow battery”, CGFB).

The ABFB technology proposes to add bipolar membranes (BPM) auxiliary to IEMs to generate not only a salinity gradient, but also a pH gradient [4,10]. A BPM is a composite membrane consisting of oppositely charged ion-exchange layers, preventing theoretically any ion transportation through it. Despite that, ions are provided by water dissociation between the two layers [11]. With this approach, water is dissociated into protons and hydroxyde ions [5]. This extra-action results in 0.83 V per membrane for 1 M acid and base, increasing significantly the voltage that could be obtained by only salinity differences.

Figure 1 shows a scheme of the ABFB technology in which both acid/base and salt/freshwater tanks are pointed out. There are two clearly differentiated processes, charging and discharging. On the one hand, during the charging process, an electric field is applied over the stack producing a dissociation into hydroxyl ions and protons. Additionally, salt is added to a third tank and being carried out across monopolar membranes, an acidic and a basic solution is obtained in one compartment [4].

On the other hand, the discharging process requires an opposite electric field over the stack, producing an electric current flow through an external load, leading to the neutralization of acid and base solutions.

For instance, using a volume of 3 L (using 3 reservoirs of 1 L each) can hold up to 75 kJ (7 kWh/m<sup>3</sup>), i.e., an energy density significantly higher than pumped hydropower systems (PHSs) and the CGFB [4]. Therefore, the ABFB system offers great potential compared to current state-of-the-art ESS regarding aspects such as safety, costs and sustainability. Consequently, it is necessary to study most-competitive scenarios and how to overcome the power grid integration of such technology.

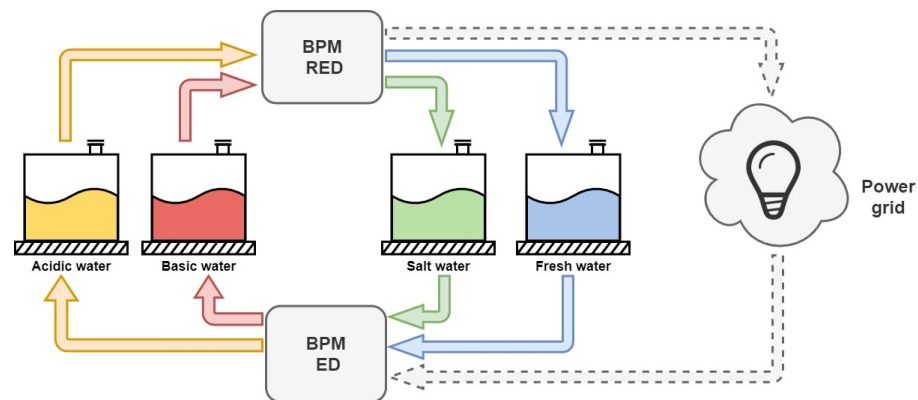


**Figure 1.** ABFB scheme: 4 tanks with different characteristics are used: acidic, base, salt, and fresh water. Two types of BPMs are used for the charge and discharge process, the BPM ED and BPM RED, respectively [4].

Consequently, the ABFB technology presents several interesting features. One of the main advantages of ABFB is that it is decoupled between the device rated power and total energy capacity because the first one is set by the membranes' size and the latter one by the water tanks capacity, resulting in an extremely flexible and modular design. Moreover, the energy and power capability have been boosted thanks to the combination of acid/base concentrations with salt/fresh ones, therefore making the technology more attractive to potential applications. Finally, no gas production inside the ABFB is also advantageous in terms of safety, compared to other battery systems based on electrolysis [12].

Due to the early development stage of ABFB technology, there are few references to this type of batteries in the literature [4]. The technology was first reported in 1983, reporting extremely low efficiencies due to the poor perm-selectivity of the early-stage membranes [13]. In the following decades, research was performed to apply the ABFB concept for a fuel cell application [14]. The developed fuel cell operated with concentrations up to 1 M HCl-NaOH, but the delamination of the BPM caused by the irreversible accumulation of water in the junction of the membrane was observed. From here, several authors [15,16] proposed important improvements such as the salt solution recirculation or techniques to avoid electrolysis in the electrode compartment of the ABFBs and subsequent gas formation. Following, Van Egmond et al. demonstrated the feasibility of the technology, showing stable operation at high current densities during charge (up to 150 A/m<sup>2</sup>) over a wide pH range, and evaluated the sources of energy losses [17]. Finally, up to date, recent studies have modelled ABFB cells and analyzed the ABFB stack in laboratory conditions [5,14,18–21].

This work contributes in the development of the ABFB technology by means of providing a study about its most-competitive potential use-cases in order to enable the future market penetration of products based on ABFB technology; moreover, it analyses how to overcome the power grid integration of the technology for the selected use-cases in order to address possible technical limitations for the interconnection of ABFB systems; and finally, it presents the first pilot-scale application example of the ABFB technology to show the feasibility of the technology and current status of development.

This paper is organized as follows. First, Section 2 describes the main characteristics of ABFB technology regarding power integration issues and presents 3 use-cases where the technology could be applied with a good trade-off between cost and functionality. Following, Section 3 describes how to overcome efficiently the power grid integration of this technology describing the features needed by a power converter interface, which is simulated in Section 4. Section 5 describes an application example with a possible implementation of an ESS based on ABFB technology in the electrical network of Pantelleria, Italy. Finally, Sections 6 and 7 summarize the most important results and conclusions of the research.

## 2. Competitive Use-Cases Applications for ABFB Technology

To properly define appropriate use-cases for the ABFB system, the strengths and weaknesses of the technology will first be compared to other mainstream ESS solutions. Following, the Smart-Grid Architecture Model (SGAM) will be used to define specific use-cases where it has been determined that the ABFB technology will be able to compete with, or surpass, current ESS solutions.

### 2.1. Comparing ABFB with Current ESS Solutions

One of the key criteria for an ESS is cost, in terms of both the capital cost (EUR/kWh) and the leveraged cost of storage (LCOS) (EUR/kWh/cycle). Large-scale PHS and compressed-air energy storage (CAES) plants typically have a very large capital cost but a much more acceptable cost per cycle, in the range of 0.05–0.15 EUR/kWh/cycle for PHS, assuming a 25 year lifespan [22–24]. These high upfront costs arise from the need for extensive civil engineering works to be carried out to prepare the site, along with expensive turbines and generators to be installed.

Other popular ESS technology is Li-ion batteries. Li-ion has a capital cost of between 150–350 EUR/kWh and a cost per cycle of around 0.30 EUR/kWh/cycle when deployed at small-scale, assuming a 10 year lifespan [25]. These costs are slightly reduced for large-scale deployment and capital costs are generally lower than a PHS or CAES facility of equivalent capacity. On the other hand, the main driver of the cost for Li-ion batteries comes from the price of the chemical storage medium [26]. These costs are unlikely to fall significantly in the future and, although successful research has been carried out to reduce the amount of material needed to produce a Li-ion cell [27], there is a floor to how much cost reduction can be achieved [26].

Vanadium Redox Flow Batteries (VRFB) and metal-air batteries have a capital expenditure (CapEx) that is lower than PHS/CAES but higher than Li-ion, while the cost per cycle is around 0.20 EUR/kWh/cycle with a 15 year lifespan [28]. The ABFB could potentially reach  $LCOS < 1.5$  EUR/kWh/cycle, which is a LCOS higher than other large-scale storage technologies but affordable enough, and considerably cheaper than contemporary smaller-scale solutions. The main costs of the ABFB systems are the membrane materials and the stack; components that are decoupled from the capacity of the system, the cost of the storage medium (water and salt) is marginal in comparison [4]. ABFB, therefore, can compete in terms of cost with the leading technology for large-scale bulk energy storage, and has a favorable cost when compared with smaller-scale ESS.

The space required is another important consideration in the selection of an appropriate ESS. The ABFB system has a theoretical energy density of 7 kWh/m<sup>3</sup> which, when operated at the target depth of discharge (DoD) of between 0.2 and 0.8, results in an obtainable energy density  $>5$  kWh/m<sup>3</sup> with a relatively high and constant output voltage. Li-ion batteries, in comparison, have a much higher energy density. Indeed, with an energy density between 250–670 kWh/m<sup>3</sup>, Li-ion batteries have some of the highest energy densities of any battery technology available today [29]. This makes Li-ion technology well suited for storage in situations where space is at a premium, for example in a residential setting or in electric vehicles. This fact is mitigated once an ESS reaches a scale where size is not as much of an issue, for example in commercial or utility-scale projects, as demonstrated by the large footprint required by PHS, which is by far the most extensively deployed large-scale ESS [23]. When comparing ABFB to PHS and CAES it is clear that ABFB holds a major advantage over the other two technologies: a lack of geographical requirement. Both PHS and CAES require very specific geography for their implementation; PHS requires a topography with a significant elevation change while CAES has the geological requirements of large, underground caverns. While a large-scale ABFB system would require a significant amount of space, the system could be installed anywhere where this space is available, without any prerequisite. Furthermore, the overall footprint of the ABFB system can be reduced using tall storage tanks as reservoirs for the storage medium.

Because ABFB is a type of flow battery, its energy capacity is decoupled from its rated power. Moreover, the system is modular, which allows for extra reservoirs to be retrofitted to increase the capacity of a system that has already been commissioned; a trait that is a rare among ESS technologies, including other types of flow batteries. Generally, when a new utility-scale ESS is planned, or replaces a smaller ESS, the size of the system is selected to accommodate for future load growth over a 15–20-year period [28]. This means that for a large amount of the system's lifetime the full investment is underused, because it is effectively oversized for much of the time, until the planned load growth has occurred. The modularity and standardization of ABFB means that the system can be sized in accordance with the short and medium-term load demand and then retrofitted with more reservoirs to increase the energy capacity as and when needed, allowing for less wasting of investment capital. Because the energy capacity and rated power are decoupled, increasing the capacity in this way would not affect the output of the system; it would just allow for the same power to be produced for a longer period of time.

Operational safety is of primary importance when designing and operating an ESS, and deployment in urban areas or in close proximity to critical grid infrastructure can be hampered because of concerns over safety. Batteries create heat when they are used, and this can become problematic if the conditions are not properly monitored and managed. Many battery technologies, including Li-ion, lead-acid and nickel-based batteries, present a risk of thermal runaway when overcharged [30], which in the worst-case scenario can lead to an explosion. Furthermore, even if an explosion is avoided, thermal runaway can irreparably damage the battery within a very short space of time. Physical damage due to manufacturing defects or improper transportation and installation can be very difficult to detect but can lead to internal short circuits within the cell or the leaking of electrolyte material, which is often toxic and/or flammable [31]; this is both a safety and an environmental hazard. Large-scale PHS introduces a different sort of environmental hazard as the engineering works required to commission one of these power plants can cause extensive ecological and environmental destruction to the surrounding area [32,33], while it has been suggested that CAES projects present a risk of soil contamination [34]. The ABFB technology does not present any of these safety or environmental hazards. Unlike most other batteries, which have storage mediums containing harmful or toxic chemicals such as lead or vanadium, the storage medium of ABFB consists of salt and water, both of which are entirely benign. Furthermore, the salt solutions and electrodes are thermally stable, and no exothermal reactions are involved within the system, meaning that there is no risk of thermal runaway and, because ABFB is a flow battery design, there is no risk presented from overcharging or indeed undercharging. These traits make ABFB particularly well suited for deployment in densely populated areas or in close proximity to essential grid infrastructure, as the safety risk is minimal.

The lifespan of contemporary battery systems is generally quite short, usually within the range of 10–15 years. Metal-ion batteries can suffer from recrystallisation of the storage medium and electrode pulverization while redox flow batteries suffer from crossover of metal ions; all of which cause irreversible degradation and a resulting loss of capacity over time [35,36]. Or other types of chemical batteries, like Pb-A, Ni-Cd, Na-S or NaNiCl<sub>2</sub> also presents lifetime expectancy no higher than 15 years in most cases [23,37]. The lifetime of PHS and CAES is much longer, usually around 40–60 years for a PHS facility; however considerable maintenance costs will be incurred over this entire period to keep the installation in good working order. The durability of the ABFB system is very desirable in comparison to these other technologies. There can be no degradation of the storage medium because it only consists of saline solutions of differing concentrations, not composition. ABFB is a closed system, which means that it does not suffer from bio-fouling or colloidal fouling that is often present in open systems, moreover the system is tolerant to contaminants such as dissolved oxygen, or other salts. Fouling can affect both the system efficiency and the lifetime of the system materials; it has been determined through laboratory experiments

that the membranes, electrodes and current collectors all have a lifespan of over 10 years due to the controlled environment of the closed system.

Not only operational safety is important but also features such as the availability, the mean time between failures (MTBF), and the failure recovery and management. Fully deployed technologies such as Li-ion have provided extensive studies about this issue [38,39]. However, it is necessary to reach enough maturity level of readiness prior to perform such studies. Therefore, the ABFB technology needs to advance in its development before stabilising the appropriate measures to mitigate or control such contingencies. Nevertheless, due to its modular scheme, as well as because the energy storage capacity (determined by the water tanks) is completely independent from the power capacity (determined by the membrane size), redundancy and complementary components can be added easily to solve this issue.

There are some ESS solutions able to provide extremely short time responses that enable its usage to provide services such as virtual inertia [40]. This is the case for example of supercapacitors energy storage (SCES) [41]. However, the response time of ABFB is too slow to provide services such as primary frequency control, spinning reserve or black start functionality. It is, however, well suited for providing services that do not require such a rapid actuation time. Although the start-up time is relatively slow, the technology can achieve a ramp rate in the region of MW/min, which is enough to provide services such as tertiary frequency control, and non-spinning or supplemental reserve functionality.

Furthermore, environmental impact is also an important issue to be considered in an ESS selection process. For different reasons, PHS, Pb-A and Ni-Cd between others have a strong impact, due to destruction of the landscape, introducing components that suppose a hazard to wildlife or other reasons [24,42]. On the other hand, there are other ESS technologies that introduce a relatively small impact in the environment, such as flywheel energy storage (FES), superconducting magnetic energy storage (SMES). The ABFB technology belongs to the latter technology, since the medium to store the energy is water.

Finally, Table 1 summarizes the main characteristics of all ESS technologies identified [4,41], and compared them to the ABFB characteristics.

## 2.2. Smart-Grid Architecture Model

The SGAM [43–46] provides a structured approach for modelling smart-grid use-cases. Its basis is a three-dimensional framework that is comprised of domains, zones and layers. The domain consists of the components of the traditional electrical energy infrastructure: generation, transmission, distribution, DER and customer premises. The zone describes a typical power system management hierarchy and is detailed further in Table 2.

The domain and zone axes form the component layer, on top of which are placed four interoperability layers: the communication, information, function and business layers.

The function layer describes functions and processes, and is used for mapping out use-cases [47]. Below, three different use-cases for ABFB are established and the relevant SGAM functional layer defined.

Table 1. Technical characteristics of typical ESS compared with ABFB technology. Data from [41].

ESS	Power Range (MW)	Energy Density (Wh/L)	Power Density (W/L)	Round Trip eff. (%)	Response Time (ms-h)	Lifetime (year)	Daily Discharge (%)	Self-Discharge (%)	Tech. Maturity	CAPEX (EUR/kW)	CAPEX (EUR/kWh)	Environ. Impact
PHS	10–5000	0.5–1.5	0.5–1.5	70–85	min	40–60	≈0.0		Full dev.	1–3 <i>k</i>	5–100	High/ Med.
FES	0–0.25	20–80	1–2 <i>k</i>	90–95	s	15	24–100		Mature	250–350	1–5 <i>k</i>	Very low
CAES	5–500	3–6	0.5–2	70–90	min	20–40	≈0.0		Proven	400–800	2–120	Med./ Low
Pb-A	0–30	50–80	10–400	70–90	10 ms	3–15	0.1–1.1		Full dev.	300–600	200–400	High
Ni-Cd	0–30	60–150	150–300	60–90	20 ms	10–20	0.1–0.7		Full dev.	0.5–2 <i>k</i>	0.8–2 <i>k</i>	High
Na-S	0–3	150–250	150–230	80–90	1 ms	10–15	20		Proven	1–3 <i>k</i>	300–500	High
NaNiCl <sub>2</sub>	0–3	150–180	220–300	85–90	<s	10–14	12–26		Proven	150–300	100–200	Med./ Low
Li-ion	0–100	200–500	0.5–2 <i>k</i>	85–100	20 ms	5–15	0.1–0.3		Proven	0.9–4 <i>k</i>	0.6–3 <i>k</i>	Med./ Low
VRFB	0.3–3	20–70	0.5–2	75–90	s	5–10	small		Proven	0.6–2 <i>k</i>	0.2–1 <i>k</i>	Med./ Low
SCES	0–0.3	2.5–15	0.5–5 <i>k</i>	90–100	8 ms	20	0.5–40		Proven	100–480	0.3–2 <i>k</i>	Very Low
SMES	0.1–10	0.2–2.5	1–4 <i>k</i>	95–100	<100 ms	20	1–15		Proven	200–490	1–10 <i>k</i>	Low
ABFB	0.01–0.5	7	17 W/m <sup>2</sup> (*)	55.9	s	10	small		Pilot	1520	50	Very Low

(\*) ABFB's energy density is related to the total membrane's area size.

**Table 2.** The power system management hierarchy represented by the zones in the SGAM model. Data from [44].

Zone	Representation
Process	Represents the transformation of energy (physical, spatial and chemical) and the physical equipment that is directly involved, such as PV panels, generators, transformers and cables.
Field	Incorporates the equipment that is required to collect, control, monitor or protect the process of the power system, such as sensors, controllers and smart devices.
Station	Denotes the aggregated level of the field zone, such as a local Supervisory Control and Data Acquisition (SCADA) system.
Operation	Provides power system control operations in the respective domain, e.g., an energy management system (EMS) in generation and transmission systems.
Enterprise	Includes commercial and organizational processes, services and infrastructures for enterprises, e.g., asset management, logistic, customer relation management, billing and procurement.
Market	Indicates potential market operations along the energy conversion chain, such as energy trading or ancillary services.

### 2.3. Use-Case 1: Light-Commercial Energy Storage

The objective of light-commercial energy storage use-case [48–50] is matching generation to consumption by peak shaving and time-shifting: both energy generation and usage; thus providing a reduction of the businesses' electricity bills. Flexibility schemes have been discussed widely during the last decade and it is foreseen a change in the power grid paradigm in the following years [51,52]. Therefore, ESS are a key component to provide it in an optimal way and has been discussed widely in the literature [53,54]. The average daily consumption of commercial premises in Europe varies greatly according to the location and function of the premises, along with the country's climate and gross domestic product (GDP). It is desirable for a light-commercial ESS to have a capacity large enough to cover a full day of demand without needing any additional energy input from the grid or rooftop solar PV. A system with a capacity of 40–70 kWh and rated power of around 5 kW should be enough to cover the daily energy needs of many light-commercial properties, such as a small office building, workshop or shop. When used alongside roof mounted PV panels the system would be able to store any excess energy during times of high generation and release it during times of low generation, providing more autonomy for the user with less reliance on the grid. These grid-connected PV/ESS systems would be equipped with grid following power converters, and functionality would include load shifting and PQ control, as well as the possibility of providing ancillary services to the grid as a constituent of a larger virtual power plant (VPP), providing extra income for the user.

In Figure 2a it can be seen that the function layer of this use-case occurs within the DER and customer premise domains, because the ESS would be situated in commercial premises equipped with rooftop solar PV panels. The zones from process through to enterprise are occupied, indicating that the system encompasses everything from the physical storage device through to the ability to save the user money on their electricity bills; the further market zone for the customer premises represents the opportunities presented by participation in the ancillary services market. Finally, Table 3 summarizes the goals and scope of this use-case.

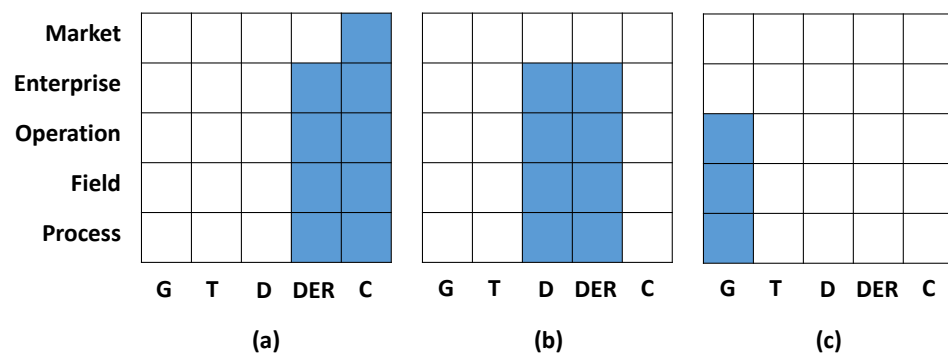


**Figure 2.** The SGAM functional layer defined for all defined use-cases: residential use-case 1 (a); low voltage network congestion use-case 2 (b); and bulk storage to support generation use-case 3 (c). All SGAM zones (market, enterprise, operation, field, and process) are correlated with the SGAM domains: generation (G), transmission (T), distribution (D), DER, and customer premises (C).

**Table 3.** Summary of the scope and objectives of Use-case 1.

Scope and Objectives of Use-Case 1	
Scope	There is a growing trend for installation of rooftop PV. Supplementary to this, installing an ESS allows the user to store excess energy generated from the PV panels for times of higher demand or lower generation, thus reducing their reliance on the grid and subsequently reducing their electricity bills. Further value can be provided to the user by promoting the localized trading of energy via a centralized ESS.
Objectives	<ul style="list-style-type: none"> <li>• Match generation to consumption by time-shifting energy use and peak shaving.</li> <li>• Increase customers' self-consumption.</li> <li>• Decrease energy bills by reducing reliance on the energy grid, enabling participation in the ancillary services market and promoting localized energy trading.</li> </ul>

#### 2.4. Use-Case 2: Low Voltage Network Congestion and Voltage Management

In low voltage network congestion use-cases [49,55,56], multiple ABFB systems would be installed at weak points of the distribution network, such as along radial feeder lines, to add flexibility to the grid, allowing for increased integration of renewables without jeopardizing grid stability. Locating the ESS at distribution level enables network congestion relief as well as allowing for the deferral of upgrades to the distribution network infrastructure. Active power management and frequency regulation can be achieved through peak shaving and active power control while reactive power control allows for voltage management. To promote strategic deployment of the device in locations that could be relatively crowded, such as suburban areas, the capacity of the device should be kept to between 15–45 kWh, with an output power of around 15 kW allowing for between 1–3 h of operation, enough time for the high demand to subside.

In Figure 2b the distribution and DER domains are occupied because the system would be deployed at distribution level. The zones from process through to enterprise are occupied which illustrates that the system provides operational benefit, such as the ability to avoid network congestion, as well as the commercial benefit of distribution network upgrade deferral. Finally, Table 4 summarizes the goals and scope of this use-case.

**Table 4.** Summary of the scope and objectives of Use-case 2.

Scope and Objectives of Use-Case 2	
Scope	Strategic deployment of ESS at distribution level and close to locations with high load demand, such as residential areas, can reduce congestion at weak points in the network and adds flexibility to the grid. Network support functionality allows for increased penetration of renewables without compromising grid stability.
Objectives	<ul style="list-style-type: none"> <li>• Reduction of congestion in the distribution network during times of high load demand.</li> <li>• Network support through control of active power, voltage and frequency.</li> <li>• Enable increased penetration of renewables without jeopardizing the stability of the grid.</li> <li>• Deferral of upgrades to the distribution network infrastructure.</li> </ul>

### 2.5. Use-Case 3: Bulk Storage to Support Generation

ESS at utility-scale is a widely studied use-case [49,57–59]. The installation of a very large ABFB system at the site of generation will enable the facility to deliver a baseload more reliably to the grid, by buffering at times of reduced generation and avoiding the need for expensive “peaker plants” when consumption is high. The capacity of such a system would likely be in the tens or even hundreds of MWh range, corresponding to many thousands of m<sup>3</sup> volume for the system’s reservoirs. A power converter with a power output of between 0.5 and 1 MW, which could be used modularly with multiple units in parallel to suit the specific need of the operator, would allow for a wide range of uses. An installation of this size could be operated similarly to a pumped-hydro plant, able to provide power when demand peaks and then recharge when cheaper energy is more abundant. Such an installation could also significantly aid in the continued integration of renewables; due to ABFB’s very low self-discharge rate, a large-scale installation could also be considered for long-term, inter-seasonal energy storage. For example, coupling a utility-scale ABFB ESS with a large PV plant could allow energy to be stored up during the summer months for use during the winter months when solar energy is less available. The advantages of ABFB at this scale are its safety and sustainability characteristics; its modularity and availability of raw materials for mass production; and it is also not limited by the geographical constraints of the former. Moreover, the ABFB technology has a good trade-off capability in terms of energy density and cost. Therefore, a system of this type would also be ideal for use on an island that has limited or no interconnection to a larger grid.

Figure 2c shows that this use-case exists solely across the generation domain, because the system would be deployed at generation level. Zones from process through to operation are occupied, showing that the purpose of the system is to provide operational benefit to the user; there is no commercial benefit other than the avoidance of regulatory penalties, for example from a power outage at times of high demand. Finally, Table 5 summarizes the goals and scope of this use-case.

**Table 5.** Summary of the scope and objectives of Use-case 3.

Scope and Objectives of Use-Case 3	
Scope	The intermittent nature of renewables is an obstacle to the provision of a reliable baseload to the grid. Furthermore, seasonal variations in generation means that excess energy is often wasted at one point of the year while generation falls short at another time of the year. A cheap, large-scale ESS solution can store energy during times of excess generation and provide a buffer during times where generation falls short of demand.
Objectives	<ul style="list-style-type: none"> <li>• Advance the ability of renewables to provide coverage for the baseload of the grid.</li> <li>• Provide a buffer for renewables for times of high demand or lower generation.</li> <li>• Reduce the need for “peaker” plants.</li> <li>• Inter-seasonal storage.</li> </ul>

### 3. ABFB Power Grid Integration

Typically, the power grid integration of ESS is an important issue to solve to enable its use in power grid support applications, and has been discussed widely in the literature [60–62]. Figure 3 shows the main components present in the ESS: the energy storage medium (ESM); the power interface stage; the power grid; the local control system (LCS); the energy management system (EMS); and the utility grid. Thus, the power grid interface provides a link between the ESS and the power grid and facilitates the charging and discharging of the battery on demand.

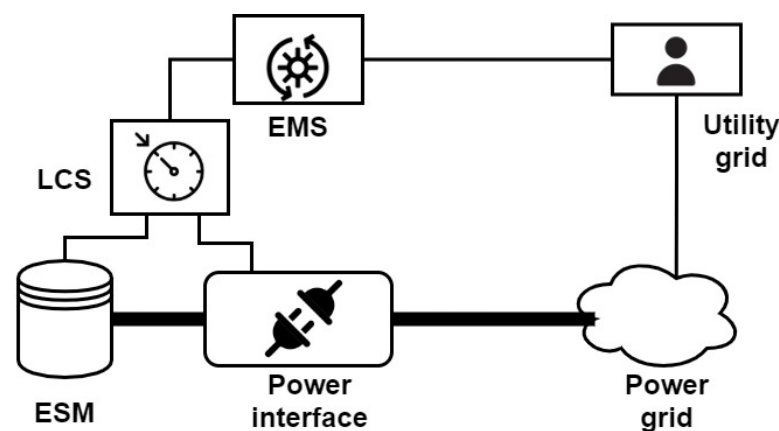


**Figure 3.** Main elements involved in the integration of an ESS: ESM; power interface stage; power grid; LCS; EMS; and the utility grid.

The design of a power grid interface should generally follow several constraints and requirements: some of them are also specifically related to the technology of the energy source behind the converter to be interfaced to the network. In the case of an electrochemical storage system, it is necessary to assess technological boundaries to avoid damage and degradation and to provide the right functionalities, as well as to establish electrical rated and ranged parameters to fulfil expected requirements. Some of the main battery technologies currently used for energy storage include Li-ion, lead-acid and flow batteries. The ABFB technology is a flow battery and thus has unique characteristics compared to batteries of other battery types.

Hereafter, a brief outline of some specifications for other ESS technologies in use today will be presented first, as it can be still useful to frame the general concepts of the problem. Then, the specific aspects related to the ABFB technology will be presented and discussed, to provide useful indications for the sizing and design of the power converters.

### 3.1. Sizing of Current ESS Applications in Selected Use-Cases

A brief description and discussion with examples for utility and residential scale specifications for power converters with storage technologies are reported in the following paragraphs. Two different scenarios have been studied, utility-scale and residential applications.

#### 3.1.1. Utility Scale

For utility use, ESS should be scalable and modular, to be able to deploy huge quantities of devices installed in parallel to adapt to every situation. The study has only looked for two types of technologies, Li-ion batteries and VRFB. This has been done for the following reasons: only solutions that need a fully controllable power electronics interface are of interest to the proper sizing of a solution based on ABFB technology; between them, the most popular technologies have been selected. Table 6 shows different examples of ESS solutions scalable to utility-scale size and their specifications.

**Table 6.** Specifications of some examples of utility-scale ESS solutions.

Utility-Scale Storage System	Technology	Charge/Discharge (kW)	Storage Capacity (kWh)
GE RSU-4000 [63]	Li-ion	1300	4184
Tesla Powerpack [64]	Li-ion	1264.5	2529
BYD Utility ESS [65]	Li-ion	1000	1000
Invinity VS3-022 [66]	VRFB	78	220
Sumimoto 250 kW-6 h [67]	VRFB	250	1500

First, Li-ion battery utility-scale solutions are built up with battery-cell stacks in series until reaching direct current (DC) voltages near the limit of low voltage definition (up to 1300 V [63]), to reduce current and enhance the efficiency of the system. In addition, they provide all-in-one containers in the range of 1 MW and 1 MWh with a scalable solution. Examples of utility-scale plants include a 10 MW/4.3 MWh installation at a thermal plant in southern California to provide supplementary spinning reserve capacity, a 7 MW/7 MWh system in Canada used to balance long duration frequency and voltage irregularities in the transmission system and a 41 MW/41 MWh system that is currently under construction in the UK in order to deliver local grid support by providing capacity and demand charge management [68].

And secondly, the characteristics of flow batteries are dependent on electrolyte type, electrode materials, the electrolyte-membrane interface, stack size, flow rate and temperature, among other factors. By far the most researched type of flow battery is VRFB. VRFB cells produce between 1.2–1.6 V across the membrane and a stack will typically consist of 100 cells [69]. Studies indicate that VRFB systems up to 100 MW are feasible and the technology is used regularly in Japan such as for load levelling at a substation (450 kW, 900 kWh), as auxiliary service in an university (500 kW, 5 MWh), and to stabilize the output of both PV (30 kW, 240 kWh) and wind (170 kW, 1.2 MWh) generators. An example of a 200 kW/400 kWh VRFB consisted of 20 different stacks that were each connected individually to the main DC line through a DC/DC converter [70]. Each stack consisted of 27 bipolar cells, each had an open-circuit voltage of 1.26 V, giving a voltage of 34.02 V across the terminals of the stacks. In [71] an 18.8 kW VRFB cell was developed and could be connected in series to increase the power output. The 18.8 kW cell had a DC voltage of 75.2 V and a DC current of 250 A. A 450 kW example was constructed by placing many cells in series.

Moreover, all ESS solutions usually provide an AC output voltage in the low voltage grid range, around 400 V depending on the country.

### 3.1.2. Residential Scale

The conventional size of domestic ESS for houses with PV is in the range of 5 kWh [72]. Table 7 shows different domestic ESS solutions and their specifications [73]. As can be seen in the table, most ESS solutions for domestic applications are based on Li-ion batteries or other electrochemical alternatives, mostly because their higher energy density factor. Moreover, the rated power and energy capacity of all of them are quite similar, because the power demands from houses only differ slightly (i.e., energy storage capacity oscillates between 4.8 and 14.5 kWh).

**Table 7.** Specifications of some examples of commercial ESS domestic solutions.

Residential Battery Storage System	Charge/ Discharge (kW)	Storage Capacity (kWh)	Useable Capacity (kWh)
Tesla Powerwall	5	13.5	13.5
SolarEdge LG Chem RESU 10	5	9.8	9.3
Puredrive Energy Storage 9.6 kWh	3.6/4.2	9.6	8.8
Powervault 3–12.3 kWh	3.3/5.5	12.3	12.3
Powervault 3–8.2 kWh	3.3/5.5	8.2	8.2
Sonnen 9.43–15 kWh	3.3	15	13.5
Sonnen 9.43–7.5 kWh	3.3	7.5	6.75
Alpha Smile 14.5 kWh	3	14.5	13.92
Solis/BYD 7 kWh	3	7	5.6
Puredrive Energy/Solis Hybrid 5 kWh	3	4.8	4.4
Moixa 4.8 kWh	2.4	4.8	3.84
Varta Pulse 6	2.3/2.5	6.5	5.9
Solax Hybrid X1 Triplepower 6.3 kWh	1.7	6.3	5.67

### 3.2. Sizing Constrains of ABFB Technology

The ABFB technology as flow battery has particular characteristics which must be considered in the process of designing the power converter to be used for the interface with the electrical network. The considerations and the requirements to be taken into account are related to the life cycle of the battery, the target efficiency, the scaling and flexibility of the solution, the guard limitations for the state of charge of the battery, sensitivity to the rate of change of voltages and currents. All these points are discussed in the following paragraphs.

#### 3.2.1. Specific Considerations Related to the Life Cycle of the Battery

The lifetime of the ABFB battery is unknown with accuracy yet due to not a single unit has been manufactured so far, but it is highly likely that the life of the system will be determined by the lifetime of the membranes. In the middle to long run, it is reasonable to aim at a lifetime of at least 10 years for a closed system (with replacement of the membranes every 5–7 years, if necessary). This consideration has a specific impact of the power electronics: the converter should in fact outlive the membranes in terms of lifetime, so it would be recommended to select a power converter with an expected lifespan of more than 10 years.

#### 3.2.2. Specific Requirements to Be Considered in the Power Converter Design

In the design of the direct current/alternating current (DC/AC) power converter, the following considerations should be also taken into account, as they can play a significant role.

- The power converter should be as efficient as possible.
- The converter should be designed in such a way that mass production is possible to keep the price per kW as low as possible, so economic considerations are clearly also important.

- Scaling/multiplication of the solution should be possible. Not all battery systems will have an identical size and therefore it should be possible to change the size of the converter to match the battery size (in terms of kW/MW). In this regard, a modular approach could work, where for instance a standard 100 kW converter could be designed and multiplied in parallel according to customers demand. However, a scaling approach might also be appropriate, where the converter could be redesigned, or parts are expanded to meet demands. Regarding the scaling requirement, the attention should be also focused on the general scale-up of the technology. Large size solutions of hundreds of MW are currently only imagined to be possible in the future: to achieve that, first smaller systems need to be built. Therefore, smaller power converters are necessary. In general, this consideration implies that the sizing of the converters could be planned according to a two-axis approach: the timeline of development of the system (from a few kW up to hundreds of MW) and the scaling of systems according to the batteries built at a certain time (a scale factor of about 10 up/down).
- In normal charge and discharge mode, the voltage can vary between 0.4 and 1.6 V. However, the battery can undergo a “reset” sequence (“charge reset”) where all solutions are purified in situ so that the solutions are restored to factory settings, extending the lifetime of the battery significantly. The charge reset function requires a minimum voltage of 2 V per ABFB cell at charge current is necessary but preferably an even higher voltage is required, up to 6 V preferably; however, any voltage higher than 6 V adds little value to the functionality. If this leads to fundamental converter design issues making the converter too expensive, a trade-off need to take place between the quality of the reset sequence and the economic considerations mentioned earlier.
- The ABFB batteries used for the pilot have 56 cells which amounts to a total theoretical open-circuit voltage (OCV) of around 48 V at 100% state of charge (SOC). In the future, for much larger power requirements, it might be possible to switch to high voltage stacks (up to several hundreds of V). This of course will impact the power converter as well. Again, this should be considered when designing the “right converter at the right time”, as discussed above with the considerations about scaling requirements.

### 3.2.3. Limitations on the State of Charge of the Battery

As with other electrochemical batteries, the ABFB technology would require recommended maximum and minimum limitations on the SOC of the batteries. This corresponds to the definition of two limits,  $SOC_{max}$  and  $SOC_{min}$ , which specify respectively maximum and the minimum SOC allowed for the battery during operation. The definition of the SOC limits varies depending on the battery type and technology, and in the case of ABFB technology, the minimum and the maximum values for the SOC have been established between 20–100% at the moment.

This consideration has an impact on the converter design, and it must be reflected in the implementation of the control system of the power converters.

### 3.2.4. Additional Limitation/Constraints on the Battery Currents

An additional constraint which could be taken into account is the limitation of the currents of the battery. Charge and discharge currents are in fact limited by the stability of the bipolar membrane and the overall internal resistance of the system. At the moment, the current density for charge is limited to about 200 A/m<sup>2</sup>. Yet in the middle to long run >1000 A/m<sup>2</sup> during the charge should be possible. For discharge, at the moment, the maximum current density is about 100 A/m<sup>2</sup>, starting with low current densities (30 A/m<sup>2</sup>) to be sure to minimize the risk of damaging the bipolar membranes. In the future, 200 up to 400 A/m<sup>2</sup> should be possible if two main obstacles can be overcome: namely lowering the resistivity of the membrane material (also needed for high charge currents) and preventing co-ion leakage to reduce potential losses during discharge.

### 3.2.5. Sensitivity to the Rate of Change

Under abnormal system conditions such as faults but also in normal operating conditions, voltages, currents and powers can vary rapidly and consistently. It is important then to also assess the possible sensitivity of the storage technology to the steepness of these variations, leading to the definition of specific limits to the rates of change (ramp-rate limiters), which is an important issue that must be considered for both: preventing damage to the unit, and to set the limits of operation of the system. For safety reasons, minimum and maximum ramp-rate limiters should be then included in the overall control and management system of the battery converters. As with the case of state of charge limitations, the considerations regarding the rate limiters are reflected in the design of the control system of the power converters. Van Egmond et al. have reported the behavior of the system describing charge and discharging cycle [17]. However, there is still not enough information regarding ABFB technology about this issue, and hence it should be studied in future research.

### 3.3. Use-Cases Sizing Specifications

The ABFB battery stack will consist of multiple cells which can be placed both in series and in parallel with each other to reach the desired DC voltage. Currently, the current density of the cells is in the range of hundreds of Amperes per square meter, and the electrical characteristics of the cells will depend upon its design features, especially the size of the membrane.

In the specific case of the pilot built for the Pantelleria island that is described in Section 5, each cell operates at a maximum discharge current of 6 A and a maximum charge current of 8 A. The voltage range for each cell is between 0.4–1.6 V in normal charging/discharging mode; however, the system has a charge reset function to increase the battery lifetime. A reset voltage of 3.3 V was found to be the best trade-off between the efficiency of the reset function and the cost of the power converter. Using these predefined parameters, the stack configuration for each use-case was calculated, shown in Table 8. However, use-case 3 is a utility-scale application, far from the pilot-scale developed operating working point and, therefore, the values achieved do not offer an optimum solution; instead of that, a redesign of the ABFB cells to reduce the number of cells to a reasonable quantity will be preferably.

**Table 8.** The ABFB proposed stack parameters calculated for each defined use-case according to the BPM cells developed in the pilot.

ABFB Stack Parameters			
Use-case	1	2	3
Number of ABFB cells in series	240	240	310
Number of ABFB stacks in parallel	2	6	205
Minimum operating voltage	96 V	96 V	124 V
Maximum operating voltage	384 V	384 V	496 V
RESET voltage	792 V	792 V	1023 V
Charge current	12 A	36 A	1230 A
Discharge current	−16 A	−48 A	−1640 A
Rated power	12.7 kW	38 kW	1678 kW
Maximum output power	4.6 kW	13.8 kW	610.1 kW

### 3.4. Power Converter Interface Configuration

In accordance with the design considerations, all three use-cases will use the same basic converter design: a two stage DC/DC–DC/AC converter. This configuration is needed

because the low input voltage range at normal conditions, below the minimum rectified AC voltage. Therefore, a first stage will be used to boost the DC voltage and achieve a steady input voltage for the inverter and will consist of an isolated bidirectional DC/DC converter. An isolated DC/DC design is recommended for two reasons: first, because doing so, a low frequency power transformer is not needed in the AC output, saving volume and weight of the unit; and secondly, thanks to this feature, a series association is possible to perform the reset operation, as explained below. Nevertheless, it is possible to use non-isolated DC/DC devices together with low frequency power transformers in the output of each power converter interface if efficiency is critical.

The secondary stage will be a DC/AC converter with a low pass filter, outputting a three-phase AC voltage with the rated low voltage distribution grid voltage and frequency (that values may change in each country).

The maximum DC bus voltage for use-cases 1 and 2 are 850 V which, according to the international standard IEC 60038, is considered to be low voltage (LV) [74]. It is necessary for these use-cases to be classified as LV to avoid the costs from the increased component specification and more stringent regulations associated with higher voltages. The maximum DC voltage for use-case 3 is 1350 V, which is close to the threshold between LV and high voltage (HV), and therefore the components used will be of the higher voltage requirements.

Finally, a scheme of the configuration is presented in Figure 4, in where a switch box has been placed to allow two possible working modes and fulfil Table 8 specifications. First, in case (a) two ABFB devices run in normal operation independently. Afterwards, when the ABFB cells need to be regenerated, the reset working state is activated, as shown in case (b), placing the two power converter interfaces in series to reach the desired input voltage level.

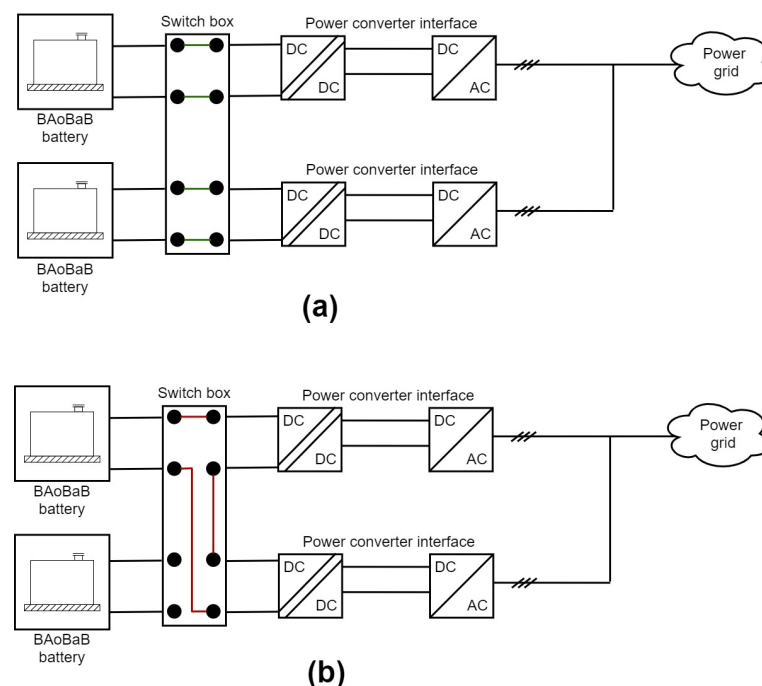


**Figure 4.** Proposed modular two-step topology for power converter interface of ABFB technology applications. The system is built up by an isolated DC/DC converter together with a 3-phase power inverter (or a single phase depending on the sizing of the system). (a) represents a configuration in which 2 modules are connected independently in “normal” operation, and (b) points out a serial configuration of the DC/DCs to perform the reset state upon one of the ABFB stacks.

#### 4. Operation of the Power Converter Interface for ABFB Technology

The behavior of two battery modules has been tested through simulation using Matlab and Simulink. For the modelling of the batteries, the parameters described in Table 8 for use-case 2 have been taken into account. For simplicity, only one battery has been simulated and the power converter number 2 is in open circuit; meanwhile the power converter 1 is in normal operation, charging and discharging the battery as Figure 5 shows. When a battery reset is required, the breaker marked with the B-tag opens and A-tag breakers close the circuit to change from a parallel connection to a serial connection, performing the reset process.

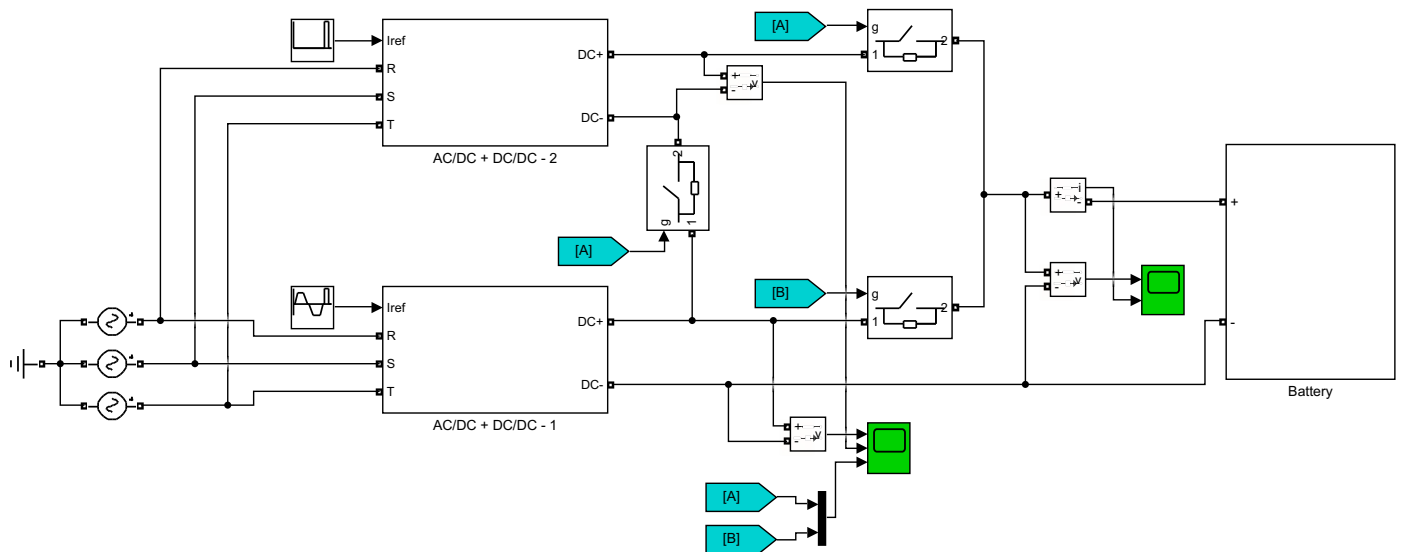


**Figure 5.** Simulation environment: the power converters are parallel connected during charge and discharge, when a reset process is required, both converters are series connected to achieve a higher working voltage.

The two first graphics of Figure 6 show the battery voltage and current. First, in the time range from  $t_C^0$  to  $t_C^f$  the battery is charged by the power converter 1, and afterwards, from  $t_D^0$  the system continues to work in normal operation until the simulation reaches  $t_D^f$  discharging the battery. As the third and fourth graphics show, the converter 2 is stopped meanwhile the converter 1 is regulating the voltage to follow the battery current reference. Then, at time  $t_{rst}^0$  a reset sequence starts. At this moment, the last graphic shows the change in state of the switches to achieve the voltage levels required to perform the reset operation (792 V) without exceeding the breakdown voltage of a single power converter (400 V).

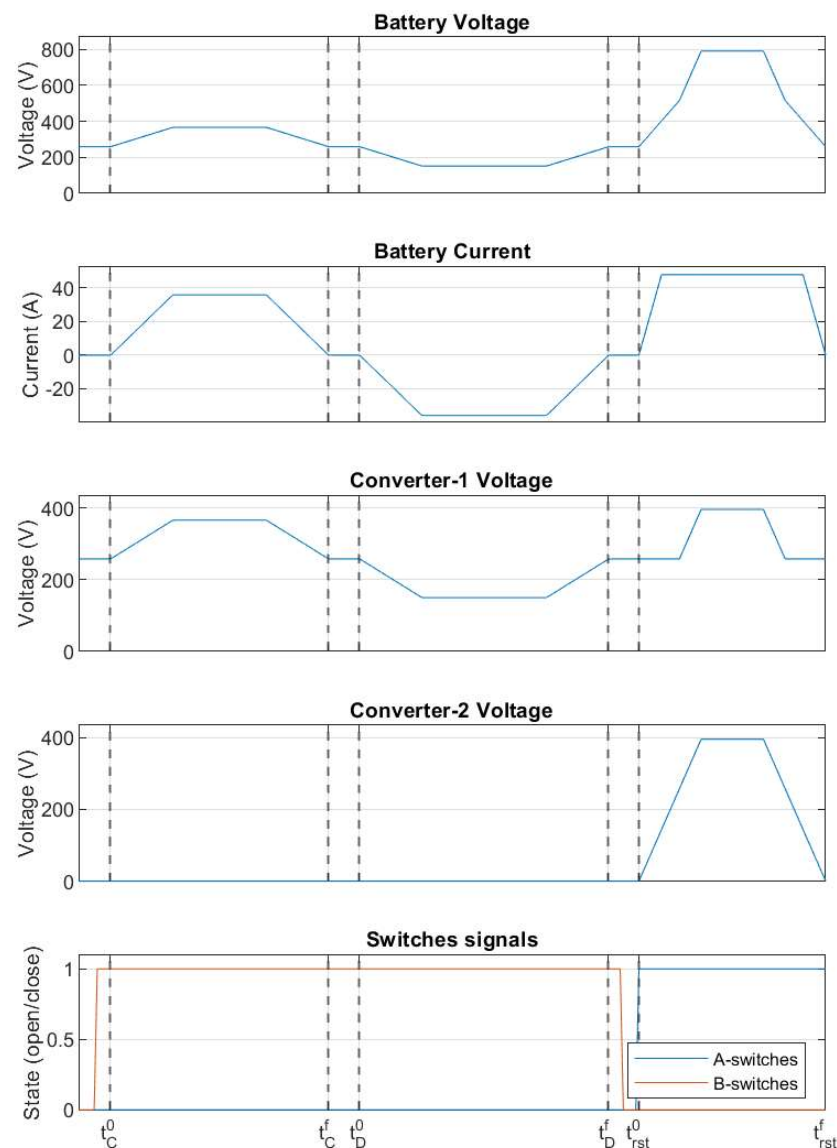


**Figure 6.** Simulation results, from top to bottom: battery voltage, battery current, converter-1 voltage, converter-2 voltage, switch control signals.

### 5. Application Example: Implementation in the Electrical Network of Pantelleria

A technology pilot demonstration of 1 kW rated power has been developed in a demo-site located in Pantelleria island (Italy), see Figure 7 [75]. The goal of the installation is to demonstrate the feasibility of this new kind of ESS technology and will be tested in the upcoming months as an ESS at the local power plant, to provide seasonal storage during the high energy demand in summer months. Following, a study about the interconnection of the system with the rest of the island power grid and how it behaves against an analysis regarding power reference step response, transient faults and SOC evolution is shown.

The power system of the island of Pantelleria is a medium voltage network, with a radial structure and the possibility of radially counter-supplying the lines or creating a meshed configuration. Currently, the island is totally dependent on external sources of energy: the supply system relies on a main thermal generation power plant, located close to the urban center of the island. The power plant is composed by eight diesel generators, for a total installed capacity of about 20 MW. The power is delivered to the loads through four main medium voltage feeders, departing from the thermal power plant. The schematic outline of the described system is shown in Figure 8. The green circle denotes the ABFB system installed in the Pantelleria network. Furthermore, Table 9 summarizes the main

parameters used for modelling Pantelleria power grid and the blue acid/base battery (BAoBaB) prototype.



Figure 7. BAoBaB 1 kW prototype installed in Pantelleria island.

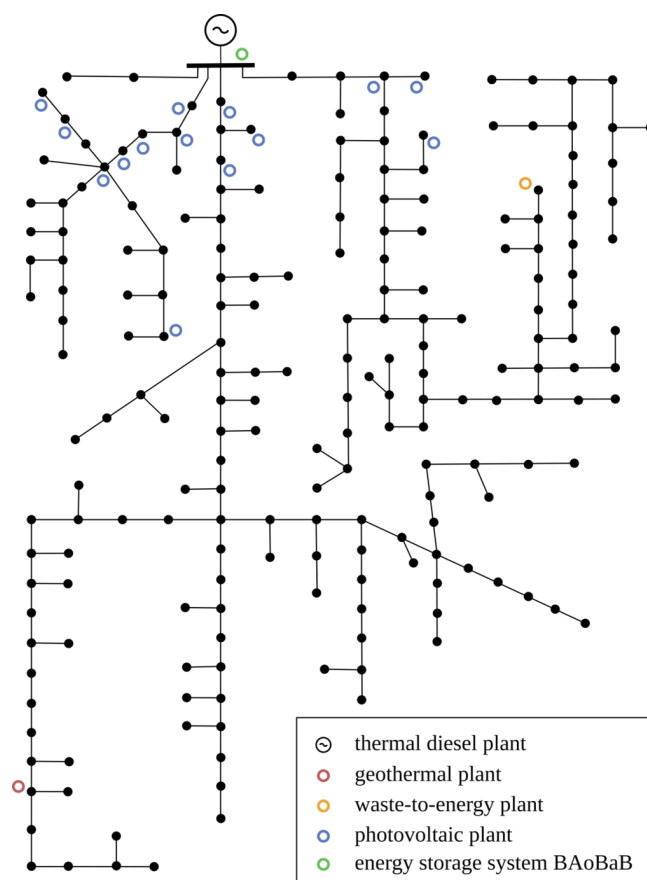


Figure 8. Network scheme of Pantelleria island, with integration of the BAoBaB technology.

**Table 9.** Parameters used to model Pantelleria demo-site.

<b>BAoBaB Prototype</b>		
<b>Parameter</b>	<b>Value</b>	<b>Units</b>
Rated power	1	kW
Minimum state of charge	20	%
Maximum state of charge	100	%
Maximum power rate limit	1	pu/s
Minimum power rate limit	−1	pu/s
Control mode of active power	open-loop	-
Control mode of reactive power	close-loop	-
Active power control time constant	0.01	s
Reactive power control proportional gain	1	pu
Reactive power control integral gain	10	pu
Terminal voltage control proportional gain	2	pu
Terminal voltage control integral gain	0	pu
Converter time constant	0.01	s
Converter PLL bandwidth	30	rad/s
<b>Pantelleria Power Grid</b>		
Power plant rated capacity	20	MW
Power plant inertia constant	2	s
Power plant frequency droop	5	%
Length range of medium voltage feeders	4–14	km
Resistance range of medium voltage feeders	0.33–0.47	$\Omega$ /km
Reactance range of medium voltage feeders	0.23–0.31	$\Omega$ /km
Capacitance range of medium voltage feeders	0.1–0.24	$\mu$ F/km

The island network including the BAoBaB storage system is analyzed with a positive-sequence RMS dynamic model, implemented in the power systems analysis software NEPLAN. The system is modelled in detail, with particular focus on the dynamic elements of the network such as synchronous machines and regulators, as well as the BAoBaB system with battery and converter control dynamics. For the common dynamic elements such as machines and regulators, the standard built-in models available in the software have been used. For the BAoBaB system instead, the model of the converter system for the DC/AC interface to the network is developed and implemented as user defined dynamic model, formulating the element equations in SYMDEF (SYMBOLIC DEFINITION), the proprietary modelling language of NEPLAN. The dynamic model of the BAoBaB system is developed according to the specifications and the principles specifically selected for the ABFB technology, to reflect in the simulation model the hardware and control design and the characteristics of the power converter system interfacing to the grid of Pantelleria. The storage system is represented as a controlled current source, keeping the power references at the terminal and following the grid variations through a phase-locked loop (PLL). The model implements then a PLL with a synchronous reference frame transformation, two dedicated control loops for the control active and reactive current components, and a current limiter representing the protection of the equipment. The model also implements the specific controls and functionalities for SOC limitations and ramp-rate limiters. The state of charge of the battery system is calculated according to a current integration method (known as Coulomb Counting) including the rated capacity of the BAoBaB storage system in Ah: the calculated value of the SOC is then sent to a block implementing the limitation logic, where the specific limit values of  $SOC_{min}$  and  $SOC_{max}$  specified for the ABFB technology are considered, respectively 20% and 100%. Specific rate limiters are also included in the model of the control system of the ABFB converter, applying them to the command and the reference signals used within the power control loops.

The results of time-domain simulations of the Pantelleria system including the operation of the BAoBaB system in grid-connected mode are reported in the following subsections.

### 5.1. Step on Power References

In Figure 9, the results for a step response on the active power reference of the converter are shown. The active power is changed from the initial value of 0.1 kW to 0.9 kW, stepping up from 10% to 90% of the rated power of the battery system. Three different cases are considered, to verify the design of the ramp-rate limiters within the converter control. From the results, it is possible to observe that with no rate limiters the converter would be able to follow the reference step almost instantaneously. However, such a fast response might affect the battery and the equipment. Ramp-rate limiters are therefore applied in the control. It can be seen that a limit of 1 kW/s can be already effective in containing the ramping up of the active power provided by the BAoBaB energy storage system, while a limit of 0.1 kW/s might prolong the step response of several seconds.

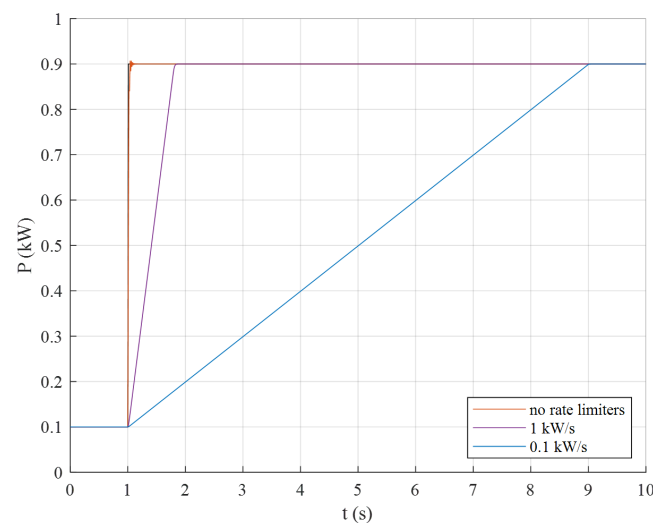


**Figure 9.** Active power output for a step on active power reference from 10% to 90%.

In Figure 10, the results for a step response on the reactive power reference of the converter are shown. The reactive power is changed from the initial value of 0 kVAR to 0.3 kVAR, stepping up to 30% of the rated power of the battery system. Similar to that done for the step response on the active power, three different ramp-rate limiters are considered in the simulations. A value of 1 kVAR/s appears to be already effective in limiting the ramp of the reactive power provided by the BAoBaB energy storage system, allowing a safe operation of the converter also in this case.

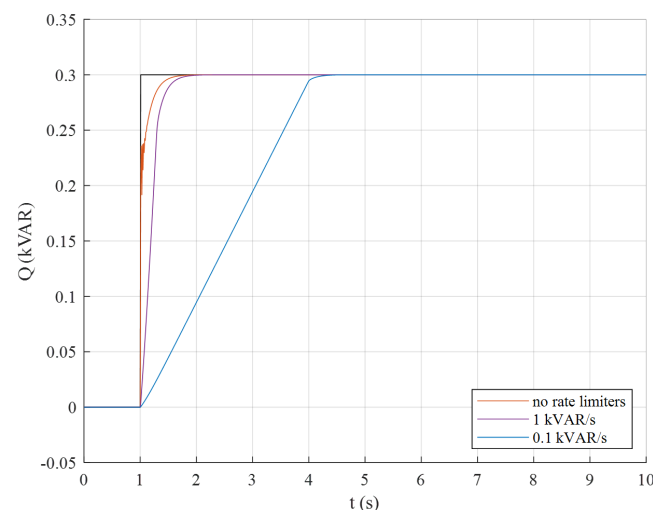


**Figure 10.** Reactive power output for a step on reactive power reference from 0% to 30%.

### 5.2. Terminal Short-Circuit

The results for a 3-phase short-circuit right at the terminal of the BAoBaB storage system are shown in Figure 11. The fault is cleared after 100 ms. For the total duration of the fault, the voltage of the converter drops to a very low value, almost to zero (top-left chart in Figure 11). From the time simulation results, it is possible to appreciate the effects of the current limiters implemented in the converter control as protection of the battery storage system: the magnitude of the current ceils to the given limit imposed by the converter control (top-right chart in Figure 11), and accordingly, the system provides a limited reactive power during the fault (bottom-right chart in Figure 11).

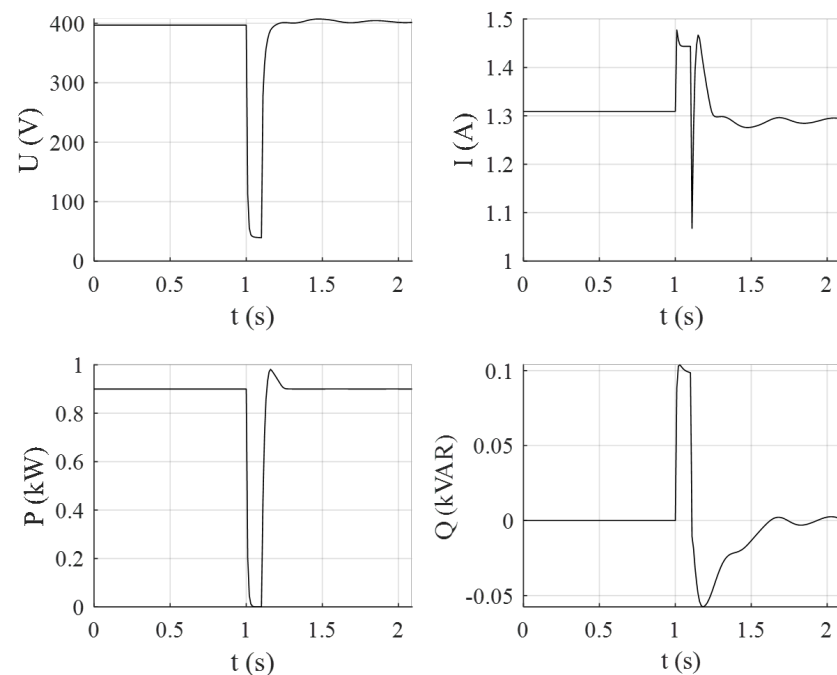


**Figure 11.** Simulation results of a 3-phase short-circuit at the storage system terminal.

### 5.3. SOC limitations

The implementation of the SOC limitations within the power converter control is also verified with specific simulations. The results are shown in Figures 12 and 13. In the first case, the BAoBaB system is assumed to be close to the minimum limit  $SOC_{min} = 20\%$ , and it is considered to be operating in discharging mode so delivering power to the grid. When the minimum limit is reached, the battery system stops to provide active power to the grid (generated current to zero). In the second case, the storage system is assumed to be in charging mode absorbing power from the grid, close to the maximum limit  $SOC_{max} = 100\%$ . When the limit is reached, the battery system quits the charging process and does not request any more power from the grid (absorbed current to zero). The transient response is verified in both simulation cases.

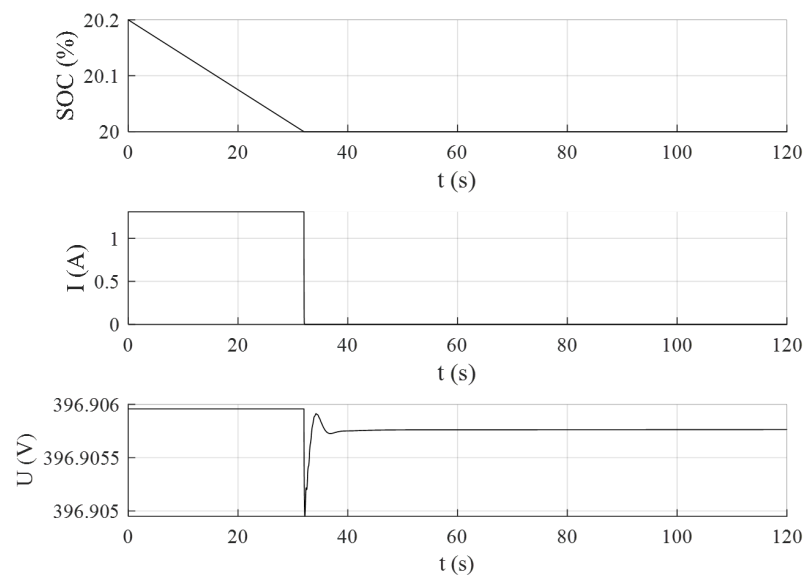


**Figure 12.** SOC limitations on the storage system for minimum value 20%.

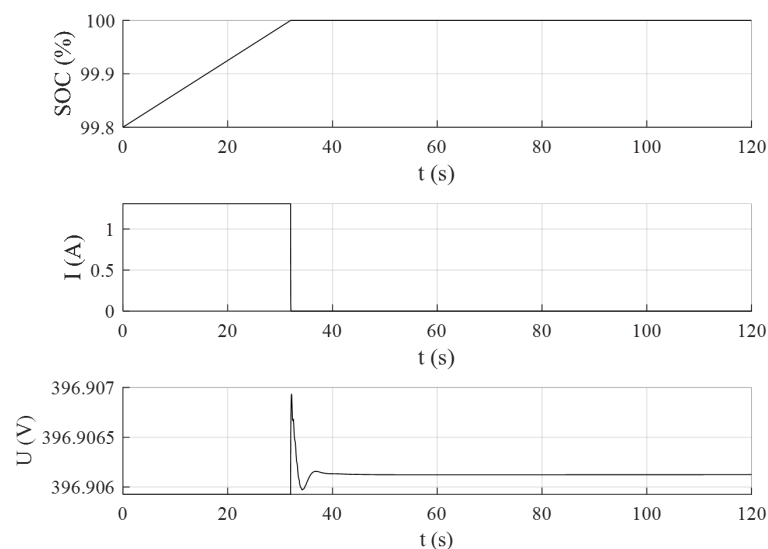


**Figure 13.** SOC limitations on the storage system for maximum value 100%.

## 6. Discussion

This paper has analyzed the characteristics and sizing of the power converter and associated ABFB ESS in the commercial and industrial scenarios in which the use of this technology could be advantageous. The ABFB technology has been first compared to other well-known ESS solutions: in Section 2 three use-cases specific for the ABFB system are therefore identified and defined, which are light-commercial energy storage, low voltage network congestions and bulk support to intermittent generation. The power conversion system which should serve as interface of the battery pack to the AC network is then properly designed for application to the ABFB technology: sizing and specifications are derived according to the particular constraints and requirements related to the ABFB technology such as cells configuration, reset sequence voltages, state-of-charge limitations and life cycle preservation.

The specific requirements of each application have been analyzed in Section 3, concluding that use-cases 1 and 2 have similar characteristics, enabling the use of the same power interface, although requiring more parallelization in the second case due to higher rated power capacity. However, applications defined by use-case 3 will require higher working voltages on the DC side, and a higher level of parallelization to reach the de-

sired rated power capacity. Thus, it will be recommended to resize the BPM system for such applications.

Currently, the restoration of electrolyte properties is done by emptying the acid and base tanks in the saltwater tanks and filling them with demineralized water again. To avoid maintenance costs derived from the battery restoration, a connection scheme that allow a change of configuration to allow on-site purification of the salty solutions has been proposed. The main parameters of the Pantelleria pilot battery have been used to simulate the reset operation in Section 4, showing the feasibility of the on-site purification of the solution known as “reset” operation state.

The behavior of two battery modules under charging/discharging normal operation, and in reset state has been shown. The simulation demonstrates how to interconnect the modules to obtain an optimum performance without incurring in significant extra-costs for the development of the power converters; the power converters individually work in the same operation range regardless they are in normal or reset condition.

Finally, Section 4 presents the Pantelleria pilot plant. The goal of the pilot is to demonstrate the feasibility of ABFB technology for seasonal storage. As a first approximation, the island network has been simulated in NEPLAN, where the influence of steps on power references, short-circuit and SOC limitations between the battery and grid have been validated prior to its commissioning.

## 7. Conclusions

ESS are expected to play a fundamental role in fostering and supporting the integration of power generation from RES. ESS can in fact alleviate some of the problems introduced by high shares of intermittent energy sources, providing a wide range of different services to the grid. To these purposes, the types and the configurations of storage systems which can provide the required functionalities are several, with different nature and characteristics. Every storage technology has natural advantages and disadvantages: among the drawbacks of storage systems, the operation costs and the environmental impact are some of the most relevant. Concerning the sustainability and the impact on the environment, the ABFB technology offers the potential of proving a storage system with the most valuable characteristic of being a cheap, clean and safe storage solution. However, the study has shown that the solution is not the best solution regarding some features: i.e., if the energy density or the response time are critical issues.

Moreover, the power converter topology needed for this application has been described. In particular, a modular approach is proposed, to scale the solution conveniently. Furthermore, the “reset” state condition of the ABFB technology needs to have an extremely large input voltage range. Therefore, this work proposes a two-step modular topology to have an optimum performance in both “normal” and “reset” conditions.

Finally, a prototype of the new ESS technology has been presented in the Pantelleria demo-site. Furthermore, the complete network of Pantelleria island integrating the BAoBaB project pilot system has been implemented and simulated in the software NEPLAN, considering the selected control system for the power converter. The simulation results have shown that the control system is effective allowing a safe operation of the converter under different possible contingencies such as power imbalance and short-circuit which can happen in the network of the island.

Future research will show the behavior of ABFB technology under a real grid scenario, once the commissioning of the plant has concluded, and will determine the feasibility of bringing ABFB technology to higher Technology Readiness Levels (TRL). Furthermore, real data will be used to confirmed or refine current design considerations and use-cases evaluation, enabling a future sensitivity analysis respect to other ESS technologies.

**Author Contributions:** Conceptualization, J.M.-C.-A., J.B.-F. and R.M.; methodology, J.M.-C.-A., and J.F.S.-O.; simulation, R.M.; formal analysis, J.M.-C.-A. and J.B.-F.; investigation, J.M.-C.-A., J.B.-F., and M.P.J.; resources, J.M.-C.-A., J.B.-F. and R.M.; writing—original draft preparation, J.M.-C.-A., R.M., J.B.-F. and J.F.S.-O.; writing—review and editing, D.M.R.-A., M.P.J., E.G. and A.C.; supervision,

J.F.S.-O., D.M.R.-A., E.G. and A.C.; project administration, D.M.R.-A., and A.C. All authors have read and agreed to the published version of the manuscript.

**Funding:** This work was performed in the framework of the BAoBaB project (Blue Acid/Base Battery: Storage and recovery of renewable electrical energy by reversible saltwater dissociation). The BAoBaB project has received funding from the European Union's Horizon 2020 Research and Innovation program under Grant Agreement no. 731187 ([www.baobabproject.eu](http://www.baobabproject.eu), accessed on 26 May 2021).

**Acknowledgments:** The authors thank to Michele Tedesco from WETSUS, and Alessandro Tamburini from University of Palermo, for his technical assistance and his comments, that greatly improved the manuscript.

**Conflicts of Interest:** The authors declare no conflict of interest.

## References

- Bergen, M. *Alphabet Wants to Fix Renewable Energy's Storage Problem—With Salt*; Bloomberg Quint: Mumbai, India, 2017.
- Cooper, J.J. *Arizona Fire Highlights Challenges for Energy Storage*; The Associated Press: New York, NY, USA, 2019.
- Frankel, T.C. *Cobalt Mining for Lithium Ion Batteries Has a High Human Cost*; The Washington Post: Washington, DC, USA, 2016.
- Pärnamäe, R.; Gurreri, L.; Post, J.; van Egmond, W.J.; Culcasi, A.; Saakes, M.; Cen, J.; Goosen, E.; Tamburini, A.; Vermaas, D.A.; et al. The Acid–Base Flow Battery: Sustainable Energy Storage via Reversible Water Dissociation with Bipolar Membranes. *Membranes* **2020**, *10*, 409. [[CrossRef](#)]
- Culcasi, A.; Gurreri, L.; Zaffora, A.; Cosenza, A.; Tamburini, A.; Micale, G. On the modelling of an Acid/Base Flow Battery: An innovative electrical energy storage device based on pH and salinity gradients. *Appl. Energy* **2020**, *277*, 115576. [[CrossRef](#)]
- Post, J.W.; Hamelers, H.V.M.; Buisman, C.J.N. Energy Recovery from Controlled Mixing Salt and Fresh Water with a Reverse Electrodialysis System. *Environ. Sci. Technol.* **2008**, *42*, 5785–5790. [[CrossRef](#)]
- Mei, Y.; Tang, C.Y. Recent developments and future perspectives of reverse electrodialysis technology: A review. *Desalination* **2018**, *425*, 156–174. [[CrossRef](#)]
- Al-Amshawee, S.; Yunus, M.Y.B.M.; Azoddein, A.A.M.; Hassell, D.G.; Dakhil, I.H.; Hasan, H.A. Electrodialysis desalination for water and wastewater: A review. *Chem. Eng. J.* **2020**, *380*, 122231. [[CrossRef](#)]
- Campione, A.; Gurreri, L.; Ciofalo, M.; Micale, G.; Tamburini, A.; Cipollina, A. Electrodialysis for water desalination: A critical assessment of recent developments on process fundamentals, models and applications. *Desalination* **2018**, *434*, 121–160. [[CrossRef](#)]
- Walther, J.F. *Process for Production of Electrical Energy from the Neutralization of Acid and Base in a Bipolar Membrane Cell (U.S. Patent 4,311,771A)*; International Atomic Energy Agency (IAEA): Vienna, Austria, 1982.
- Pärnamäe, R.; Mareev, S.; Nikonenko, V.; Melnikov, S.; Sheldeshov, N.; Zabolotskii, V.; Hamelers, H.V.; Tedesco, M. Bipolar membranes: A review on principles, latest developments, and applications. *J. Membr. Sci.* **2021**, *617*, 118538. [[CrossRef](#)]
- Sáez, A.; Montiel, V.; Aldaz, A. An Acid-Base Electrochemical Flow Battery as energy storage system. *Int. J. Hydrogen Energy* **2016**, *41*, 17801–17806. [[CrossRef](#)]
- Emrén, A.T.; Holmström, V.J. Energy storage in a fuel cell with bipolar membranes burning acid and hydroxide. *Energy* **1983**, *8*, 277–282. [[CrossRef](#)]
- Pretz, J.; Staude, E. Reverse electrodialysis (RED) with bipolar membranes, an energy storage system. *Berichte Bunsenges. Phys. Chem.* **2010**, *102*, 676–685. [[CrossRef](#)]
- Zholkovskij, E.K.; Müller, M.C.; Staude, E. The storage battery with bipolar membranes. *J. Membr. Sci.* **1998**, *141*, 231–243. [[CrossRef](#)]
- Kim, J.H.; Lee, J.H.; Maurya, S.; Shin, S.H.; Lee, J.Y.; Chang, I.S.; Moon, S.H. Proof-of-concept experiments of an acid-base junction flow battery by reverse bipolar electrodialysis for an energy conversion system. *Electrochem. Commun.* **2016**, *72*, 157–161. [[CrossRef](#)]
- van Egmond, W.J.; Saakes, M.; Noor, I.; Porada, S.; Buisman, C.J.N.; Hamelers, H. Performance of an environmentally benign acid base flow battery at high energy density. *Int. J. Energy Res.* **2018**, *42*, 1524–1535. [[CrossRef](#)]
- Xia, J.; Eigenberger, G.; Strathmann, H.; Nieken, U. Acid-Base Flow Battery, Based on Reverse Electrodialysis with Bi-Polar Membranes: Stack Experiments. *Processes* **2020**, *8*, 99. [[CrossRef](#)]
- Veerman, J.; Post, J.W.; Saakes, M.; Metz, S.J.; Harmsen, G.J. Reducing power losses caused by ionic shortcut currents in reverse electrodialysis stacks by a validated model. *J. Membr. Sci.* **2008**, *310*, 418–430. [[CrossRef](#)]
- Tang, A.; McCann, J.; Bao, J.; Skyllas-Kazacos, M. Investigation of the effect of shunt current on battery efficiency and stack temperature in vanadium redox flow battery. *J. Power Source* **2013**, *242*, 349–356. [[CrossRef](#)]
- Culcasi, A.; Gurreri, L.; Zaffora, A.; Cosenza, A.; Tamburini, A.; Cipollina, A.; Micale, G. Ionic shortcut currents via manifolds in reverse electrodialysis stacks. *Desalination* **2020**, *485*, 114450. [[CrossRef](#)]
- Electric Power Research Institute. *Quantifying the Value of Hydropower in the Electric Grid: Plant Cost Elements*; Technical Report; Electric Power Research Institute: Washington, DC, USA, 2011.
- Das, C.K.; Bass, O.; Kothapalli, G.; Mahmoud, T.S.; Habibi, D. Overview of energy storage systems in distribution networks: Placement, sizing, operation, and power quality. *Renew. Sustain. Energy Rev.* **2018**, *91*, 1205–1230. [[CrossRef](#)]

24. Sabihuddin, S.; Kiprakis, A.; Mueller, M. A Numerical and Graphical Review of Energy Storage Technologies. *Energies* **2014**, *8*, 172–216. [[CrossRef](#)]
25. Few, S.; Schmidt, O.; Offer, G.J.; Brandon, N.; Nelson, J.; Gambhir, A. Prospective improvements in cost and cycle life of off-grid lithium-ion battery packs: An analysis informed by expert elicitations. *Energy Policy* **2018**, *114*, 578–590. [[CrossRef](#)]
26. Stampatori, D.; Raimondi, P.P.; Noussan, M. Li-Ion Batteries: A Review of a Key Technology for Transport Decarbonization. *Energies* **2020**, *13*, 2638. [[CrossRef](#)]
27. Horie, H. Future Lithium-ion Batteries. In *Future Lithium-ion Batteries*; Eftekhari, A., Ed.; Royal Society of Chemistry: London, UK, 2019; Chapter 7—Creatio, p. 367. [[CrossRef](#)]
28. Mongird, K.; Fotedar, V.; Viswanathan, V.; Koritarov, V.; Balducci, P.; Hadjerioua, B.; Alam, J. *Energy Storage Technology and Cost Characterization Report*; Technical Report July; U.S. Department of Energy: Washington, DC, USA, 2019.
29. Chen, J. *Lithium-Ion Battery*; Clean Energy Institute: Seattle, WA, USA, 2020.
30. Belov, D.; Yang, M.H. Failure mechanism of Li-ion battery at overcharge conditions. *J. Solid State Electrochem.* **2008**, *12*, 885–894. [[CrossRef](#)]
31. Doughty, D.; Roth, E.P. A general discussion of Li Ion battery safety. *Electrochem. Soc. Interface* **2012**, *21*, 37–44. [[CrossRef](#)]
32. Normyle, A.; Pittock, J. A review of the impacts of pumped hydro energy storage construction on subalpine and alpine biodiversity: Lessons for the Snowy Mountains pumped hydro expansion project. *Aust. Geogr.* **2020**, *51*, 53–68. [[CrossRef](#)]
33. Kobler, U.G.; Wüest, A.; Schmid, M. Effects of lake-reservoir pumped-storage operations on temperature and water quality. *Sustainability* **2018**, *10*, 1968. [[CrossRef](#)]
34. Liu, W.; Ramirez, A. State of the art review of the environmental assessment and risks of underground geo-energy resources exploitation. *Renew. Sustain. Energy Rev.* **2017**, *76*, 628–644. [[CrossRef](#)]
35. Deng, D. Li-ion batteries: Basics, progress, and challenges. *Energy Sci. Eng.* **2015**, *3*, 385–418. [[CrossRef](#)]
36. Perry, M.L.; Saraidaridis, J.D.; Darling, R.M. Crossover mitigation strategies for redox-flow batteries. *Curr. Opin. Electrochem.* **2020**, *21*, 311–318. [[CrossRef](#)]
37. Aneke, M.; Wang, M. Energy storage technologies and real life applications—A state of the art review. *Appl. Energy* **2016**, *179*, 350–377. [[CrossRef](#)]
38. Scarabaggio, P.; Carli, R.; Cavone, G.; Dotoli, M. Smart control strategies for primary frequency regulation through electric vehicles: A battery degradation perspective. *Energies* **2020**, *13*, 4586. [[CrossRef](#)]
39. Maheshwari, A.; Paterakis, N.G.; Santarelli, M.; Gibescu, M. Optimizing the operation of energy storage using a non-linear lithium-ion battery degradation model. *Appl. Energy* **2020**, *261*, 114360. [[CrossRef](#)]
40. Toma, L.; Sanduleac, M.; Baltac, S.A.; Arrigo, F.; Mazza, A.; Bompard, E.; Musa, A.; Monti, A. On the virtual inertia provision by BESS in low inertia power systems. In Proceedings of the 2018 IEEE International Energy Conference, ENERGYCON 2018, Limassol, Cyprus, 3–7 June 2018; pp. 1–6. [[CrossRef](#)]
41. Behabtu, H.A.; Messagie, M.; Coosemans, T.; Bercebar, M.; Fante, K.A.; Kebede, A.A.; Van Mierlo, J. A review of energy storage technologies' application potentials in renewable energy sources grid integration. *Sustainability* **2020**, *12*, 10511. [[CrossRef](#)]
42. Rohit, A.K.; Rangnekar, S. An overview of energy storage and its importance in Indian renewable energy sector: Part II—Energy storage applications, benefits and market potential. *J. Energy Storage* **2017**, *13*, 447–456. [[CrossRef](#)]
43. Smart Grid Coordination Group. *Smart Grids Methodology and New Applications*; Technical Report; CEN-CENELEC-ETS: Brussels, Belgium, 2014.
44. Uslar, M.; Delfs, C.; Gottschalk, M. *The Use Case and Smart Grid Architecture Model Approach*; Springer: Berlin, Germany, 2017; pp. 41–61. ISBN 978-3319492285.
45. Santodomingo, R.; Uslar, M.; Göring, A.; Gottschalk, M.; Nordstrom, L.; Saleem, A.; Chenine, M. SGAM-based methodology to analyse Smart Grid solutions in DISCERN European research project. In Proceedings of the ENERGYCON 2014—IEEE International Energy Conference, Cavtat, Croatia, 13–16 May 2014; pp. 751–758. [[CrossRef](#)]
46. Andrén, F.P.; Strasser, T.; Kastner, W. Applying the SGAM methodology for rapid prototyping of smart Grid applications. In Proceedings of the IECON 2016—42nd Annual Conference of the IEEE Industrial Electronics Society, Florence, Italy, 23–26 October 2016; pp. 3812–3818. [[CrossRef](#)]
47. Wilker, S.; Meisel, M.; Sauter, T. Smart grid architecture model standardization and the applicability of domain language specific modeling tools. In Proceedings of the 2017 IEEE 26th International Symposium on Industrial Electronics (ISIE), Edinburgh, UK, 19–21 June 2017; pp. 152–157. [[CrossRef](#)]
48. Liu, J.; Zhang, N.; Kang, C.; Kirschen, D.; Xia, Q. Cloud energy storage for residential and small commercial consumers: A business case study. *Appl. Energy* **2017**, *188*, 226–236. [[CrossRef](#)]
49. Malhotra, A.; Battke, B.; Beuse, M.; Stephan, A.; Schmidt, T. Use cases for stationary battery technologies: A review of the literature and existing projects. *Renew. Sustain. Energy Rev.* **2016**, *56*, 705–721. [[CrossRef](#)]
50. Ballestín-Fuertes, J.; Muñoz-Cruzado-alba, J.; Sanz-Osorio, J.F.; Laporta-Puyal, E. Role of wide bandgap materials in power electronics for smart grids applications. *Electronics* **2021**, *10*, 677. [[CrossRef](#)]
51. Cochran, J.; Miller, M.; Zinaman, O.; Milligan, M.; Arent, D.; Palmintier, B.; O'Malley, M.; Mueller, S.; Lannoye, E.; Tuohy, A.; et al. *Flexibility in 21st Century Power Systems*; Technical Report; NREL: Golden, CO, USA, 2014; [[CrossRef](#)]
52. Akrami, A.; Doostizadeh, M.; Aminifar, F. Power system flexibility: An overview of emergence to evolution. *J. Mod. Power Syst. Clean Energy* **2019**, *7*, 987–1007. [[CrossRef](#)]

53. Sperstad, I.B.; Korpås, M. Energy storage scheduling in distribution systems considering wind and photovoltaic generation uncertainties. *Energies* **2019**, *12*, 1231. [[CrossRef](#)]
54. Scarabaggio, P.; Grammatico, S.; Carli, R.; Dotoli, M. Distributed Demand Side Management with Stochastic Wind Power Forecasting. *IEEE Trans. Control. Syst. Technol.* **2021**. [[CrossRef](#)]
55. van Westering, W.; Hellendoorn, H. Low voltage power grid congestion reduction using a community battery: Design principles, control and experimental validation. *Int. J. Electr. Power Energy Syst.* **2020**, *114*, 105349. [[CrossRef](#)]
56. Agbonaye, O.; Keatley, P.; Huang, Y.; Bani Mustafa, M.; Hewitt, N. Design, Valuation and Comparison of Demand Response Strategies for Congestion Management. *Energies* **2020**, *13*, 6085. [[CrossRef](#)]
57. Pavić, I.; Luburić, Z.; Pandžić, H.; Capuder, T.; Andročec, I. Defining and evaluating use cases for battery energy storage investments: Case study in Croatia. *Energies* **2019**, *12*, 376. [[CrossRef](#)]
58. Muñoz-Cruzado-Alba, J.; Rojas, C.A.; Kouro, S.; Díez, E.G. Power production losses study by frequency regulation in weak-grid-connected utility-scale photovoltaic plants. *Energies* **2016**, *9*, 317. [[CrossRef](#)]
59. International Renewable Energy Agency. *Utility-Scale Batteries Innovation Landscape Brief*; IRENA: Abu Dhabi, United Arab Emirates, 2019.
60. Torres, J.; Blanco, M.; Lafoz, M.; Navarro, G.; Nájera, J.; Santos-Herran, M. Dimensioning methodology of energy storage systems for power smoothing in a wave energy conversion plant considering efficiency maps and filtering control techniques. *Energies* **2020**, *13*, 3380. [[CrossRef](#)]
61. Daud, M.Z.; Mohamed, A.; Hannan, M.A. A review of the integration of energy storage systems (ESS) for utility grid support. *Prz. Elektrotechniczny* **2012**, *88*, 185–191.
62. Chang, L.; Zhang, W.; Xu, S.; Spence, K. Review on Distributed Energy Storage Systems for Utility Applications. *CPSS Trans. Power Electron. Appl.* **2017**, *2*, 267–276. [[CrossRef](#)]
63. General Electric. *GE Energy Storage Unit RSU-4000*; Technical Report January; General Electric: Boston, MA, USA, 2020.
64. Megapack | Tesla. Available online: <https://www.tesla.com/megapack> (accessed on 5 April 2021).
65. Utility ESS—BYD USA. Available online: <https://en.byd.com/energy/utility-ess/> (accessed on 5 April 2021).
66. Vanadium Flow Battery Energy Storage | Invinity. Available online: <https://invinity.com/solutions/vanadium-flow-batteries/> (accessed on 2 April 2021).
67. Redox Flow Battery | Sumitomo Electric Industries. Available online: <https://sumitomoelectric.com/products/redox> (accessed on 7 April 2021).
68. Energy, S.; Inverter, S. *GE Energy Storage Reservoir Inverter Unit*; Technical Report; General Electric: Boston, MA, USA, 2021.
69. Lotspeich, C. A Comparative Assessment of Flow Battery Technologies. In Proceedings of the 2002 EESAT Conference, San Francisco, CA, USA, 15–17 April 2002; pp. 1–6.
70. Bryans, D.; Amstutz, V.; Girault, H.H.; Berlouis, L.E. Characterisation of a 200 kw/400 kwh vanadium redox flow battery. *Batteries* **2018**, *4*, 54. [[CrossRef](#)]
71. Tokuda, N.; Kanno, T.; Hara, T.; Shigematsu, T.; Tsutsui, Y.; Ikeuchi, A.; Itou, T.; Kumamoto, T. Development of a redox flow battery system. *SEI Tech. Rev.* **2000**, *50*, 88–94.
72. Marra, F.; Yang, G.; Træholt, C.; Østergaard, J.; Larsen, E. A decentralized storage strategy for residential feeders with photovoltaics. *IEEE Trans. Smart Grid* **2014**, *5*, 974–981. [[CrossRef](#)]
73. Solar Battery Storage: Including Tesla Powerwall, LG Chem, Powervault. Available online: <https://naked solar.co.uk/storage/> (accessed on 2 April 2021).
74. International Electrotechnical Commission. *IEC 60038: IEC Standard Voltages*; Technical Report; IEC: Geneva, Switzerland, 2002.
75. Technology | BAoBaB. Available online: <http://www.baobabproject.eu/technology> (accessed on 26 June 2020).

# Capítulo 7

## **Implementación de servicios auxiliares en cargadores públicos para vehículo eléctrico y evaluación de su efecto en la red**

**RESUMEN:** La creación de nuevos dispositivos para la prestación de servicios auxiliares puede ser, en muchas ocasiones, costoso económicamente y técnicamente difícil debido a la falta de espacio para la instalación de estos equipos en ambientes urbanos. El artículo *Four-leg EV Chargers for Grid Supporting* toma los conceptos desarrollados en los capítulos anteriores, propone su integración en otros elementos del mobiliario urbano como los cargadores para vehículo eléctrico, y analiza los efectos de su instalación en cuatro modelos de redes urbanas europeas.

# Four-leg EV Chargers for Grid Supporting

Antonio Miguel Muñoz<sup>1</sup>, Javier Ballestín-Fuertes<sup>1</sup>, Gregorio Fernandez<sup>1</sup>, Daniel Marquina<sup>1</sup>, Ricardo Igea<sup>1</sup>.

<sup>1</sup> Fundación CIRCE, Spain.

Corresponding author: Antonio Miguel Muñoz, amimuno@fcirce.es

The Power Point Presentation will be available after the conference.

## Abstract

Despite the benefits of transport electrification, such as improved efficiency energy use or reduced environmental impact, a wide spread of incorrectly managed charging facilities can generate problems for the electricity system, mainly in the distribution grids. In recent years, the paradigm is changing and the use of EV charging facilities as support elements for grid operation is being proposed. Following this idea, this document shows a high-power EV charger with a 4-leg grid side for grid support, highlighting among its functionalities the possibility of charging or discharging EV batteries in an unbalanced way or the management of reactive power

## 1 Introduction

Fossil fuel use has been proven is the main cause of the climate change and the global warming [1]. Renewable energy and electrification of transportation is leading this change of paradigm to break this tendency, pushed by social awareness [2] and new regulations [3].

To significantly reduce the world's dependence on fossil fuels and the correlative global warming, it is generally accepted on solution is the integration of transportation and electricity sectors, in combination with EVs and renewable energy [4].

Despite its benefits, EV charging and high penetration of renewable energies could have important impacts on the electric grid. On the one hand, due to demand increase and power quality disturbances originated by the involved power electronic converters [5]. And on the other hand, due to seasonal, intermittent, and uncontrollable nature, forcing new operation, structures, and maintenance techniques in the grid system [6].

In particular, the distribution grid will undergo the greatest transformation following this electrification process. Power quality and voltage stability are the main issues in power systems. In addition, the low-voltage distribution system is supplied by a three-phase four-wire network, where single-

phase and three phase devices coexist. This characteristic generates imbalances that cause a series of problems in distribution networks that must be addressed [7]–[9]:

- Neutral conductor overload.
- Neutral to ground voltage (NGV) increase.
- Power quality reduction.
- Line losses increase.
- Distribution transformer overheating and degradation.
- Maloperation of protection relays.
- Vibration and malfunction in induction equipment.

To minimize these issues, the most important standards define different parameters to quantify and limit the main causes of all these problems. However, all of them agree on the restriction of the unbalance factor. The American National Standards Institute (ANSI) defines the percent voltage unbalance as

$$\begin{aligned} \text{Percent voltage unbalance} &= \\ &= 100 \cdot \frac{\text{max deviation from average voltage}}{\text{average voltage}} \end{aligned}$$

and recommends limiting it to 3% [10], since the International electrotechnical commission (IEC)

and CIGRE define the voltage unbalance factor (VUF)

$$VUF(\%) = 100 \cdot \frac{V_-}{V_+}$$

where  $V_+$  and  $V_-$  are the positive and negative symmetric components, respectively. Both institutions set the VUF limit to 2%, allowing to reach 3% in grids with a high presence of single-phase customers [11], [12].

To reduce the effect of imbalances several methods are proposed in literature [7]. On the one hand, the reconfiguration techniques, consist in acting on switches distributed in the grid to alter the topology of the network, known as feeder reconfiguration [13], [14], or to switch the phase connection among phases, called phase swapping [15], [16]. On the other hand, some techniques mitigate network imbalances by adding special current compensating devices [17]–[21]. Specifically, one of these techniques proposes the use of power electronics converters known as active power filters (APF) to eliminate imbalances.

The deployment of APF has a series of drawbacks, like power losses increase, lack of public space in cities and the investment required, that may be its installation unfeasible. However, this technology can be included with minimal changes in public equipment such as public EV chargers. Thus, different APF topologies are proposed [7]. Most of them can be classified into three single phase H-bridge, three-legs four-wire (3L-4W) and four-leg (4L) topologies [22]–[24].

Considering the effects in the grid of the EV charging stations deployment and integration of renewable energies, this document shows how a high-power EV charger with a 4L grid side can be feasible to use for grid support, and the results of several test and simulation performed to prove the usefulness of the system.

## 2 Proposed solution

To provide public equipment, the ability to give additional grid services an enhanced EV charger has been designed. This power converter consists of a DC/DC and an AC/DC converter with a bi-level 3L split-capacitor plus a fourth capacitor-balancing leg topology, based on SiC MOSFETs, shown in Fig. 1. In this topology, the converter has three active phases while providing a return path to the neutral current through the capacitor midpoint, in case the load is unbalanced. In this way, the proposed converter allows to handle active and reactive unbalanced currents whether vehicles are connected or not. As illustrated in Fig. 2, the

AC/DC converter was tested in a relevant environment through Power Hardware in the Loop emulation. The AC/DC converter main characteristics are listed in Table 1.

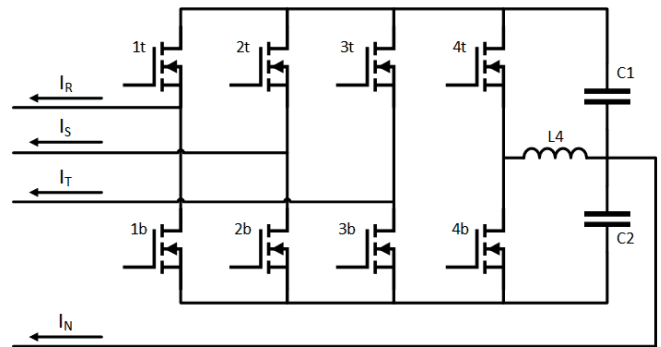


Fig. 1: 4W-4L split capacitor topology chosen to allow unbalanced operation.

Specification	Description
AC/DC characteristics:	AC/DC Converter 4-Leg Bidirectional High frequency switching SiC semiconductors technology Low harmonic current Accurate operation Noiseless, switching frequency >20 kHz
Main functions	Active and reactive power compensation Phase independent control capability
Main circuitry	4x HF SiC Phase, DC Bus, Input grid filter, current, voltage and temperature measurements.
Refrigeration	By air, forced
Dimensions	400x400x200 mm
Protection	Without IP environmental protection, it must be provided/covered with an external envelope.

Table 1: AC/DC converter main characteristics

In the literature, the benefits of current balancing have been demonstrated by the addition of equipment specifically designed for this purpose, both through simulation [25] and in pilots installed in real distribution grids [26]. However, it is possible to add the capability to manage unbalanced loads to grid-deployed equipment, such as EV chargers, without the need to install equipment specifically designed for this purpose.

By introducing slight modifications to convert the common 3W chargers installed on public roads into 4W chargers, they are able to charge the vehicle without increasing the consumption of the most heavily loaded phase, consuming energy

only from the less loaded phases (3 (a)); to discharge the vehicle on a single phase to mitigate occasional congestion (3 (b)); or even to balance the line currents when no vehicle is plugged in (3 (c)).



Fig. 2.: AC/DC converter tested with PHIL in CIRCE Laboratory.

### 3 System simulations, electric vehicle charge grid impact reduction

The effect on the grid that an electric vehicle charger as the one described in previous sections has been evaluated through computer simulations. The software used is DigSILENT PowerFactory [27] and it has been tested in two groups of grids with different objectives: the IEEE LV benchmark grid, to evaluate effect on grid losses and voltage issues, in four real grids, to evaluate effect in terms of energy losses and voltage unbalances reduction.

#### 3.1 IEEE LV benchmark grid tests

A description of the “IEEE European Low Voltage Test Feeder” can be seen [28]. For the simulations

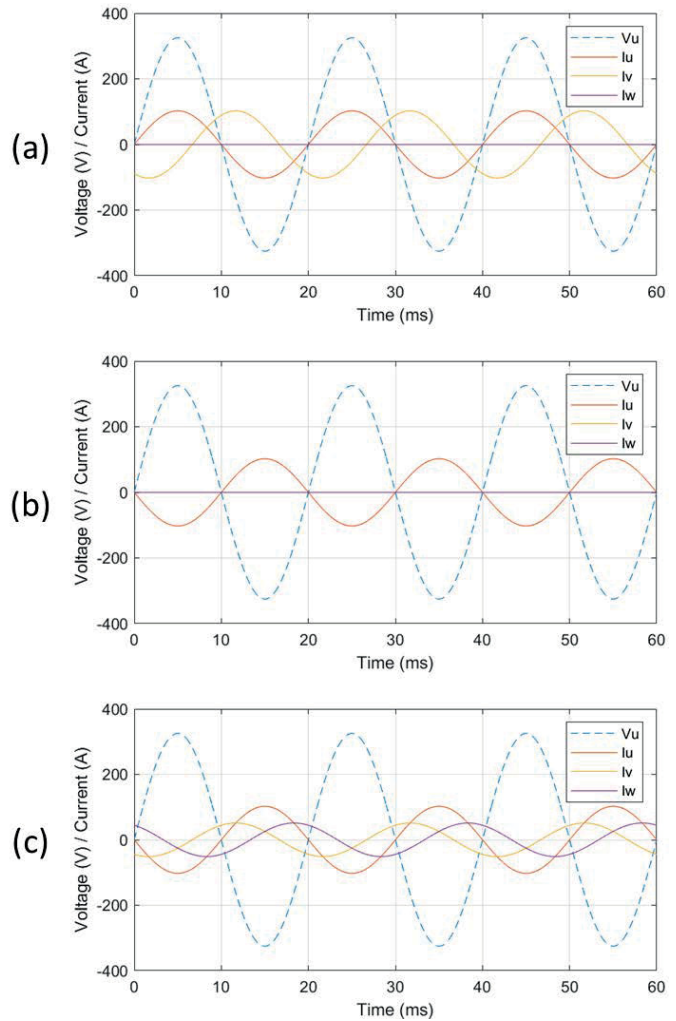


Fig. 3: EV charger providing different services: (a) charging the EV at 33 kW, consuming power from U and V phases; (b) injecting 16.6 kW into U phase, taking the power from the EV batteries; (c) balancing the line, consuming 33 kW from V and W phases and injecting it in U.

in this grid, to make it more general, three commercial consumers have been added directly downwards of the transformer.

The effect of the EV charger has been tested near the MV/LV transformer (in parallel to the new commercial consumers) and in one of the furthest points of the grid.

An electric vehicle charger as the described in this paper can provide unbalanced charge, V2G and reactive power management functionalities. The most interesting results are:

- Unbalanced charge. Can reduce energy losses reducing charging power and balancing voltages. Depending on the charger location, additional issues could be generated as the connection of new loads in remote areas of the network

can produce new congestions and voltage problems.

- V2G. Discharging EV batteries always reduces energy provided by the transformer and grid distribution losses. The effect on congestions and undervoltage problems is greater in the case of the charger installation near the most distant loads.

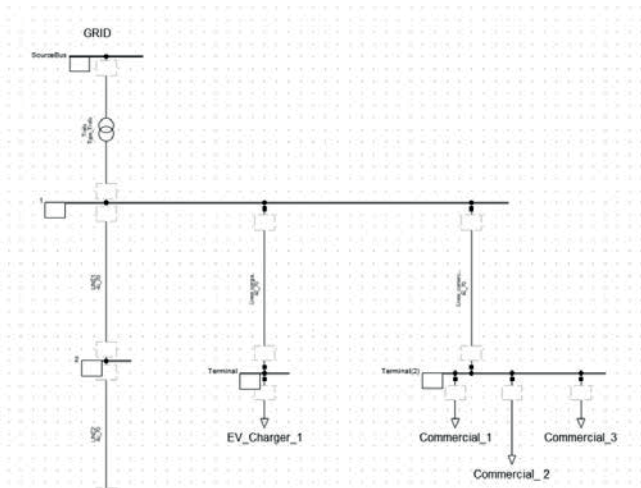


Fig. 4: Single line diagram of the newly added loads to the IEEE European Low Voltage Test Feeder benchmark grid.

- Reactive power management. The effect on the reduction of under voltages and congestions is much greater if the charger is located far from the transformer, near the most problematic points. It also has been seen that high power charges, although not at the nominal power, combined with a reactive power injection could congest the grid to undesirable levels.

The main conclusion of these simulations is that although EV chargers as the described in this document can provide a proper support to grid operators, its location must be carefully selected to avoid undesired effects.

### 3.2 Real grid tests

One of the main benefits of the chargers equipped with a 4L grid side is that it can provide grid services even when no EV is connected to it, compensating reactive power or unbalanced demands, as a D-STATCOM system would do. Reactive power compensation has been evaluated in previous grid. The effect of an EV charger when no vehicles are connected has been tested in four real grids in different locations in terms of energy

losses reductions due to the balance of phase voltages through demand unbalances compensation.

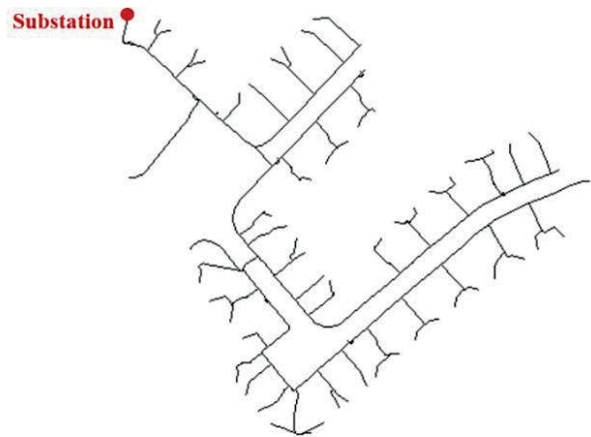


Fig. 5: One-line diagram of the European low voltage test feeder.

Four real grids from different locations along Europe and long term (more than 7 months for some grids and until a year for others) related consumption/generation data of have been used: Southern Europe rural grid, Northern Europe urban-residential grid, Central Europe Rural-Residential grid and Southern Europe urban grid.

In order to evaluate the possible effect of the charger on the networks studied, it has been placed in multiple locations until the one where the losses due to voltage unbalance are reduced the most (see Fig. 6, Fig. 7, Fig. 8, Fig. 9). The best results reducing energy losses in the previous grids is shown in the next table:

Grid	Energy Savings (kWh)	Energy Savings (%)
Southern Europe rural grid.	311.89	3.325
Northern Europe urban-residential grid.	1.65	0.019
Central Europe Rural-Residential grid.	112.96	2.076
Southern Europe urban grid.	217.71	6.396

Table 2. Energy losses savings in four real grids using an EV charger with a 4L grid side.



Fig. 6. Image of the optimal location of the EV charger compensating voltage unbalances in the Southern Europe rural grid.

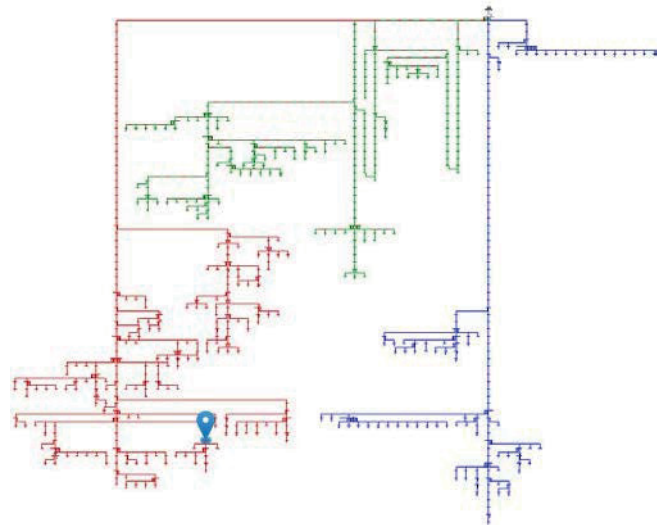


Fig. 9.. Image of the optimal location of the EV charger compensating voltage unbalances in the Southern Europe urban grid.

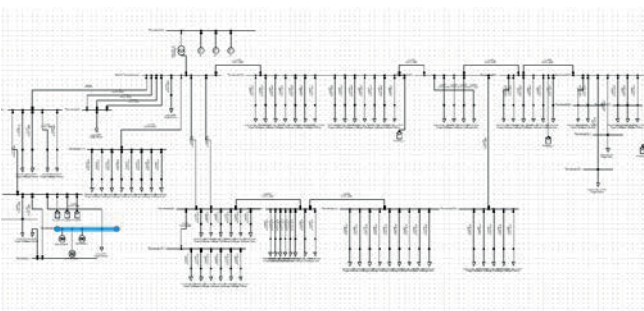


Fig. 7. Image of the optimal location of the EV charger compensating voltage unbalances in the Northern Europe urban-residential grid.

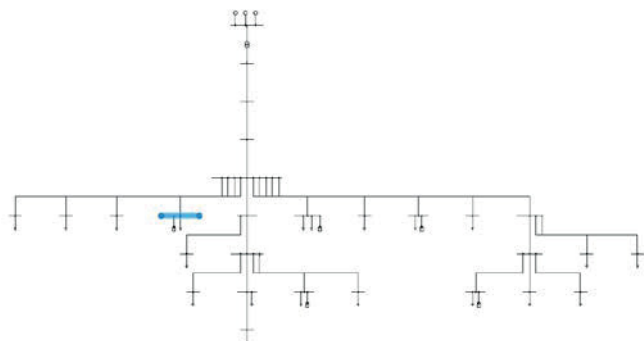


Fig. 8. Image of the optimal location of the EV charger compensating voltage unbalances in the Central Europe Rural-Residential grid.

## 4 Conclusion

This document presents a high-power electric vehicle charger with a 4L side to provide grid support. The developed device consists in a 50-kW DC CHAdeMO + CSS charger with V2G and V2V capabilities. In addition to describing the charger, the results of several simulations made to evaluate the benefits of this device on the electric grid are shown. Specifically, the effect of these chargers has been simulated in a low voltage benchmark network and in four real grids. It has been seen how losses, voltage deviation and congestions can be reduced, but these results are highly dependent on the location and characteristics of the grids, so detailed studies are recommended to choose the optimal location for these devices.

## Declaration of Competing Interest

The authors declare that they have no known competing financial interests or personal relationships that could have appeared to influence the work reported in this article.

## Acknowledgments

The research has been carried out in the framework of the INCIT-EV project (<https://www.in>

[cit-ev.eu/](http://cit-ev.eu/)), funded by the European Union under the Horizon 2020 Programme (H2020-LC-GV-2019).

## 5 Reference

- [1] T. M. L. Wigley, P. D. Jones, and P. M. Kelly, "Global warming of 1.5 °C," *Nature*, vol. 291, no. 5813, p. 285, 1981, doi: 10.1038/291285a0.
- [2] *Going climate-neutral by 2050: A strategic long-term vision for a prosperous, modern, competitive and climate-neutral EU economy*. © European Union, 2019.
- [3] European Commission, "Energy topics," 2020. [https://ec.europa.eu/energy/topics/energy-strategy/clean-energy-all-europeans\\_en](https://ec.europa.eu/energy/topics/energy-strategy/clean-energy-all-europeans_en) (accessed Oct. 15, 2021).
- [4] "Global EV Outlook 2021," Paris (France), 2021.
- [5] C. H. Dharmakeerthi, N. Mithulananthan, and T. K. Saha, "Overview of the impacts of plug-in electric vehicles on the power grid," *2011 IEEE PES Innov. Smart Grid Technol. ISGT Asia 2011 Conf. Smarter Grid Sustain. Afford. Energy Futur.*, 2011, doi: 10.1109/ISGT-Asia.2011.6167115.
- [6] R. A. Verzijlbergh, L. J. De Vries, G. P. J. Dijkema, and P. M. Herder, "Institutional challenges caused by the integration of renewable energy sources in the European electricity sector," *Renew. Sustain. Energy Rev.*, vol. 75, no. November 2016, pp. 660–667, 2017, doi: 10.1016/j.rser.2016.11.039.
- [7] M. R. Islam, H. Lu, M. J. Hossain, and L. Li, "Mitigating unbalance using distributed network reconfiguration techniques in distributed power generation grids with services for electric vehicles: A review," *J. Clean. Prod.*, vol. 239, 2019, doi: 10.1016/j.jclepro.2019.117932.
- [8] C. I. Ciontea and F. Iov, "A Study of Load Imbalance Influence on Power Quality Assessment for Distribution Networks," *Electr. 2021, Vol. 2, Pages 77-90*, vol. 2, no. 1, pp. 77–90, Mar. 2021, doi: 10.3390/ELECTRICITY2010005.
- [9] S. Deleanu, M. Iordache, M. Stanculescu, and D. Niculae, "The induction machine operating from a voltage supply, unbalanced and polluted with harmonics: A practical approach," *2019 15th Int. Conf. Eng. Mod. Electr. Syst. EMES 2019*, pp. 181–184, 2019, doi: 10.1109/EMES.2019.8795212.
- [10] "ANSI C84.1-2011 - Electric Power Systems and Equipment - Voltage Ratings (60 Hertz)," 2011.
- [11] "IEC 61000-3-6:1996 – Assessment of Emission Limits for Distorting Loads in MV and HV Power Systems, technical report type 3," 2008.
- [12] Cigré WG C4.07, "CIGRE Technical Brochure 261, 'Power quality indices and objectives,'" 2004. doi: 10.1049/cp:20051074.
- [13] A. R. Abbasi, "Investigation of simultaneous effect of demand response and load uncertainty on distribution feeder reconfiguration," *IET Gener. Transm. Distrib.*, vol. 14, no. 8, pp. 1438–1449, 2020, doi: 10.1049/iet-gtd.2019.0854.
- [14] H. Lotfi, R. Ghazi, and M. bagher Naghibi-Sistani, *Multi-objective dynamic distribution feeder reconfiguration along with capacitor allocation using a new hybrid evolutionary algorithm*, vol. 11, no. 3. Springer Berlin Heidelberg, 2020.
- [15] B. Cortés-Cañedo, L. S. Avellaneda-Gómez, O. D. Montoya, L. Alvarado-Barrios, and C. Álvarez-Arroyo, "An improved crow search algorithm applied to the phase swapping problem in asymmetric distribution systems," *Symmetry (Basel)*, vol. 13, no. 8, pp. 1–20, 2021, doi: 10.3390/sym13081329.
- [16] O. D. Montoya, J. A. Alarcon-Villamil, and J. C. Hernández, "Operating cost reduction in distribution networks based on the optimal phase-swapping including the costs of the working groups and energy losses," *Energies*, vol. 14, no. 15, 2021, doi: 10.3390/en14154535.
- [17] A. Hiranandani, "Calculation of cable ampacities including the effects of harmonics," *IEEE Ind. Appl. Mag.*, vol. 4, no. 2, pp. 42–51, 1998, doi: 10.1109/2943.655660.
- [18] K. Nikum, A. Wagh, R. Saxena, and A. Singh, "Power Quality Problems in Large Commercial Load and their Mitigation: A Case Study," *2019 IEEE 1st Int. Conf. Energy, Syst. Inf. Process. ICESIP 2019*, vol. 3, no. 2, 2019, doi: 10.1109/ICESIP46348.2019.8938339.
- [19] C. Dai and Y. Sun, "Investigation of the imbalance current compensation for transformers used in electric railways," *Asia-Pacific Power Energy Eng. Conf.*

- APPEEC*, vol. 1, no. 1, pp. 10–13, 2010, doi: 10.1109/APPEEC.2010.5448337.
- [20] P. Jayaprakash, B. Singh, and D. P. Kothari, “Three-phase 4-wire DSTATCOM based on H-bridge VSC with a star/hexagon transformer for power quality improvement,” *IEEE Reg. 10 Colloq. 3rd Int. Conf. Ind. Inf. Syst. ICIIIS 2008*, pp. 1–6, 2008, doi: 10.1109/ICIINFS.2008.4798378.
- [21] T. H. Chen, “Comparison of Scott and Leblanc transformers for supplying unbalanced electric railway demands,” *Electr. Power Syst. Res.*, vol. 28, no. 3, pp. 235–240, Jan. 1994, doi: 10.1016/0378-7796(94)90038-8.
- [22] J. Gong, D. Li, T. Wang, W. Pan, and X. Ding, “A comprehensive review of improving power quality using active power filters,” *Electr. Power Syst. Res.*, vol. 199, p. 107389, Oct. 2021, doi: 10.1016/J.EPSR.2021.107389.
- [23] A. Teke, L. Saribulut, M. E. Mehmet Emin, and M. Tümay, “Active power filter: Review of converter topologies and control strategies,” *Gazi Univ. J. Sci.*, vol. 24, no. 2, pp. 283–289, 2011.
- [24] D. Chen and S. Xie, “Review of the control strategies applied to active power filters,” *Proc. 2004 IEEE Int. Conf. Electr. Util. Deregulation, Restruct. Power Technol.*, vol. 2, no. April, pp. 666–670, 2004, doi: 10.1109/drpt.2004.1338067.
- [25] G. Fernández *et al.*, “Optimal d-statcom placement tool for low voltage grids,” *Energies*, vol. 14, no. 14, pp. 1–31, 2021, doi: 10.3390/en14144212.
- [26] J. Ballestín-Fuertes, J. F. Sanz-Osorio, J. Muñoz-Cruzado-Alba, E. L. Puyal, J. Leiva, and J. R. Rivero, “Four-Legs D-STATCOM for Current Balancing in Low-Voltage Distribution Grids,” *IEEE Access*, vol. 10, pp. 779–788, 2022, doi: 10.1109/ACCESS.2021.3138827.
- [27] “DigSILENT | POWER SYSTEM SOLUTIONS.”  
<https://www.digsilent.de/en/powerfactory.html>.
- [28] “IEEE PES Test Feeder.”  
<https://cmte.ieee.org/pes-testfeeders/resources/>.

# Capítulo 8

## Discusión

**RESUMEN:** En este capítulo se presentan las principales aportaciones de cada uno de los estudios realizados al conjunto de la tesis. De este modo, se ofrece una visión global de la contribución de esta tesis al ámbito de estudio en el que se engloba y al progreso del estado del arte del sector.

## 8. DISCUSIÓN

### 8.1 Estudio 1

La EL es el fenómeno por el cual las células FV emiten radiación electromagnética cuando se realiza la polarización directa de las mismas. Esto implica que, cuando a un panel FV se le aplica una tensión en bornes superior a su tensión de circuito abierto este deja de generar corriente, como un foto-diodo, para absorber energía eléctrica y transformarla en radiación, como lo haría un diodo LED. En particular, en el caso de los paneles de silicio esta radiación es emitida en el espectro del infrarrojo cercano.

La Figura 8.1 muestra el comportamiento de la corriente en función de la tensión e irradiancia aplicadas al panel. En ella se aprecia que, para valores de tensión por debajo de la tensión de circuito abierto, el valor de la corriente permanece en el primer cuadrante, lo que denota un comportamiento del panel como generador. Sin embargo, en el momento en el que se supera la tensión de circuito abierto, la cual depende de la irradiancia, el signo de la corriente se invierte pasando a consumir energía y emitir radiación electromagnética.

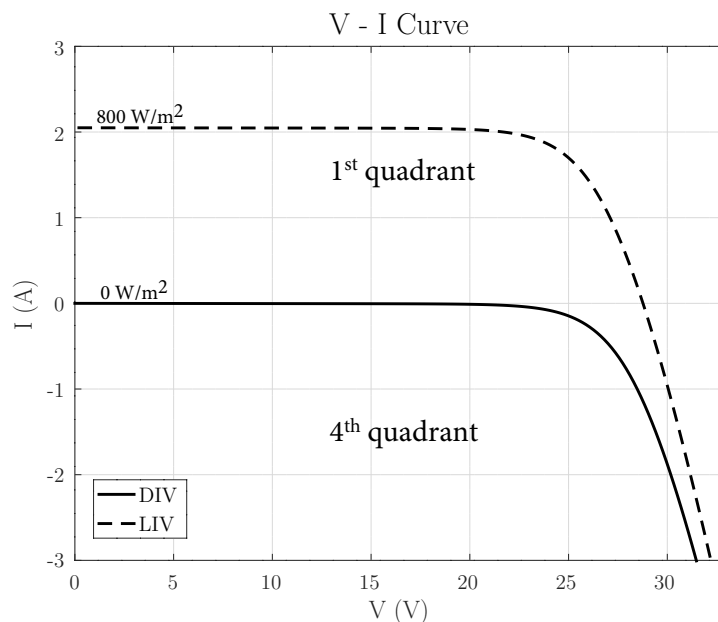


**Figura 8.1:** Curvas IV de un módulo FV para una radiación incidente de  $0 \text{ W/m}^2$  y  $800 \text{ W/m}^2$ .

La aplicación de la EL al mantenimiento de plantas FV resulta una de las técnicas más precisas para la detección de células en mal estado, defectos y roturas presentes en los paneles FV. En la actualidad, la realización de esta técnica requiere la desconexión de los módulos y el desmontaje de los mismos. Posteriormente estos son transportados a unas instalaciones acondicionadas para este fin, donde son evaluados y posteriormente instalados en la planta de nuevo.

En el primer artículo del compendio de publicaciones se propone la utilización del propio inversor instalado en la planta FV para llevar a cabo la polarización directa de los paneles, evitando la necesidad de desconexión y transporte de los mismos, con el objetivo de reducir los costes de mantenimiento de la instalación. A continuación, se muestra el desarrollo de un inversor de pequeña potencia para la validación de los paneles de una planta piloto. Finalmente, se analizan las características eléctricas necesarias para la aplicación de esta técnica, tales como tensiones y potencias requeridas para la polarización de los paneles.

La principal aportación de este estudio al conjunto de la tesis se encuentra en la sección 3 de la publicación. En ella se realiza el estado del arte de las topologías de convertidores trifásicos de electrónica de potencia más utilizadas en inversores FV. Este estudio destaca que no hay una solución única, y que la elección de una u otra topología dependerá de varios factores como la necesidad o no de aislamiento galvánico, si la conversión de potencia se realizará en una o más etapas, el número de niveles del convertidor, su modo de funcionamiento como fuente de corriente, tensión o impedancia, el modo de conmutación, etc.

En primer lugar, la topología más simple y una de las más empleadas en el mercado hoy en día es el inversor trifásico de dos niveles (Figura 8.2(a)). Esta topología requiere el mínimo número de semiconductores con tan solo 6 dispositivos controlables, típicamente MOSFETs o IGBTs.

Como evolución de la topología binivel aparecen las topologías multinivel. Estas, a su vez, pueden dividirse en el caso de 3, 5 o N niveles, con el objetivo de reducir la tensión máxima que debe soportar cada dispositivo. Además, se consigue una mejora en la calidad de onda de salida del equipo y, de esta forma, reducir las necesidades de filtrado. Por contra, aumentar el número de niveles implica también un aumento en el número de semiconductores necesarios y en la complejidad de las estrategias de modulación requeridas para su operación.

## 8. DISCUSIÓN

---

Dentro de las topologías multinivel aparecen diferentes variantes, entre las más comunes destacan las topologías de punto medio anclado, más conocidas como NPC por sus siglas en inglés. Dentro de las topologías NPC también existen variantes, siendo las más comunes la variante tipo-I y la tipo-T, mostradas en la Figura 8.2(b) y 8.2(c), respectivamente.

La topología NPC tipo-I presenta un punto medio flotante en su bus de continua que permite aplicar una tensión de 0 V a la salida del convertidor, además de las tensiones máxima y mínima de bus,  $+V_{DC}$  y  $-V_{DC}$ . Esta topología presenta varias ventajas frente a la binivel como un menor contenido en armónicos, la necesidad de menores componentes pasivos para el filtrado, una mayor eficiencia, así como que la tensión máxima requerida por sus dispositivos semiconductores es la mitad que en la topología binivel. Sin embargo, se deben implementar técnicas de control que eviten el desequilibrio de los condensadores del bus de continua.

Por otro lado, la topología NPC tipo-T reduce el número de semiconductores respecto a la tipo-I, pues esta no requiere de los diodos de *clamping*, y presenta una eficiencia ligeramente superior a esta debido a que solo conduce un semiconductor en cada momento. Por el contrario, los semiconductores deben tener una mayor tensión de rotura pues, en esta topología, sí deben bloquear la tensión de bus completa.

En paralelo a las topologías NPC, otra variante de los convertidores multinivel son las denominadas topologías de condensador flotante (Figura 8.2(d)). Esta alternativa consigue un menor contenido de armónicos y una mejor regulación de la tensión en los condensadores. Por contra, el número de condensadores necesarios aumenta con el número de niveles, lo que hace de estos inversores más voluminosos que los basados en topologías NPC.

Existen ciertas variaciones para todas las topologías analizadas que permiten ligeras mejoras en las características del inversor. Un ejemplo de ello es la mostrada en la Figura 8.2(e), que combina características de las topologías NPC y condensador flotante presentadas anteriormente. Además, cabe destacar que todas estas topologías son bidireccionales, pudiendo tanto absorber como entregar potencia a la red, y permiten un control total sobre la componente reactiva de la corriente, lo que hace de estas configuraciones aptas para todo tipo de equipos como inversores FV, cargadores de VE, sistemas de baterías, etc.

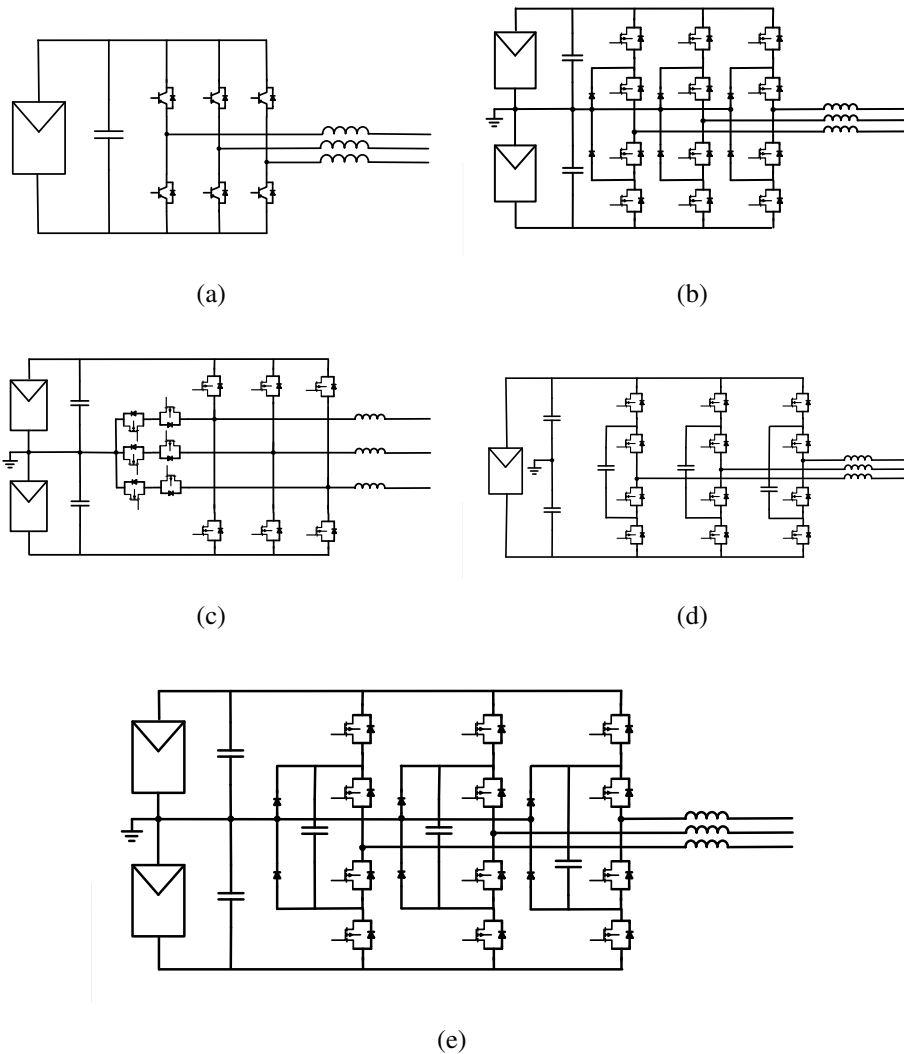


**Figura 8.2:** Topologías representativas de inversores trifásicos para aplicaciones de fotovoltaica: (a) inversor binivel; (b) inversor trinivel NPC tipo-I; (c) inversor trinivel NPC tipo-T; (d) inversor trinivel de condensador flotante; y (e) inversor trinivel NPC tipo-I modificado.

Finalmente, se realiza un análisis de las principales partes que componen el control de la mayoría de inversores trifásicos, las cuales se muestran en la Figura 8.3:

- El control de alto nivel es el encargado de la generación de las consignas de

## 8. DISCUSIÓN

---

potencia activa y reactiva en función de las necesidades de cada aplicación. Algunos ejemplos son la reducción de la potencia generada en aplicaciones de FV debido a la necesidad de aplicar curtailments, la generación de reactiva de acuerdo a los códigos de red, etc. Este control se realiza a una frecuencia menor que los controles de bajo nivel, que puede ir desde el orden de los segundos hasta los minutos.

- El control intermedio toma las consignas de potencia y se encarga del control de las variables eléctricas instantáneas en tiempo real. Las variables a controlar típicamente son la corriente de salida del convertidor o la tensión en bornes del mismo, en función de si el convertidor funciona en modo *grid following* o *grid forming*, respectivamente. Existen numerosas técnicas para el control de tensión/corriente en convertidores trifásicos. Una de las más sencillas y ampliamente utilizada en este tipo de aplicaciones es el control en DQ por medio de la aplicación de las transformaciones de Park y Clarke. Estas transformaciones permiten cambiar la base de proyección de los valores de tensión y corriente sobre unos ejes sincronizados con la fase de la red, facilitando el control de la misma. Por otro lado, existen técnicas que permiten realizar la regulación sobre los valores instantáneos de tensión y corriente, consiguiendo habitualmente una respuesta más rápida del sistema.
- El control de bajo nivel se encarga de tomar la acción determinada por el regulador anterior, habitualmente la tensión aplicada a la salida del puente inversor, y establecer en todo momento las señales de activación de los elementos semiconductores controlables. Este control está íntimamente ligado a la topología empleada en el inversor y, por lo tanto, debe ser cuidadosamente estudiada de acuerdo a esta. Dos de las modulaciones más empleadas son la modulación en vector de estados y las basadas en una onda portadora, SVM y CBM por sus siglas en inglés, respectivamente. La mayoría de las topologías de inversores de este tipo disponen de uno o más grados de libertad, generando estados redundantes que pueden ser empleados por las técnicas de modulación con el objetivo de conseguir diferentes beneficios

adicionales, como una mejora de la calidad de la onda a la salida, una reducción del modo común inyectado por el convertidor, la regulación de la tensión de los condensadores en topologías multinivel, etc.

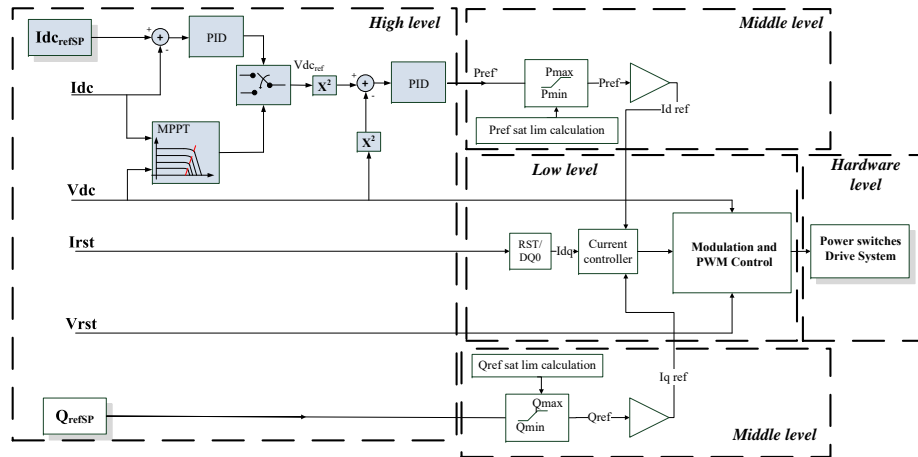


**Figura 8.3:** Principales elementos que componen el control de un inversor de electrónica de potencia.

## 8. DISCUSIÓN

---

### 8.2 Estudio 2

El cambio climático representa un reto a nivel global, y las energías renovables tendrán un rol decisivo ayudando a satisfacer las necesidades energéticas mundiales en el futuro. En la actualidad, más del 30 % de la generación eléctrica en la UE proviene de fuentes de energías renovables. En el año 2000, las energías renovables suponían apenas un 12 %, mientras que, para el año 2030, la UE se ha fijado la meta de alcanzar el 45 % de la generación eléctrica total. Del mismo modo, reducir el consumo energético es una medida igualmente efectiva, por lo que la CE ha fijado el objetivo de incrementar el ahorro energético un 1,5 % anual desde 2024 a 2030.

La esperada electrificación del sector energético hace que el rol de las *Smart Grids* juegue un papel importante. La siguiente generación de estas redes inteligentes debe integrarse en un escenario con un gran número de dispositivos conectados a la red, y con una gran capacidad de coordinación entre ellos. Por un lado, las grandes centrales térmicas serán sustituidas por plantas de generación renovable a gran escala. Por el otro lado, se espera que emerjan las ciudades inteligentes; con una alta penetración de DERs, los consumidores dejarán de tener un rol pasivo para participar más activamente en el sistema eléctrico; combinando diferentes sistemas como micro-fotovoltaica, VE, BESS, sistemas de climatización eléctrica, etc.

Sin embargo, para alcanzar este escenario, los nuevos dispositivos de las redes inteligentes deben satisfacer algunos requisitos antes de convertirse en tecnologías viables: deben ser económicos, tener una alta eficiencia, ser silenciosos, fiables y compactos. En la actualidad, los equipos de electrónica de potencia no cumplen con estos requisitos y se está trabajando en el desarrollo de nuevos convertidores que sí los satisfagan. Además, se están alcanzando los límites teóricos del silicio como material semiconductor, lo que ha obligado al sector de la electrónica a buscar nuevos materiales con unas mejores propiedades eléctricas. En este contexto, los materiales WBG están surgiendo como la solución a las actuales limitaciones del silicio.

En línea con lo descrito anteriormente, el Estudio 2 completa el estado del arte realizado en la presente tesis. Las *Smart Grids* requerirán una mayor conectividad y capacidad de regulación a los dispositivos que se conecten en ella. Así, en este

artículo, en primer lugar, se realiza una clasificación de los convertidores de electrónica de potencia en función de su capacidad para proporcionar servicios auxiliares a la red. Según la clasificación mostrada en la Tabla 8.1, solo los convertidores de Tipo 2, y especialmente Tipo 3 y 4, son viables para la integración de DERs en una *Smart Grid*.

**Tabla 8.1:** Clasificación de los convertidores de electrónica de potencia en función de su capacidad de adaptación a la red.

Tipo	Comunicaciones con la red	Control sobre potencia activa	Control sobre potencia reactiva	Topología
1	No	No	No	Monofásico Trifásico
2	Sí	Sí	No	Monofásico Trifásico
3	Sí	Sí	Sí	Monofásico Trifásico
4	Sí	Control monofásico	Control monofásico	Cuatro hilos

- Los convertidores de Tipo 1 tienden a ser dispositivos de una potencia inferior que los siguientes tipos. Estos equipos no disponen de comunicaciones que les permitan gestionar su demanda, de forma que, estos convertidores son totalmente controlados por la carga o la fuente renovable a la que se encuentran conectados. Algunos de estos dispositivos no tienen la capacidad de controlar la inyección de reactiva, mientras que otros añaden una etapa para corregir el factor de potencia a un valor predeterminado y no variable, típicamente un factor de potencia unidad. En esta categoría se incluyen cargadores de VE modo-2 y micro-fotovoltaica.
- Las características del Tipo 2 son similares al Tipo 1, sin embargo, estos equipos añaden un enlace de comunicaciones con un elemento externo que les permite realizar tareas de gestión de la demanda. Un ejemplo típico son las grandes estaciones de carga de VE que incluyen sistemas de gestión de la demanda.

## 8. DISCUSIÓN

---

- Los dispositivos Tipo 3 añaden algunas herramientas para el soporte a la red, añadiendo la posibilidad de regular la potencia activa y reactiva, para proveer servicios auxiliares a la red. En este grupo se contemplan los cargadores de VE bidireccionales y las grandes plantas de generación eólica y fotovoltaica.
- El Tipo 4 introduce, en comparación con el Tipo 3, la posibilidad de controlar independientemente las consignas de potencia activa y reactiva en cada una de sus fases, añadiendo la posibilidad de proveer soporte a la red en escenarios desequilibrados.

De los dispositivos descritos anteriormente, los Tipo 2, pero especialmente los Tipo 3 y 4, permiten la implementación de funcionalidades avanzadas con el objetivo de proveer nuevos servicios que serán importantes para el control y regulación de redes urbanas con una gran penetración de DERs. Entre estas funcionalidades se destacan el despeje de distorsiones de tensión y frecuencia, la limitación de potencia activa y *slew rate*, emulación de curvas de generador síncrono, regulación de tensión por medio de curvas V-Q, implementación de técnicas anti-isla, respuesta frente a huecos de tensión, *black-start* y el funcionamiento en modo aislado.

A continuación, el artículo analiza los requisitos indispensables que los materiales semiconductores deben satisfacer en las que se han detectado como las aplicaciones más importantes de los DERs en las ciudades inteligentes: micro generación FV, cargadores de VE, BESS y direccionadores de energía y FACTS de distribución. Del estudio realizado se destacan los siguientes:

- Tensiones de ruptura superiores a 1200 V.
- El tamaño de los semiconductores no es relevante respecto a otros componentes como elementos pasivos y componentes necesarios para la disipación térmica.
- Altas frecuencias de conmutación para minimizar el tamaño de los pasivos y evitar frecuencias audibles.
- Alta temperatura de funcionamiento y buena disipación térmica.
- Bajas pérdidas de conducción y conmutación.
- Cumplimiento de requisitos Compatibilidad Electro-Magnética (EMC) e Interferencia Electro-Magnética (EMI).

- Debe permitir su fabricación a gran escala, requiriendo materias prima asequibles y procesos de fabricación industrializables.

El silicio es una tecnología madura que ha estado presente en aplicaciones de electrónica de potencia desde la década de 1950, sin embargo, este material está alcanzando sus límites teóricos en aplicaciones de potencia. En la actualidad, las principales limitaciones de los semiconductores basados en silicio radica en sus altas pérdidas, baja frecuencia de conmutación y pobres propiedades térmicas.

Mientras que sí es posible conseguir frecuencias de conmutación elevadas con semiconductores unipolares basados en silicio, estos ofrecen unas características de tensión y corriente demasiado pobres. En el otro extremo se encuentran los dispositivos bipolares, que sí alcanzan tensiones y corrientes, y por lo tanto potencias, más elevadas; sin embargo operan a frecuencias máximas de pocas decenas de kilohercios, resultando los elementos pasivos necesarios demasiado voluminosos para el tipo de aplicaciones estudiadas.

Entre los principales materiales WBG que prometen superar las limitaciones del silicio (Si) se encuentran el carburo de silicio (SiC), nitruro de galio (GaN), diamante, óxido de galio ( $\text{Ga}_2\text{O}_3$ ), algunos compuestos derivados del nitruro de aluminio (AlN), nitruro de boro (BN) y el óxido de zinc (ZnO). A continuación se realiza una breve descripción de cada uno de estos materiales; a su vez, la Tabla 8.2 muestra un resumen de las características más importantes de los mismos:

- **SiC:** Desde 1987 el SiC ha experimentado un gran desarrollo, convirtiéndose en el más maduro de todos los materiales WBG. Es un compuesto cristalino con más de 170 politipos diferentes, resultando el 2H-SiC el más interesante para aplicaciones de electrónica de potencia. Este material ofrece una tensión de ruptura diez veces mayor que el Si, útil en aplicaciones de alta potencia y temperaturas (hasta 350 °C). Además, el silicio es el segundo material más abundante en la corteza terrestre, por lo que no se prevé una falta de suministro a diferencia de otros materiales WBG.

En la actualidad, se disponen de obleas de comerciales de SiC de hasta 200 mm. Desde 1993 este material se ha empleado para una gran variedad de dispositivos de potencia: U-MOSFETs, D-MOSFETs, JFETs, diodos PIN, etc.

## 8. DISCUSIÓN

---

Hoy en día, los MOSFETs basados en SiC se han convertido en el dispositivo más empleado a escala industrial, con módulos de 1200 V y 1700 V, y un amplio rango de corrientes, disponibles por la mayoría de fabricantes.

- **GaN:** Este material ha sido empleado en diodos LED y equipos de radio durante décadas y, desde el año 2000, se ha convertido en una opción interesante para aplicaciones de potencia. El ancho de la banda de valencia del GaN es ligeramente superior a la del SiC, y ambos tienen una tensión de ruptura similar. Sin embargo, su principal ventaja es la elevada movilidad de los electrones que este material presenta, permitiendo frecuencias de conmutación mucho más elevadas que el SiC. Por el contrario, su baja conductividad térmica, similar a la del Si, pueden suponer un inconveniente para aplicaciones de potencia.

Actualmente, las características de los dispositivos de GaN están limitadas a 650 V y 150 A en la mayoría de fabricantes, y se está trabajando en el desarrollo de módulos de hasta 1200 V. El principal obstáculo para obtener dispositivos de más tensión es debida a la dificultad de obtener estructuras verticales y la falta de disponibilidad de obleas de alta calidad.

- **Diamante:** Esta forma alotrópica del carbono es conocida por ser un material excepcional en muchos aspectos y, del mismo modo, también presenta unas propiedades como semiconductor superiores a la mayor parte de los materiales. Debido a su alta tensión de ruptura, alta conductividad térmica, alta movilidad de sus electrones y su baja constante dieléctrica, se espera que los semiconductores basados en diamante reduzcan considerablemente tanto las pérdidas de conducción como de conmutación en aplicaciones de alta potencia y temperatura. Sin embargo, las investigaciones llevadas a cabo en este material como semiconductor desde la década de 1980 hasta la actualidad han obtenido pobres resultados debido a la dificultad de sintetizar diamantes de alta calidad.

En consecuencia, no se esperan unidades de diamante disponibles en el mercado a corto ni medio plazo. Aun así, se ha logrado demostrar a nivel de laboratorio transistores de 1 kV con densidades de corriente superiores a 500 A/cm<sup>2</sup>; y hay proyectos en curso para desarrollar los primeros MOSFETs de 6,5 kV, 10 kV y 20 kV.

- **Ga<sub>2</sub>O<sub>3</sub>**: Pese a que el Ga<sub>2</sub>O<sub>3</sub> ha sido reportado desde 1952, y usado como material aislante desde la década de 1970, ha sido en la última década cuando se han intensificado las investigaciones en este material como semiconductor. El Ga<sub>2</sub>O<sub>3</sub> tiene cinco politipos diferentes siendo el β-Ga<sub>2</sub>O<sub>3</sub> el más interesante para aplicaciones de electrónica de potencia. Presenta un ancho de banda y una tensión de ruptura superior a SiC y GaN, ofreciendo una potencial mejora sobre las características de estos materiales en aplicaciones de alta tensión y alta potencia. La facilidad para trabajar este material permite crear grandes estructuras monocristalinas y se han demostrado obleas de hasta 6 pulgadas. Sin embargo, los mayores inconvenientes de este material son su baja conductividad térmica y la falta de dopantes positivos, que hacen que se mantenga como una tecnología menos madura que SiC y GaN.  
Pese a que no es posible encontrar dispositivos de Ga<sub>2</sub>O<sub>3</sub> en el mercado, la disponibilidad de sustratos de alta calidad ha permitido demostrar MOSFETs de hasta 8,03 kV recientemente.
- **AlN**: El AlN se comenzó a estudiar en 1980 como material semiconductor, y ofrece un ancho de banda superior que el diamante, una alta estabilidad y conductividad térmica, y una gran tensión de ruptura de 12 MV/cm, que lo hacen una opción muy atractiva para aplicaciones de potencia. La aleación AlGaN ofrece unas propiedades excepcionales, combinando las ventajas de GaN y AlN. Sin embargo, los altos costes de fabricación debidos a la dificultad de procesar este material ha sido un importante limitante en el desarrollo de este material como semiconductor.
- **BN**: En su estructura cúbica presenta un elevado ancho de banda y se prevé una tensión de ruptura de 15 MV/cm, y una altísima conductividad térmica. Pese a que promete propiedades superiores incluso a las del diamante, la dificultad de desarrollo de sustratos de BN hacen que apenas se hayan reportado resultados como material semiconductor hasta la fecha.
- **ZnO**: Sus propiedades como semiconductor fueron ampliamente estudiadas durante las décadas de los 50 y 60. El ZnO presenta un gran ancho de banda, alto punto de fusión, baja expansión térmica y alta movilidad de sus electrones. Sin embargo, las dificultades en el dopado del material y en la generación de sustratos hace que las aplicaciones de este material queden limi-

## 8. DISCUSIÓN

tadas a fotónica, optoelectrónica, LED ultravioleta, sensores, piezoeléctricos y células solares.

**Tabla 8.2:** Principales características de los diferentes materiales semiconductores [30, 31, 32]: ancho de banda ( $E_g$ ), constante dieléctrica ( $\epsilon_r$ ), movilidad de los portadores ( $\mu_n$ ), tensión de ruptura ( $E_C$ ), velocidad de saturación ( $v_{sat}$ ), Conductividad térmica ( $\lambda$ ) y máxima temperatura de funcionamiento ( $T_{max}$ )

	Si	SiC	GaN	Ga <sub>2</sub> O <sub>3</sub>	AlN	Diamond
$E_g$ (eV)	1,12	3,26	3,49	4,9	6,2	5,0
$\epsilon_r$ (-)	11,7	9,7	9,0	10,0	8,5	5,7
$\mu_n$ (cm <sup>2</sup> /Vs)	1480	1000	1200	200	300	2800
$E_C$ (MV/cm)	0,3	3,18	3,0	8,0	12,0	5,7
$v_{sat}$ (10 <sup>7</sup> cm/s)	2,3	2,2	1,5	2,0	1,7	2,7
$\lambda$ (W/(cmK))	1,48	4,5	1,3	0,27	2,85	20,0
$T_{max}$ (°C)	175	600	400	600	250	700

Las “figuras de mérito” son una herramienta empleada en diferentes ámbitos del conocimiento. Una figura de mérito es una expresión numérica tomada como representativa del desempeño de un sistema o dispositivo. En ocasiones, las características que resultan de interés en los dispositivos semiconductores no son directamente medibles en el propio material, pero pueden ser estimadas a través de otras que sí lo son.

Las primeras figuras de mérito aplicadas al campo de los semiconductores fueron publicadas en la década de 1960. En este estudio se ha hecho una revisión de las figuras de mérito más importantes presentes en la literatura aplicadas a los materiales WBG, resultando en los resultados reflejados en la Tabla 8.3. En la tabla, se han añadido dos filas para cuantificar dos parámetros clave: la disponibilidad del material y el coste de fabricación de los semiconductores. A continuación, se muestra una breve descripción de las figuras de mérito empleadas:

- **Johnson’s Figure of Merit (JFOM):** Define el producto potencia-frecuencia y es comúnmente usada para determinar la capacidad de conmutar potencia a frecuencias elevadas.

- **Keyes' Figure of Merit (KFOM):** Predice las limitaciones térmicas del transistor.
- **Baliga's Figure of Merit (BFOM):** Define las pérdidas de conducción en dispositivos unipolares, asumiendo que estas están dominadas por el flujo de corriente a través de la resistencia entre drenador y fuente.
- **Baliga's High Frequency Figure of Merit (BHFFOM):** Su cálculo depende de las propiedades de cada dispositivo y no del material en sí mismo, por lo que no puede ser empleada en este estudio.
- **Huang's Material Figure of Merit (HMFOM):** Determina el mejor material para aplicaciones de alta frecuencia. Puede considerarse una simplificación de BHFFOM donde el término dependiente del dispositivo se ha omitido.
- **Huang's Chip Area Figure of Merit (HCAFOM):** Determina los materiales que posibilitan un menor tamaño del semiconductor.
- **Huang's Termal Figure of Merit (HTFOM):** Del mismo modo que KFOM, define la máxima temperatura de trabajo. En ella se presta especial atención a que los materiales con una elevada tensión de ruptura pueden ser embebidos en dispositivos más pequeños y, por consiguiente, con una menor superficie de disipación.

**Tabla 8.3:** Comparación de las figuras de mérito seleccionadas de los diferentes materiales semiconductores (normalizadas frente al Si).

	Si	SiC	GaN	Ga <sub>2</sub> O <sub>3</sub>	AlN	Diamond
JFOM	1	10,1	6,5	23,2	29,6	22,3
KFOM	1	3,3	0,8	0,2	1,9	21,0
BFOM	1	13,8	18,9	9,7	25,0	82,0
HMFOM	1	8,7	9,0	9,8	18,0	26,1
HCAFOM	1	76,6	69,3	223,4	523,3	241,9
HTFOM	1	0,35	0,11	0,01	0,07	1,46
Disponibilidad	5	4	2	2	2	1
Fabricación	5	4	3	2	1	1

## 8. DISCUSIÓN

---

A continuación, el artículo realiza una comparación entre los materiales WBG de acuerdo a los criterios descritos a continuación:

1. Se descartan los materiales que no presentan la viabilidad de estar disponibles en el mercado en un corto-medio plazo.
2. Se descartan los semiconductores que no disponen de la capacidad para soportar las tensiones requeridas en la aplicación estudiada.
3. Propiedades que mejoran las características de los convertidores de potencia actuales en base a tres factores:
  - a) Propiedades eléctricas.
  - b) Propiedades térmicas.
  - c) Disponibilidad del material y coste de fabricación.

En base al primer criterio, el AlN y el diamante han sido descartados por encontrarse lejos de alcanzar la viabilidad técnica y económica para ser producidos en masa. De acuerdo al segundo criterio, todos los materiales alcanzan una tensión de ruptura suficiente para las aplicaciones necesarias en *Smart Grids*. A continuación, para evaluar las propiedades de los materiales, la Figura 8.4 compara las propiedades destacadas en el criterio 3: la frecuencia de conmutación (JFOM y HMFOM); las propiedades térmicas, por medio de la disipación térmica (KFOM) y la temperatura máxima de funcionamiento ( $T_{max}$ ); y la viabilidad de los dispositivos en el mercado, a través de la disponibilidad de obleas de calidad (Availability) y una estimación de los costes de producción de dispositivos (Manufacturing).

De la Tabla 8.3 y la Figura 8.4 se puede concluir que, como las figuras JFOM y HMFOM destacan, el  $Ga_2O_3$  presenta las mejores propiedades eléctricas, con lo que cabe esperar que se consiga una mayor tensión de ruptura y velocidad de conmutación. Además, presenta una alta temperatura de funcionamiento, similar a la del SiC. Por el contrario, debido a su pobre conductividad térmica, podría no ser viable para usarse en muchas de las aplicaciones estudiadas. Sin embargo, debido a que los convertidores que operan en conmutación blanda reducen drásticamente las pérdidas en los semiconductores, estas aplicaciones podrían verse beneficiadas de las altas frecuencias de conmutación y altas tensiones de bloqueo que proporciona este material.

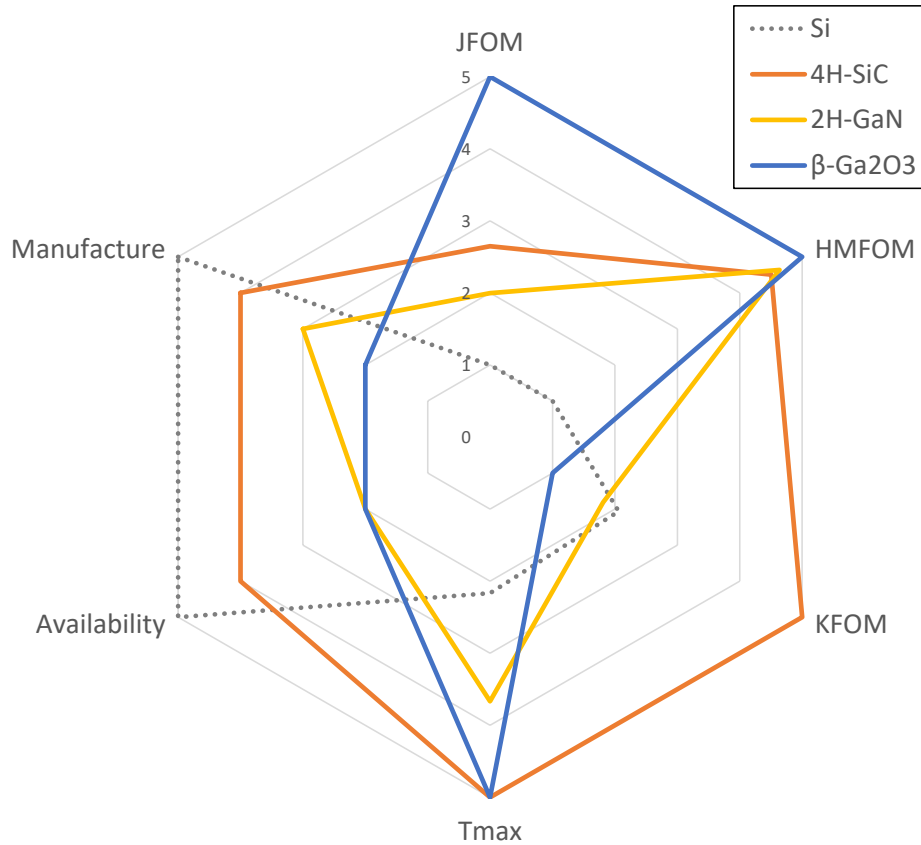


**Figura 8.4:** Comparación de las propiedades más importantes de los materiales semiconductores para aplicaciones en *Smart Grids*. Los valores han sido escalados asignando 1 al peor material y 5 al mejor.

Los convertidores de electrónica de potencia en *Smart Grids* requieren altas frecuencias de conmutación, pero también potencias medias y altas. A pesar de que el GaN es conocido por su alta frecuencia de conmutación, su capacidad de corte es relativamente baja. Por contra, el SiC presenta una conductividad térmica tres veces más grande que el Si y el GaN, y hasta 16 veces más que el Ga<sub>2</sub>O<sub>3</sub>. Además, el SiC presenta unas propiedades eléctricas muy superiores a las del Si y similares a las del GaN. Estas características, unidas al hecho de que es un material abundante en la naturaleza, harán de los dispositivos basados en SiC adecuados para la mayoría de equipos en estas aplicaciones.

## 8. DISCUSIÓN

---

### 8.3 Estudios 3 y 4

El rápido despliegue de energías renovables, para reemplazar las centrales de combustión, está favoreciendo el cambio de un modelo energético centralizado hacia un modelo distribuido, donde la red de distribución está tomando un papel cada vez más importante. Además, la creciente importancia de la red de distribución se está viendo incrementada por cambios en los hábitos de consumo de la población, típicamente conectada a la red de baja tensión. La sustitución de las calefacciones de gas y gasoil por sistemas de climatización eléctricos y los vehículos de combustión por otros propulsados por baterías, junto con la creciente rentabilidad de las pequeñas instalaciones fotovoltaicas, está evidenciando un cambio en el consumo energético.

Además, en la red de distribución de baja tensión coexisten cargas monofásicas y trifásicas, alimentadas por una red de tres fases y cuatro hilos, y comúnmente conectadas a la red de media tensión a través de un transformador de distribución con una configuración triángulo-estrella.

Si el consumo en cada una de las fases en la red es diferente se genera una situación de desequilibrio, que puede ocasionar una amplia variedad de problemas que pueden poner en compromiso la estabilidad de la red: sobrecargas del cable de neutro, calentamiento del transformador de distribución y disminución de la eficiencia, entre otros.

Tomando como punto de partida las topologías más comunes analizadas en el **Estudio 1**, los **Estudio 3 y 4** proponen introducir ligeras modificaciones sobre ellas, con el objetivo de facilitar la implementación de servicios auxiliares en este tipo de convertidores de potencia.

Los STATCOMs son equipos usados habitualmente para la regulación de tensión en la red de transporte. Estos no disponen ninguna clase de almacenamiento, generación o consumo, por lo que no son capaces de realizar un intercambio energético neto con la red. En la actualidad, los STATCOMs se conectan de una forma trifásica a la red, pues en la red de transporte no se dispone de cable de neutro, como se muestra en la Figura 8.5.

La falta de conexión del cable de neutro impide el retorno de las corrientes a través de este conductor. Este hecho impide la inyección de corrientes de secuencia

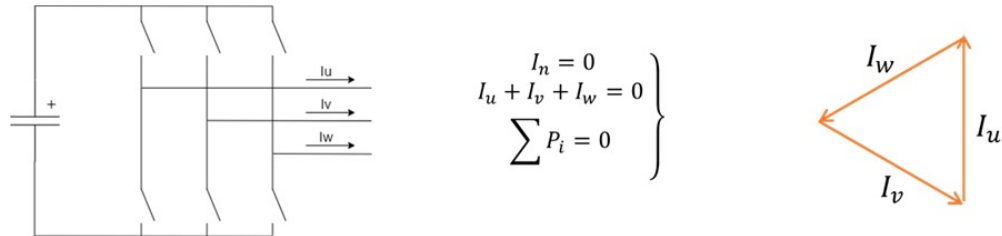


**Figura 8.5:** Descripción de las limitaciones de funcionamiento de un STATCOM de 3 ramas.

homopolar, con lo que solo las componentes de secuencia directa e inversa son soportadas por estas configuraciones. Asumiendo una red perfecta de tensiones sinusoidales desfasadas 120 °, la componente directa de la corriente en fase con la tensión determina la potencia activa transferida por el sistema, mientras que la componente en cuadratura se corresponde con la parte reactiva de la potencia. Dado que el STATCOM no dispone de ningún elemento que pueda absorber o inyectar potencia activa, las corrientes que puede manejar este tipo de convertidores quedan limitadas a la componente en cuadratura de la secuencia directa y a la secuencia inversa.

Por el contrario, la red de distribución de baja tensión sí que dispone de un neutro físico que permite la adición de una cuarta rama al convertidor. Este conductor proporciona un camino de retorno a las corrientes desequilibradas, como puede apreciarse en la Figura 8.6.

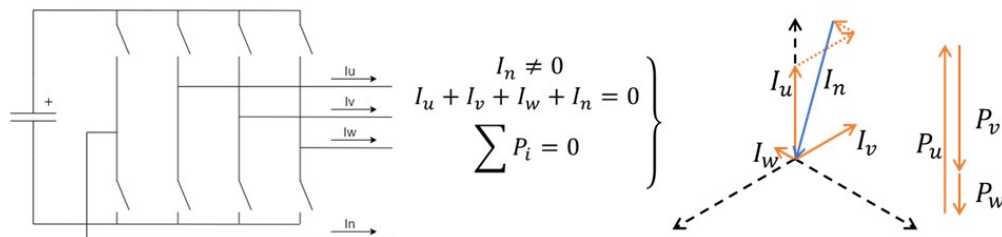


**Figura 8.6:** Descripción del funcionamiento de un D-STATCOM de 4 ramas.

Esta ligera modificación permite el manejo de corrientes homopolares, que añaden una gran flexibilidad. Puede demostrarse que si el fasor de la corriente homopolar es exactamente el conjugado de la corriente de secuencia inversa respecto a la tensión, las potencias monofásicas resultantes están compuestas exclusiva-

## 8. DISCUSIÓN

mente de componente activa, positiva en una o dos fases y negativa en las restantes, resultando en una potencia total nula. Este hecho se traduce en un trasvase efectivo de potencia entre las diferentes fases de la red.

La posibilidad de realizar un control totalmente independiente de la potencia en cada una de las fases posibilita, mediante la conexión en paralelo a la línea de un D-STATCOM con conexión a neutro, la compensación de los desequilibrios presentes en la red. De esta forma, el balanceo de las fases permite que, aguas arriba, la corriente en cada una de las fases sea idéntica y la corriente en el conductor de neutro sea totalmente eliminada, tal y como se muestra en la Figura 8.7.

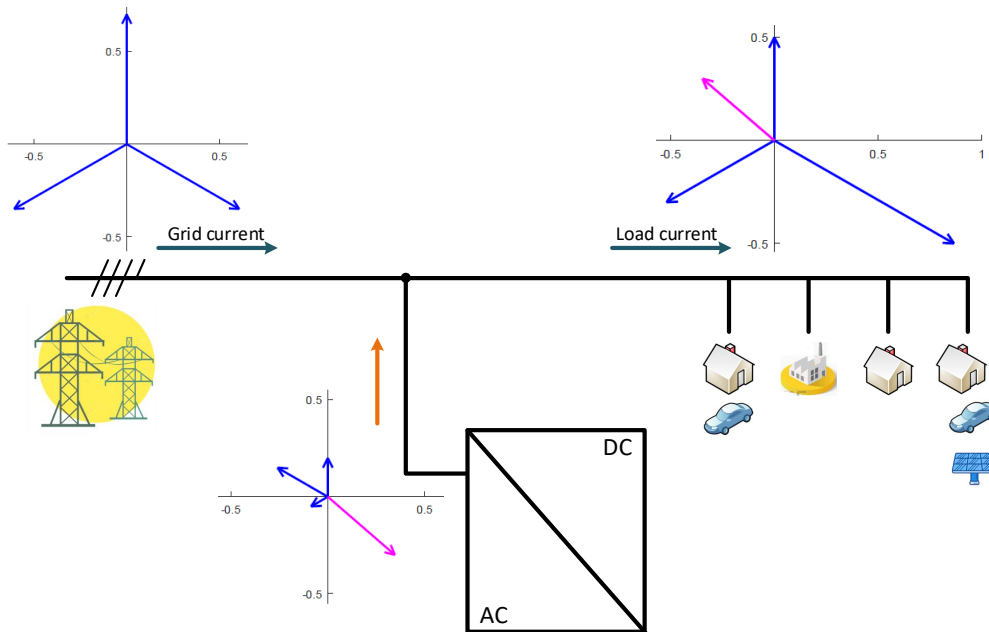


**Figura 8.7:** Esquema de conexión del D-STATCOM propuesto para la compensación de desequilibrios de corriente en la red. Los fasores de las tensiones de fase se representan en azul y el de la corriente de neutro en rosa.

Para demostrar la capacidad de recirculación de potencia entre fases, mediante la introducción de un equipo de electrónica de potencia, se ha diseñado de un prototipo de D-STATCOM de una potencia nominal trifásica de 30 kVA, el cual se muestra en la Figura 8.8. El convertidor emplea una topología NPC tipo-I basada en módulos IGBT de silicio que conmutan a una frecuencia de 20 kHz, haciendo su funcionamiento completamente inaudible. La conexión del convertidor a la red

se realiza a través de un filtro de segundo orden con una configuración LCL amortiguado de forma pasiva para atenuar el comportamiento resonante del mismo.

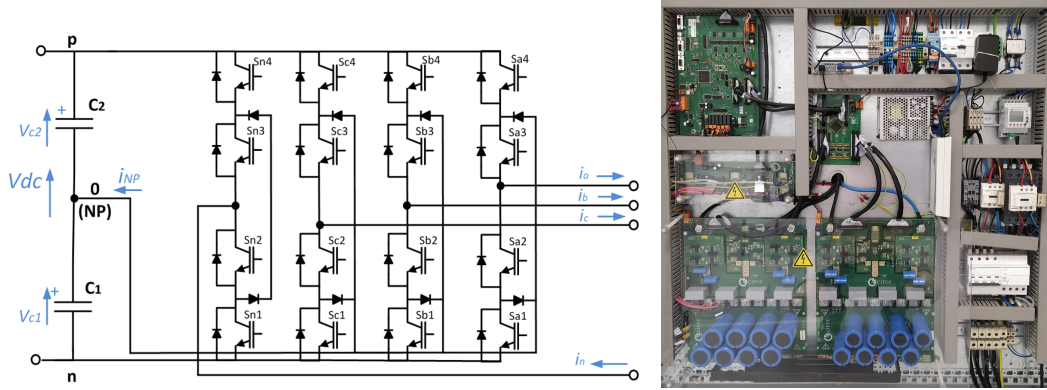


**Figura 8.8:** Topología NPC tipo-I con cuatro ramas empleada en el prototipo (izquierda) y disposición de la electrónica de potencia instalada en el interior de la envoltura.

La Figura 8.9 muestra el esquema de control implementado en el prototipo de D-STATCOM para la realización del equilibrado de la red. En primer lugar, se necesita determinar las consignas de potencia activa y reactiva necesarias para equilibrar la línea. Para ello se calcula la potencia activa y reactiva en la red ( $P_i^{down}$ ,  $Q_i^{down}$ ), a partir de los valores de tensión y corriente ( $V_i^{down}$ ,  $I_i^{down}$ ) medidos en cada una de las fases de la línea ( $i = a, b, c$ ):

$$\left. \begin{aligned} P_i^{down} &= Re\{\bar{V}_i^{down} \cdot \bar{I}_i^{down*}\} \\ Q_i^{down} &= Im\{\bar{V}_i^{down} \cdot \bar{I}_i^{down*}\} \end{aligned} \right\}$$

De ambas componentes únicamente la potencia activa contribuye a la transmisión de potencia, de forma que eliminando la componente reactiva de la corriente se eliminarán las pérdidas por conducción que esta ocasiona. Por otro lado, las pérdidas por conducción son proporcionales al cuadrado de la corriente que circula por el cable. De esta forma, la manera más eficiente de transportar potencia a través de la línea es que esta circule igualmente distribuida entre las tres fases de la red, descendiendo esta eficiencia cuanto mayor sea el desequilibrio. Por consiguiente, la potencia deseada aguas arriba del D-STATCOM ( $P_i^{up}$ ,  $Q_i^{up}$ ) se determina de acuerdo a la siguiente expresión:

## 8. DISCUSIÓN

$$\left. \begin{aligned} P_i^{up} = \bar{P} = \frac{\sum P_i^{down}}{3} \\ Q_i^{up} = 0 \end{aligned} \right\}$$

Así, la consigna de potencia a inyectar por el D-STATCOM puede ser calculada como la diferencia de la corriente aguas abajo y aguas arriba del equipo:

$$\left. \begin{aligned} P_i^{STAT} = P_i^{down} - P_i^{up} = P_i^{down} - \bar{P} \\ Q_i^{STAT} = Q_i^{down} - Q_i^{up} = Q_i^{down} \end{aligned} \right\}$$

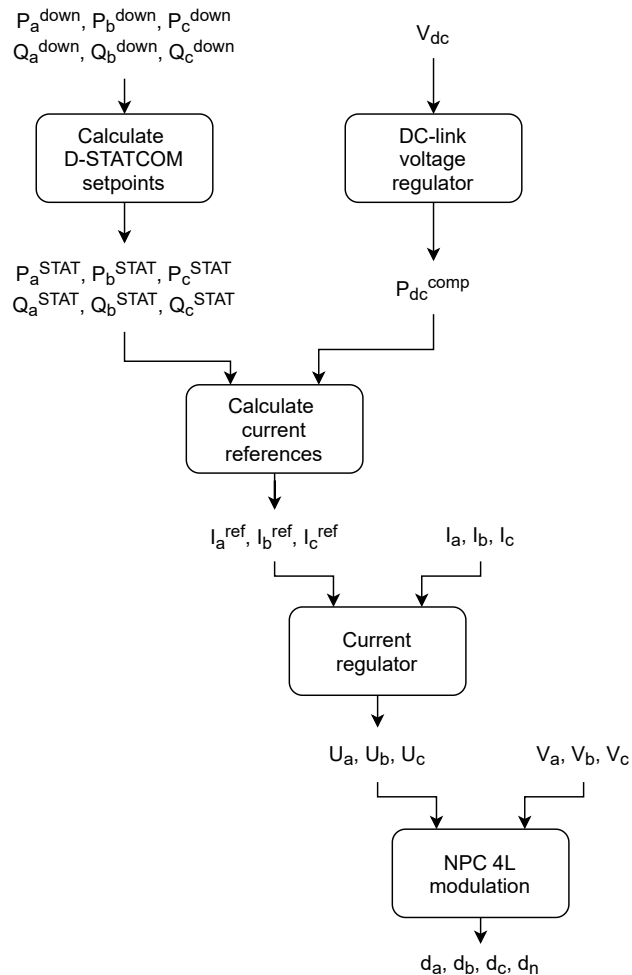


**Figura 8.9:** Diagrama de control del prototipo de D-STATCOM.

Además, la tensión del bus de continua ( $V_{dc}$ ) es regulada por el propio D-STATCOM sin la necesidad de ninguna fuente de tensión externa, para lo cual un

controlador PI estima la potencia requerida para mantener esta tensión constante ( $P_{dc}^{comp}$ ). A continuación, se aplica un filtro SOGI para obtener las componentes instantáneas directa y en cuadratura de la tensión de cada una de las fases de la red, que son empleadas para la determinación de las referencias de corriente ( $I_i^{ref}$ ) a partir de las consignas de potencia activa y reactiva. Después, a partir del error de corriente, calculado como la diferencia entre la referencia de corriente instantánea y la medida de la corriente a la salida del equipo, determina la tensión que debe ser aplicada por el convertidor ( $U_i$ ). Finalmente, se calcula el ciclo de trabajo de cada uno de los semiconductores ( $d_i$ ) mediante una técnica de modulación basada en onda portadora que, a su vez, se encarga del equilibrado de las tensiones de los dos semibuses de continua.

De manera previa a la instalación en campo, el funcionamiento del prototipo ha sido verificado a nivel experimental a nivel de laboratorio. En la Figura 8.10 puede observar el funcionamiento del equipo en un punto de operación desequilibrado. La imagen muestra la inyección de corriente a la red por la fase a, mientras esta potencia es tomada de la fase c.

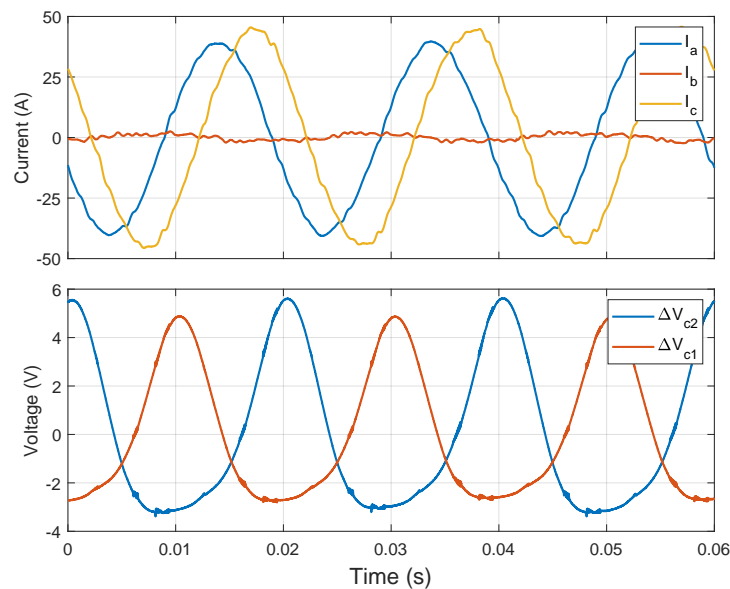


**Figura 8.10:** Captura de osciloscopio del funcionamiento del prototipo de manera desequilibrada. Se muestran las tres corrientes de red (arriba) y la componente oscilante de ambas tensiones de semibus (abajo).

## 8. DISCUSIÓN

---

En la parte inferior de la imagen se muestran las tensiones de ambos semibus de condensadores. Estos muestran un comportamiento oscilante debido a dos factores principalmente, a la componente oscilante de 100 Hz en la potencia introducido por la corriente de secuencia inversa, y a la incapacidad de la modulación empleada de controlar completamente la corriente introducida al punto medio de los condensadores a través de los diodos de *clamping*. Posteriormente, se ha medido la eficiencia del prototipo a diferentes factores de carga, cuyos resultados se reflejan en la Tabla 8.4, registrando una eficiencia de acuerdo a la California Energy Commission (CEC) del 97,7 %.

**Tabla 8.4:** Pérdidas y eficiencia del prototipo de D-STATCOM en función de la potencia de salida del convertidor.

Carga (%)	Potencia (kVA)	Pérdidas (W)	Eficiencia (%)
5	1,96	174	91,1
10	3,56	170	95,2
20	7,03	187	97,3
30	10,54	250	97,6
50	17,54	370	97,8
60	21,03	450	97,8
75	26,28	580	97,7
90	31,53	730	97,6
100	34,68	810	97,6

Para la obtención de resultados de la operación real del equipo en campo, el equipo ha sido instalado en un área residencial de la red de distribución en la ciudad de Málaga. La Figura 8.11 muestra el diagrama unifilar de la red en la que el prototipo ha sido instalado, donde pueden observarse las ocho líneas que parten de este centro de transformación. Al final de la línea F8, sección marcada en rojo en la imagen, existe una alta concentración de cargas monofásicas conectadas a la misma fase, las cuales ocasionan frecuentes desequilibrios en la línea. Esta localización ha sido escogida para la instalación del prototipo, tratando de compensar los desequilibrios en el punto más cercano a su origen.

Con el objetivo de obtener una muestra de datos significativa para el estudio, se ha analizado el funcionamiento del convertidor durante un periodo de tiempo

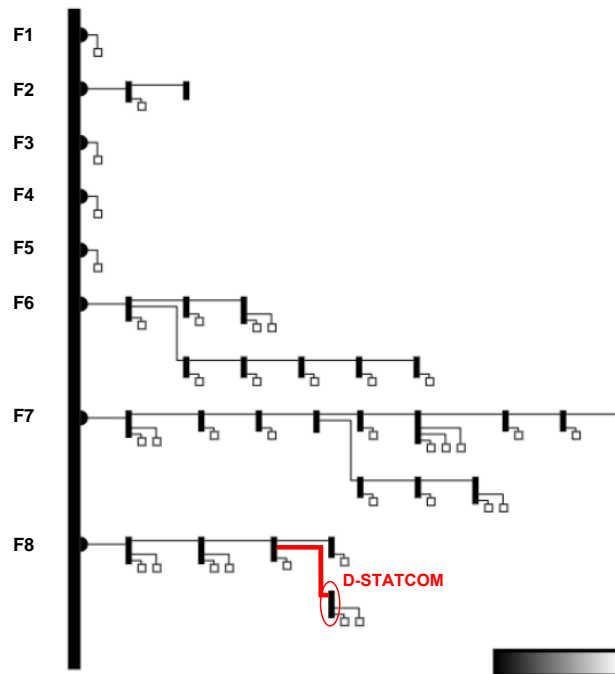


**Figura 8.11:** Esquema eléctrico de la red donde se ha instalado el prototipo, destacando la ubicación exacta del D-STATCOM.

de un mes, el mes de febrero de 2021. Durante la realización del estudio se ha realizado la monitorización de las tensiones y corrientes eficaces, así como de la potencia activa y reactiva, tanto aguas abajo del D-STATCOM como aguas arriba del mismo, donde se observarán los efectos de este. Estas medidas se han realizado con una granularidad de 2 segundos y han sido enviadas a un servidor para su posterior procesado.

El primero de los parámetros estudiados es el factor de desequilibrio de corriente (CUF), dado que está directamente relacionado con la operación del D-STATCOM. La Figura 8.12 muestra a la izquierda los percentiles 25, 50, 75 y 95 de los valores del CUF para cada uno de los días analizados aguas abajo (naranja) y aguas arriba (azul) del D-STATCOM. En ella puede apreciarse una notable reducción del área sombreada (rango entre los percentiles 25 y 75) del 15 % – 30 % aguas abajo del equipo a un 0 % – 2,5 % aguas arriba. Igualmente, el CUF máximo se ha reducido de un 45 % aguas abajo a menos del 10 % aguas arriba, y el valor mediano ha caído del 21,9 % al 0,9 %.

## 8. DISCUSIÓN

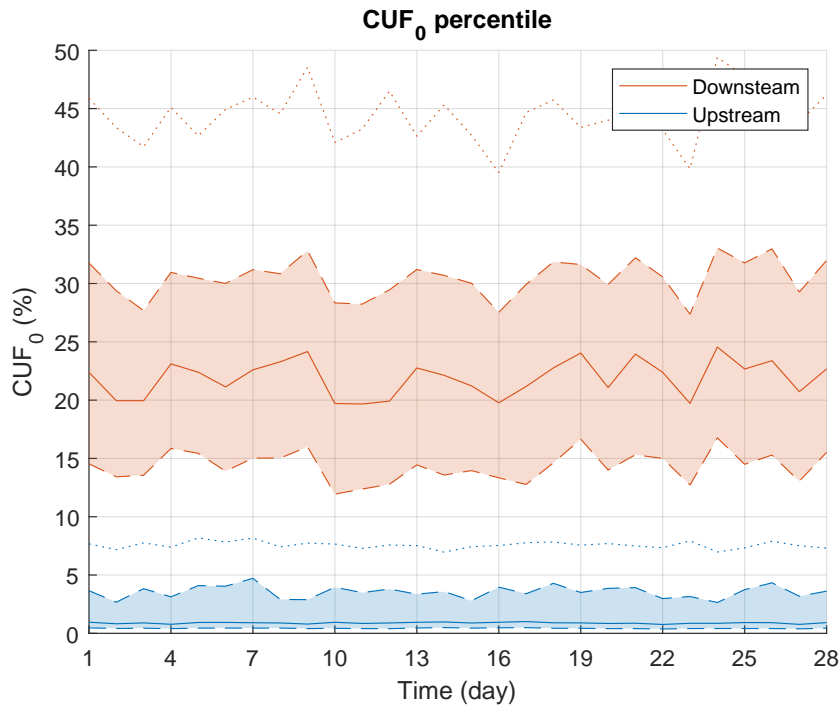


**Figura 8.12:** Percentiles 25, 50, 75 y 95 del CUF aguas abajo (naranja) y aguas arriba (azul) del prototipo.

Del mismo modo, a la derecha de la Figura 8.13 se muestran los mismo percentiles para la corriente circulante a través del conductor de neutro. En ella, el área sombreada ha disminuido del rango 5 A – 15 A a 0 A – 2,5 A. Además, los picos de corriente a través de este cable han pasado de un máximo de 25 A a menos de 10 A. Así, se ha conseguido prácticamente eliminar la corriente de neutro, pasando de un valor medio de 10,3 A a 0,4 A.

IEEE define el factor de potencia efectivo ( $PF_e$ ) como un parámetro representativo de la eficiencia de un sistema eléctrico. Para ello define la potencia aparente efectiva ( $S_e$ ) asumiendo un sistema trifásico balanceado con exactamente las mismas pérdidas en la línea que el sistema a estudiar. Esta equivalencia conduce a la definición de la corriente efectiva ( $I_e$ ) como

$$3rI_e^2 = r(I_a^2 + I_b^2 + I_c^2 + \rho I_n^2)$$

donde  $r$  es la resistencia de la línea y  $\rho$  el ratio entre la resistencia del cable de

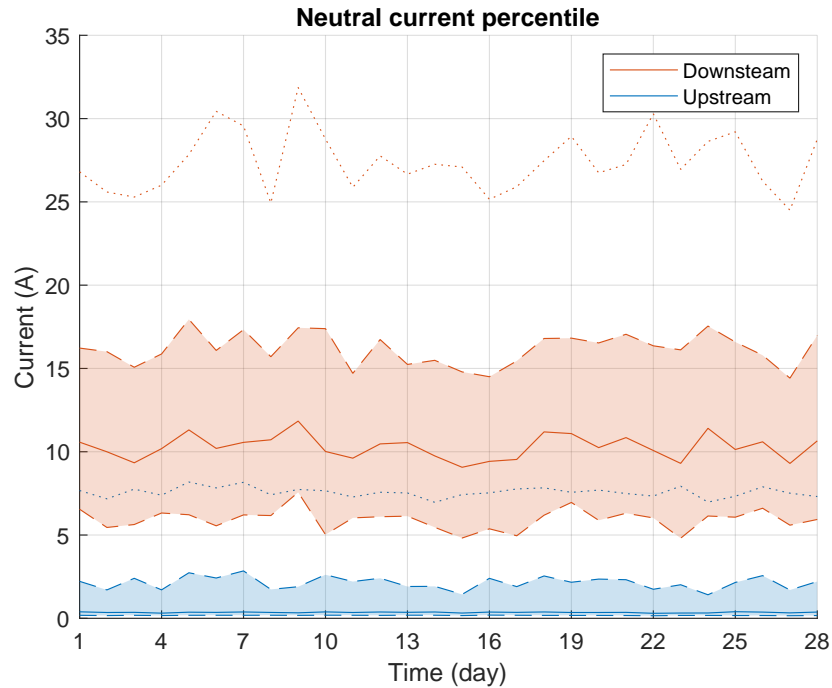


**Figura 8.13:** Percentiles 25, 50, 75 y 95 de la corriente de neutro aguas abajo (naranja) y aguas arriba (azul) del prototipo.

neutro y los de fase. Además, define la tensión efectiva ( $V_e$ ) de forma que la  $S_e$  puede calcularse de la misma forma que en una línea equilibrada

$$S_e = 3V_e I_e \quad ((1))$$

conduciendo a la definición del factor de potencia efectivo como

$$PF_e = \frac{P}{S_e} \quad ((2))$$

Además, estas expresiones tienen en cuenta armónicos generados por cargas no lineales. Esta aproximación ha sido empleada para calcular el  $PF_e$  durante el periodo de tiempo analizado, de forma que la Figura 8.14 muestra la media diaria del  $PF_e$  aguas abajo y aguas arriba. Durante los 28 días de funcionamiento del prototipo, el  $PF_e$  medio ha pasado del 0,901 al 0,967, lo que se traduce en una reducción de las pérdidas técnicas en el tramo afectado de la línea del 13 %.

## 8. DISCUSIÓN

---

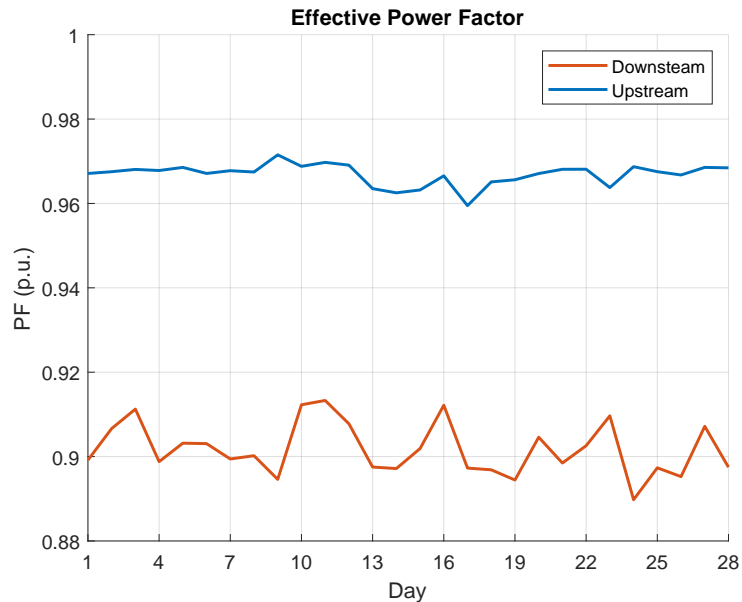


**Figura 8.14:** Factor de potencia medio diario aguas abajo (naranja) y aguas arriba (azul).

El factor de desequilibrio de tensión (VUF) es un parámetro clave regulado por la legislación actual. Puesto que, a diferencia de la corriente, la función que relaciona la tensión y la posición en la línea es continua, resulta imposible analizar las variaciones en el VUF aguas arriba y aguas abajo como se ha hecho con el resto de los parámetros estudiados. Por este motivo, se han estudiado las medidas de tensión de un medidor inteligente cercano al D-STATCOM y en la transformación de distribución, en la cabecera de la línea; durante los meses de febrero de 2020, cuando el D-STATCOM no había sido instalado todavía, y febrero de 2021.

Así, las medidas de ambas localizaciones y fechas han sido estudiadas para analizar los efectos del prototipo en la línea. La Figura 8.15 muestra la probabilidad acumulada de encontrar el VUF por debajo de cada valor en el centro de transformación (izquierda) y en la ubicación en la que el D-STATCOM ha sido instalado. Por un lado, se puede observar que no existen diferencias significativas en la cabecera de la línea entre ambos años. Sin embargo, en el área de influencia del dispositivo, puede apreciarse un sensible cambio de tendencia. Los resultados muestran un claro descenso en el tiempo en el que la red se encuentra desequilibrada. Esto es especialmente notable para desequilibrios de entorno al 0,5 %. Mientras

que en febrero de 2020 el valor del VUF se encontraba por debajo del 1 % aproximadamente el 75 % del tiempo, con el D-STATCOM en funcionamiento, este valor se incrementó al 97 %.

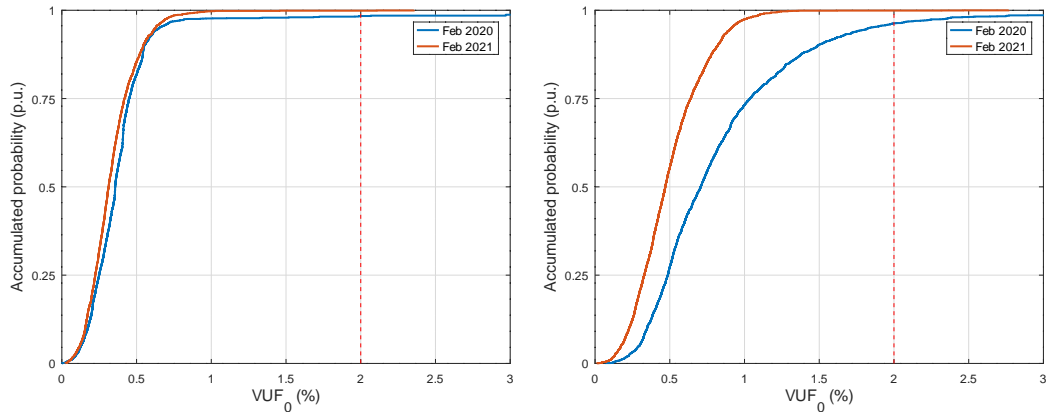


**Figura 8.15:** Comparación del VUF con D-STATCOM (febrero 2021) y sin D-STATCOM (febrero 2020), en el centro de transformación (izquierda) y en el punto de conexión del prototipo (derecha)

Estos resultados evidencian la utilidad de este tipo de dispositivos en redes de distribución largas con un alto número de consumidores monofásicos. El equilibrio de la línea permite la reducción de pérdidas técnicas y reducción de la sección de los conductores, así como una sensible mejora en la calidad de suministro.

## 8. DISCUSIÓN

---

### 8.4 Estudio 5

Históricamente, una gran proporción de la energía ha sido generada mediante la quema de combustibles fósiles. Este método de generación eléctrica es altamente controlable, haciendo posible igualar generación y demanda, y responder a cualquier diferencia entre ambos en la red. Dada la naturaleza intermitente de las fuentes de energía renovables, emparejar generación y demanda se vuelve una tarea mucho más compleja cuando las renovables constituyen una proporción significativa del mix energético. Por este motivo, los sistemas de almacenamiento energético jugarán un papel clave para aliviar este problema. Es un desafortunado hecho que, en la actualidad, una parte de la energía generada debe descartarse por ser producida en momentos de demanda baja, mientras que las energías renovables son insuficientes para cubrir la demanda total. Con los sistemas de almacenamiento adecuados integrados en la estructura de la red, se posibilitaría el almacenamiento del exceso de energía renovable generada en los momentos en que esta supera la demanda para su suministro durante picos de demanda. De este modo se lograría incrementar la controlabilidad y sostenibilidad de la red.

Hay muchas tecnologías de almacenamiento disponibles en la actualidad, y son varias las funcionalidades que ellas puede proporcionar, así como los inconvenientes que cada una de ellas presenta. Recientemente se ha propuesto un nuevo tipo de baterías de flujo ácido-base, para ayudar a la integración de energías renovables a un precio asequible y, además, evitando potenciales problemas medioambientales. Estas baterías usan como medio de almacenamiento tanques de agua fresca y agua salada a través de un proceso de electrodiálisis. Para ello, combinan membranas de intercambio de iones con membranas bipolares, de forma que, no se genera únicamente un gradiente de salinidad, sino un gradiente de pH también. Estas baterías pueden alcanzar una densidad energética de hasta  $7 \text{ kWh/m}^3$ , un valor significativamente superior al almacenamiento por bombeo. Por este motivo, es necesario estudiar los escenarios más competitivos para esta tecnología, antes de abordar su integración en la red.

La principal aportación de esta publicación a la tesis se encuentra en la sección 2 del artículo, donde se presentan tres casos de uso en los cuales esta tecnología de baterías puede ser aplicada con un buen compromiso entre funciona-

lidad y coste. En primer lugar, se realiza una comparación de todos los sistemas de almacenamiento energético disponibles en la actualidad. Para ello se comparan diferentes aspectos como escala de potencia a la que es aplicable cada tecnología, densidad energética y de potencia, eficiencia, costes de instalación y de operación, tiempo de vida e impacto ambiental.

Posteriormente, en esta publicación se realiza un análisis de diferentes casos de usos de inversores, particularizando para el caso de los interfaces de potencia para baterías de flujo. En este estudio se ha usado el modelo de arquitectura de *Smart Grid*, o SGAM, para definir los casos de uso donde estas baterías pueden resultar competitivas. En este artículo se analizan los 3 casos de uso siguientes:

1. **Almacenamiento energético para el pequeño comercio:** Combinado los sistemas de almacenamiento con pequeñas plantas fotovoltaicas, almacenaría energía durante las horas de máxima generación para emplearla cuando la producción cae. De este modo se lograría maximizar el autoconsumo, reduciendo su dependencia de la red y, por lo tanto, su factura eléctrica. A su vez, esto puede ser combinado con la participación en mercados energéticos locales con el objetivo de compartir los excedentes de energía, recibiendo un rendimiento económico adicional. En la mayoría de aplicaciones, como tiendas o pequeños edificios de oficinas, las necesidades de almacenamiento se sitúan en el orden de los 40 – 70 kWh, con potencias máximas de en torno a 5 kW.
2. **Gestión de congestiones y regulación de tensión en la red de Baja Tensión (BT):** En este caso, los sistemas de almacenamiento se instalarían en puntos débiles de la red de distribución, como líneas radiales largas, con el objetivo de añadir flexibilidad a la red, permitiendo una mayor penetración de energías renovables sin perjudicar la estabilidad del sistema. Estos sistemas permitirían contribuir a la reducción de congestiones en momentos de alta demanda, y proveer servicios auxiliares para la regulación de la tensión y frecuencia de la red. La capacidad necesaria en estas aplicaciones se situaría entre los 15 – 45 kWh con una potencia pico de 15 kW, permitiendo el soporte durante periodos de 1 a 3 horas, tiempo suficiente para que las sobrecargas desaparezcan.

## 8. DISCUSIÓN

---

### 3. **Grandes sistemas de almacenamiento para el soporte a la generación:**

Debido a la naturaleza intermitente de las energías renovables, las grandes centrales de almacenamiento permitirán una mayor generación renovable a través de la amortiguación de las variaciones estacionales en la producción energética. Esto es llevado a cabo por medio del almacenamiento de energía durante picos de producción que la red no es capaz de absorber, evitando la necesidad de instalar una mayor generación potencia para cubrir los picos de consumo en periodos de menor generación. La capacidad de estos sistemas llegaría a las decenas o incluso centenas de MWh, con potencias nominales de hasta 1 MW, el cual podría ser modular con múltiples unidades en paralelo.

Posteriormente, se realiza un estudio de mercado de las tecnologías disponibles a las diferentes escalas destacadas anteriormente, fijando las principales condiciones de diseño y determinando los requisitos más importantes que debe satisfacer un convertidor de potencia destinado a aplicaciones de almacenamiento energético: alta eficiencia, producción en masa económica, alta escalabilidad, etc.

Debido al rápido cambio esperado en las redes de distribución en BT, así como la creación de *Smart Grids*, se ha destacado el potencial del segundo de los casos de uso analizado por dos razones. En primer lugar, por la serie de desafíos que trae consigo la electrificación de estas redes. Y en segundo lugar, por el esperado rápido despliegue de convertidores de electrónica de potencia que ofrecen la posibilidad de implementar de forma masiva nuevas técnicas que conviertan inversores FV, cargadores de VE y baterías en DERs, aportando servicios adicionales importantes a la red.

## **8.5 Estudio 6**

Se ha demostrado que los combustibles fósiles son la principal causa del cambio climático. Para reducir la dependencia mundial de los estos combustibles y frenar el calentamiento global, se considera una solución aceptada la integración del transporte en el sector eléctrico.

A pesar de los beneficios de la movilidad eléctrica, la carga de VE y la alta penetración de energías renovables puede tener un importante impacto en la red. Por un lado, debido al incremento de la demanda y las perturbaciones en la calidad de suministro originadas por los convertidores de electrónica de potencia. Por otro lado, por la intermitencia y la naturaleza incontrolable de estos servicios, forzando nuevas estructuras y estrategias de operación y mantenimiento del sistema.

En particular, la red de distribución sufrirá la mayor parte de la transformación en este proceso de electrificación. Como se ha visto a lo largo de este documento, la calidad de suministro y la estabilidad del sistema son importantes retos que deben ser afrontados en este proceso.

Los **Estudios 3 y 4** proponen el empleo de convertidores D-STATCOM para contribuir a la estabilidad de redes débiles de distribución en baja tensión. Sin embargo, el despliegue de estos equipos tienen una serie de inconvenientes. Durante su funcionamiento, estos convertidores tienen pérdidas que deben sumarse a las pérdidas de la red, además de la falta de espacio en las vías públicas para desplegar estos dispositivos y la inversión necesaria para su fabricación e instalación, son algunos factores que pueden hacer inviable su implantación.

Esta publicación unifica los resultados obtenidos en el resto de los estudios realizados en la presente tesis. En primer lugar, se parte del análisis de las necesidades y aplicaciones de los nuevos DERs en las *Smart Grids* del futuro, realizado en el **Estudio 2**. De este también se toman las conclusiones obtenidas en el estudio de los semiconductores de WBG. Por otro lado, se emplea el análisis de los casos de uso de los sistemas de baterías abordados en el **Estudio 5**. Usando esto como base, se propone la implementación de las técnicas de equilibrado, desarrollada en los **Estudios 3 y 4**, en convertidores de electrónica de potencia destinados a otras aplicaciones, con el objetivo de que equipos que no están concebidos con este propósito puedan proporcionar servicios auxiliares a la red.

## 8. DISCUSIÓN

Se han identificado como un posible vector de implantación de este tipo de servicios los equipos destinados a la carga de VE por varios motivos. Por un lado, la posibilidad de contar con las baterías de los vehículos eléctricos que sirvan de respaldo energético en cargadores bidireccionales. Y, en segundo lugar, el rápido despliegue esperado de estos cargadores, tanto a nivel particular como cargadores públicos ubicados en las calles de las ciudades, confieren a estos sistemas un gran potencial para la implantación de servicios auxiliares de soporte a la red.

En particular, este artículo propone la implementación de las técnicas de equilibrio de corriente en un cargador de VE de 50 kW, construido a partir de módulos de 25 kW. En este caso, el uso de carburo de silicio como material semiconductor ha permitido la simplificación de la topología trinivel, empleada en el prototipo de D-STATCOM, por la topología binivel mostrada en la Figura 8.16, más sencilla, fácilmente paralelizable y con un menor número de componentes, así como de una significativa reducción de su tamaño.

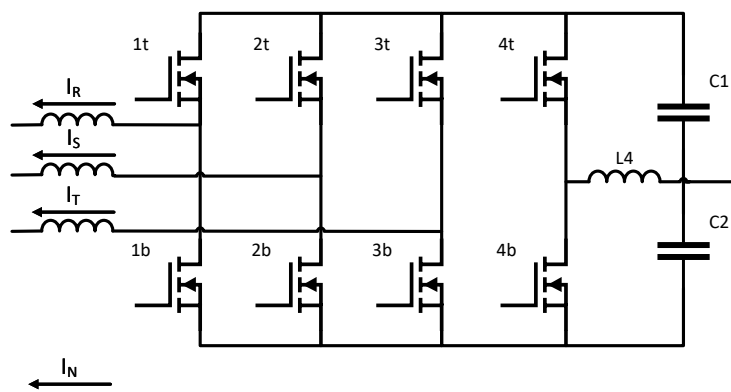


**Figura 8.16:** Topología 4 hilos y 4 ramas con condensador partido empleada en los módulos ACDC del cargador para permitir un funcionamiento desequilibrado.

De forma previa a la instalación del cargador en campo, el funcionamiento del convertidor ha sido probado a nivel de laboratorio, probando de manera satisfactoria la validez de la topología empleada para el equilibrio de corriente.

Posteriormente, la operación del cargador ha sido simulada en el modelo de red referencia de IEEE para pruebas de BT. Finalmente, se ha empleado un algoritmo que realiza la búsqueda del emplazamiento óptimo donde el equilibrio de la red sea más efectivo. Este, además, proporciona el ahorro energético conseguido por

la instalación del cargador en el punto seleccionado. Para ello, se han utilizado los modelos eléctricos de cuatro redes reales pertenecientes a diferentes países de la UE: una red rural en el sur de Europa, una red urbana en el norte de Europa, una red rural en el centro de Europa y una red urbana en el sur de Europa. La Tabla 8.5 muestra los resultados obtenidos con el algoritmo de optimización para cada una de estas redes.

**Tabla 8.5:** Ahorro energético conseguido, en cada uno de los cuatro casos estudiados, mediante la instalación de un cargador de 50 kW con equilibrado de corriente.

	Ahorro energético (kWh)	Ahorro energético (%)
Red rural sur de Europa	311,89	3,325
Red urbana norte de Europa	1,65	0,019
Red rural centro de Europa	112,96	2,076
Red urbana sur de Europa	217,71	6,396

Las simulaciones han arrojado resultados muy dispares en cada una de las redes estudiadas. Mientras la cuarta de las redes muestra una reducción de las pérdidas técnicas en la línea del 6,4 %, la segunda ha registrado una mejora insignificante en su eficiencia. Es por este motivo que, las conclusiones de este estudio destacan la importancia de determinar el lugar más apropiado para realizar el equilibrado, pudiendo conseguir ahorros energéticos muy significativos en las pérdidas de la red, mejorando por consiguiente la eficiencia del transporte de energía.



# Capítulo 9

## Conclusiones

**RESUMEN:** En este capítulo se presentan las principales conclusiones de los estudios expuestos, así como las principales líneas para la continuación del trabajo realizado en el presente documento.

## 9. CONCLUSIONES

---

### 9.1 Conclusiones del estudio

De los resultados de las seis publicaciones que componen esta investigación se derivan tres bloques de conclusiones. El primero de estos bloques se relaciona con los **Estudios 1 y 2**, donde se han establecido las necesidades de los convertidores de electrónica de potencia, así como las principales tendencias en su diseño.

- Los nuevos convertidores empleados en las *Smart Grids* deberán ser capaces de proveer una mayor flexibilidad, así como otras características definidas en los códigos de red. Con este fin, deberán diseñarse empleando topologías bidireccionales y sistemas de comunicación con la red que permitan las funcionalidades exigidas.
- Para cumplir con los requisitos de los usuarios, además, estos equipos deberán satisfacer necesidades adicionales como la limitación de tamaño, operación silenciosa, eficiencia energética y un coste reducido. Para ello, estos convertidores deberán tener unas prestaciones en cuanto a frecuencia de funcionamiento, térmicas y pérdidas, superiores a los proporcionados por los semiconductores de silicio.
- Ante esta necesidad surgen los semiconductores fabricados en materiales de gran ancho de banda, que sí satisfacen estos requisitos. Entre ellos destacan los fabricados carburo de silicio y nitruro de galio, disponibles comercialmente, y los basados en óxido de galio, cuyos primeros prototipos ya han sido probados con éxito.

El segundo bloque está compuesto por los **Estudios 3 y 4**, y recoge el diseño y evaluación de los principales desarrollos llevados a cabo en la tesis.

- Se ha propuesto el diseño de un convertidor capaz de funcionar con cargas desequilibradas. Partiendo de una de las topologías trifásicas más empleadas comercialmente, se han aplicado las modificaciones necesarias para adaptarla a un convertidor de cuatro ramas. Posteriormente se ha efectuado el dimensionamiento del hardware y el montaje de un prototipo de D-STATCOM.
- Se ha elaborado el estudio e implementación de la estrategia de control necesaria para el funcionamiento del equipo, abordando el control de potencia, generación de consignas, control de corriente y modulación.

## 9.1 Conclusiones del estudio

---

- Se ha ejecutado una primera fase de validación del prototipo a nivel de laboratorio, evaluando parámetros como eficiencia y la calidad de la corriente generada. En una segunda fase se ha instalado el prototipo en una línea eléctrica de la red de distribución, analizando los beneficios del equilibrio de corrientes.
- El estudio del funcionamiento del prototipo durante un periodo de un mes, confirma la efectividad del equipo para mejorar la calidad de la potencia suministrada a los consumidores (reducción del VUF), así como una mejora en la eficiencia de la línea (reducción de pérdidas del 13 %) y una reducción de la corriente máxima en los conductores (de un 73 % en el cable de neutro), lo que posibilitaría una reducción en la sección de los cables empleados en la línea.

El último bloque está formado por los **Estudios 5 y 6** y se centra en la aplicación de las técnicas estudiadas y experiencia adquirida para su implantación masiva en sistemas comerciales.

- Se han estudiado las posibles aplicaciones de la instalación de un sistema de este tipo de forma conjunta a sistemas de baterías, destacando tres casos de uso: almacenamiento energético para el pequeño comercio, donde se emplearían convertidores de potencias inferiores a 10 kW; aplicaciones en la red de BT, con potencias requeridas de decenas de kilovatios; y grandes sistemas de almacenamiento, alcanzando potencias de hasta 1 MW.
- Dada la creciente importancia de las redes de baja tensión y el rápido crecimiento de las *Smart Grids* se ha destacado el segundo caso de uso, donde los inversores de electrónica de potencia podrían ser utilizados como recursos energéticos distribuidos para la gestión de congestiones y regulación de tensión en estas redes.
- Se ha destacado como aplicación con gran proyección la implementación de las técnicas desarrolladas en cargadores de vehículo eléctrico, y se ha realizado el diseño de un prototipo de 50 kW para carga rápida en modo 4.
- Se ha estudiado mediante simulación los efectos de la instalación de estos cargadores en cuatro redes reales, concluyendo la importancia de estudiar la ubicación del equipo para optimizar los beneficios que puede aportar a la red,

## **9. CONCLUSIONES**

---

consiguiendo una reducción de las pérdidas técnicas del 6,4 % en el mejor de los casos estudiados.

### 9.2 Líneas de trabajo futuro

La creación de *Smart Grids*, la implementación de recursos energéticos distribuidos y el despliegue masivo de fuentes de energía renovables son ámbitos de estudio en pleno crecimiento y que todavía requieren un gran esfuerzo, tanto a nivel de investigación como de industrialización. Esta tesis ha profundizado en el uso de los convertidores electrónicos de potencia para la prestación de servicios auxiliares a la red. Sin embargo, durante la realización de este trabajo se han detectado posibles líneas de continuación que no han sido abordadas, puesto que su extensión y alcance serían suficientes para el desarrollo tesis doctoral completa. En esta sección se resumen brevemente algunas de las posibles líneas de continuación del trabajo realizado.

En primer lugar, los nuevos materiales semiconductores de gran ancho de banda están alcanzando la madurez y fiabilidad tecnológica suficiente para emplearse en sistemas de electrónica de potencia. Sin embargo, estos apenas han comenzado a emplearse a nivel industrial. Para favorecer su adopción para la fabricación en masa, todavía debe trabajarse en su caracterización, la disminución de la inductancia parásita y la creación de protecciones aptas para el funcionamiento a las altas frecuencias de conmutación proporcionadas por estos elementos [33].

En segundo lugar, conseguir elevar la penetración de energías renovables más allá de los límites alcanzados hoy en día supondrá un cambio en el paradigma del funcionamiento de los convertidores conectados a la red. Los generadores síncronos, presentes en las grandes centrales térmicas, proporcionan a la red una inercia y una capacidad de regulación que en el futuro deberá ser proporcionado por sistemas electrónicos. En la actualidad, se está realizando un gran esfuerzo de investigación en el desarrollo de técnicas *grid-forming*, que permitan altas tasas de generación renovable [34].

Por último, el futuro del sistema eléctrico pasa por una red más interconectada. En ella los distintos sistemas conectados a la red prestarán servicios de flexibilidad en función de la previsión de generación y demanda, y del estado de la red. Con este fin, se están desarrollando varios proyectos a nivel internacional con el objetivo de desarrollar las plataformas que permitan las transacciones de energía entre usuarios [35].



# Bibliografía

- [1] The Intergovernmental Panel on Climate Change (IPCC), “Special Report on the impacts of global warming of 1.5°C,” 2018. [Online]. Available: <https://www.ipcc.ch/sr15/> (Accessed 2022-05-19).
- [2] Intergovernmental Science-Policy Platform on Biodiversity and Ecosystem Services (IPBES), “Global Assessment Report on Biodiversity and Ecosystem Services,” 2019. [Online]. Available: <https://ipbes.net/global-assessment> (Accessed 2022-05-19).
- [3] “Qué es la Convención Marco de las Naciones Unidas sobre el Cambio Climático — CMNUCC.” [Online]. Available: <https://unfccc.int/es/process-and-meetings/the-convention/que-es-la-convencion-marco-de-las-naciones-unidas-sobre-el-cambio-climatico> (Accessed 2022-08-01).
- [4] “¿Qué es el Protocolo de Kyoto? — CMNUCC.” [Online]. Available: <https://unfccc.int/es/kyoto{ }protocol> (Accessed 2022-08-01).
- [5] “El Acuerdo de París — CMNUCC.” [Online]. Available: <https://unfccc.int/es/process-and-meetings/the-paris-agreement/el-acuerdo-de-paris> (Accessed 2022-08-01).
- [6] D. Jones, A. Sakhel, M. Buck, and P. Graichen, “Agora Energiewende and Sandbag (2018): The European Power Sector in 2017. State of Affairs and Review of Current Developments,” Agora Energiewende, 10178 Berlin, Tech. Rep., 2018.

## BIBLIOGRAFÍA

---

- [7] European Commission, “Europe leads the global clean energy transition: commission welcomes ambitious agreement on further renewable energy development in the EU.” Tech. Rep., 2018.
- [8] “A European Green Deal — European Commission.” [Online]. Available: <https://ec.europa.eu/info/strategy/priorities-2019-2024/european-green-deal> (Accessed 2022-04-26).
- [9] European Commission, “REPowerEU Plan,” 2022. [Online]. Available: <https://eur-lex.europa.eu/resource.html?uri=cellar:fc930f14-d7ae-11ec-a95f-01aa75ed71a1.0001.02/DOC> (Accessed 2022-04-26).
- [10] “Energy efficiency targets.” [Online]. Available: <https://energy.ec.europa.eu/topics/energy-efficiency/energy-efficiency-targets-directive-and-rules/energy-efficiency-targets> (Accessed 2022-08-03).
- [11] “Renewable energy targets.” [Online]. Available: <https://energy.ec.europa.eu/topics/renewable-energy/renewable-energy-directive-targets-and-rules/renewable-energy-targets> (Accessed 2022-08-03).
- [12] “Plan Nacional Integrado de Energía y Clima (PNIEC) 2021-2030.” [Online]. Available: <https://www.miteco.gob.es/es/prensa/pniec.aspx> (Accessed 2022-04-26).
- [13] “Energy and the Green Deal — European Commission,” 2020. [Online]. Available: <https://ec.europa.eu/info/strategy/priorities-2019-2024/european-green-deal/energy-and-green-deal> (Accessed 2022-05-22).
- [14] Banco Mundial, “PIB (US\$ a precios actuales) - European Union — Data.” [Online]. Available: <https://datos.bancomundial.org/indicador/NY.GDP.MKTP.CD?locations=EU> (Accessed 2022-05-22).
- [15] Federal Government, “Integrated National Energy and Climate Plan - Germany,” 2019. [Online]. Available: <https://energy.ec.europa.eu/system/>

- files/2020-07/de{ }final{ }necp{ }main{ }en{ }0.pdf (Accessed 2022-05-22).
- [16] “Integrated National Energy and Climate Plan - France,” 2020. [Online]. Available: <https://energy.ec.europa.eu/system/files/2020-09/fr{ }final{ }necp{ }main{ }en{ }0.pdf> (Accessed 2022-05-22).
- [17] Ministry of Economic Development, Ministry of the Environment and Protection of Natural Resources and the Sea, and Ministry of Infrastructure and Transport, “Integrated National Energy and Climate Plan - Italy,” 2019. [Online]. Available: <https://energy.ec.europa.eu/system/files/2020-02/it{ }final{ }necp{ }main{ }en{ }0.pdf> (Accessed 2022-05-22).
- [18] Ministry of Economic Affairs and Climate Policy, “Integrated National Energy and Climate Plan - The Netherlands,” 2021, (Accessed 2022-05-22).
- [19] “EU strategy on energy system integration.” [Online]. Available: <https://energy.ec.europa.eu/topics/energy-system-integration/eu-strategy-energy-system-integration{ }en> (Accessed 2022-05-22).
- [20] “CIRCE — Centro Tecnológico en I+D+i.” [Online]. Available: <https://www.fcirce.es/> (Accessed 2022-05-23).
- [21] G. Fernandez Aznar, M. Á. Oliván Monge, J. Sediles Ortiz, A. Munoz Zuara, J. Bruna Romero, H. Bludszuweit, and I. Prieto Borrero, “Transformation of a microgrid in a distribution grid support asset,” in *CIREN 2019, 25th International Conference on Electricity Distribution*. Madrid (Spain): CIREN, 2019. [Online]. Available: <https://www.cired-repository.org/handle/20.500.12455/328>
- [22] “FLEXICIENCY - Consumo de energía según demanda - Fundación CIRCE.” [Online]. Available: <https://www.fcirce.es/redes-electricas-del-futuro/flexiency-2> (Accessed 2022-05-24).
- [23] G. Fernandez, J. Almajano, E. García, H. Bludszuweit, S. MacHín, and J. F. Sanz, “Control structure for optimal demand-side management with a multi-technology battery storage system,” *IEEE International Conference on*

## BIBLIOGRAFÍA

---

*Emerging Technologies and Factory Automation, ETFA*, vol. 2019-Septe, pp. 754–759, sep 2019.

- [24] “Proyecto EV-OPTIMANAGER — Optimización de la Demanda Eléctrica.” [Online]. Available: <https://www.fcirce.es/smart-mobility-es/ev-optimanager> (Accessed 2022-05-24).
- [25] J. Ballestín-Fuertes, J. Muñoz-Cruzado-Alba, and J. F. Sanz-Osorio, “4-legs electronic active load for anti-islanding evaluation,” in *CIGRE - 2020 E-session*. Paris (France): CIGRE, 2020.
- [26] “REDACTIVA - Circe.” [Online]. Available: <https://www.fcirce.es/redes-electricas-del-futuro/redactiva> (Accessed 2022-05-24).
- [27] European Commission, “HORIZON 2020 WORK PROGRAMME 2016 – 2017 20 . General Annexes (European Commission Decision C (2017) 2468 of 24 April 2017), Annex G, Technology Readiness Levels (TRL),” pp. 1–39, 2017. [Online]. Available: <https://ec.europa.eu/research/participants/data/ref/h2020/other/wp/2016-2017/annexes/h2020-wp1617-annex-ga{ }en.pdf> (Accessed 2022-04-24).
- [28] European Commission, “Powering a climate-neutral economy: An EU Strategy for Energy System Integration,” 2020. [Online]. Available: <https://ec.europa.eu/energy/topics/energy-strategy/clean-energy-all-europeans{ }en>. (Accessed 2022-04-26).
- [29] “IEEE PES Test Feeder.” [Online]. Available: <https://cmte.ieee.org/pes-testfeeders/resources/> (Accessed 2022-05-02).
- [30] K. Shenai, “High-Density Power Conversion and Wide-Bandgap Semiconductor Power Electronics Switching Devices,” *Proceedings of the IEEE*, vol. 107, no. 12, pp. 2308–2326, 2019.
- [31] T. P. Chow, I. Omura, M. Higashiwaki, H. Kwarada, and V. Pala, “Smart power devices and ICs using GaAs and wide and extreme bandgap semiconductors,” *IEEE Transactions on Electron Devices*, vol. 64, no. 3, pp. 856–873, 2017.

- [32] M. Higashiwaki and S. Fujita, “Introduction,” in *Gallium Oxide: Materials Properties, Crystal Growth, and Devices*, 1st ed. Springer, 2020, vol. 293, pp. 1–12.
- [33] P. R. Wilson, B. Ferreira, J. Zhang, and C. DiMarino, “IEEE ITRW: International Technology Roadmap for Wide-Bandgap Power Semiconductors: An Overview,” *IEEE Power Electronics Magazine*, vol. 5, no. 2, 2018. [Online]. Available: <https://ieeexplore-ieee-org.cuarzo.unizar.es/9443/document/8386966/>
- [34] J. Matevosyan, B. Badrzadeh, T. Prevost, E. Quitmann, D. Ramasubramanian, H. Urdal, S. Achilles, J. Macdowell, S. H. Huang, V. Vital, J. Osullivan, and R. Quint, “Grid-forming inverters: Are they the key for high renewable penetration?” *IEEE Power and Energy Magazine*, vol. 17, no. 6, pp. 89–98, nov 2019.
- [35] G. Pressmair, E. Kapassa, D. Casado-Mansilla, C. E. Borges, and M. Themistocleous, “Overcoming barriers for the adoption of Local Energy and Flexibility Markets: A user-centric and hybrid model,” *Journal of Cleaner Production*, vol. 317, p. 128323, oct 2021.



# Anexo A

## **Lista de publicaciones**



## A.1 Publicaciones en revistas científicas

1. Ballestín-Fuertes, J.; Muñoz-Cruzado-Alba, J.; Sanz-Osorio, J.F.; Hernández-Callejo, L.; Alonso-Gómez, V.; Morales-Aragones, J.I.; Gallardo-Saavedra, S.; Martínez-Sacristan, O.; Moretón-Fernández, Á. “Novel Utility-Scale Photovoltaic Plant Electroluminescence Maintenance Technique by Means of Bidirectional Power Inverter Controller”. *Appl. Sci.* 2020, 10, 3084. doi: 10.3390/app10093084.
2. Gallardo-Saavedra, S.; Hernández-Callejo, L.; Alonso-García, M.d.C.; Muñoz-Cruzado-Alba, J.; Ballestín-Fuertes, J. “Infrared Thermography for the Detection and Characterization of Photovoltaic Defects: Comparison between Illumination and Dark Conditions”. *Sensors* 2020, 20, 4395. doi: 10.3390/s20164395.
3. Ballestín-Fuertes, J.; Muñoz-Cruzado-Alba, J.; Sanz-Osorio, J.F.; Laporta-Puyal, E. “Role of Wide Bandgap Materials in Power Electronics for Smart Grids Applications”. *Electronics* 2021, 10, 677. doi: 10.3390/electronics10060677.
4. Muñoz-Cruzado-Alba, J.; Musca, R.; Ballestín-Fuertes, J.; Sanz-Osorio, J.F.; Rivas-Ascaso, D.M.; Jones, M.P.; Catania, A.; Goosen, E. “Power Grid Integration and Use-Case Study of Acid-Base Flow Battery Technology”. *Sustainability* 2021, 13, 6089. doi: 10.3390/su13116089.
5. Fernández, G.; Martínez, A.; Galán, N.; Ballestín-Fuertes, J.; Muñoz-Cruzado-Alba, J.; López, P.; Stukelj, S.; Daridou, E.; Rezzonico, A.; Ioannidis, D. “Optimal D-STATCOM Placement Tool for Low Voltage Grids”. *Energies* 2021, 14, 4212. <https://doi.org/10.3390/en14144212>.
6. J. Ballestín-Fuertes, J. F. Sanz-Osorio, J. Muñoz-Cruzado-Alba, E. L. Puyal, J. Leiva and J. R. Rivero, “Four-Legs D-STATCOM for Current Balancing in Low-Voltage Distribution Grids” *IEEE Access*, vol. 10, pp. 779-788, 2022, doi: 10.1109/ACCESS.2021.3138827.

### A.2 Publicaciones en congresos

1. E. García-Martínez, J. Ballestín, J. Muñoz-Cruzado and J. F. Sanz, “Analysis of a switched and linear power amplifier for Power Hardware-in-the-Loop testing of Smartgrid systems”. 2019 24th IEEE International Conference on Emerging Technologies and Factory Automation (ETFA), 2019, pp. 747-753, doi: 10.1109/ETFA.2019.8868952.
2. J. Ballestín-Fuertes, D. Cervero, H. Bludszuweit, et al. “Fault Location in Low-Voltage Distribution Networks based on Reflectometry – A Case Study”. 18th International Conference on Renewable Energies and Power Quality (ICREPQ’20), Granada (Spain), 1st to 2nd April 2020.
3. J. Ballestín-Fuertes, J. Muñoz-Cruzado-Alba, J.F. Sanz Osorio. “4-legs electronic active load for anti-islanding evaluation”. CIGRE e-session 2020, París (Francia), August 2020.
4. Javier Ballestín Fuertes, Jesús Muñoz-Cruzado Alba y José Francisco Sanz Osorio. “4L D-STATCOM para redes débiles desbalanceadas de baja tensión”. VII Congreso Smart Grids, Madrid (España), 16 de Diciembre de 2020.
5. Javier Ballestín Fuertes. “4-Leg D-STATCOM for the balancing of the low-voltage distribution grid”. Semana Virtual 2020 – Comité Nacional de CIGRE España, online, 24-26 de Noviembre de 2020.
6. A. M. Munoz, J. Ballestin-Fuertes, G. Fernandez, D. Marquina and R. Igea, ”Four-leg EV Chargers for Grid Supporting,”PCIM Europe 2022; International Exhibition and Conference for Power Electronics, Intelligent Motion, Renewable Energy and Energy Management, 2022, pp. 1-7, doi: 10.30420/565822235.
7. J. Munoz-Cruzado Alba, J. B. Fuertes, A. M. Munoz Gomez, J. F. Sanz Osorio and E. Laporta Puyal, ”50-kW Modular V2G SiC Charger Station in Energy Island Microgrids: a Real Use-Case in Madeira Island,”PCIM Europe 2022; International Exhibition and Conference for Power Electronics, Intelligent Motion, Renewable Energy and Energy Management, 2022, pp. 1-9, doi: 10.30420/565822018.